



3 1176 00027 1479

Copy
RM L57A23

C.2

NACA RM L57A23

RESEARCH MEMORANDUM

WIND-TUNNEL MEASUREMENT OF STATIC FORCES ON INTERNALLY
CARRIED BOMBS OF TWO DIFFERENT BLUFF SHAPES IN THE
FLOW FIELD OF A SWEEPED-WING FIGHTER-BOMBER
CONFIGURATION AT A MACH NUMBER OF 1.6

By Douglas J. Geier and A. Warner Robins

Langley Aeronautical Laboratory
Langley Field, Va.

LIBRARY COPY

APR 12 1957

LANGLEY AERONAUTICAL LABORATORY
LIBRARY, NACA
LANGLEY FIELD, VIRGINIA

CLASSIFIED DOCUMENT

This material contains information affecting the National Defense of the United States within the meaning of the espionage laws, Title 18, U.S.C., Secs. 793 and 794, the transmission or revelation of which in any manner to an unauthorized person is prohibited by law.

**NATIONAL ADVISORY COMMITTEE
FOR AERONAUTICS**

WASHINGTON

April 1, 1957

~~CONFIDENTIAL~~

UNCLASSIFIED

ASHA (CQUID) 11-7-57
11-30-57
1-14-78

NATIONAL ADVISORY COMMITTEE FOR AERONAUTICS

RESEARCH MEMORANDUM

WIND-TUNNEL MEASUREMENT OF STATIC FORCES ON INTERNALLY
CARRIED BOMBS OF TWO DIFFERENT BLUFF SHAPES IN THE
FLOW FIELD OF A SWEEP-WING FIGHTER-BOMBER
CONFIGURATION AT A MACH NUMBER OF 1.6

By Douglas J. Geier and A. Warner Robins

SUMMARY

Forces and moments on a fighter-bomber airplane configuration with an open bomb bay and on two bluff bomb shapes located in various positions below the fuselage and in the plane of symmetry of the airplane were measured in the Langley 4- by 4-foot supersonic pressure tunnel at a Mach number of 1.61. These data were taken as part of an extensive program in which static force and moment measurements on various bombs in the flow field of an airplane configuration could be used to predict the bomb motions and drop paths in the immediate vicinity of the airplane. No drop-path calculations, however, are presented in this paper.

The data indicate that the wing has a noticeable effect on bomb forces and that these bluff bombs affect the longitudinal characteristics of the wing-fuselage combination as the strong shocks from the bomb pass over the airplane horizontal tail.

INTRODUCTION

This investigation is an extension of a program in the Langley 4- by 4-foot supersonic pressure tunnel for the determination at Mach number 1.61 of static forces and moments of various bombs in the flow field of an airplane configuration so that bomb-release motions and drop paths in the immediate vicinity of the airplane might be calculated. Reference 1 presents such data for several internally carried bombs located in the flow field of an open bomb bay and shows the method for calculating bomb motions and bomb drop paths. Reference 2 presents data for several bomb shapes tested below a closed bomb bay and below a swept wing. This paper presents the results of tests of two bluff-shaped bombs in the vicinity of an open bomb bay and gives data which

UNCLASSIFIED

By authority of

NACA RM L57A23

UNCLASSIFIED

CLASSIFIED

1-14-78

END

1-36-79

show some effects of these bombs on the airplane configuration (same airplane configuration as in ref. 1) with and without horizontal tail. The data are presented with limited analysis.

SYMBOLS

$C_{D_{wf}}$	drag coefficient of wing-fuselage or wing-fuselage-tail combination, $\frac{\text{Drag}}{qS}$
$C_{L_{wf}}$	lift coefficient of wing-fuselage or wing-fuselage-tail combination, $\frac{\text{Lift}}{qS}$
$C_{m_{wf}}$	pitching-moment coefficient of wing-fuselage or wing-fuselage-tail combination, referred to $\frac{\bar{c}}{4}$, $\frac{\text{Pitching moment}}{qS\bar{c}}$
C_{D_b}	drag coefficient of bomb, $\frac{\text{Drag}}{qF}$
C_{L_b}	lift coefficient of bomb, $\frac{\text{Lift}}{qF}$
C_{m_b}	pitching-moment coefficient of bomb (moment center at bomb nose), $\frac{\text{Pitching moment}}{qFl}$
\bar{c}	mean aerodynamic chord of wing, in.
S	total area of wing, sq ft
F	maximum frontal area of bomb, sq ft
l	length of bomb, in.
q	dynamic pressure, lb/sq ft
x	longitudinal distance between bomb midpoint and bomb-bay midpoint, in. (fig. 1(b))
z	vertical distance between bomb midpoint and horizontal line drawn through the fuselage center line at bomb-bay center line (station 20), in., (fig. 1(b))

α_b angle of attack of bomb referenced to free-stream direction,
deg

α_{wf} angle of attack of wing-fuselage or wing-fuselage-tail refer-
enced to free-stream direction, deg

Subscript:

i isolated

TESTS AND METHODS

Models and Tests

The general arrangement of models, the fuselage coordinates, and the wing dimensions are shown in figure 1. The wing-fuselage combination was designed to simulate a swept-wing fighter-bomber airplane. A detailed description of the airplane configuration and model setup is given in reference 1.

The bombs are described in figure 2. These two bluff bomb shapes will be referred to in this paper as the spool (fig. 2(a)) and cylindrical (fig. 2(b)) bombs. The bombs were tested in various locations under the fuselage in the plane of symmetry of the airplane.

The nominal ranges of angles of attack and positions used in the investigation and a convenient index to the bomb and wing-fuselage configurations involved are presented in table I.

Precision of Data

The repeatability or relative accuracies are estimated from an inspection of repeat test points, zero shifts, and static-deflection calibrations to be as follows:

x, in.	±0.05
z, in.	±0.10
Bomb:	
C_{D_b}	±0.01
C_{L_b}	±0.03

C_{m_b}	± 0.03
α_b , deg	± 0.10

Wing-fuselage:

$C_{D_{wf}}$	± 0.001
$C_{L_{wf}}$	± 0.002
$C_{m_{wf}}$	± 0.001
α_{wf} , deg	± 0.10

PRESENTATION AND DISCUSSION OF DATA

Bomb Data

Isolated bomb data.- Isolated lift, drag, and pitching-moment coefficients for the bombs are presented in figure 3. Schlieren photographs of the bombs at various angles of attack are shown in figure 4. The flat sections of the curves of lift and moment coefficient at $\alpha = 0^\circ$ and the hump at $\alpha = 0^\circ$ in the drag coefficient curve in figure 3(a) for the spool bomb can be explained by inspection of the schlieren photographs in figure 4(a). At angles of attack of -1° , 0° , and $3/4^\circ$, the flow over the center section of the spool has not fully separated and a strong shock exists before the rear flange of the spool, which produces the high drag shown in figure 3(a). Since at these low angles of attack the strong rear shock appears to be uniform about the bomb, no strong moments or lifts result. As bomb angle increases beyond 1° , however, the flow separates over the center section of the spool on the downstream side of the bomb. This separation reduces the drag, and, because of its asymmetry, produces a restoring moment and a lift.

Basic bomb data.- Drag, lift, and pitching-moment coefficients for the spool bomb and the cylindrical bomb in the presence of the airplane configuration are presented in figures 5, 6, 7, and 8. Table I gives a convenient index to the contents of these basic-data figures. These data are presented in the form of plots of aerodynamic coefficients against z . From these plots contour maps of bomb forces and calculations of bomb drop paths can be made.

Contour maps of bomb data.- The lift, drag, and pitching-moment coefficients for the spool bomb and cylindrical bomb in the presence of

the wing-fuselage combination are presented in contour map form in figures 9 to 14. The bomb midpoint is the reference point (the point at which the force coefficient is plotted) for these plots. The bomb and bomb bay are shown to scale on each plot.

These contour maps in general show rapid changes in bomb forces and moments with changes of x and z . Rapid changes are also shown with changes in bomb angle of attack. The data in this form illustrate well the complexity of the flow field in which the bomb is located. An evaluation of the effect of these measured forces and moments on the bomb drop path can be obtained only by utilizing these data on the calculation of bomb drop paths, as in reference 1.

Effects of wing.- Figure 15 shows the effects of the wing on the bomb forces and moments. Data taken with wing on and off show, in general, that the wing has a noticeable effect on the bomb coefficients. These effects, however, are not as significant as the effects of the wing on the longer bombs with fins of reference 1.

Comparison of spool and cylindrical bombs.- A comparison of the spool and cylindrical bomb forces and moments in the flow field of the wing-fuselage combination are presented in figure 16. The shapes of the curves in general are the same and, as may be seen from the isolated bomb data (fig. 3), the drag of the cylindrical bomb is less than that of the spool bomb.

Airplane Data

Basic wing-fuselage data.- The drag, lift, and pitching-moment coefficients measured on the wing-fuselage combination in the presence of the two bluff bombs are shown in figures 17 to 25. An inspection of these figures shows that, in general, rapid changes in the pitching moments of the wing-fuselage combination occur with changes in bomb position and that lift and drag coefficients exhibit much less change with either bomb position or bomb angle of attack.

Contour maps of wing-fuselage data.- Wing-fuselage data are also presented in contour maps of lift, drag, and pitching-moment coefficients for the wing-fuselage combination in the presence of the spool bomb (figs. 26 to 28) and the cylindrical bomb (figs. 29 to 31).

Wing-fuselage data with and without tail.- A comparison of the wing-fuselage force and moment data for the configuration with and without a tail in the presence of the spool bomb is presented in figures 32 and 33. These figures give data for the configurations with the bomb

in a forward position ($x = 2.95$ inches) and a rearward position ($x = 10.95$ inches), respectively. The most significant effect is seen in the difference in the influence of the bomb in the rearward location. In this position the bow shock passing across the horizontal tail of the wing-fuselage-tail configuration produces a much greater nose-down increment in pitching moment than is evidenced for the configuration without tail.

Effect of bomb shape.- Figure 34 presents the force and moment coefficients for the wing-fuselage combination in the presence of the spool and cylindrical bombs. The data show no significant differences in the effects of these two bomb shapes.

Effect of bomb angle of attack.- It appears from the basic wing-fuselage data (figs. 17 to 25) that the effects of bomb angle of attack on wing-fuselage coefficients are not significant except when the bow shocks from the bombs are falling near the trailing edge of the wing or the leading or trailing edges of horizontal-tail surfaces. As the bomb angle of attack varies, the bow shock deforms so that, for example, a shock impinging on a wing or tail surface when the bomb is at zero angle of attack might be off the surface at an angle of attack. This may be seen by superimposing sketches of the bomb schlieren photographs on figure 1(b).

CONCLUDING REMARKS

Forces and moments have been measured in the Langley 4- by 4-foot supersonic pressure tunnel at a Mach number of 1.6 on bombs of two different bluff shapes and on a swept-wing fighter-bomber airplane configuration for a large number of positions of the bombs under an open bomb bay. The results show that, in general, the wing has a noticeable effect on bomb forces and moments. These effects, however, are not as large as the effects of the wing on the streamlined bombs of NACA RM L56I18. The bluff bombs have a significant effect on airplane longitudinal characteristics as the strong bow shock of the bombs passes

over the airplane horizontal tail. The bomb data are presented in the form of contour maps suitable for trajectory calculations.

Langley Aeronautical Laboratory,
National Advisory Committee for Aeronautics,
Langley Field, Va., January 2, 1957.

REFERENCES

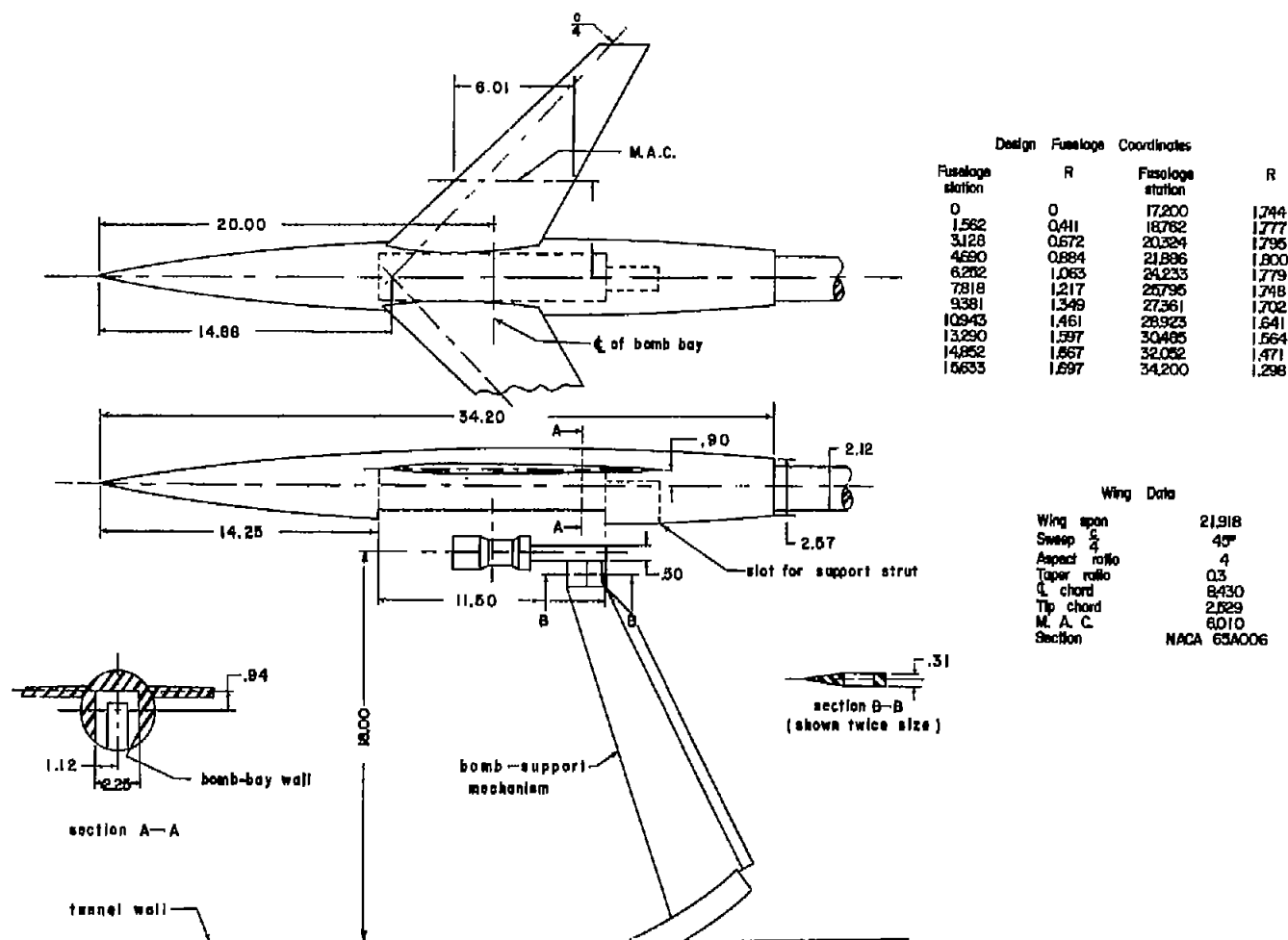
1. Smith, Norman F., and Carlson, Harry W.: Measurement of Static Forces on Internally Carried Bombs of Three Fineness Ratios in Flow Field of a Swept-Wing Fighter-Bomber Configuration at a Mach Number of 1.61 With Illustrative Drop-Path Calculations. NACA RM L56I18, 1956.
2. Geier, Douglas J., and Carlson, Harry W.: Measurement of Static Forces on Externally Carried Bombs of Fineness Ratios 7.1 and 10.5 in the Flow Field of a Swept-Wing Fighter-Bomber Configuration at a Mach Number of 1.6. NACA RM L56K30, 1957.
3. Smith, Norman F., and Carlson, Harry W.: The Origin and Distribution of Supersonic Store Interference From Measurement of Individual Forces on Several Wing-Fuselage-Store Configurations. III.- Swept-Wing Fighter-Bomber Configuration With Large and Small Stores. Mach Number, 1.61. NACA RM L55H01, 1955.

TABLE I

INDEX TO MODEL CONFIGURATIONS AND BASIC-DATA FIGURES

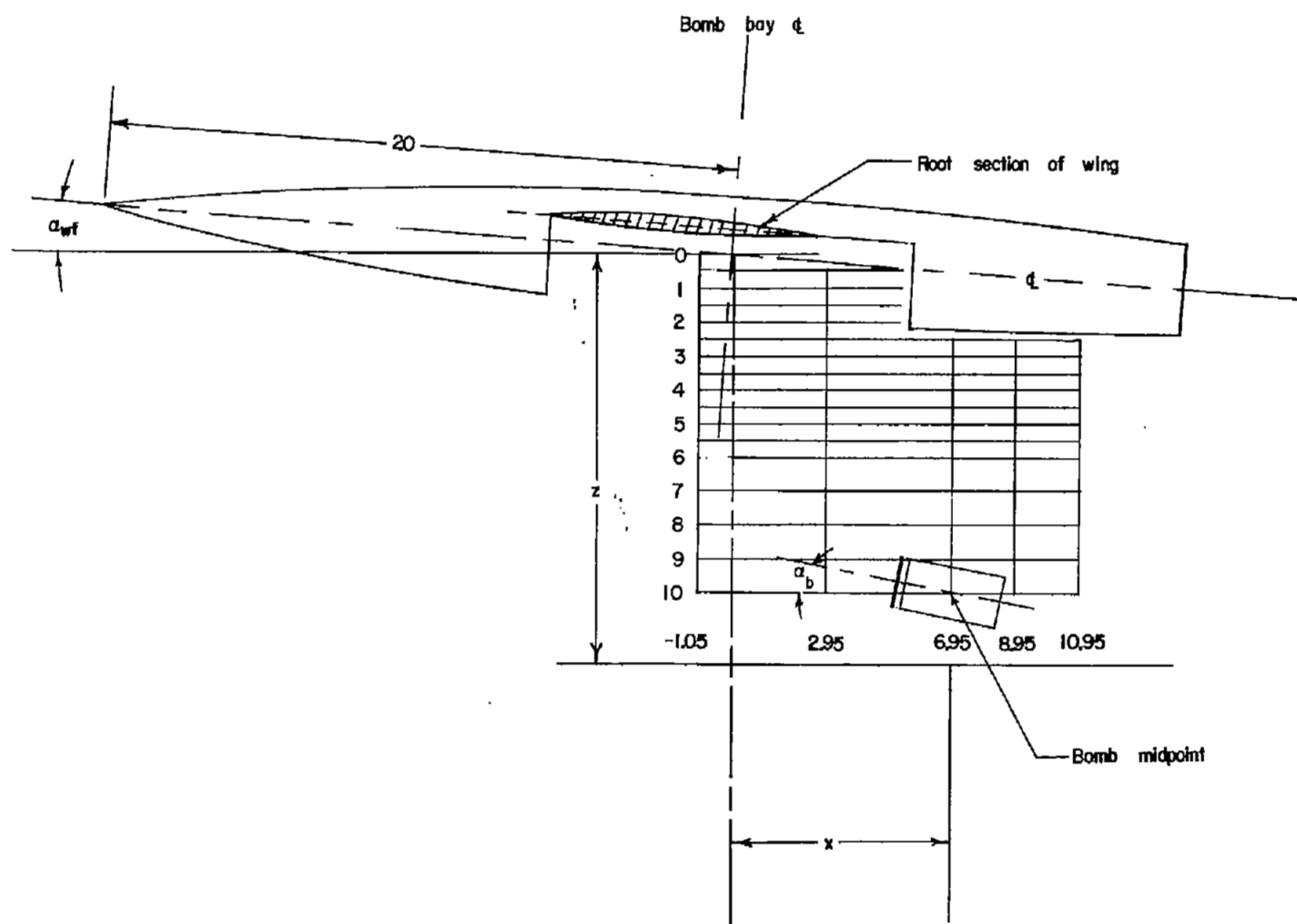
Bomb	Wing	Tail	α_b , deg	α_{wf} , deg	x, in.	Range of z, in.	Figure
Spool	On	Off	0, ± 10	0	-1.30, 2.70, 6.70	0 to 6	5
					8.70, 10.70	0 to 10	
			0	4	-1.05, 2.95, 6.95, 8.95, 10.95	^a 0 to 20	
					-1.05, 2.95, 6.95	0 to 6	
			$\pm 5, \pm 10, \pm 15$	4	8.95, 10.95	0 to 10	
					-1.17, 2.83, 6.83	0 to 6	
			0, ± 10	8	8.83, 10.83	0 to 10	
	On	On	0	0	2.70	^a 0 to 18 or 20	6
			0, ± 10		10.70	0 to 10	
			0, ± 10	4	2.95	^a 0 to 18 or 20	
			0		10.95	^a 0 to 20	
			± 10		10.95	0 to 10	
			0	8	2.83	^a 0 to 18	
			0, ± 10		10.83	0 to 10	
	Off	Off	0, ± 10	0	-1.30	0 to 6	7
			0	4	-1.05	^a 0 to 20	
			$\pm 5, \pm 10, \pm 15$		-1.05	0 to 6	
			0, ± 10	8	-1.17	0 to 6	
Cylindrical	On	Off	0, ± 10	0	-1.30, 2.70, 6.70	0 to 6	8
					10.7	0 to 10	
			0	4	-1.05, 2.95, 6.95, 10.95	^a 0 to 20	
					-1.05, 2.95, 6.95	0 to 6	
			$\pm 5, \pm 10, \pm 15$	4	10.95	0 to 10	
					-1.17, 2.83, 6.83	0 to 6	
			0, ± 10	8	10.83	0 to 10	

^aDrag coefficients for values of z greater than 10.0 are not plotted.



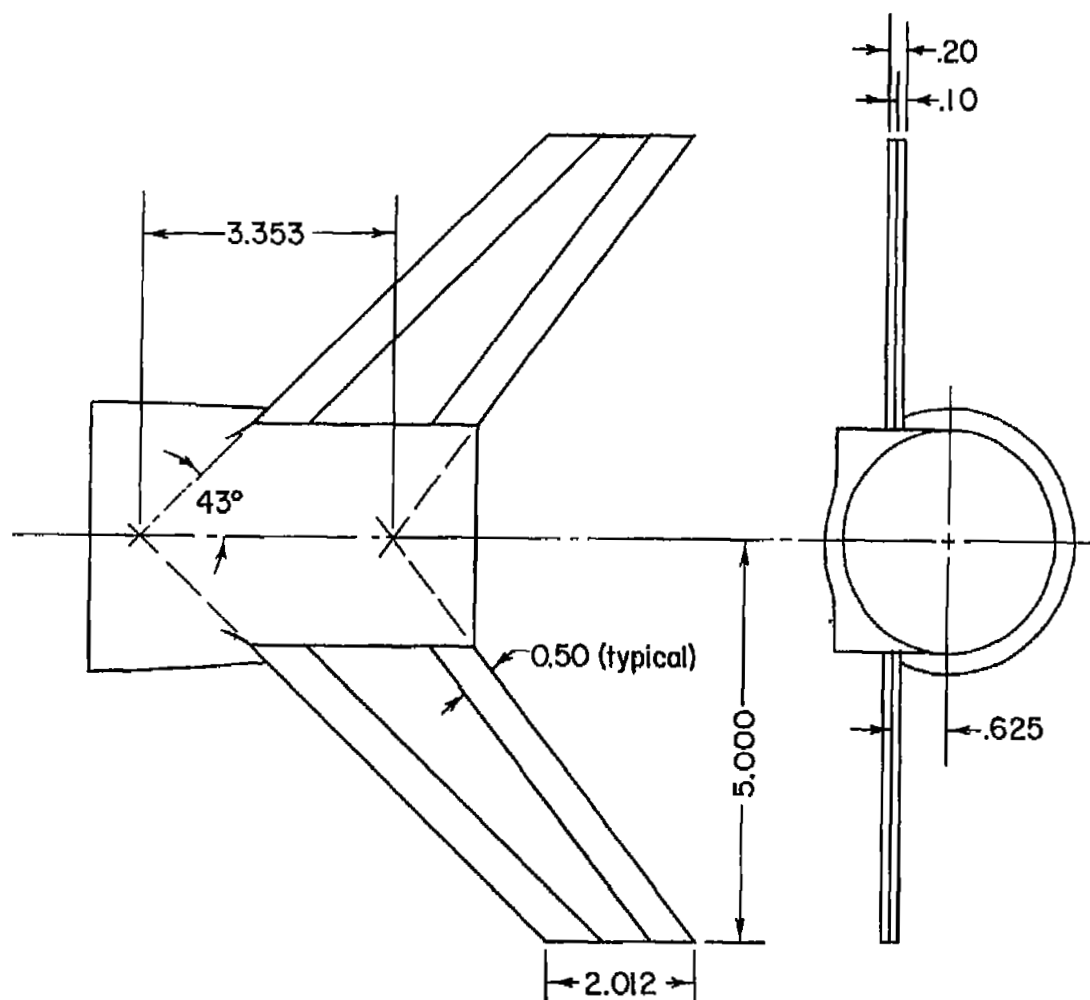
(a) Model setup.

Figure 1.- Layout of models, dimensions, and fuselage coordinates. Dimensions are in inches.



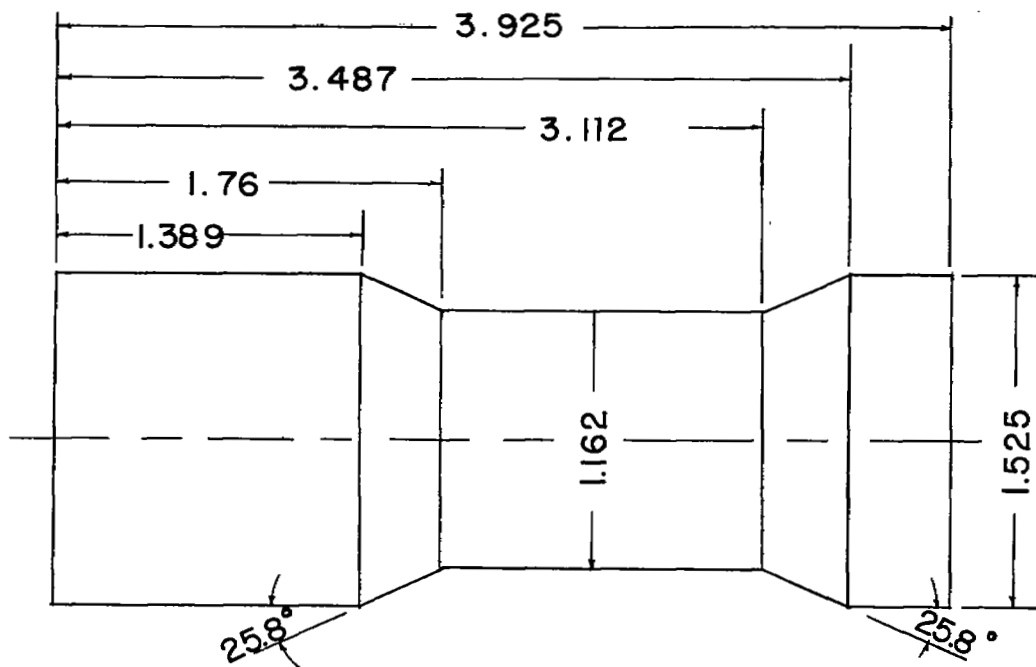
(b) Sketch showing bomb orientation in plane of symmetry of airplane.

Figure 1.- Continued.

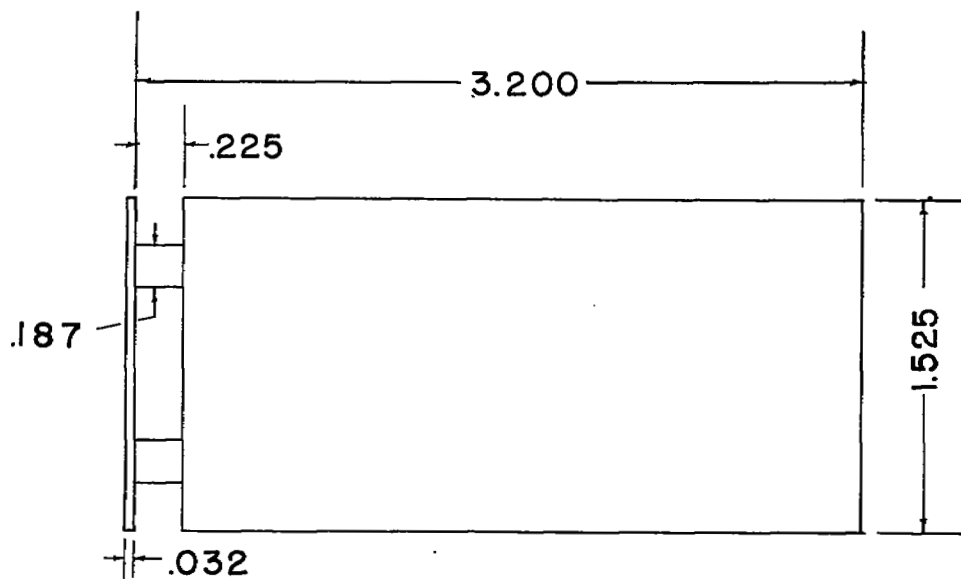


(c) Horizontal tail.

Figure 1.- Concluded.

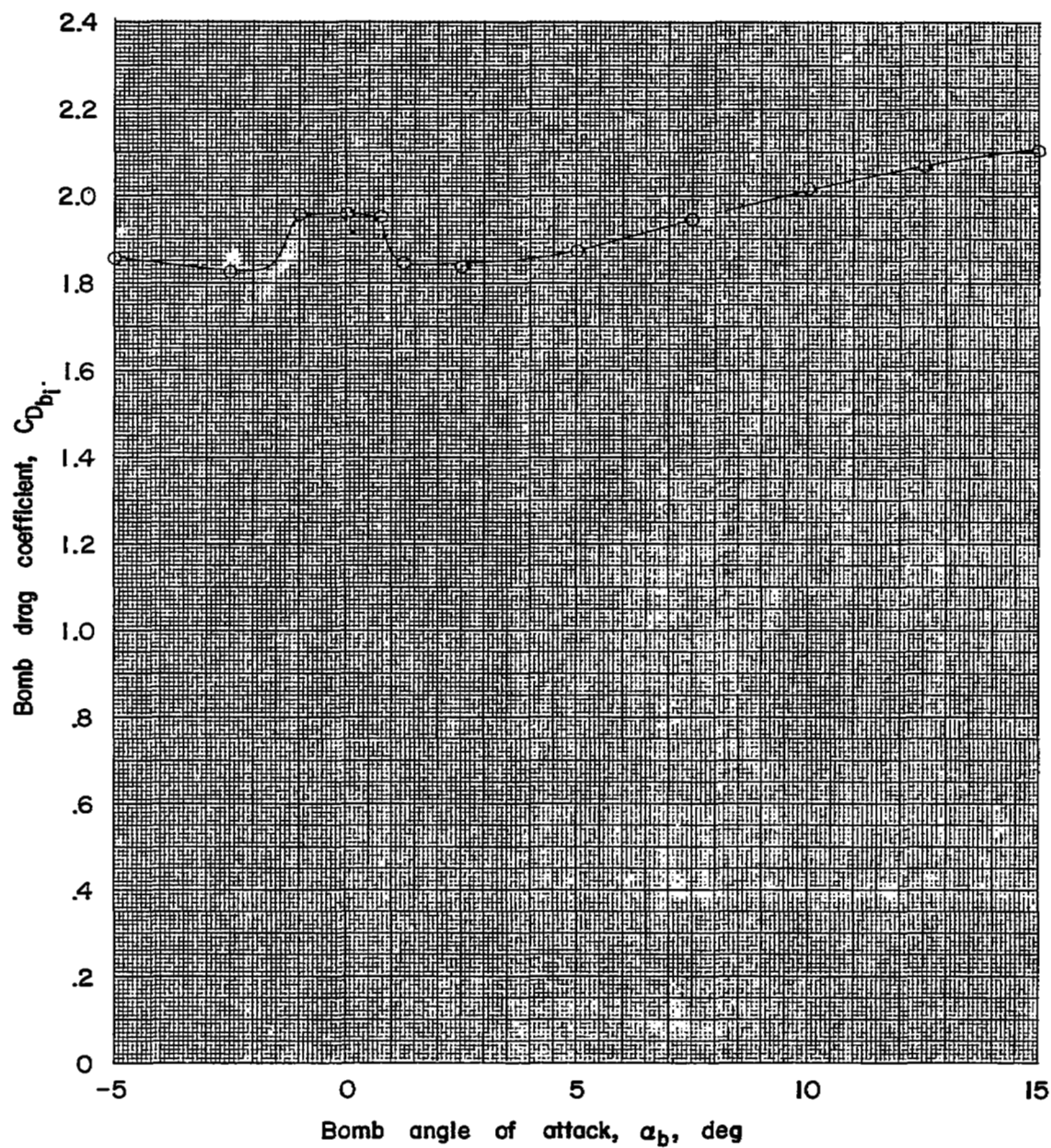


(a) Spool bomb.



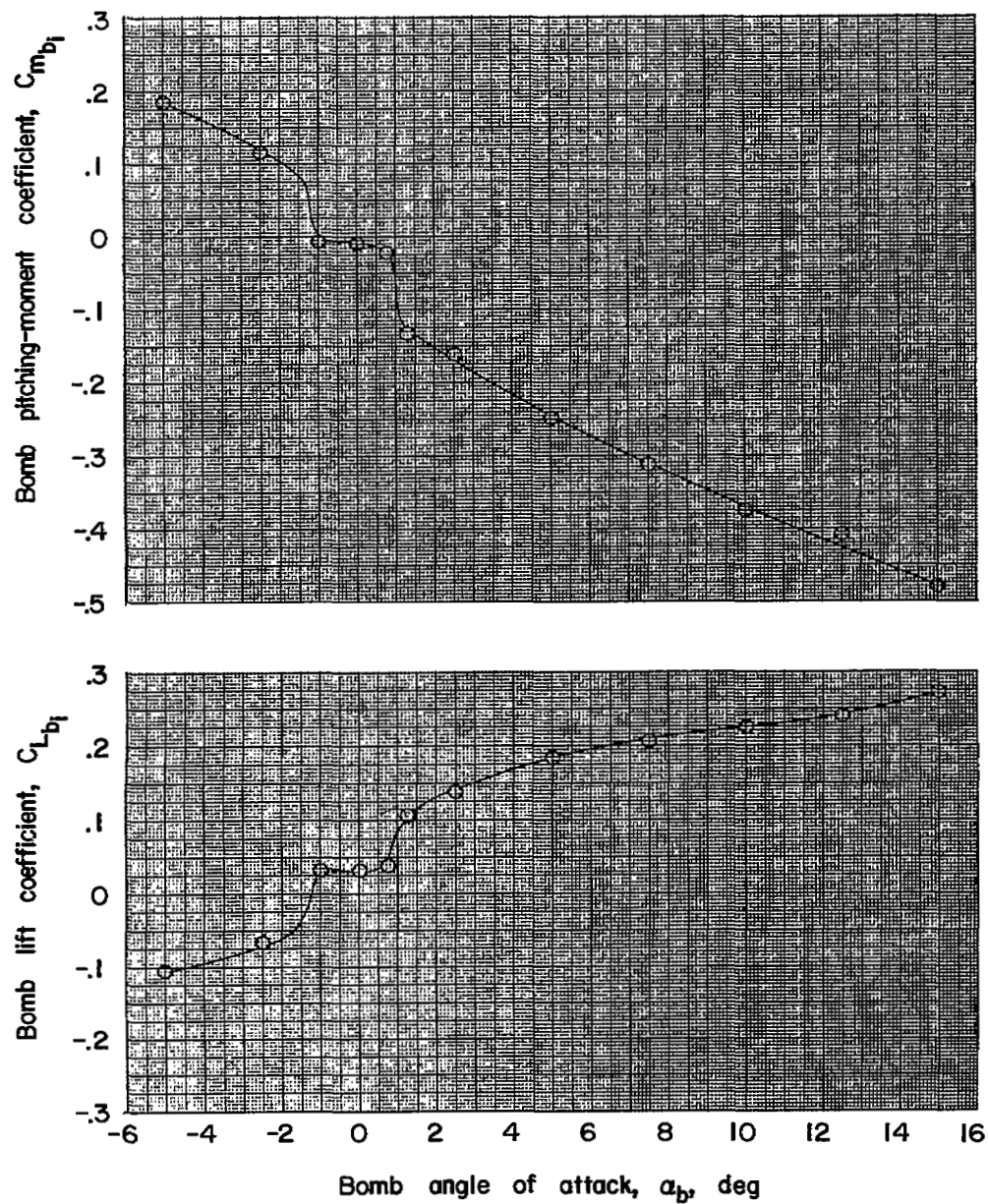
(b) Cylindrical bomb.

Figure 2.- Sketches of bombs. Dimensions are in inches.



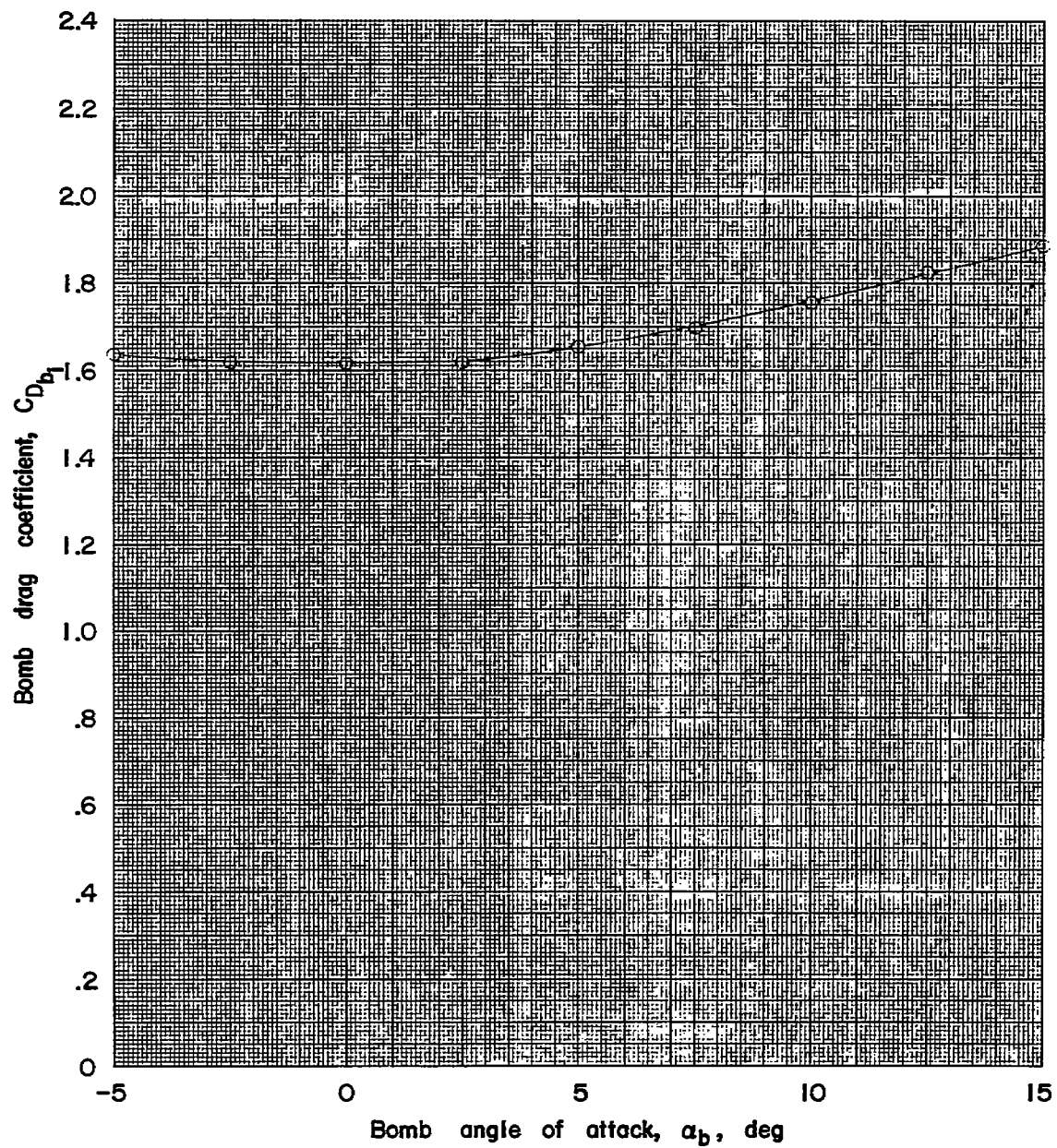
(a) Spool bomb.

Figure 3.- Aerodynamic characteristics of the isolated bombs.



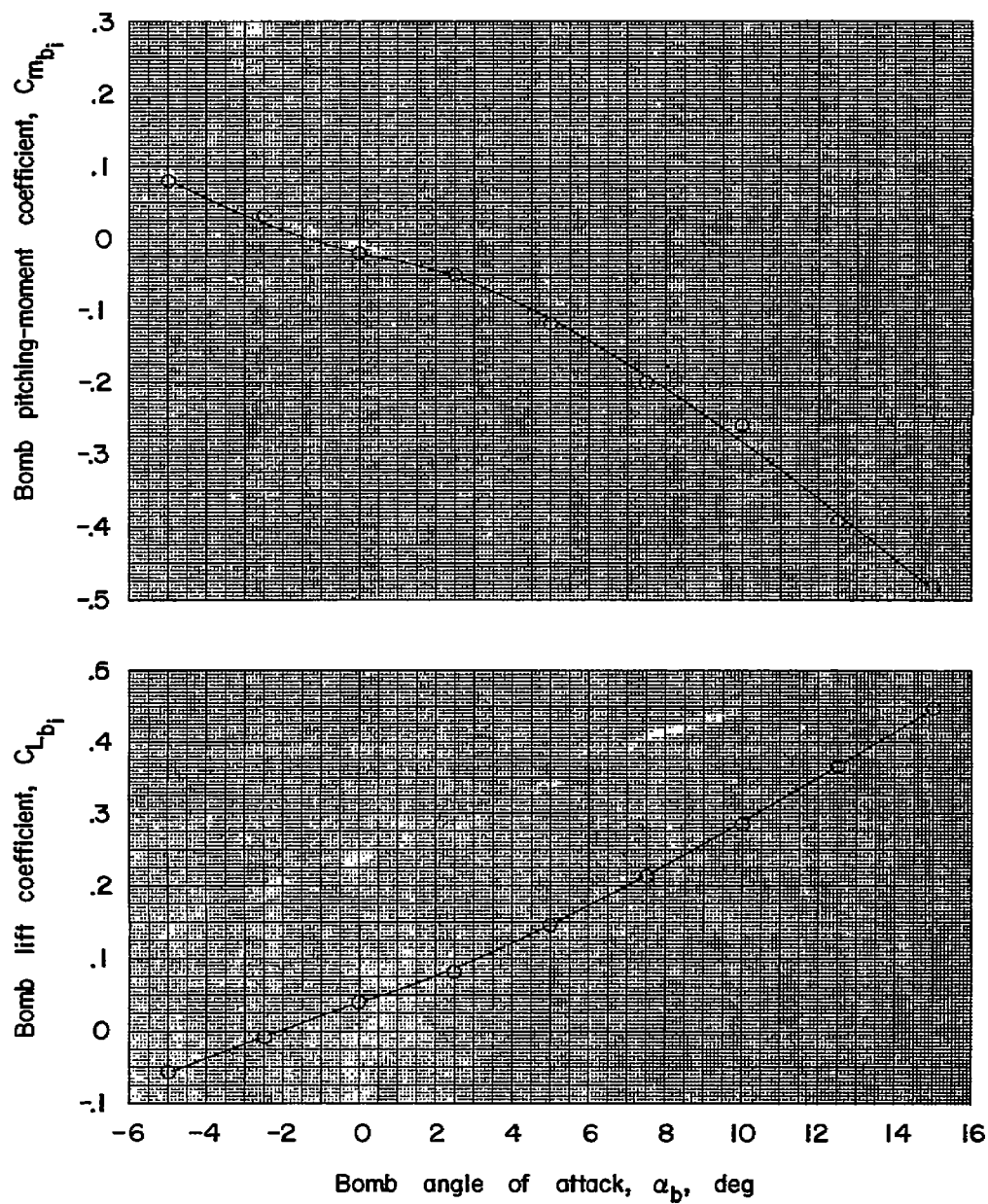
(a) Concluded.

Figure 3.- Continued.



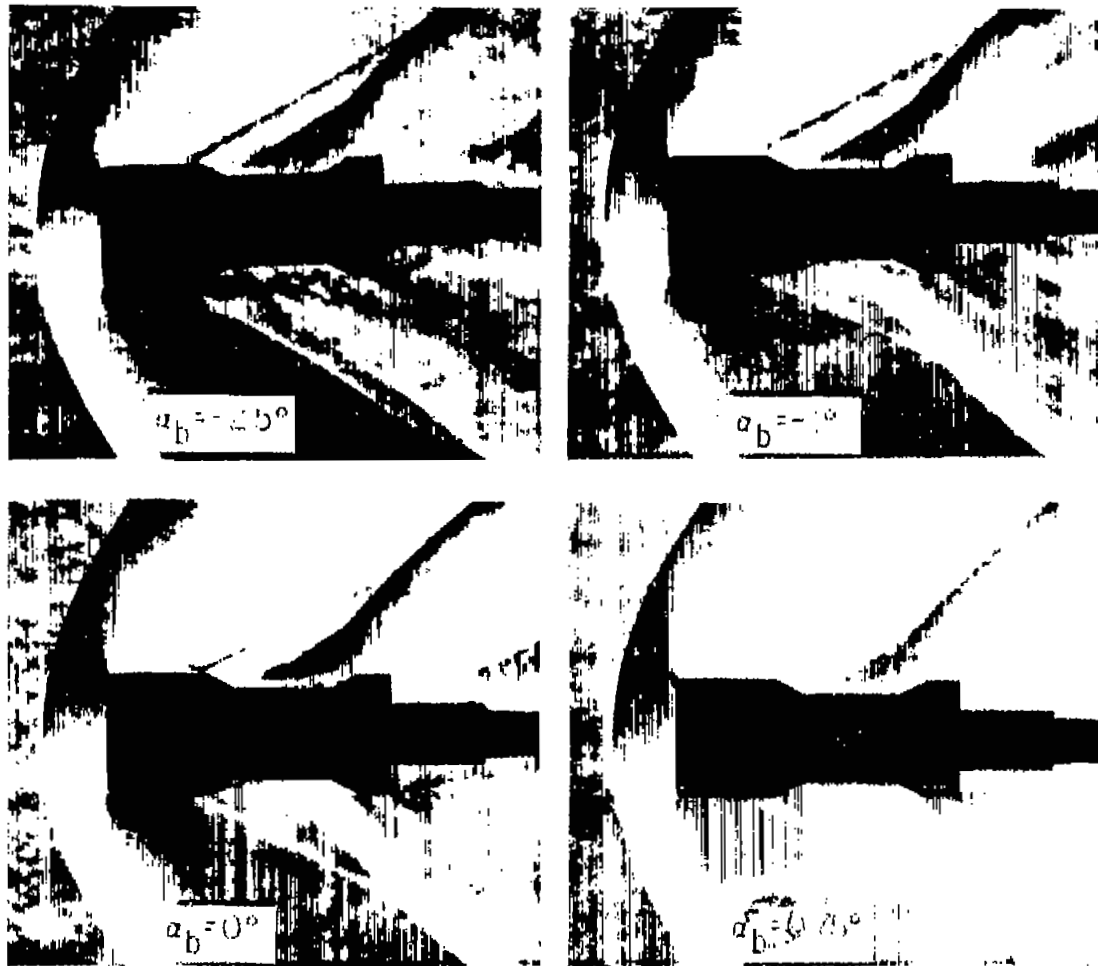
(b) Cylindrical bomb.

Figure 3.- Continued.



(b) Concluded.

Figure 3.- Concluded.



(a) Spool bomb.

L-57-113

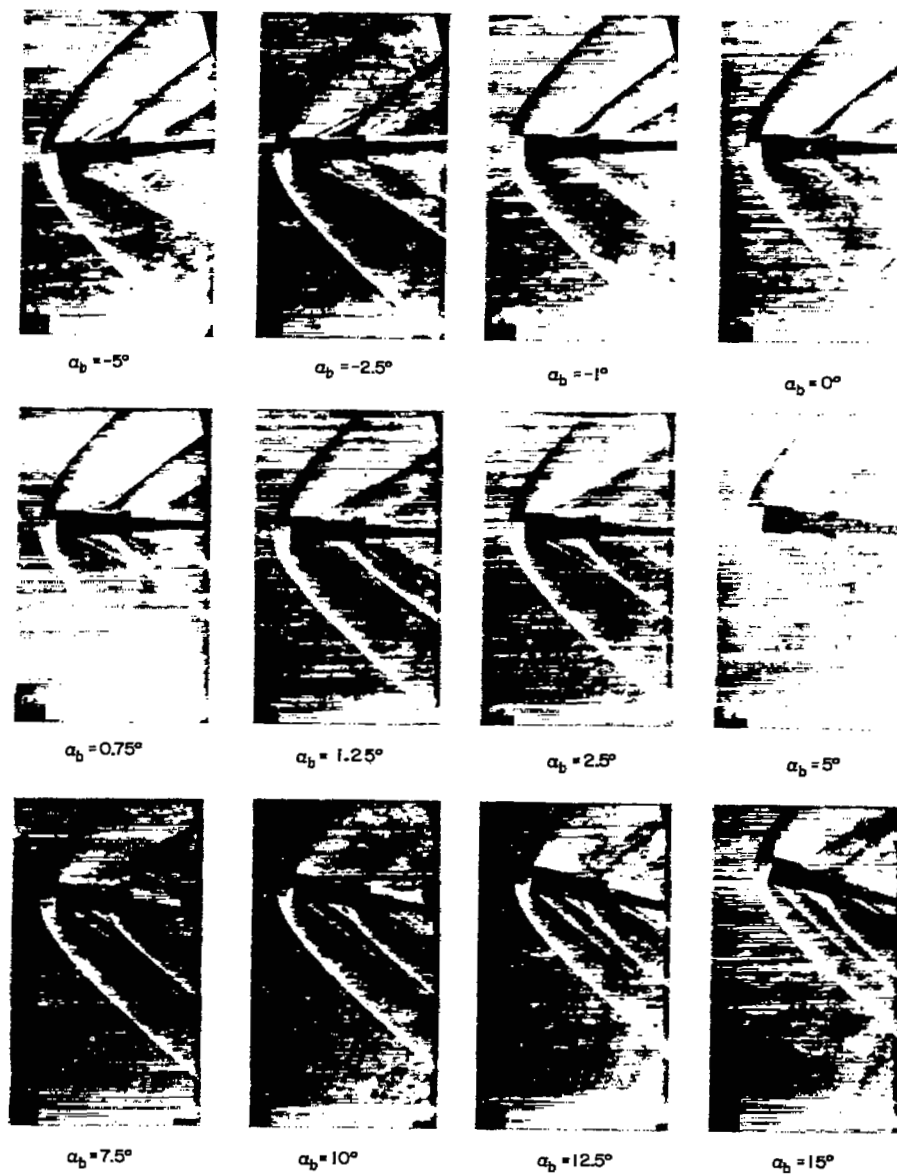
Figure 4.- Schlieren photographs of flow fields about two bluff-shaped bombs through an angle-of-attack range.



(a) Continued.

L-57-114

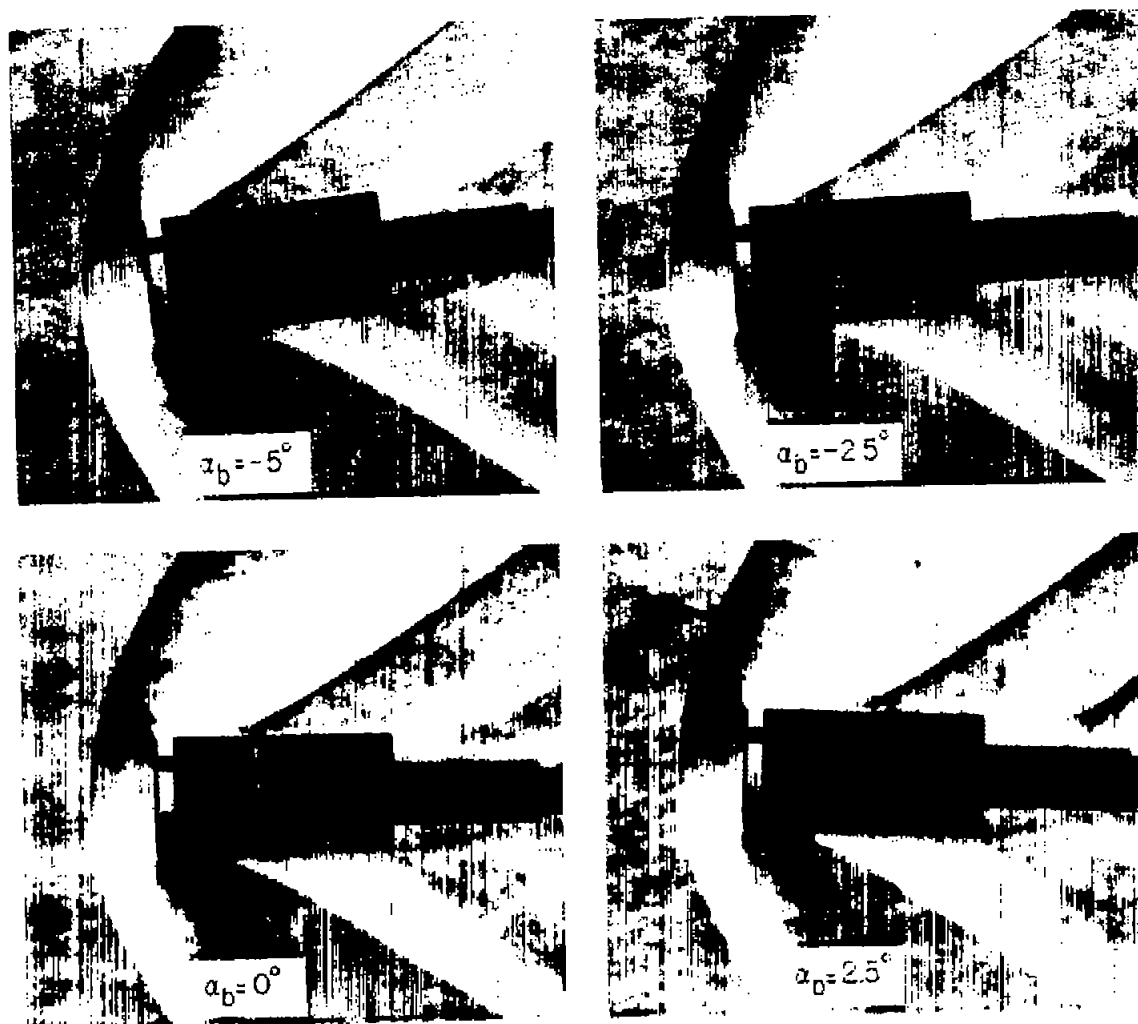
Figure 4.- Continued.



(a) Concluded.

L-95876

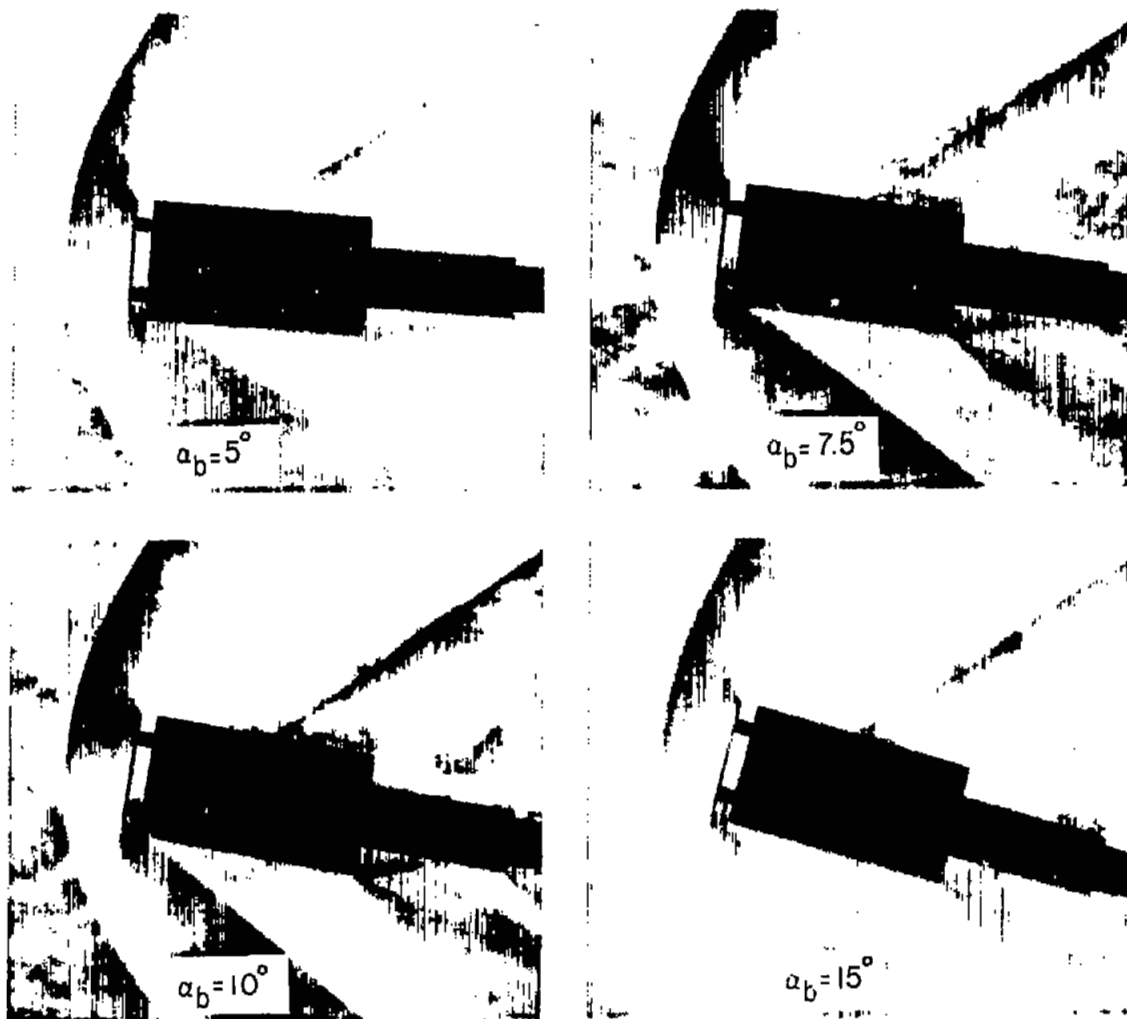
Figure 4.- Continued.



(b) Cylindrical bomb.

L-57-115

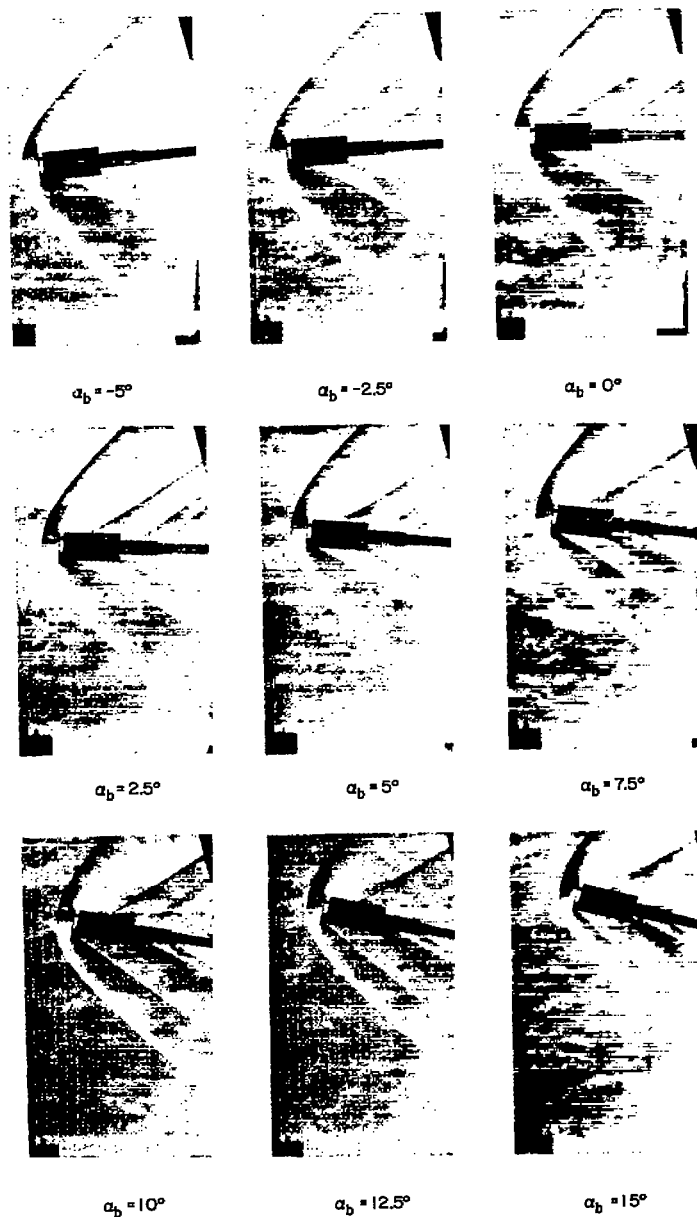
Figure 4.- Continued.



(b) Continued.

L-57-116

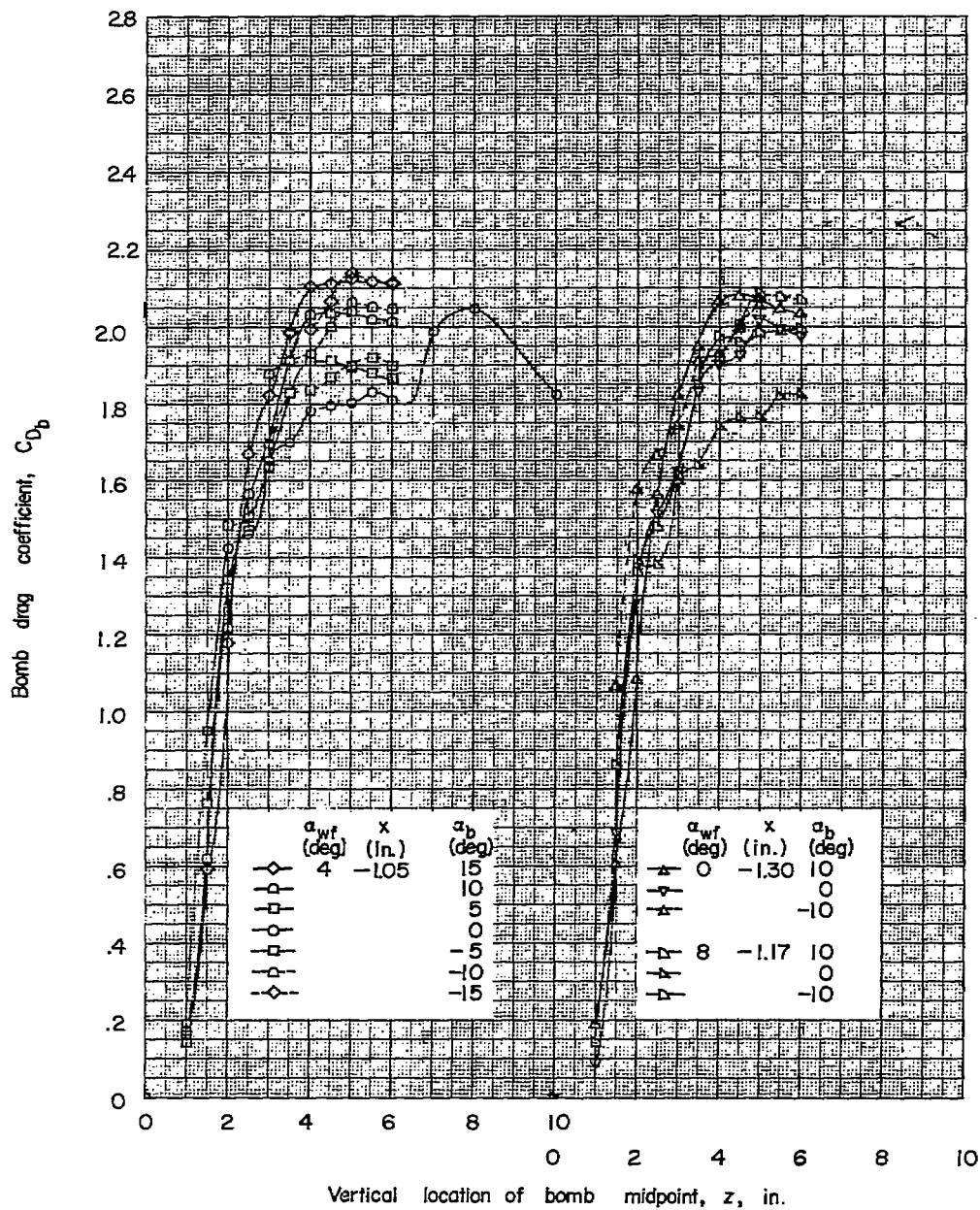
Figure 4.- Continued.



(b) Concluded.

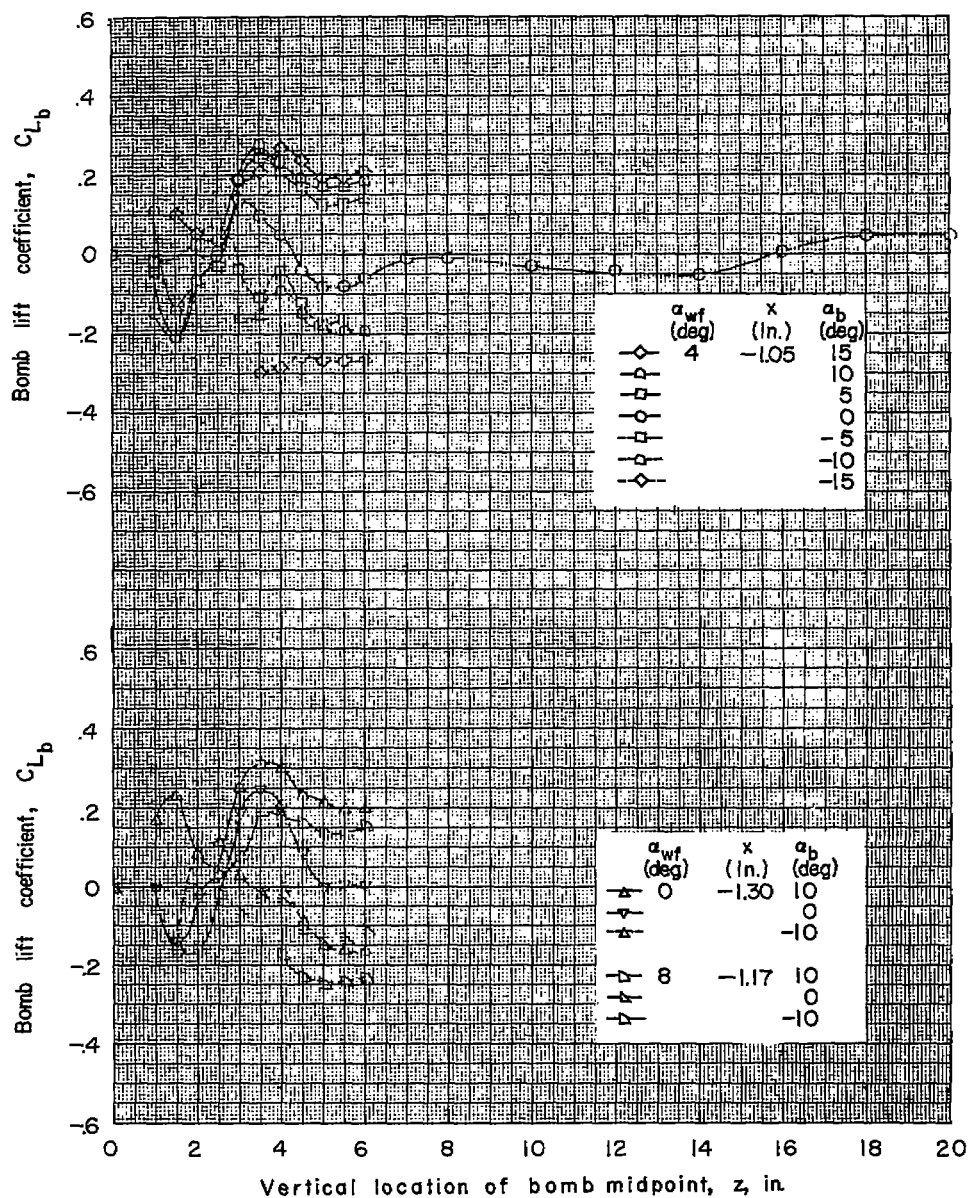
L-95877

Figure 4.- Concluded.



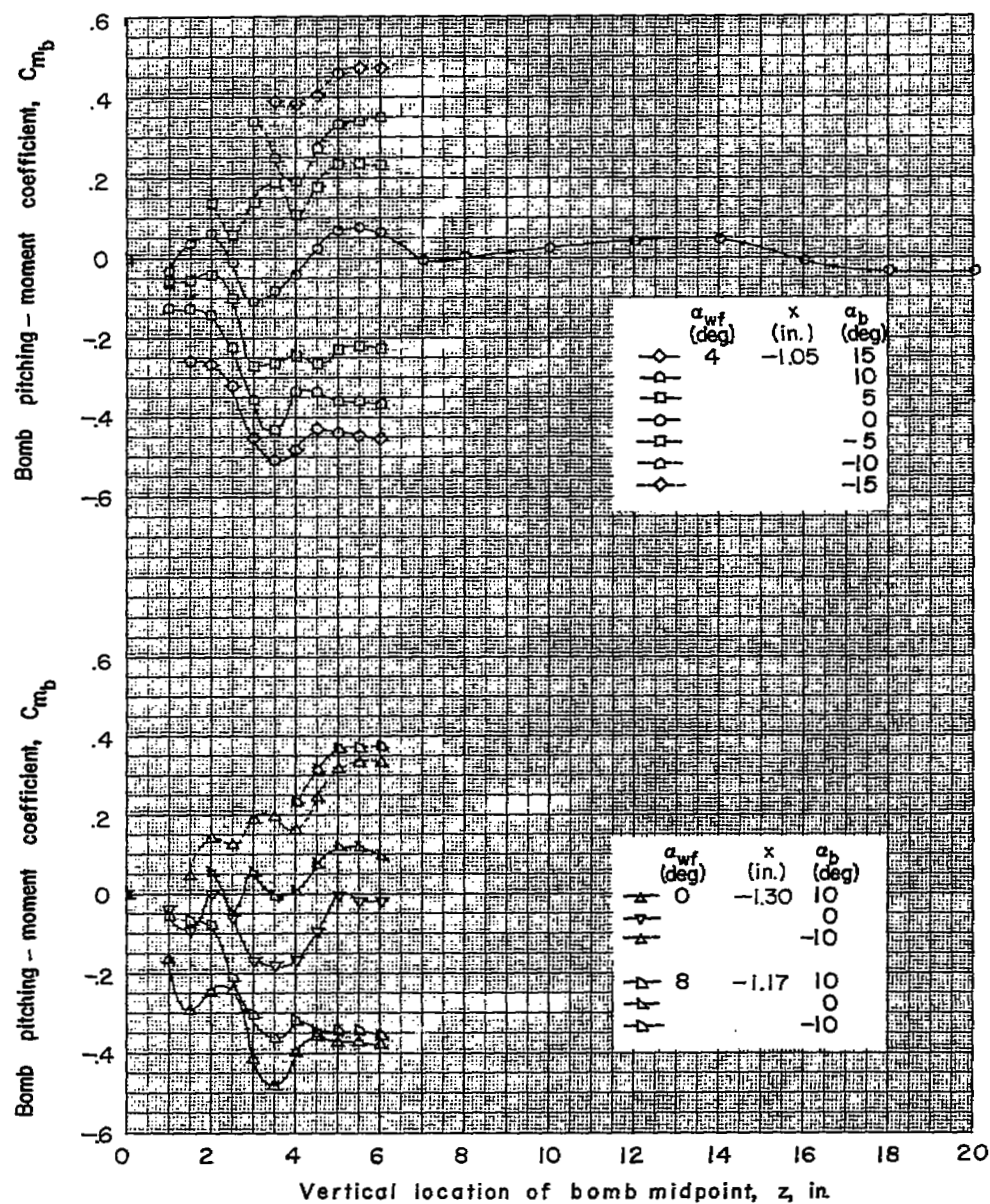
(a) Values of x from -1.05 to -1.30 inches.

Figure 5.- Force data for spool bomb in presence of wing-fuselage combination.



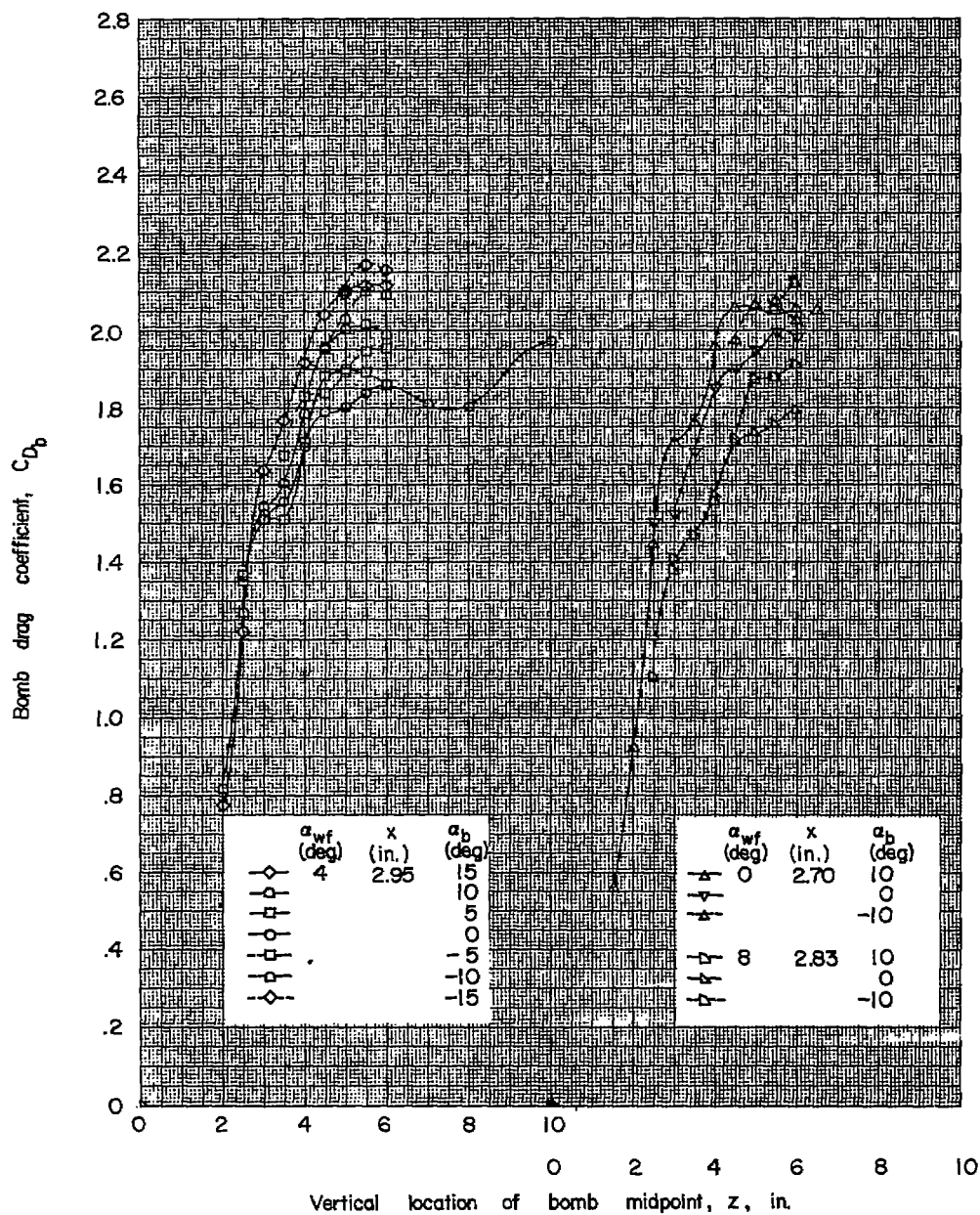
(a) Continued.

Figure 5.- Continued.



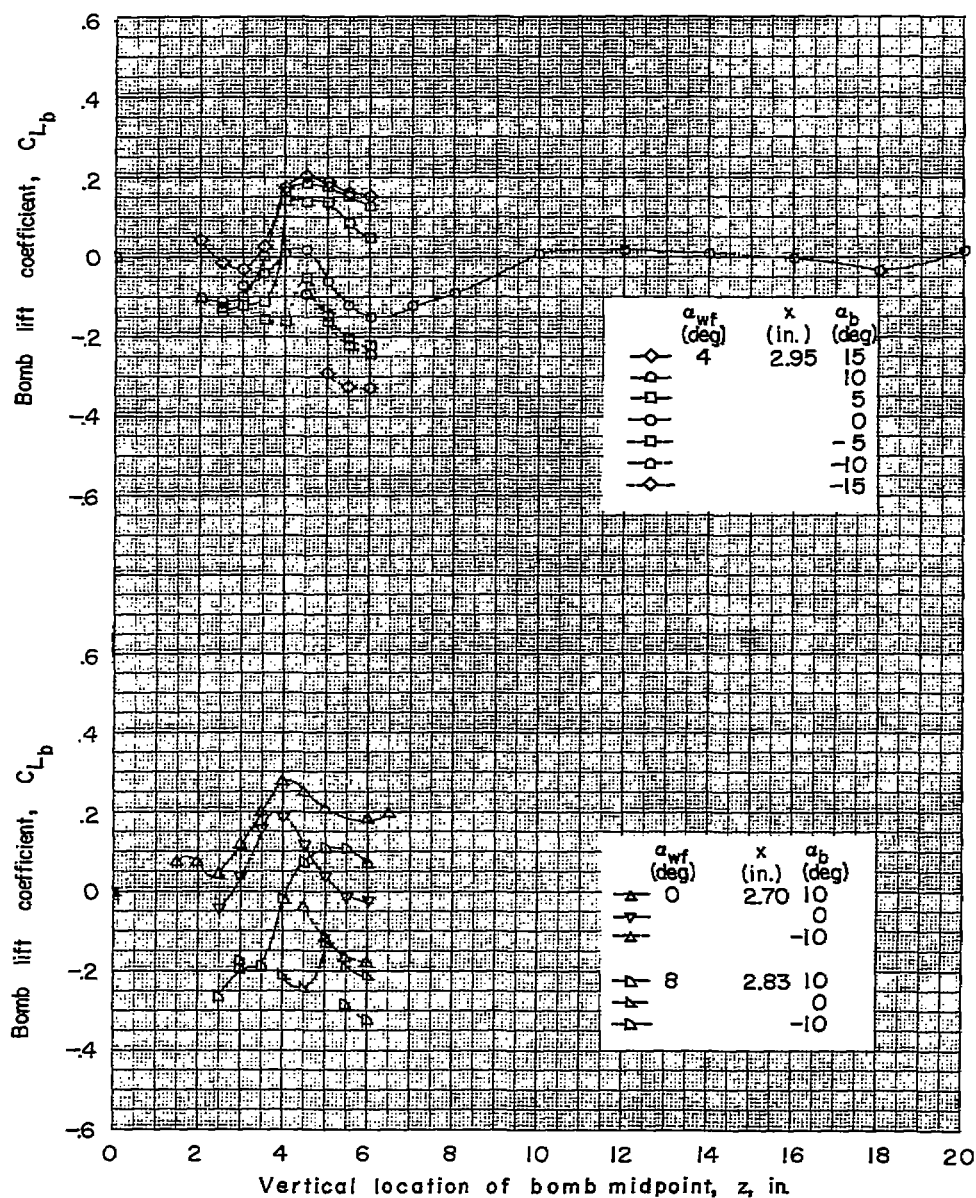
(a) Concluded.

Figure 5.- Continued.



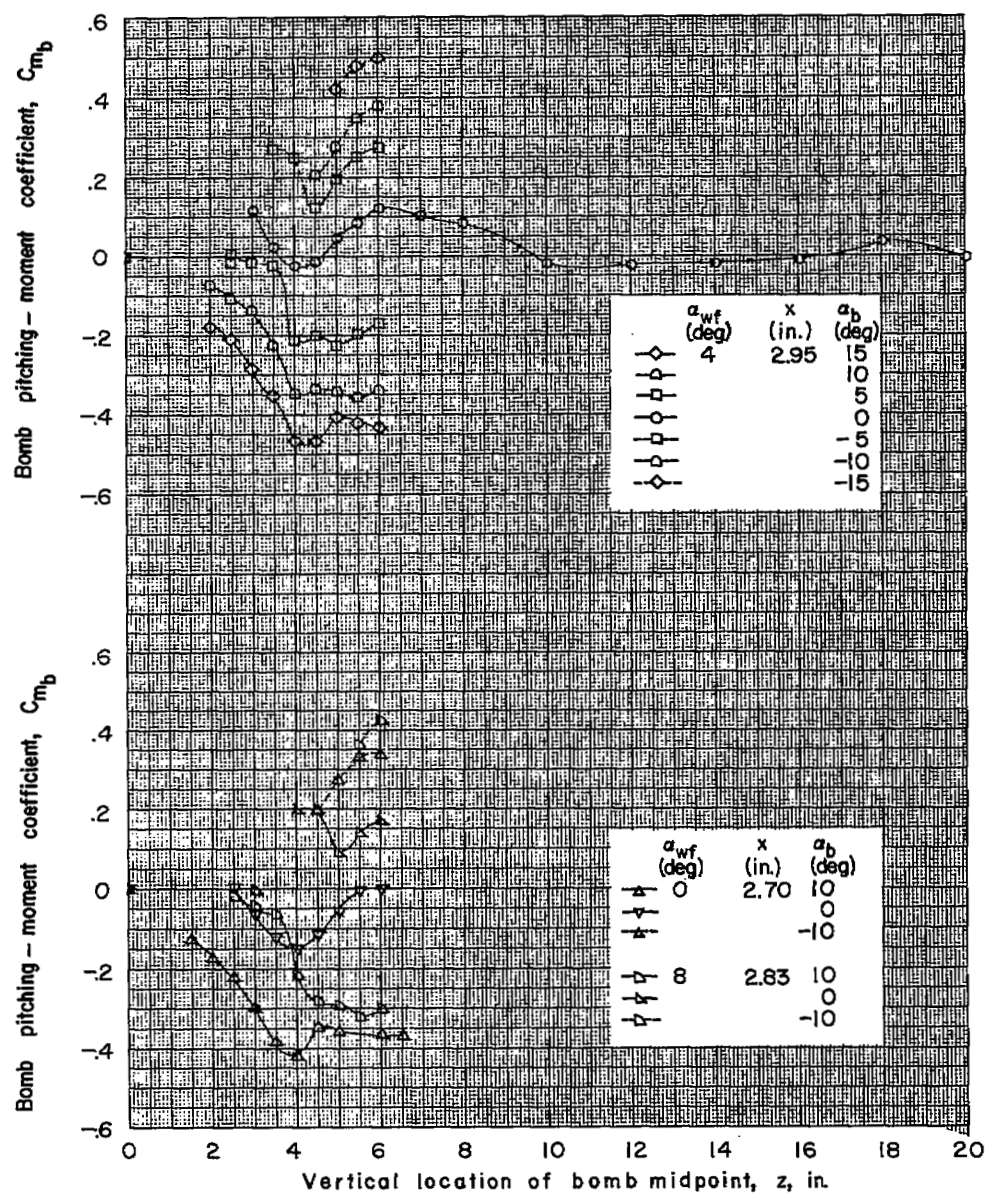
(b) Values of x from 2.70 to 2.95 inches.

Figure 5.- Continued.



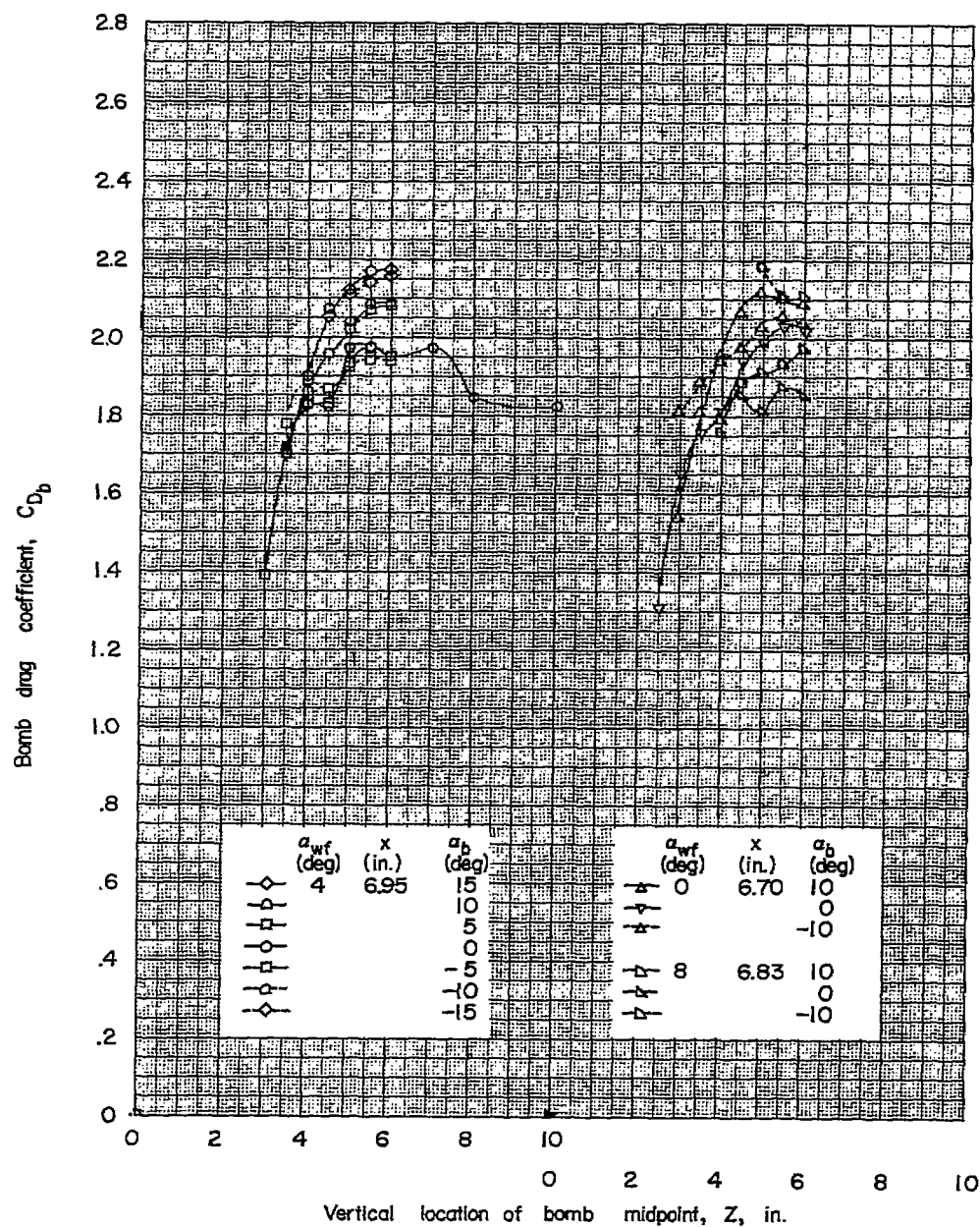
(b) Continued.

Figure 5.- Continued.



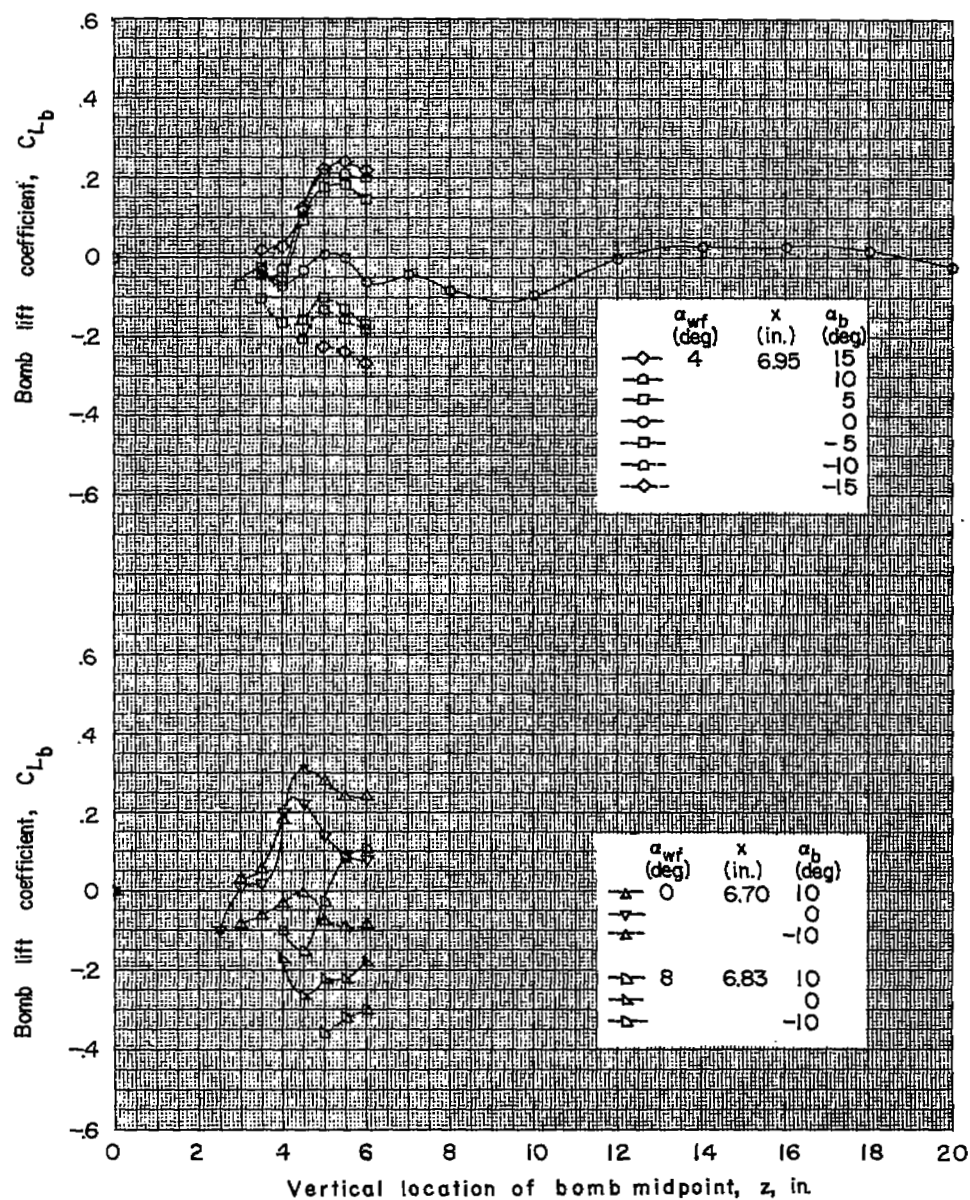
(b) Concluded.

Figure 5.- Continued.



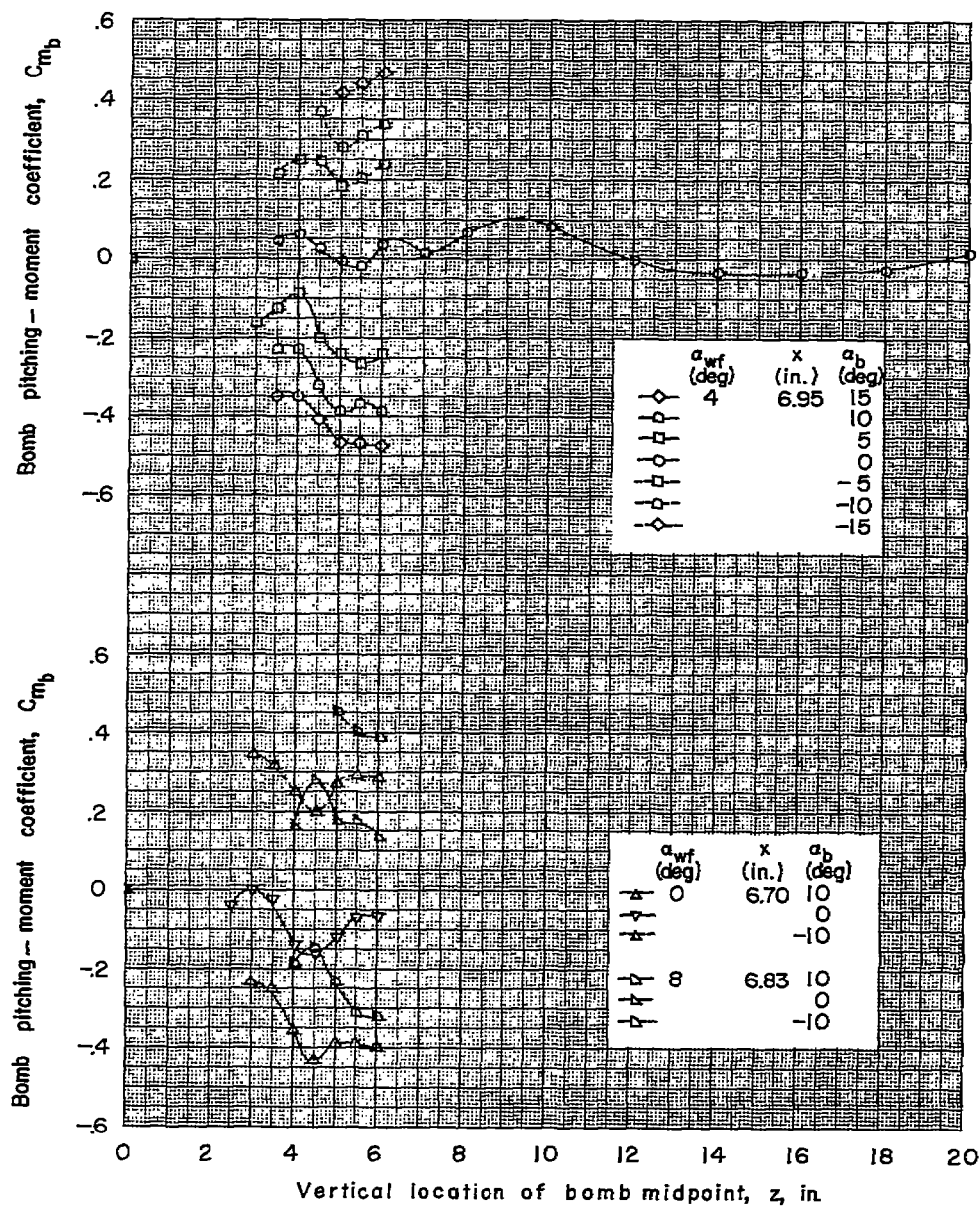
(c) Values of x from 6.70 to 6.95 inches.

Figure 5.- Continued.



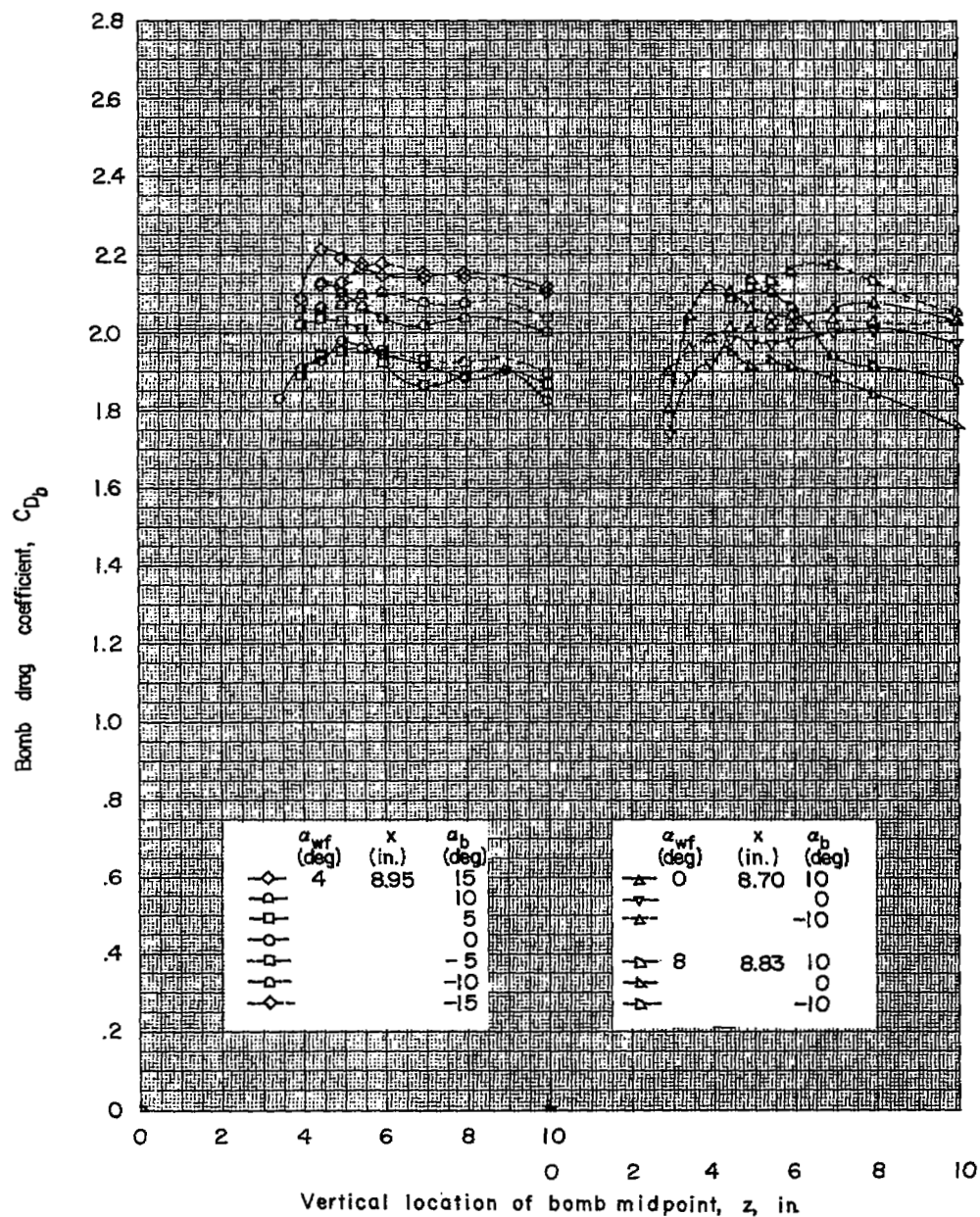
(c) Continued.

Figure 5.- Continued.



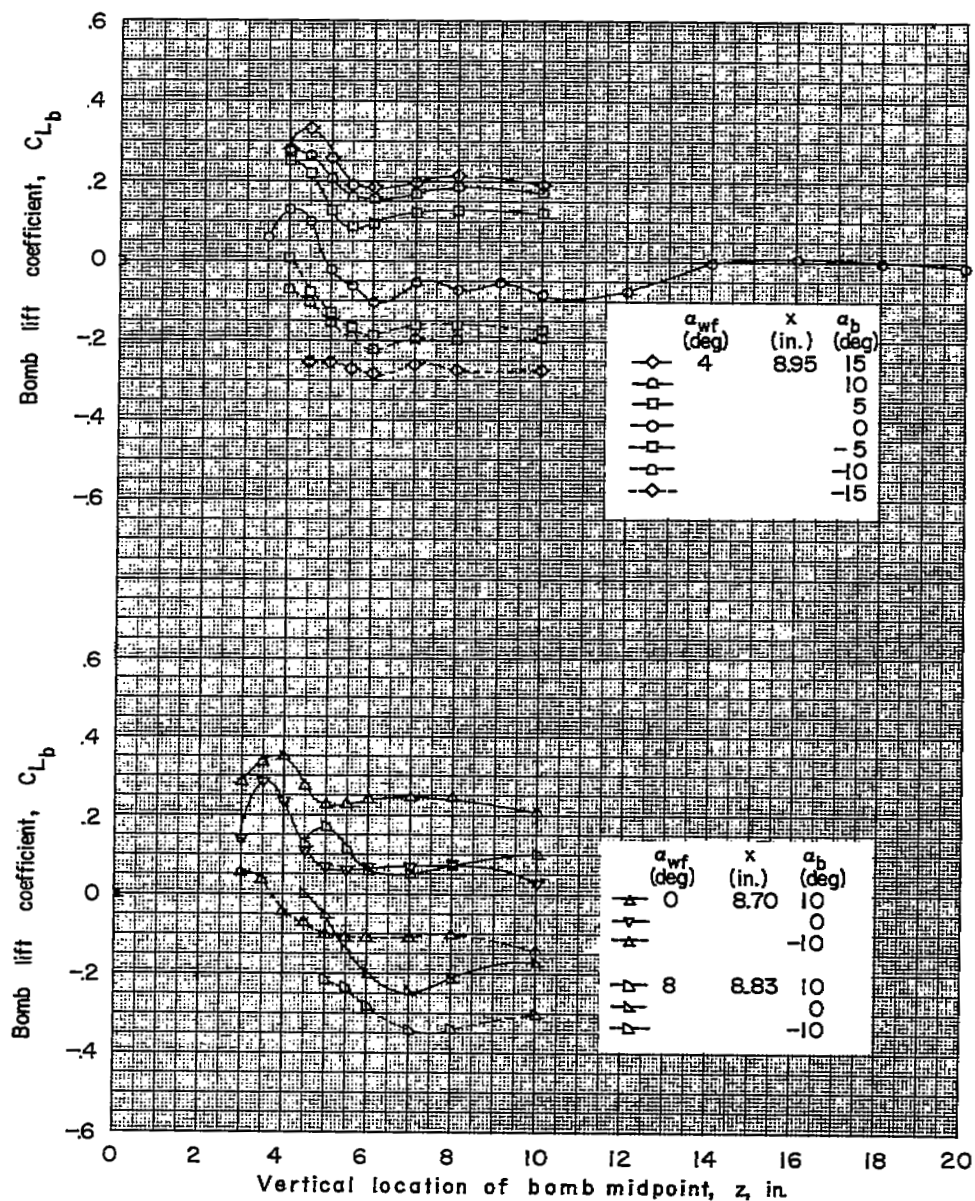
(c) Concluded.

Figure 5.- Continued.



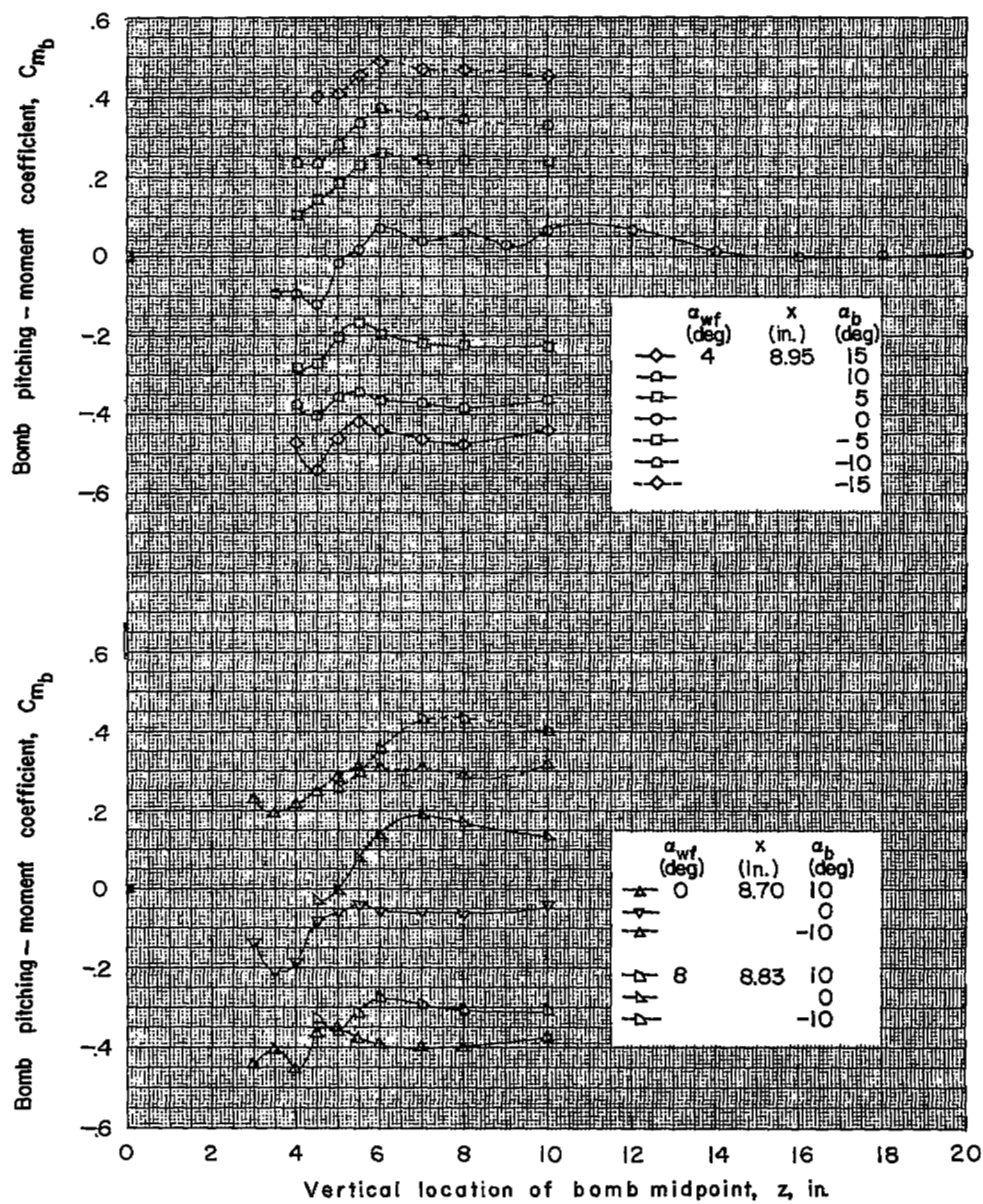
(d) Values of x from 8.70 to 8.95 inches.

Figure 5.- Continued.



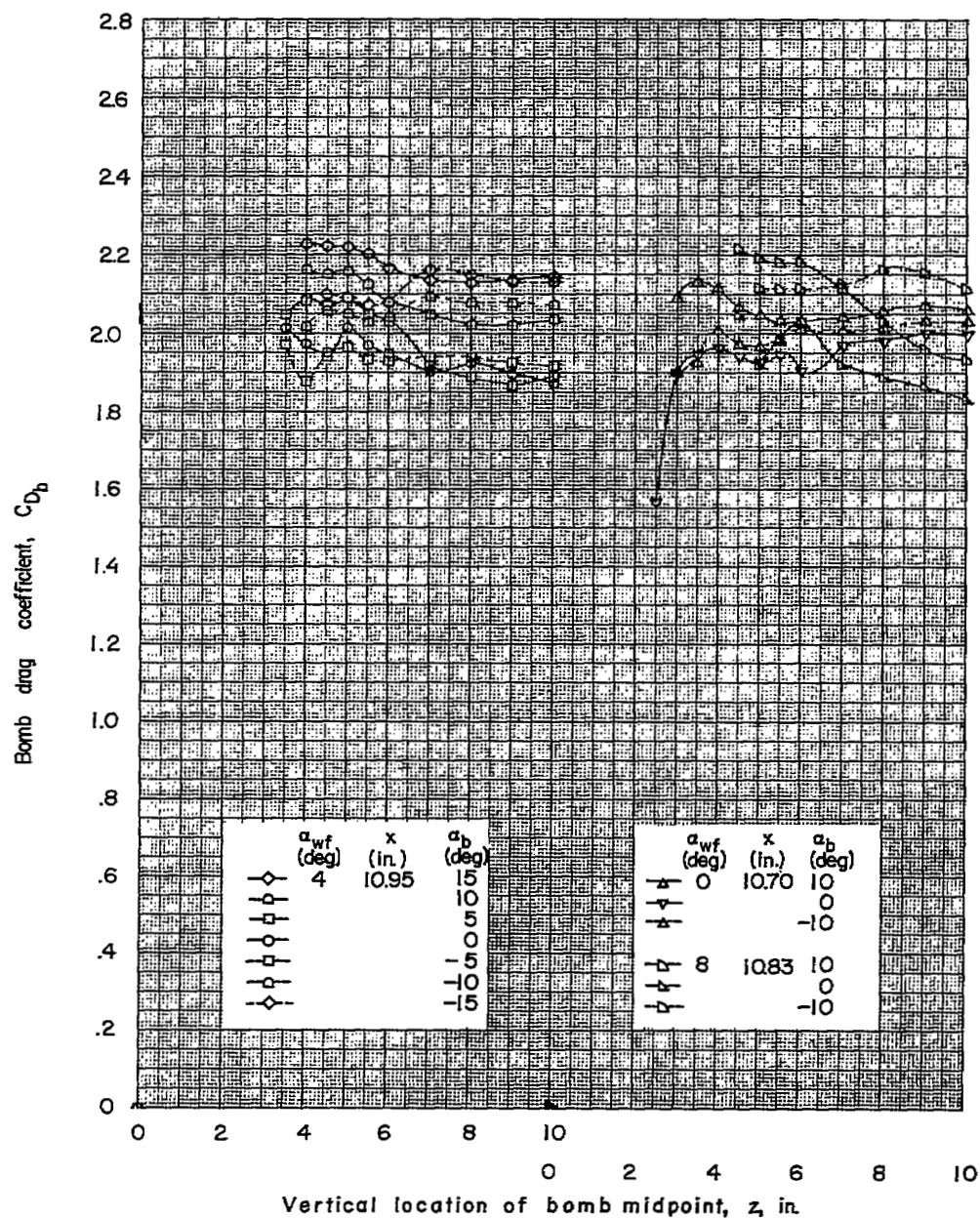
(d) Continued.

Figure 5.- Continued.



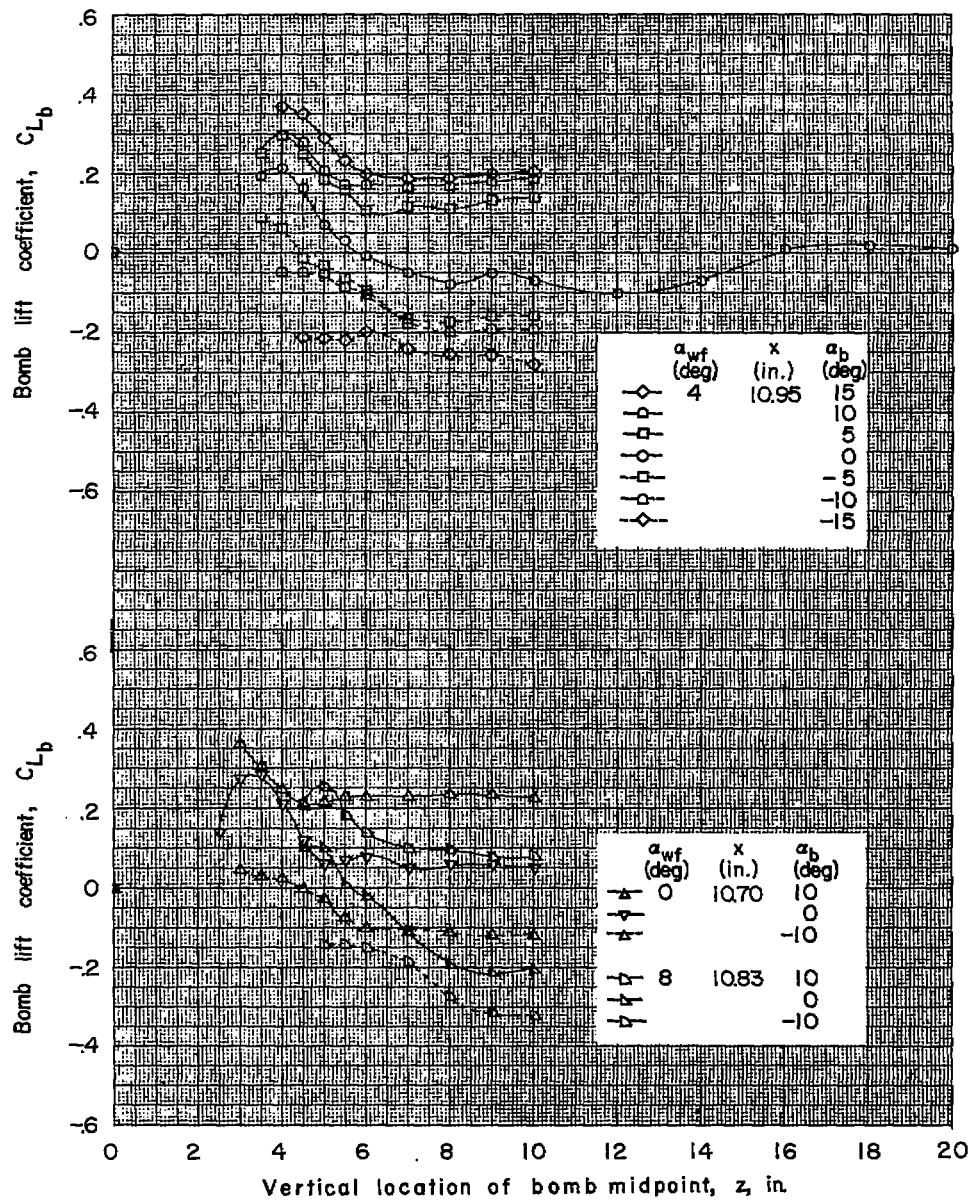
(d) Concluded.

Figure 5.- Continued.



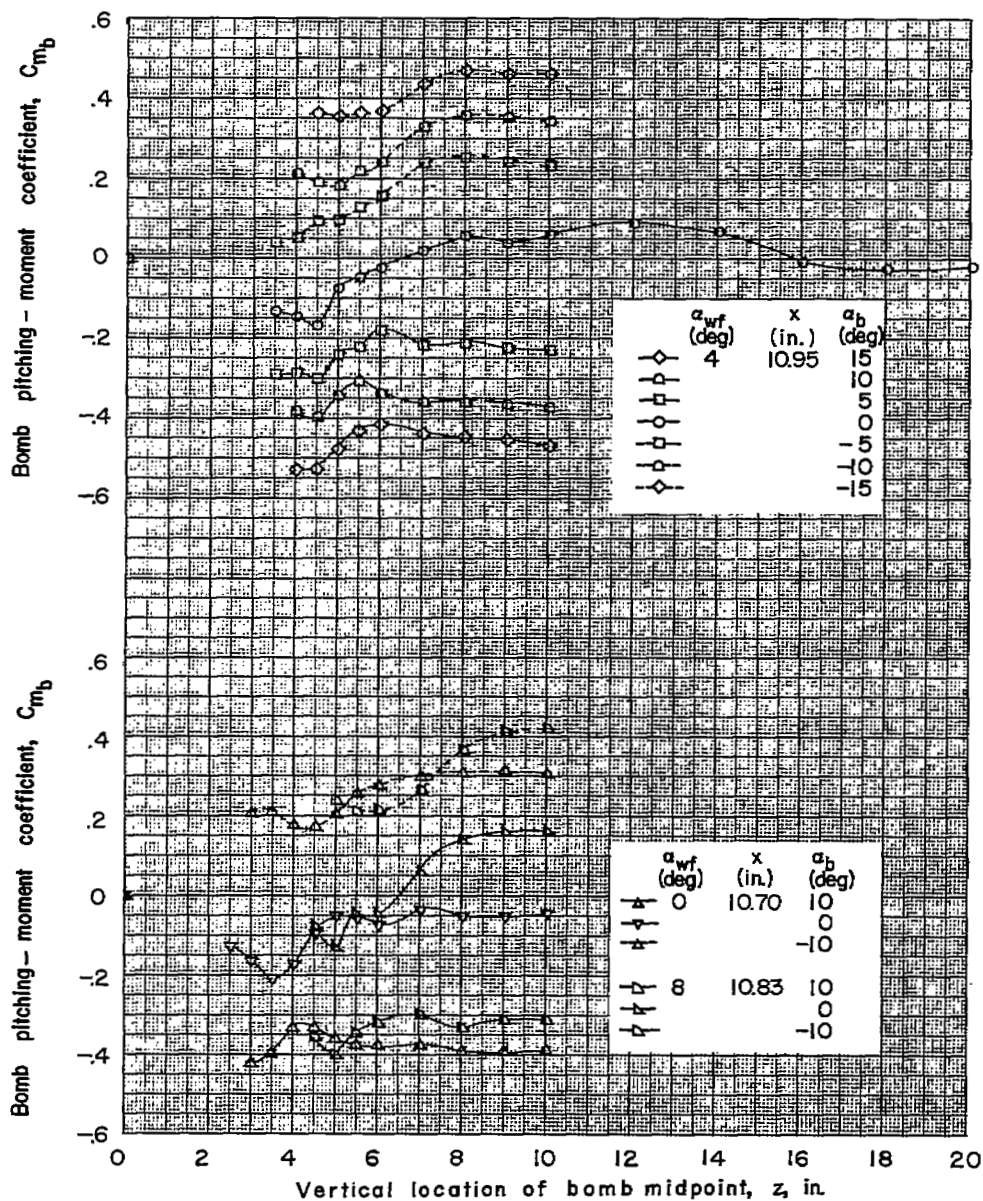
(e) Values of x from 10.70 to 10.95 inches.

Figure 5.- Continued.



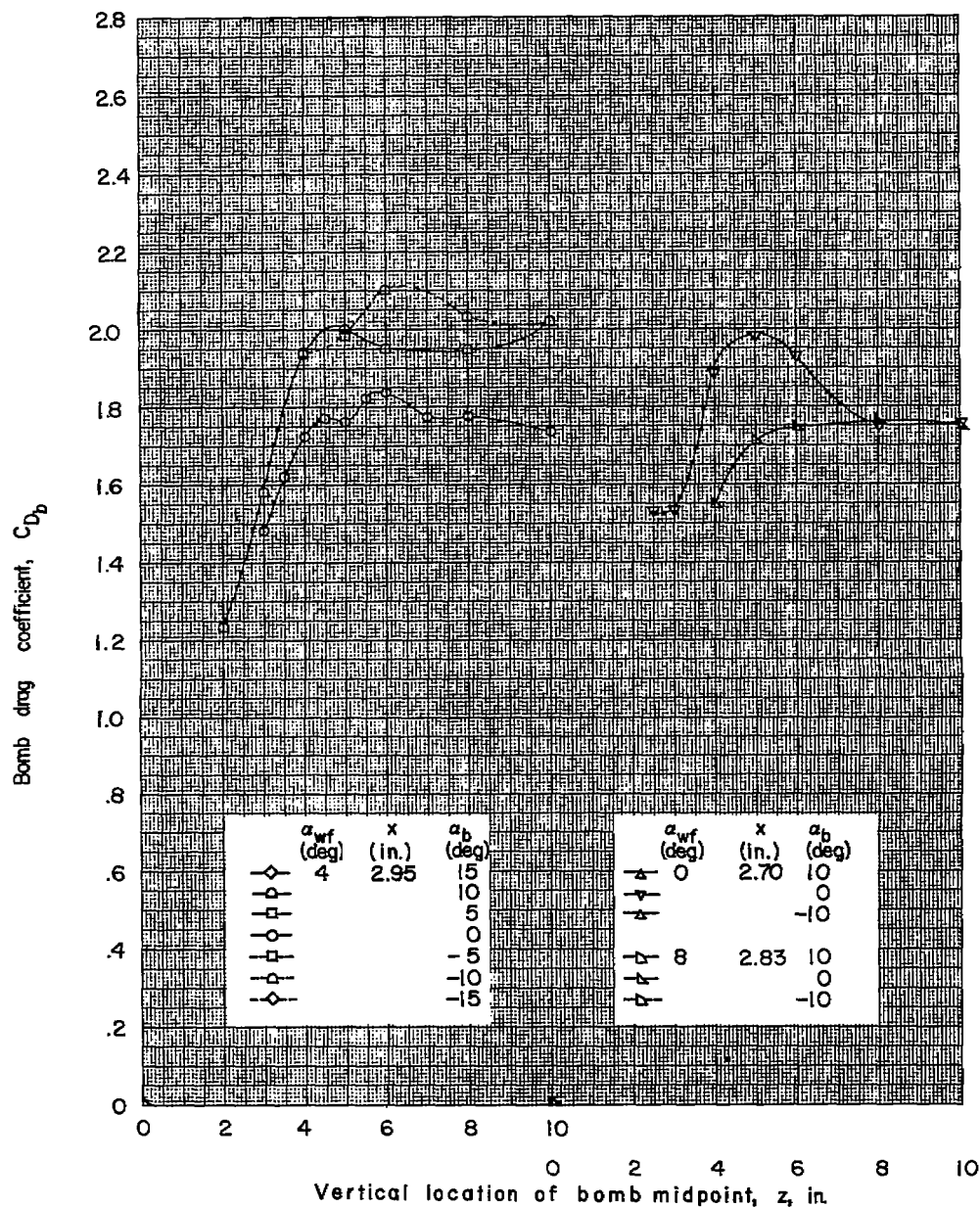
(e) Continued.

Figure 5.- Continued.



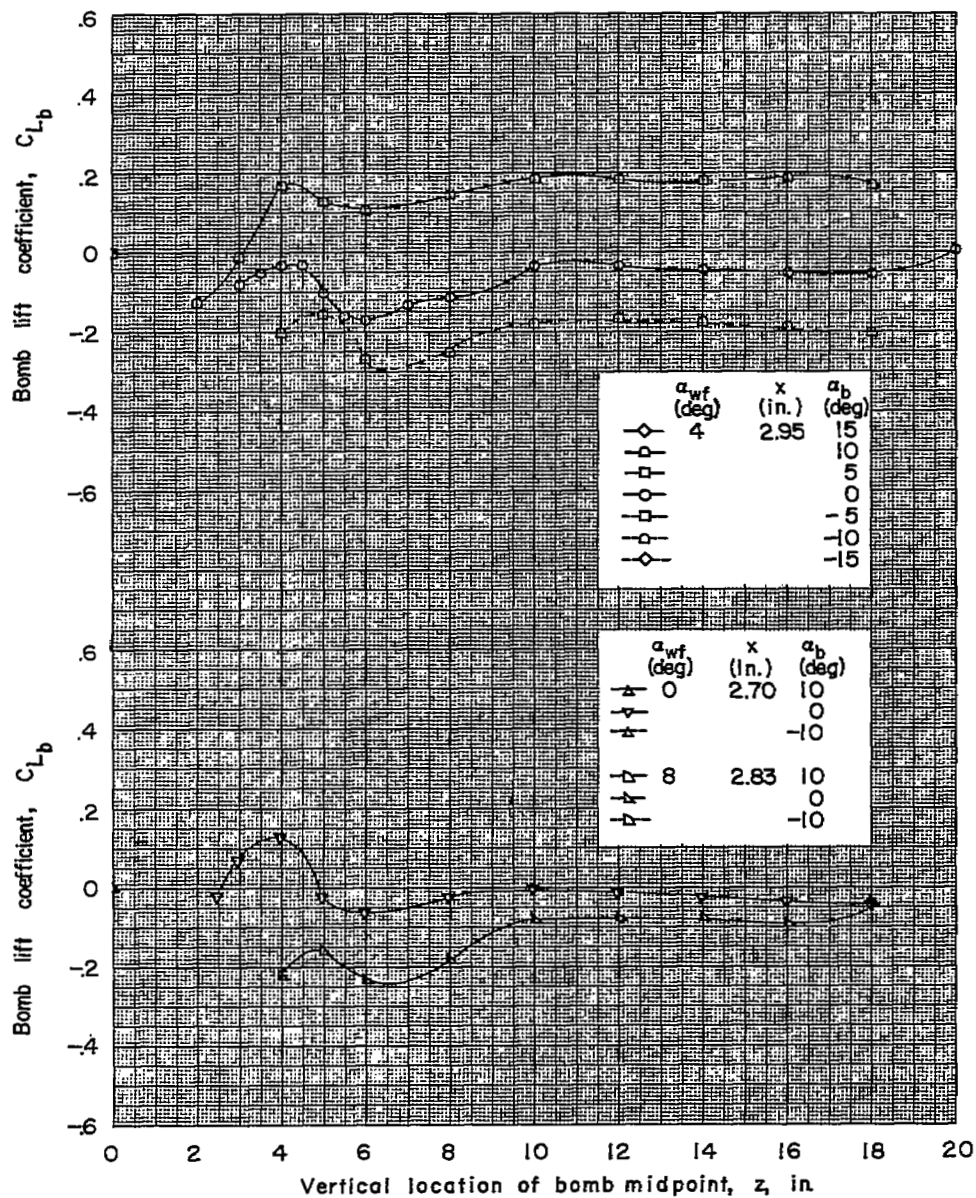
(e) Concluded.

Figure 5.- Concluded.



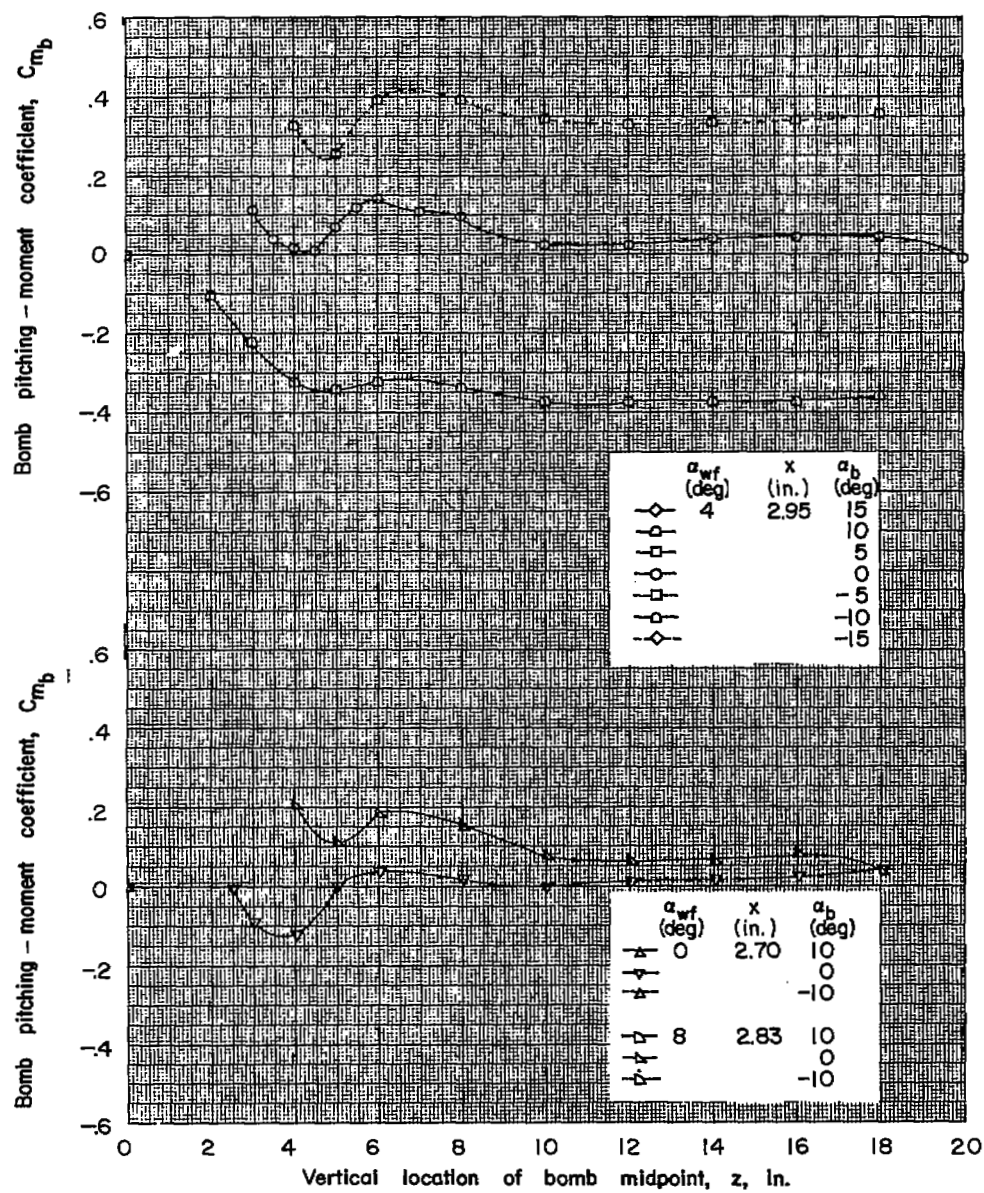
(a) Values of x from 2.70 to 2.95 inches.

Figure 6.- Force data for spool bomb in presence of wing-fuselage-tail combination.



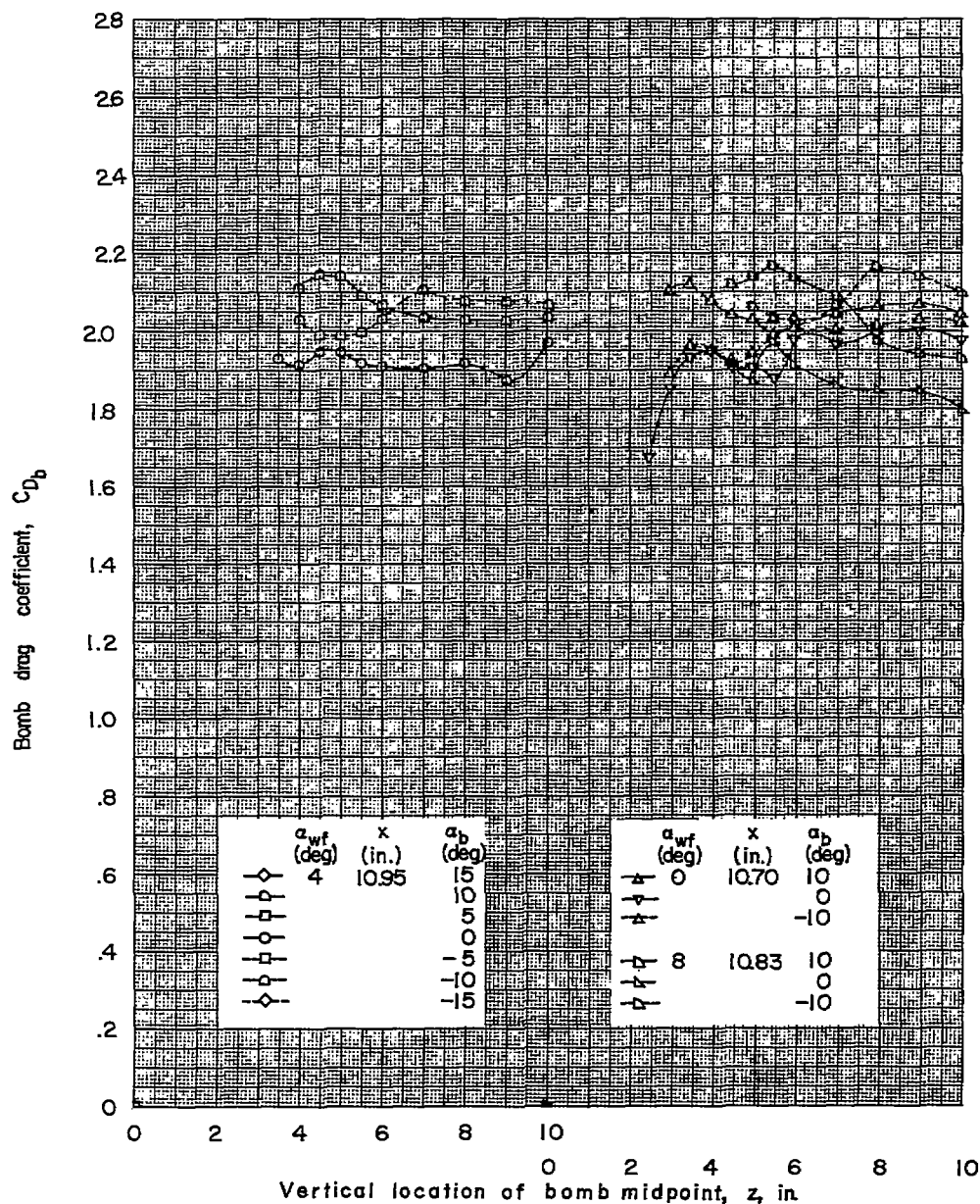
(a) Continued.

Figure 6.- Continued.



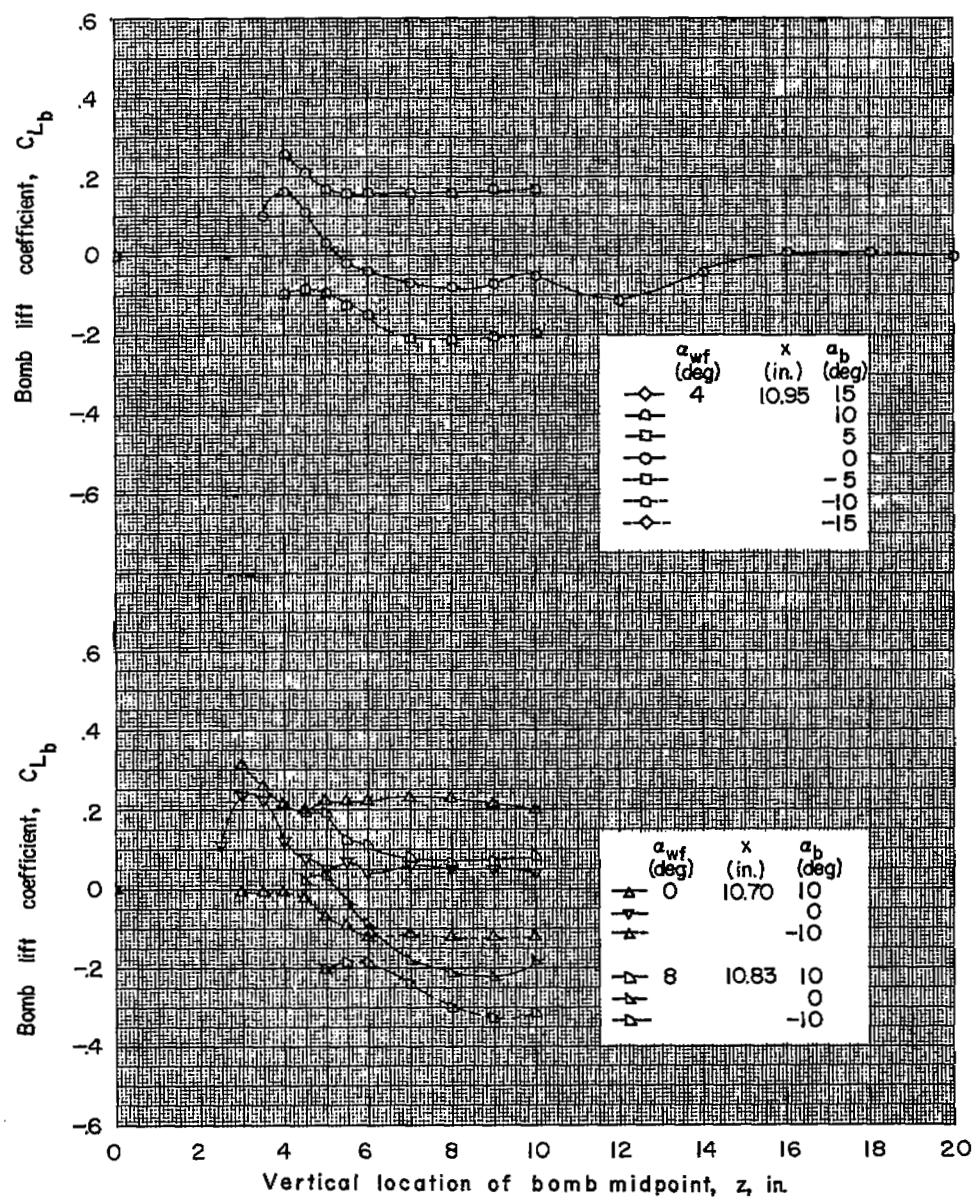
(a) Concluded.

Figure 6.- Continued.



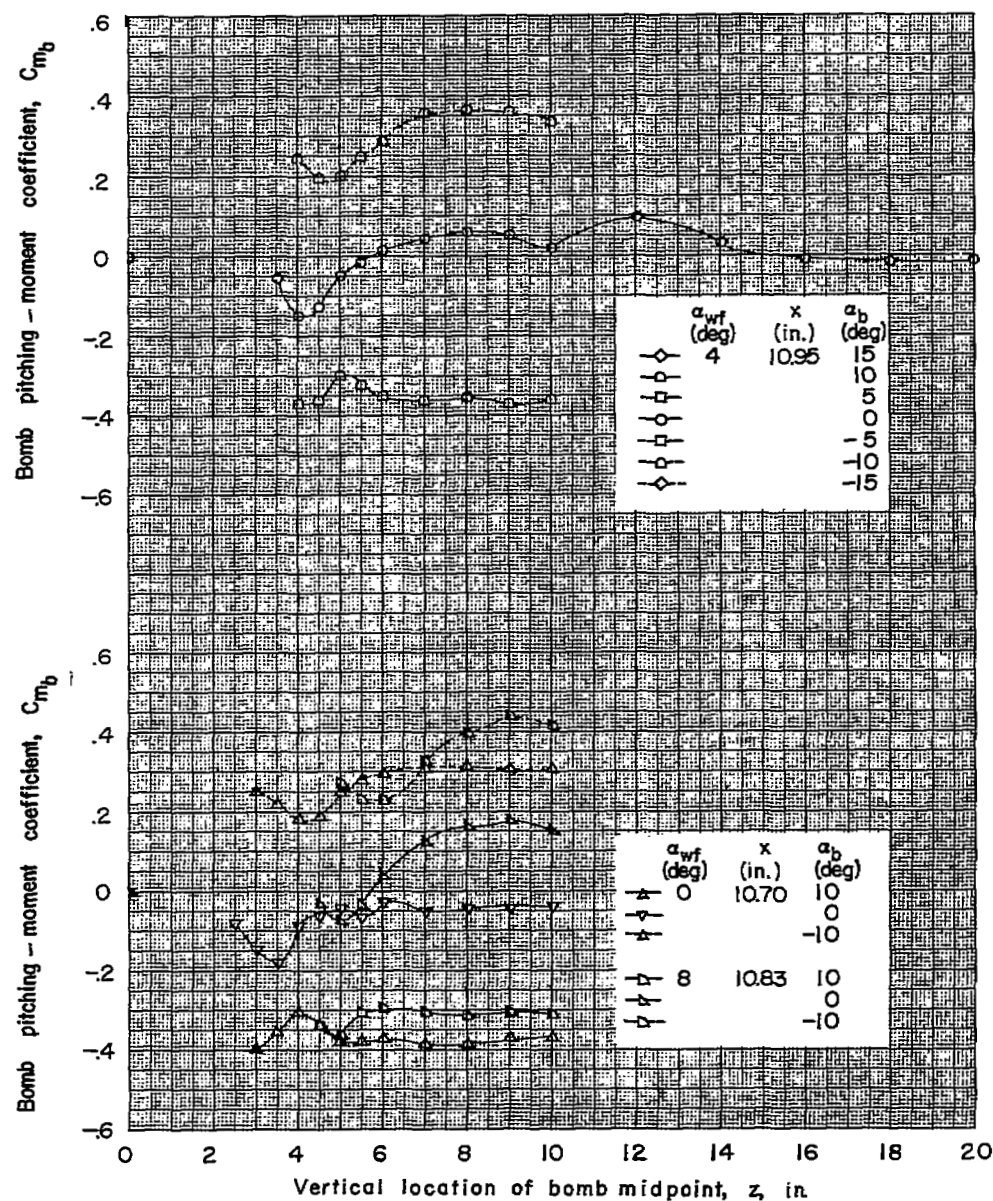
(b) Values of x from 10.70 to 10.95 inches.

Figure 6.- Continued.



(b) Continued.

Figure 6.- Continued.



(b) Concluded.

Figure 6.- Concluded.

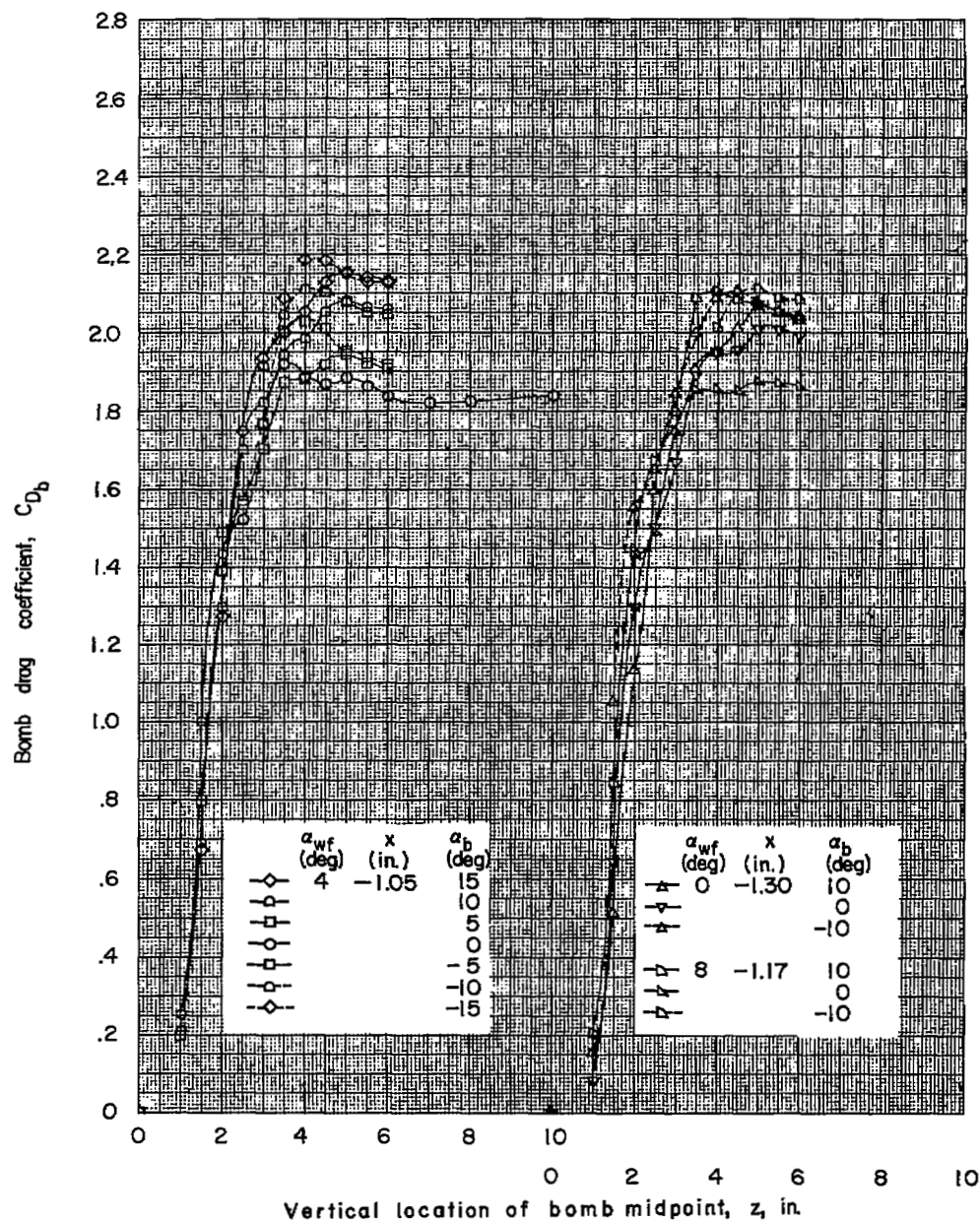


Figure 7.- Force data for spool bomb in presence of fuselage. Values of x from -1.05 to -1.30 inches.

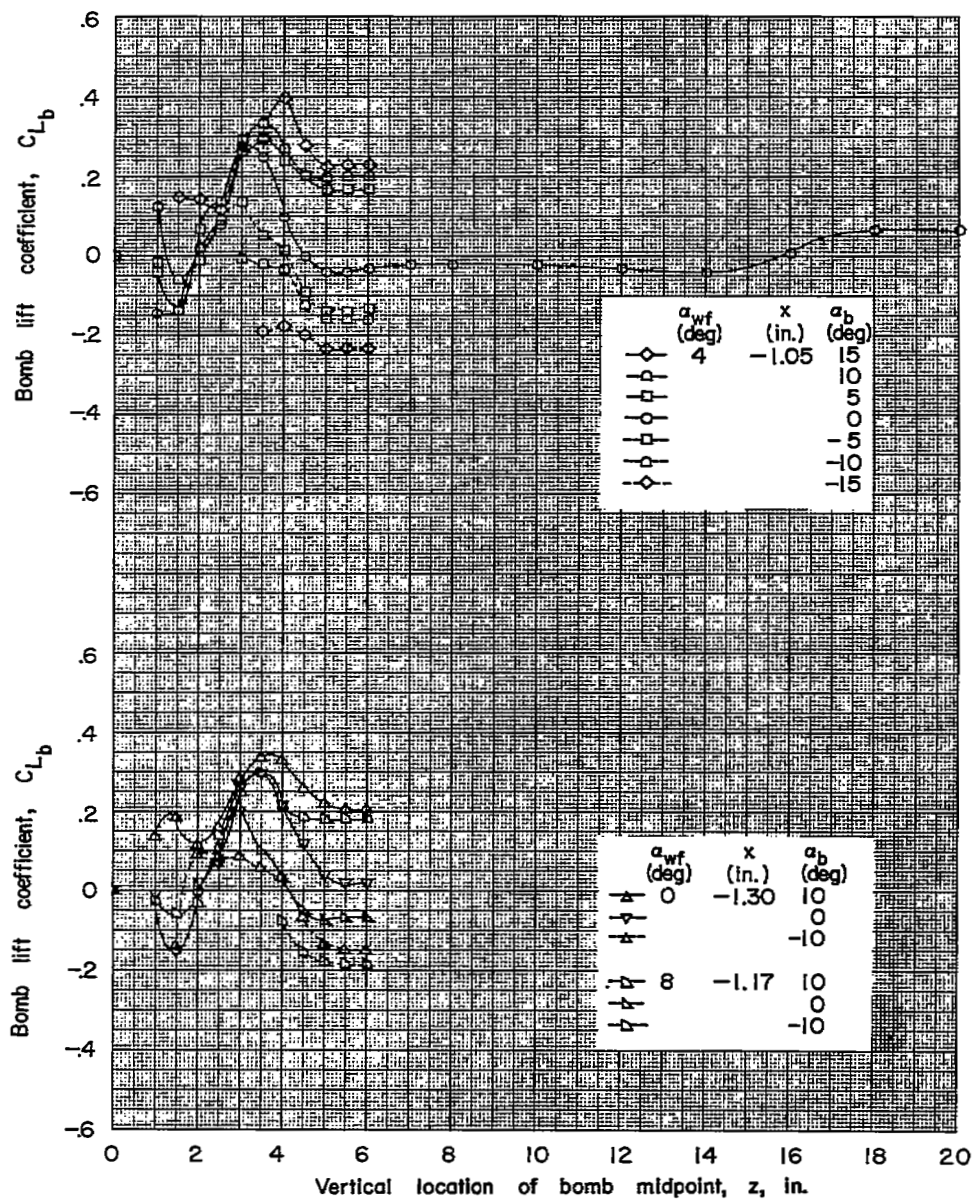


Figure 7.- Continued.

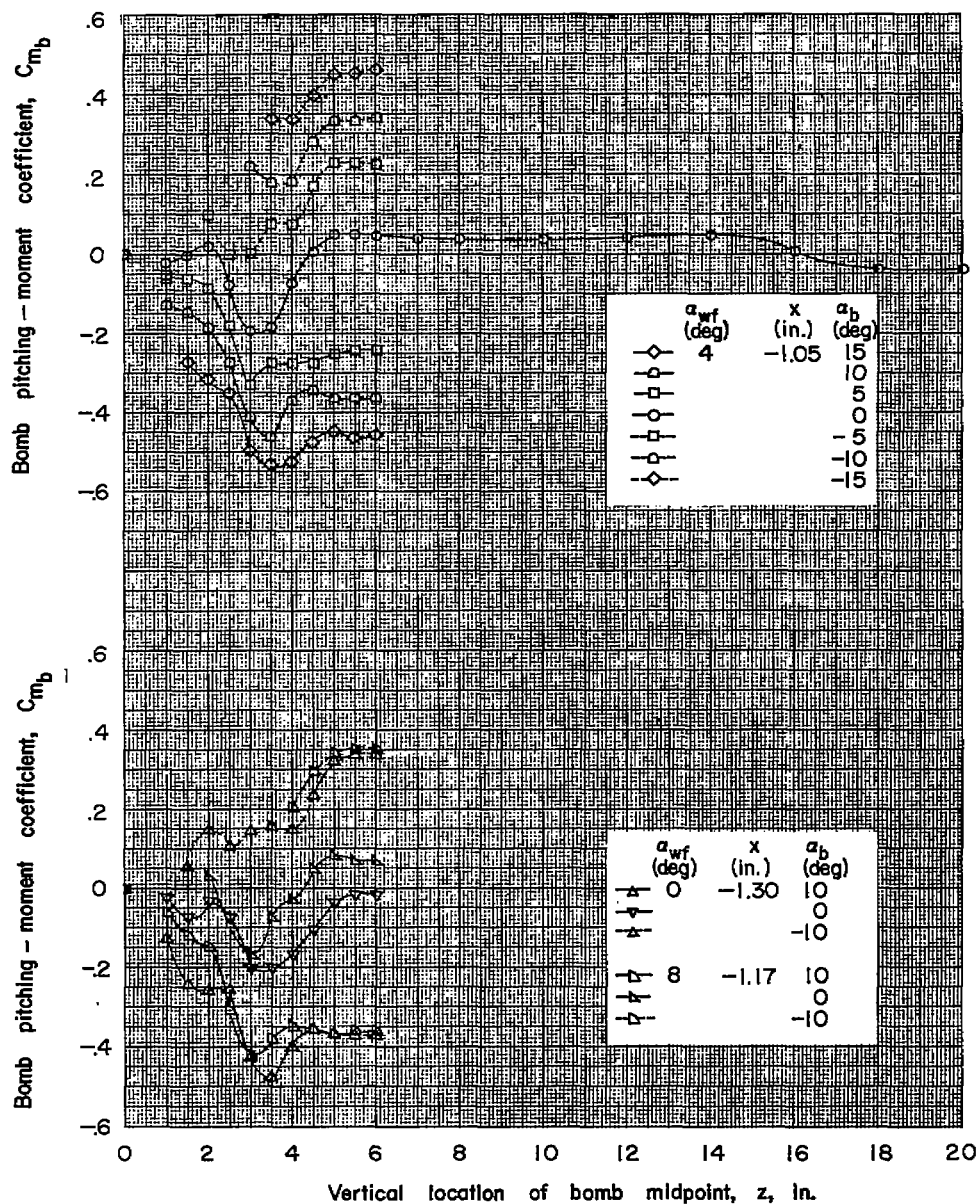
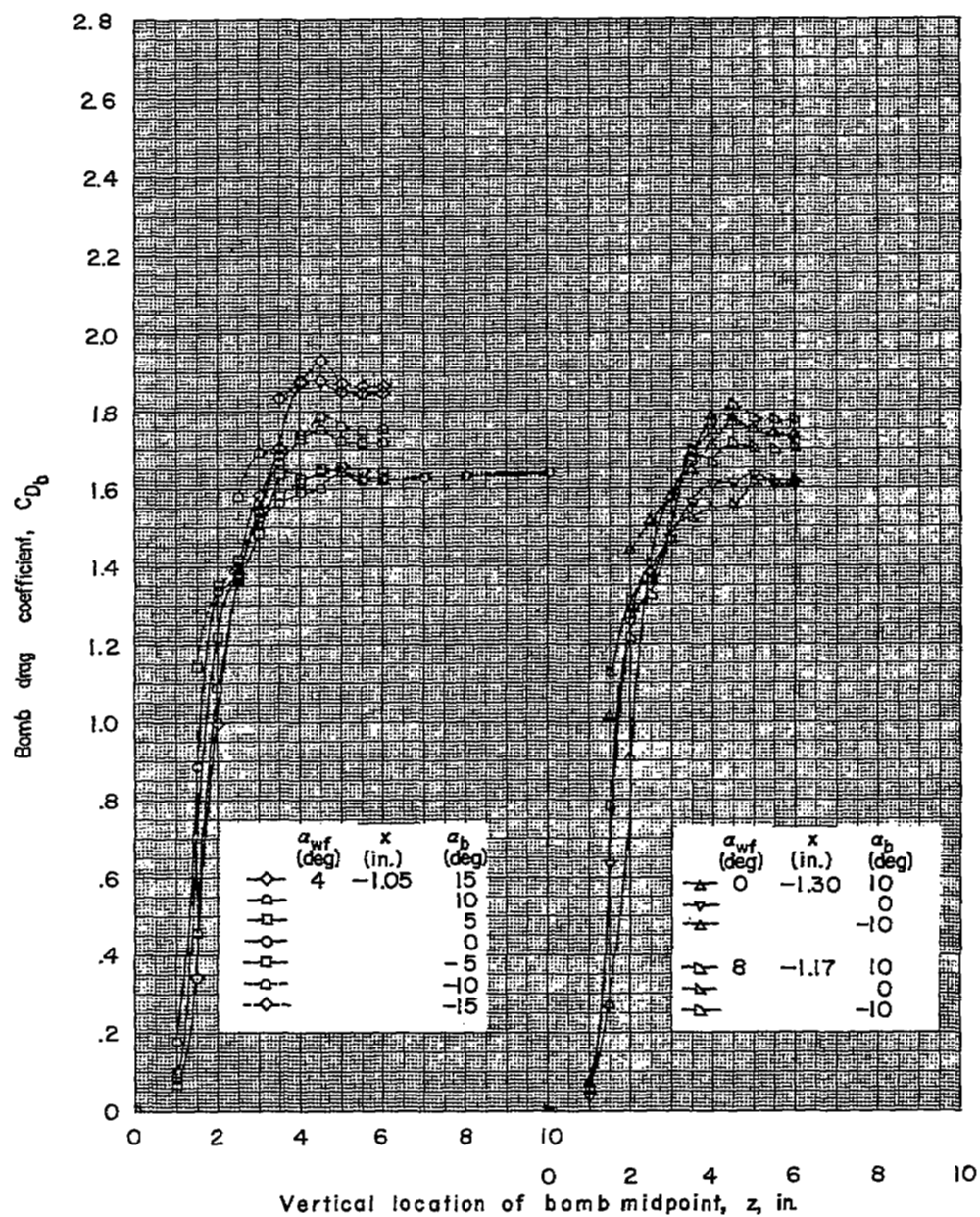
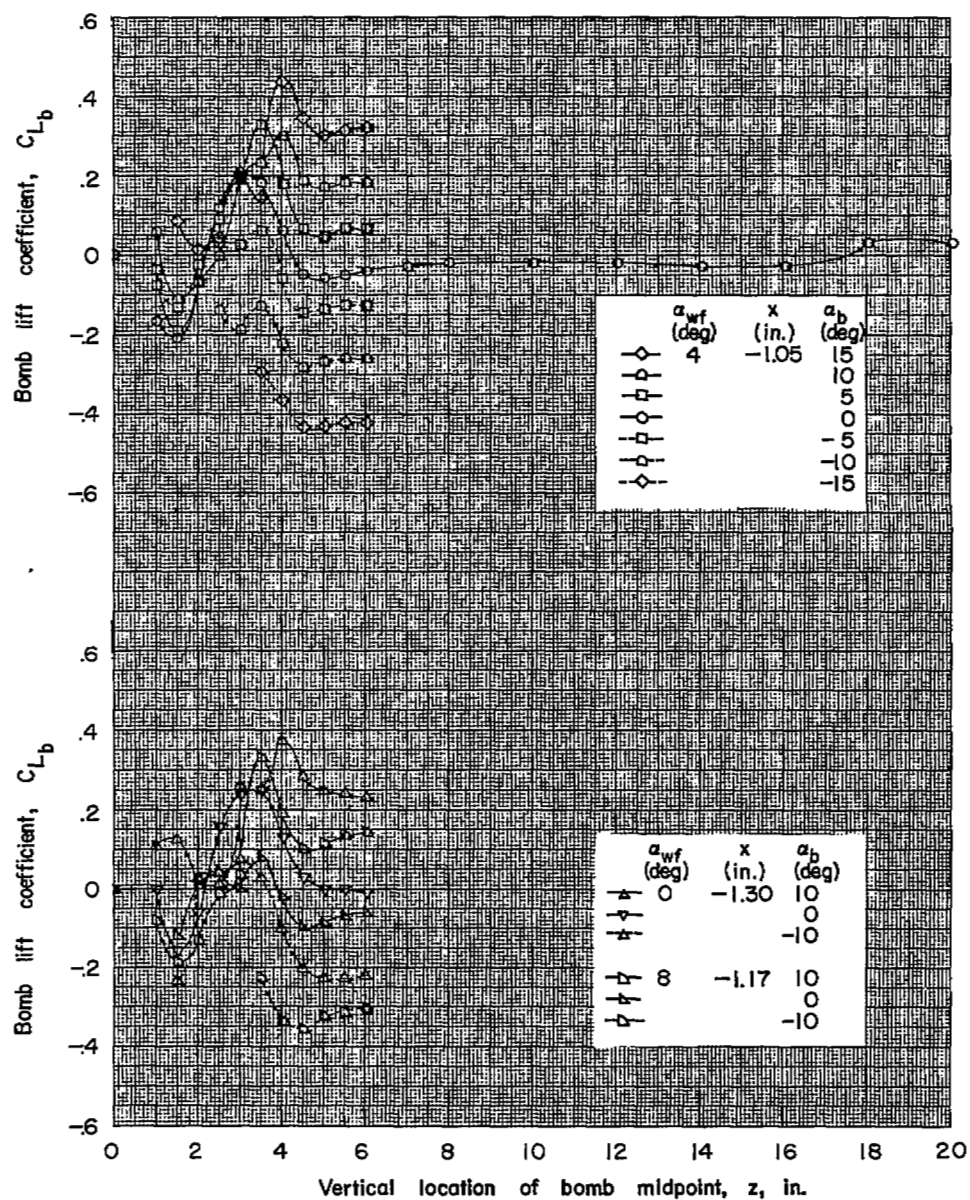


Figure 7.- Concluded.



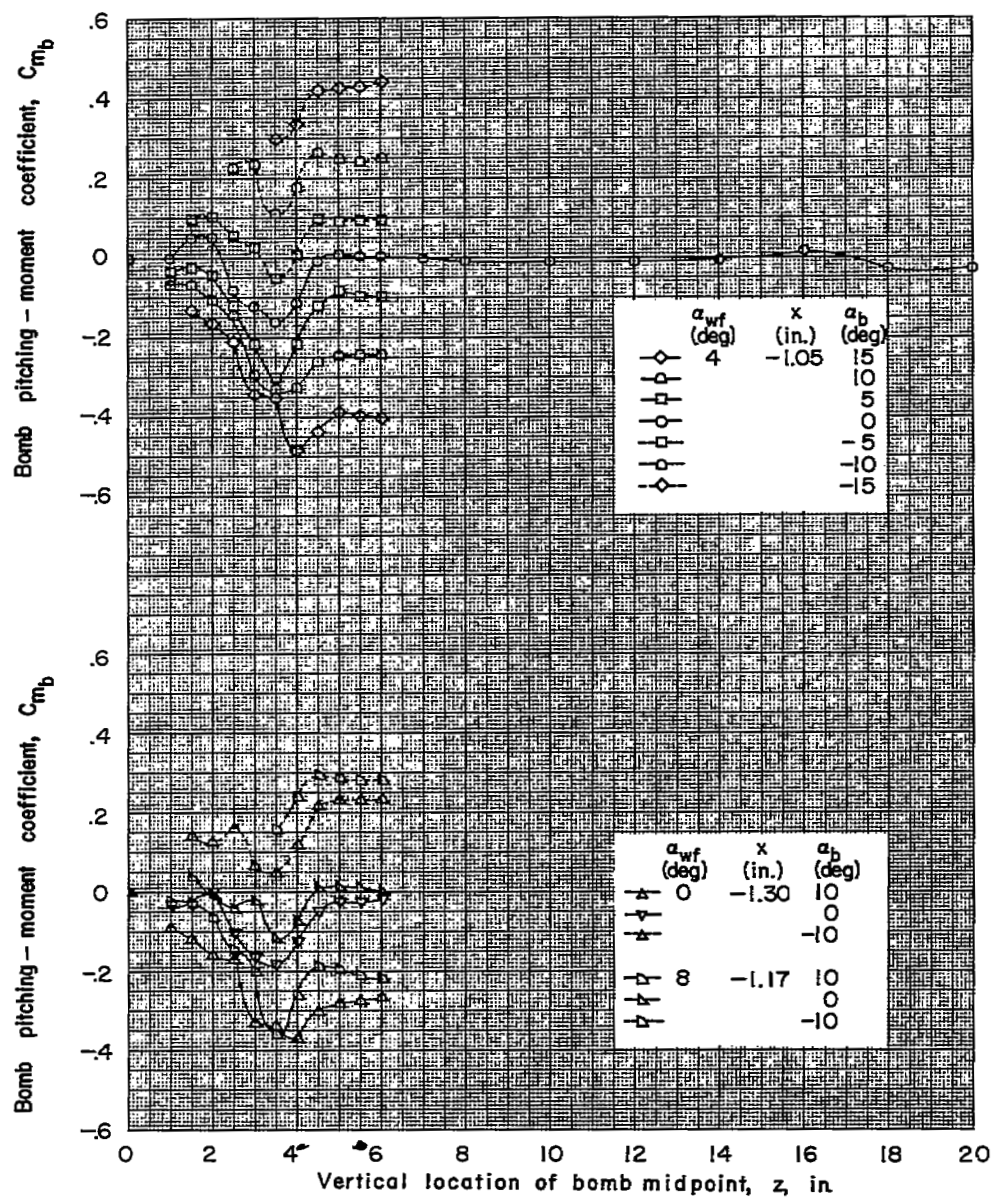
(a) Values of x from -1.05 to -1.30 inches.

Figure 8.- Force data for cylindrical bomb in presence of wing-fuselage combination.



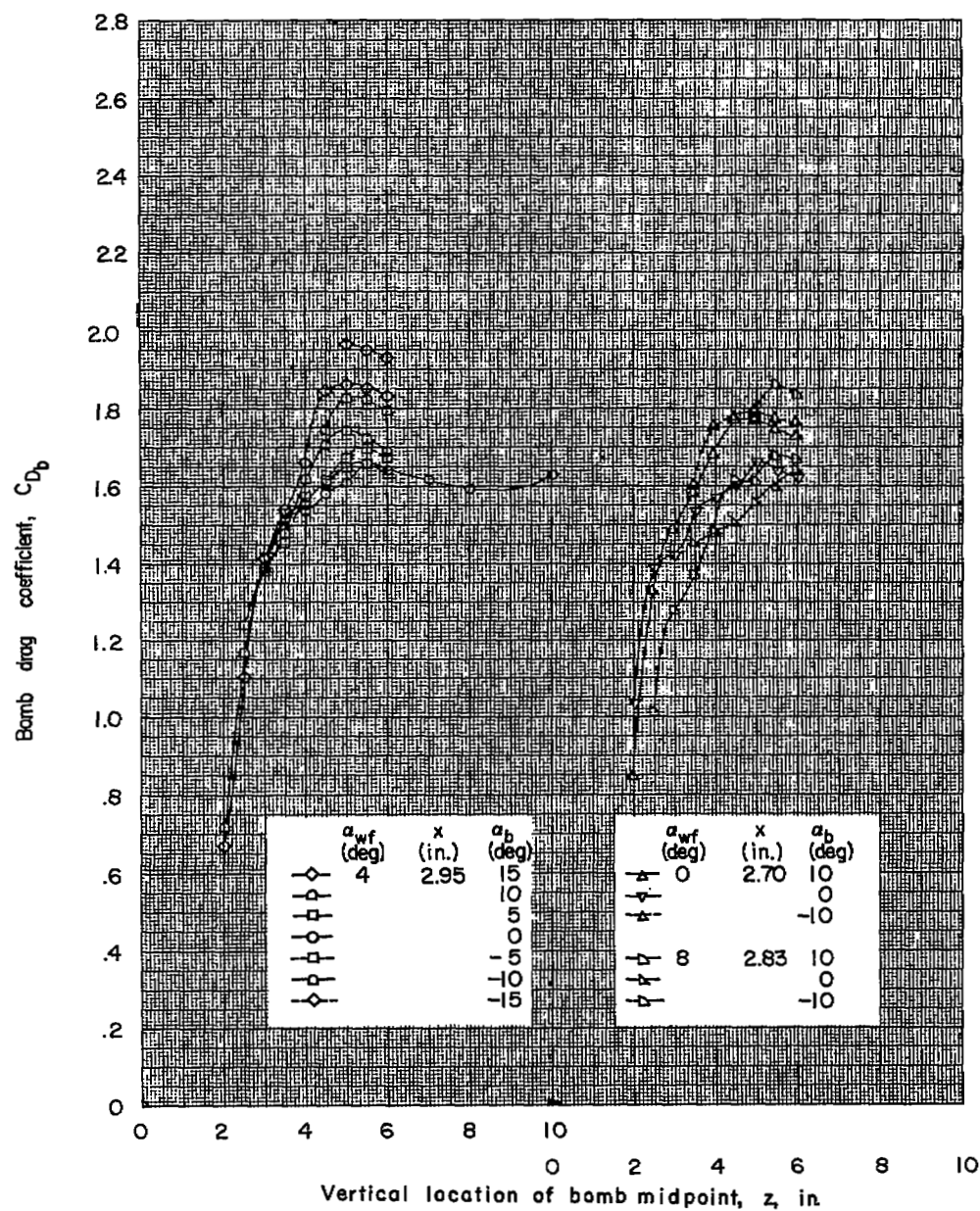
(a) Continued.

Figure 8.- Continued.



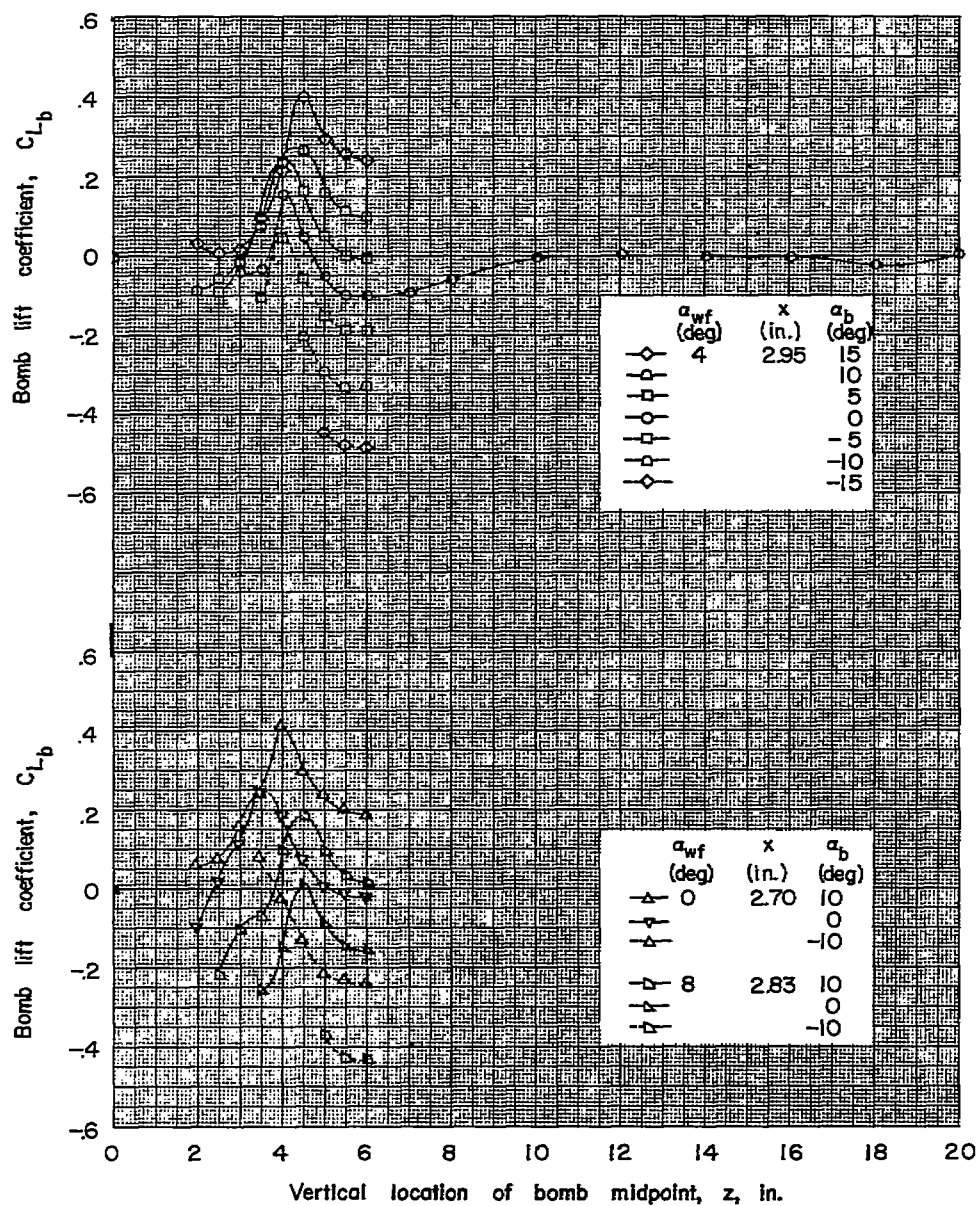
(a) Concluded.

Figure 8.- Continued.



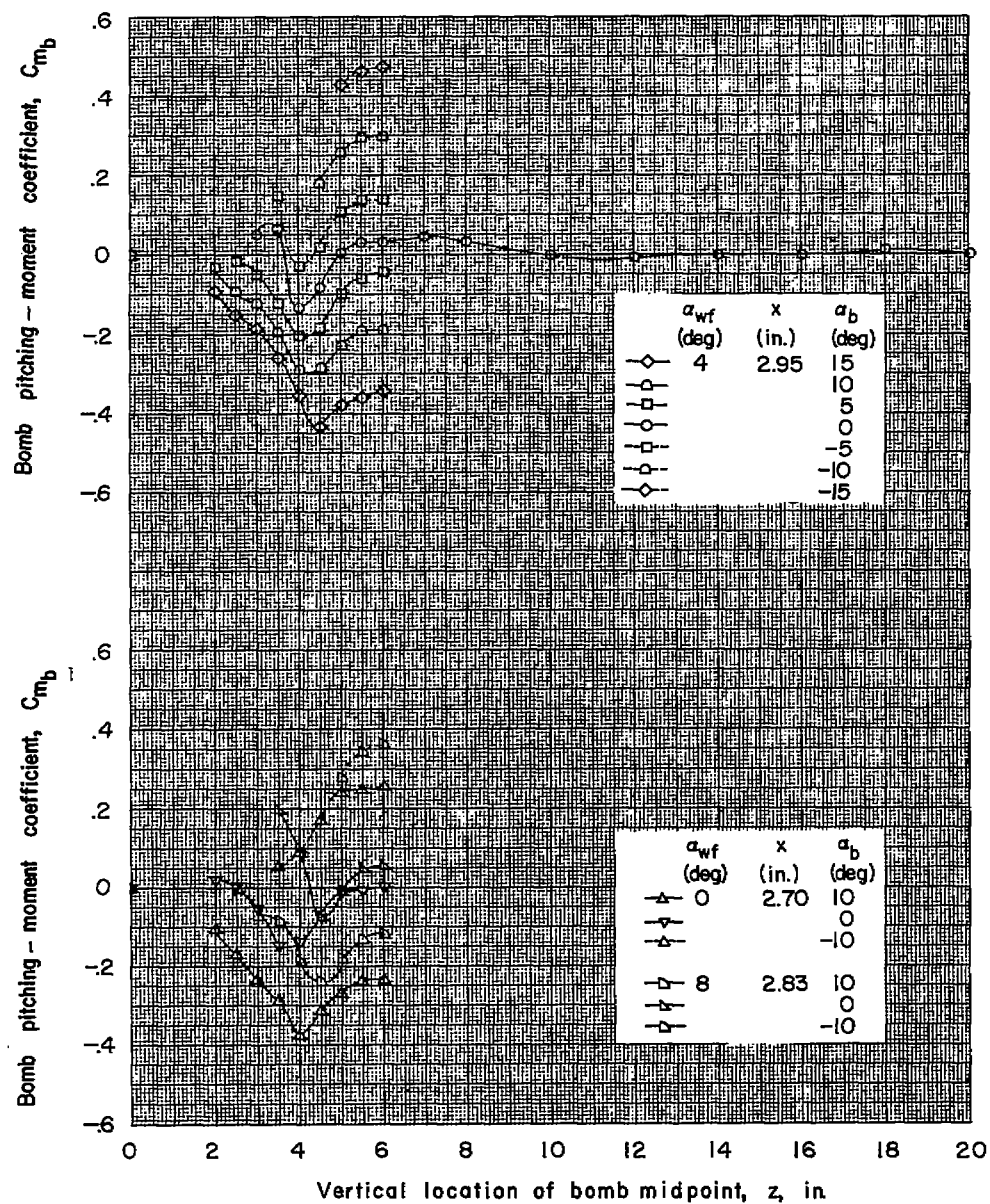
(b) Values of x from 2.70 to 2.95 inches.

Figure 8.- Continued.



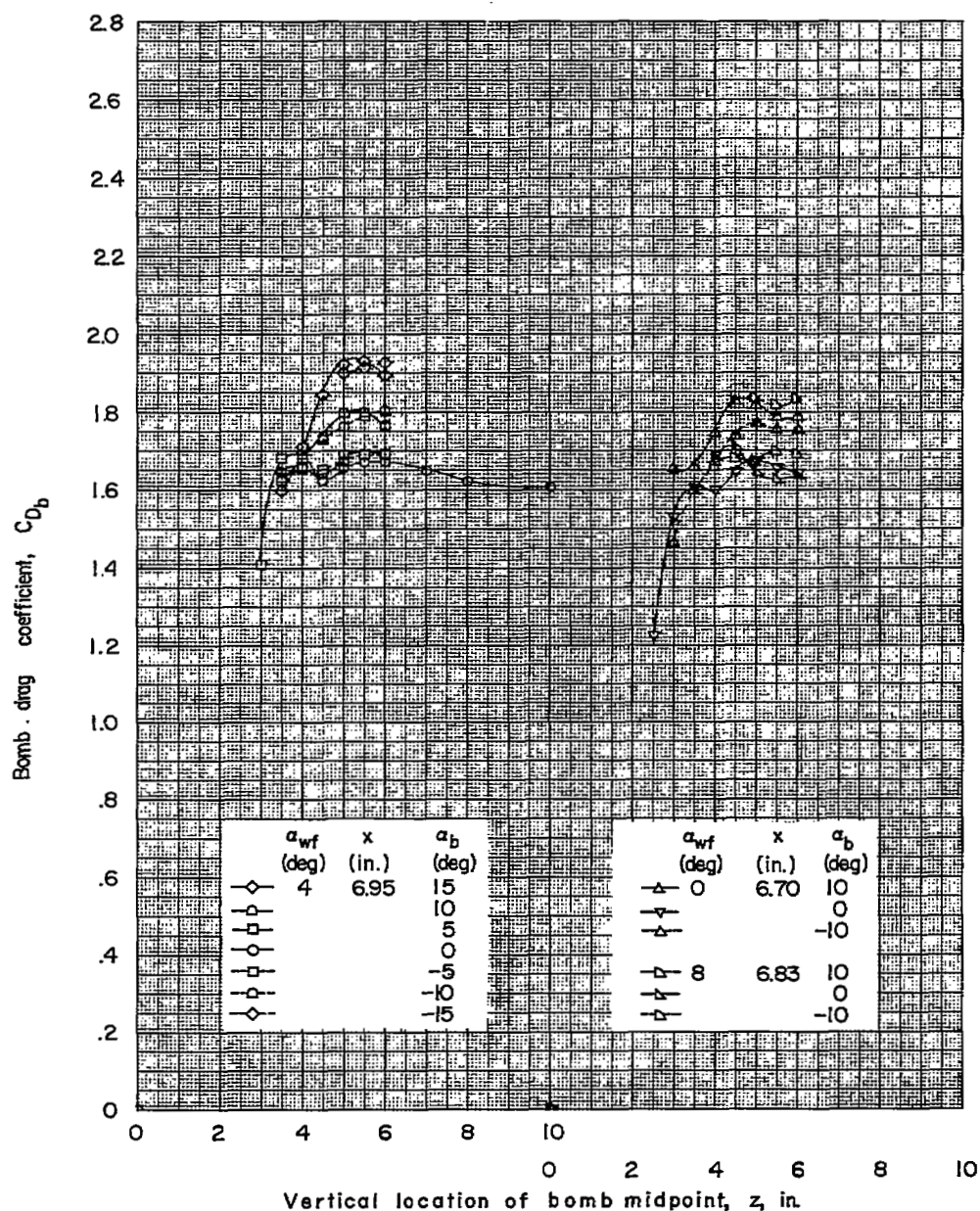
(b) Continued.

Figure 8.- Continued.



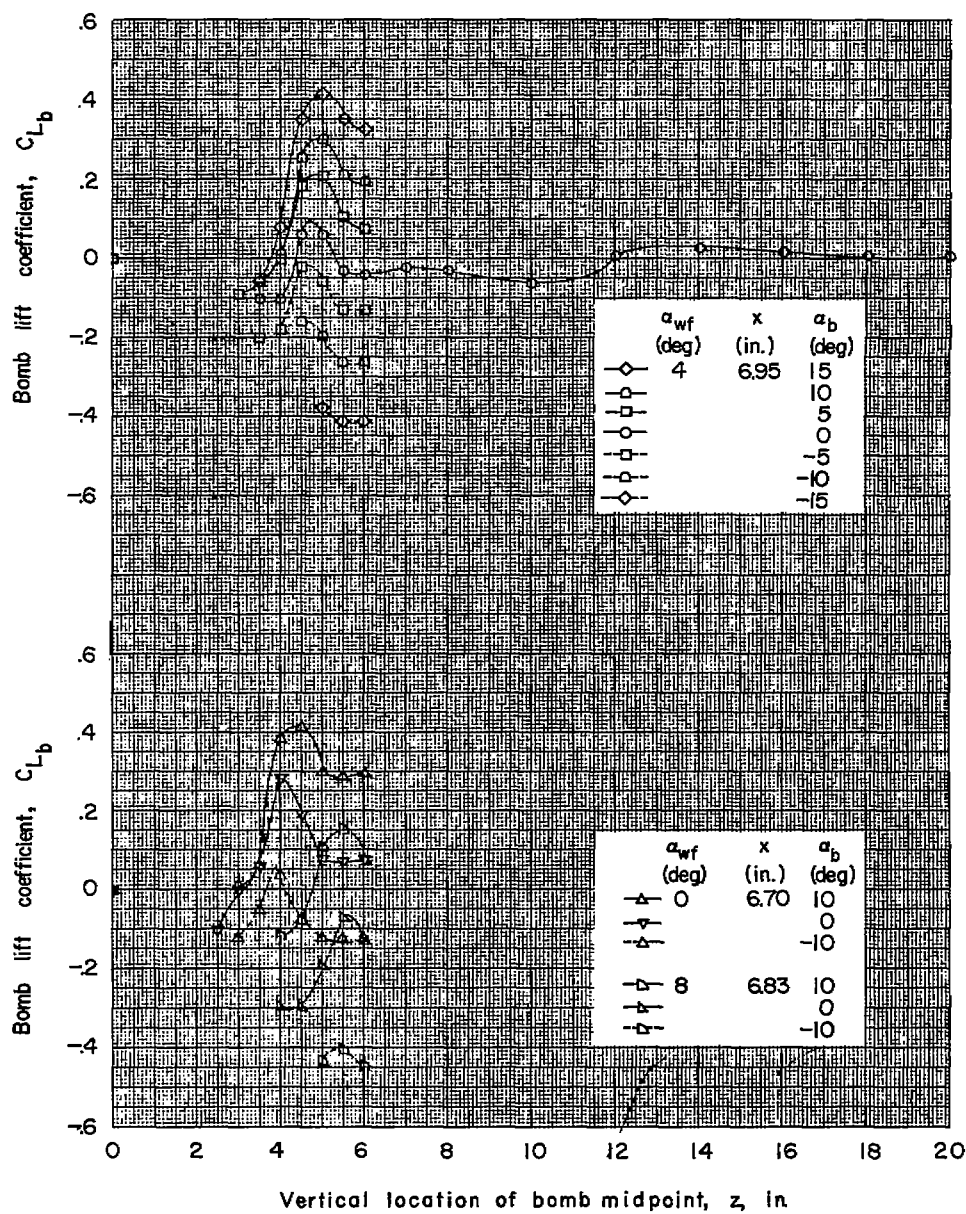
(b) Concluded.

Figure 8.- Continued.



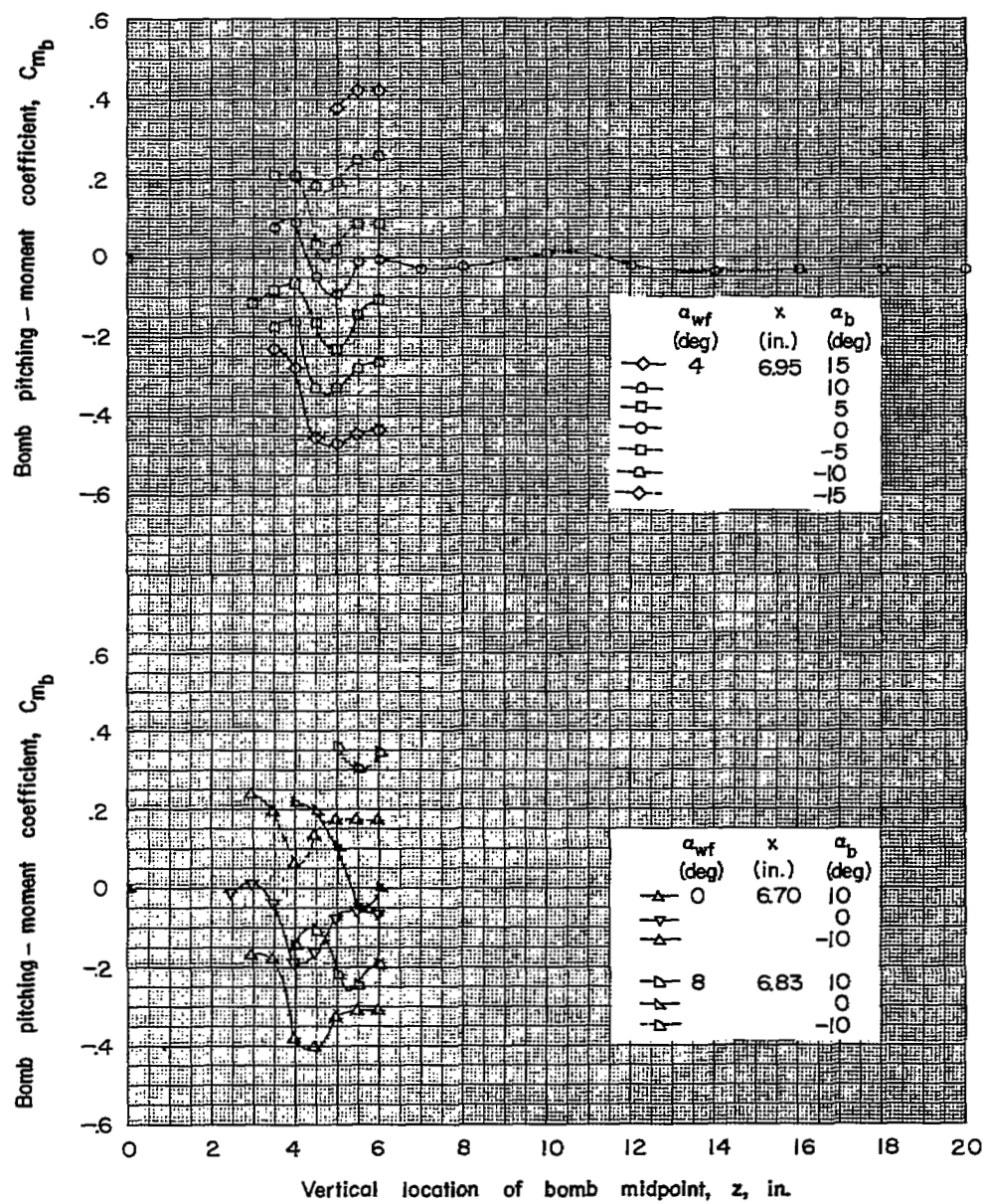
(c) Values of x from 6.70 to 6.95 inches.

Figure 8.- Continued.



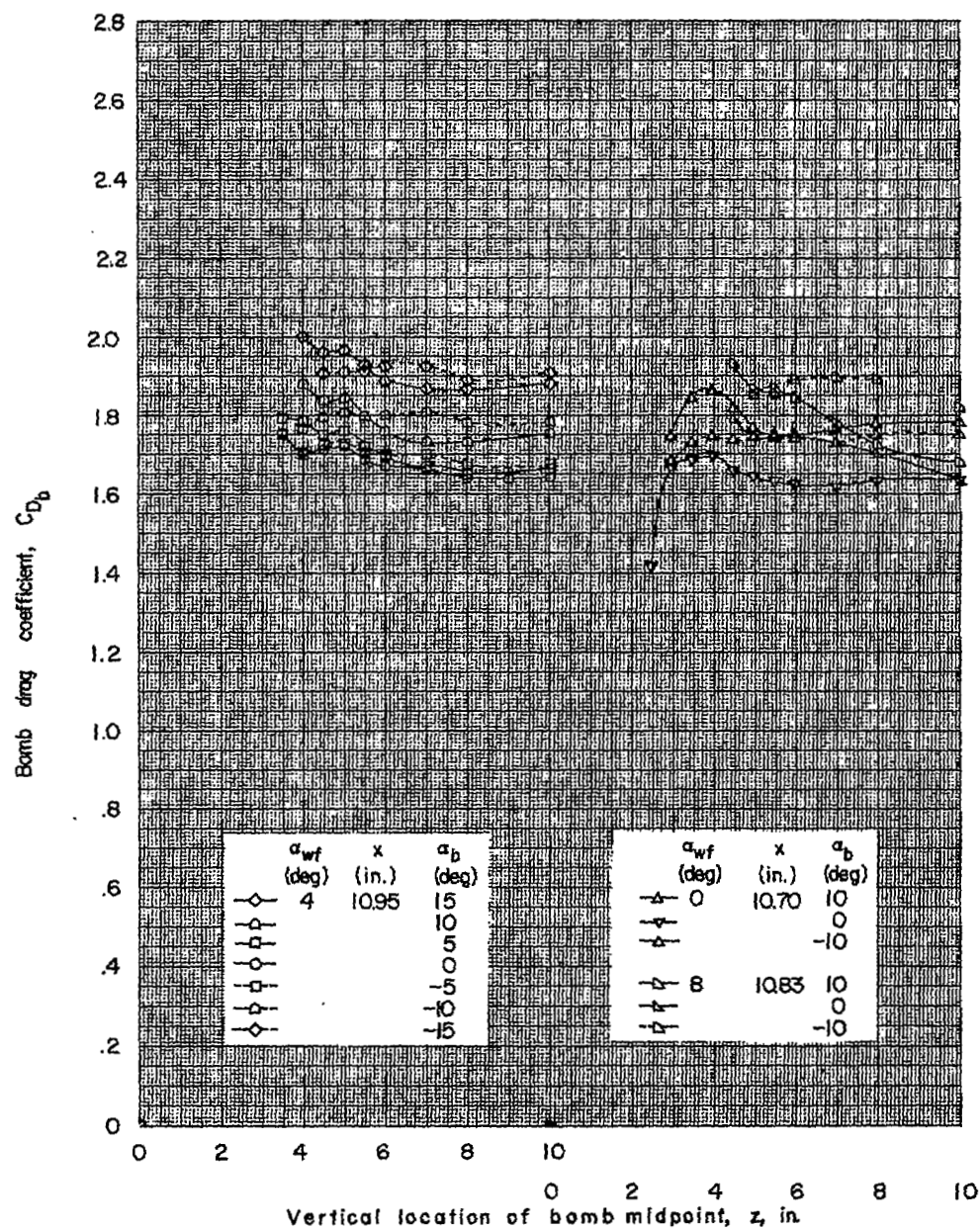
(c) Continued.

Figure 8.- Continued.



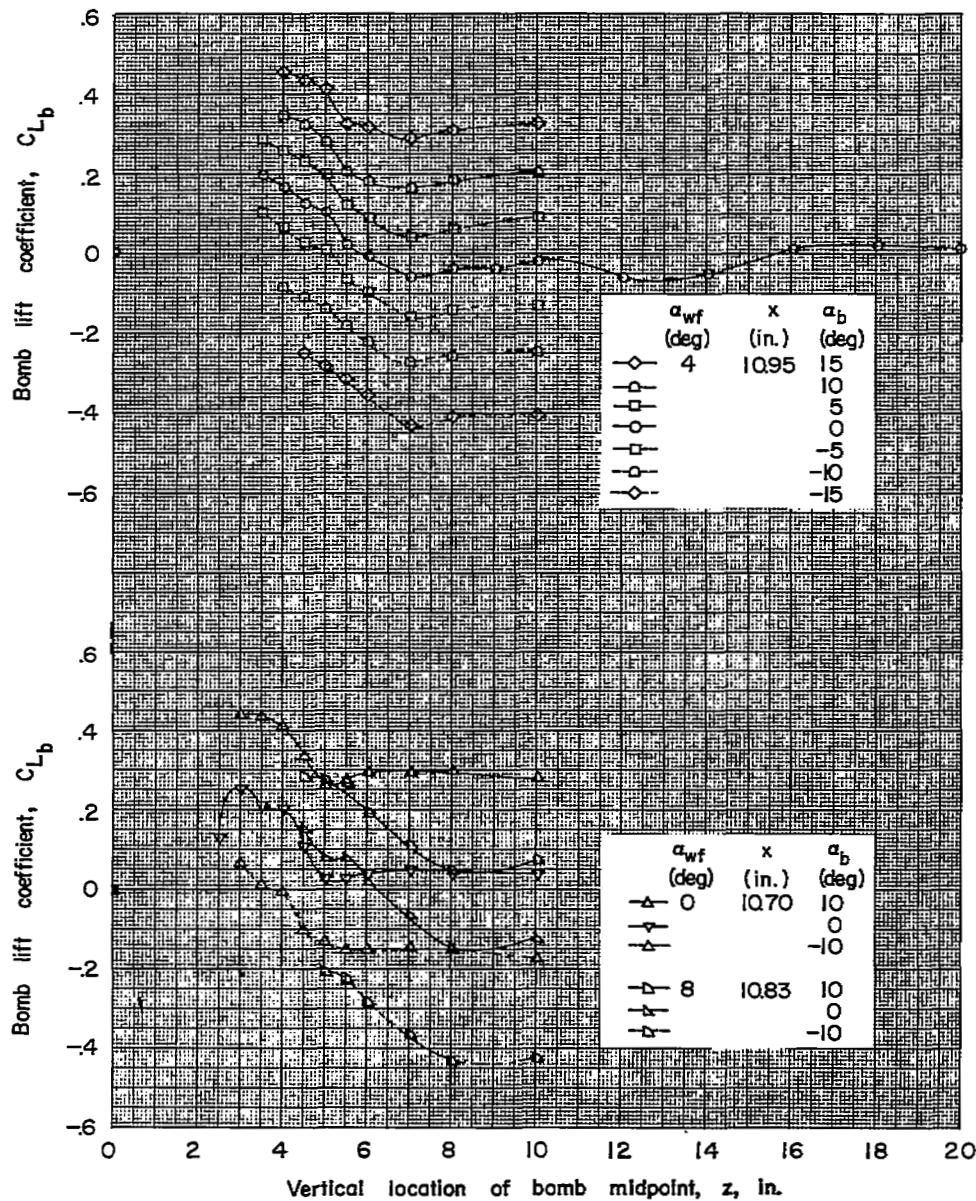
(c) Concluded.

Figure 8.- Continued.



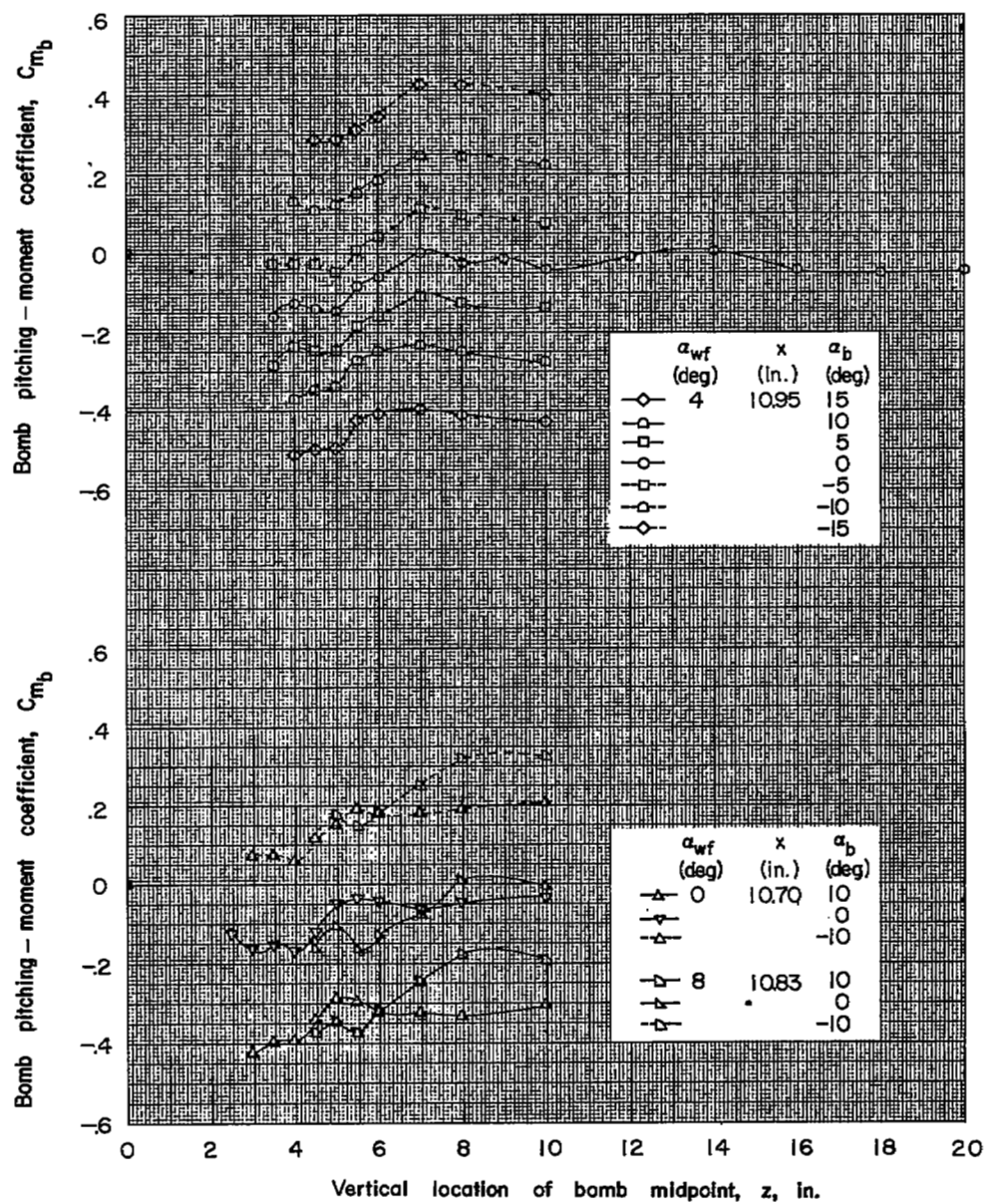
(d) Values of x from 10.70 to 10.95 inches.

Figure 8.- Continued.



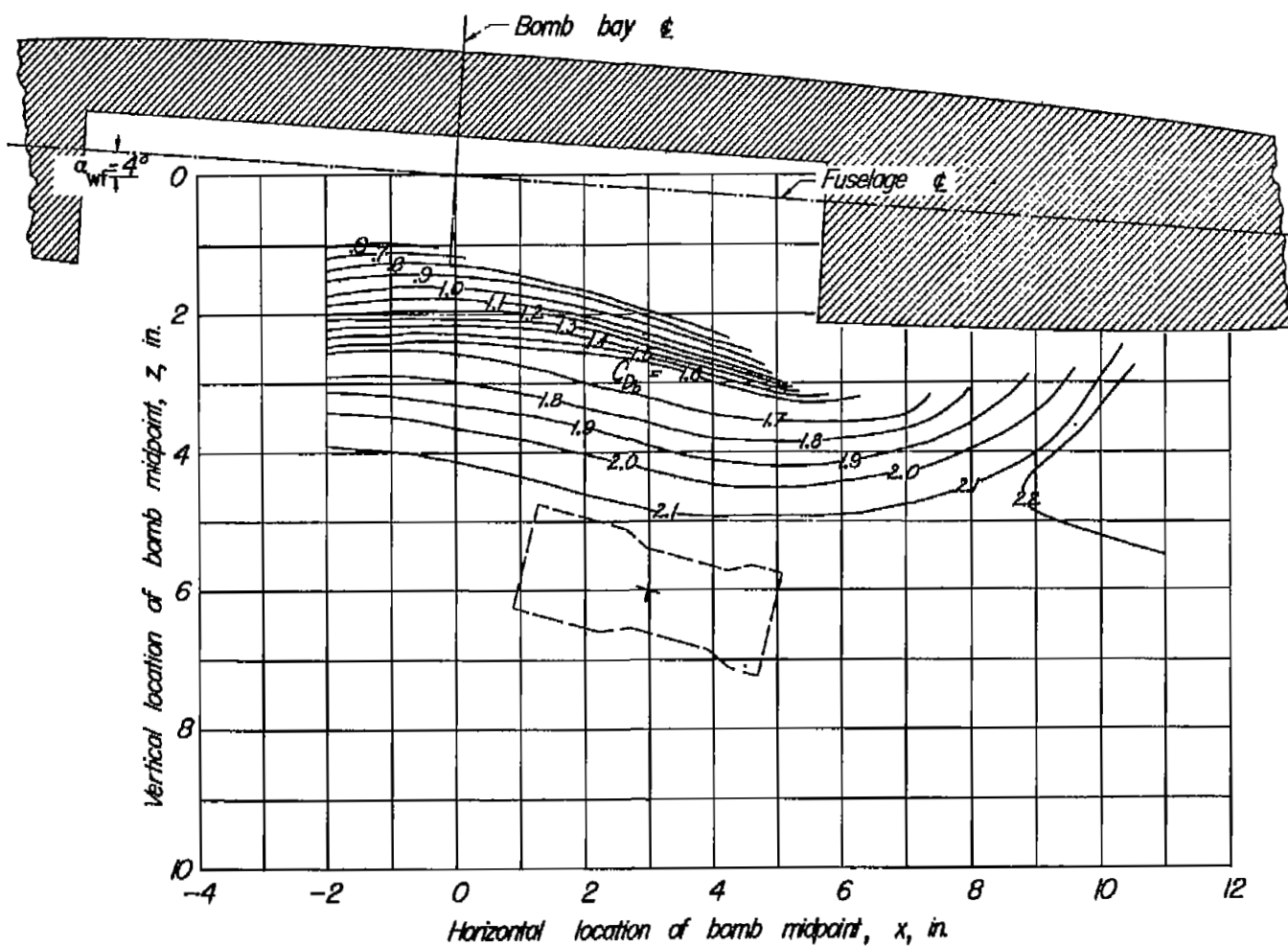
(d) Continued.

Figure 8.- Continued.



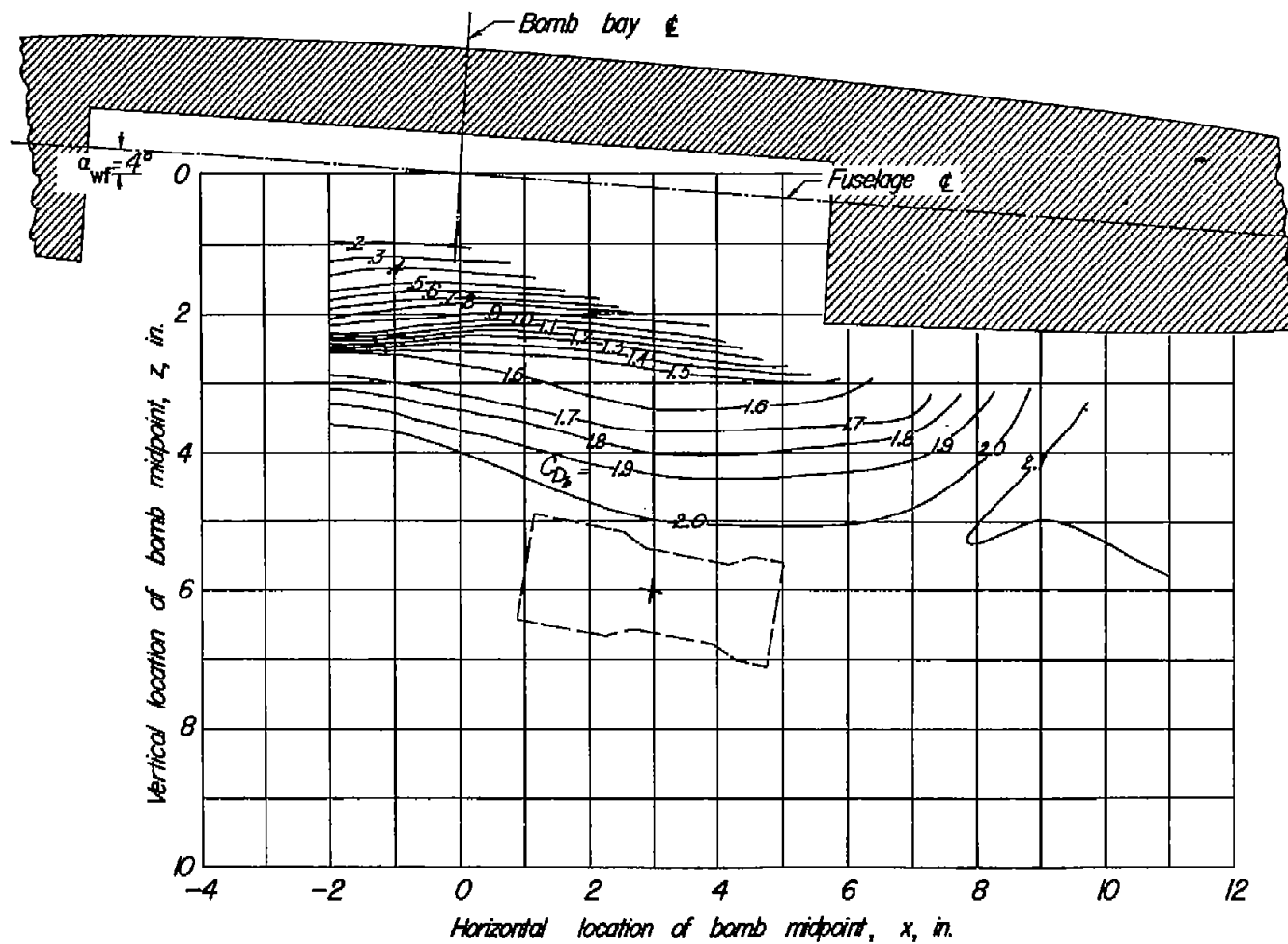
(d) Concluded.

Figure 8.- Concluded.



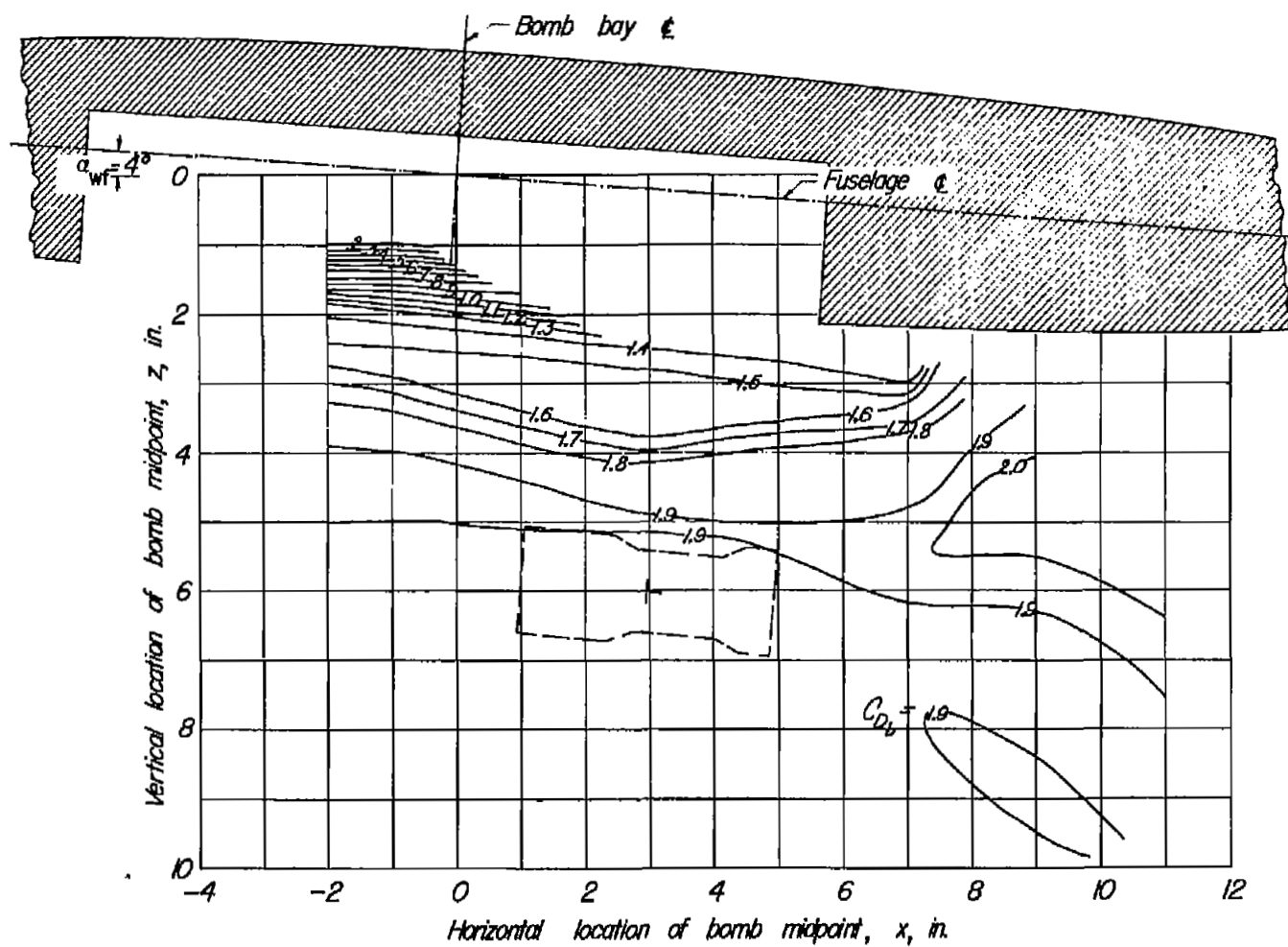
(a) $\alpha_b = 15^\circ$.

Figure 9.- Contour plot of drag coefficients of spool bomb in presence of wing-fuselage combination.



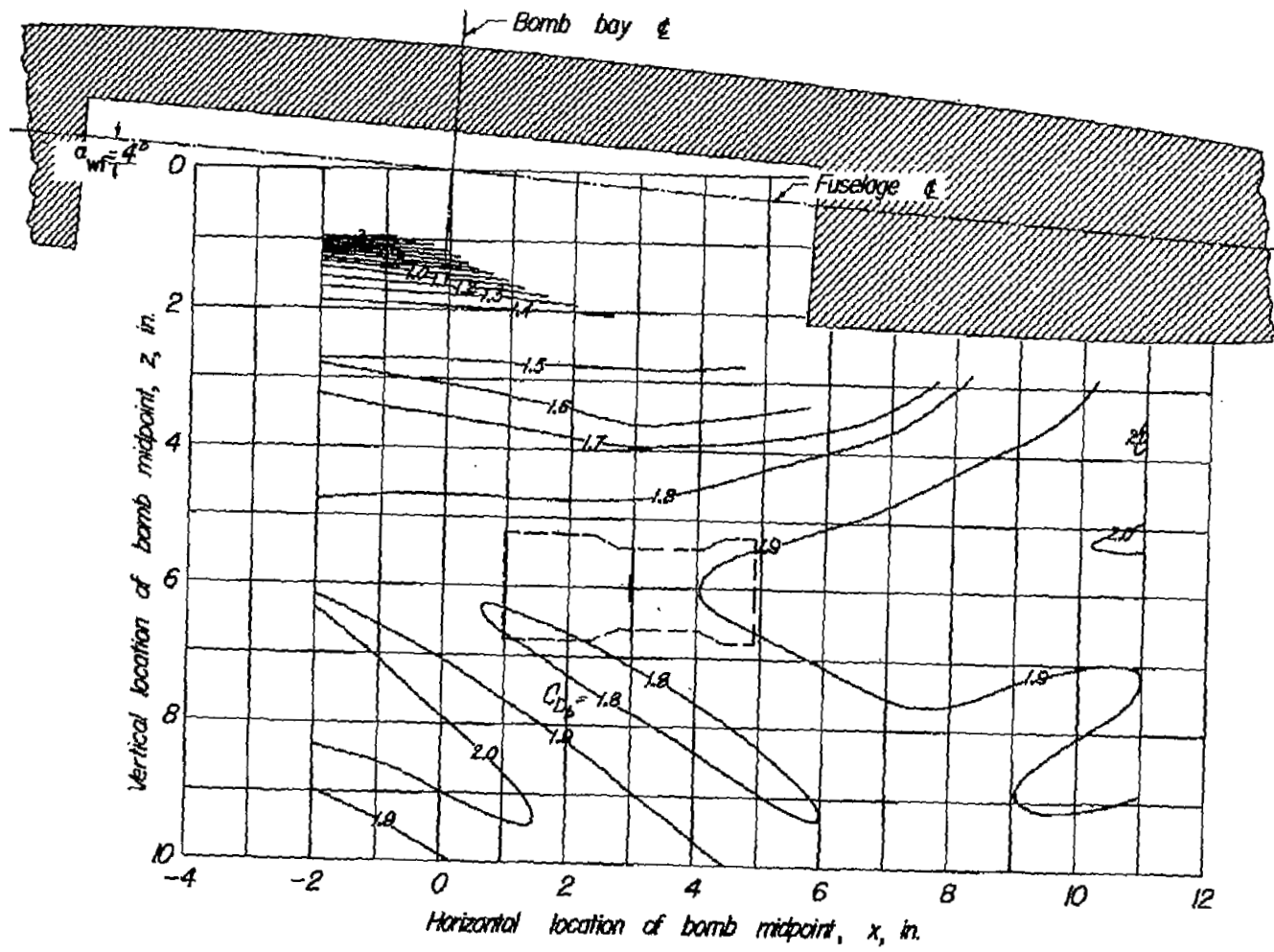
(b) $\alpha_0 = 10^\circ$.

Figure 9.- Continued.



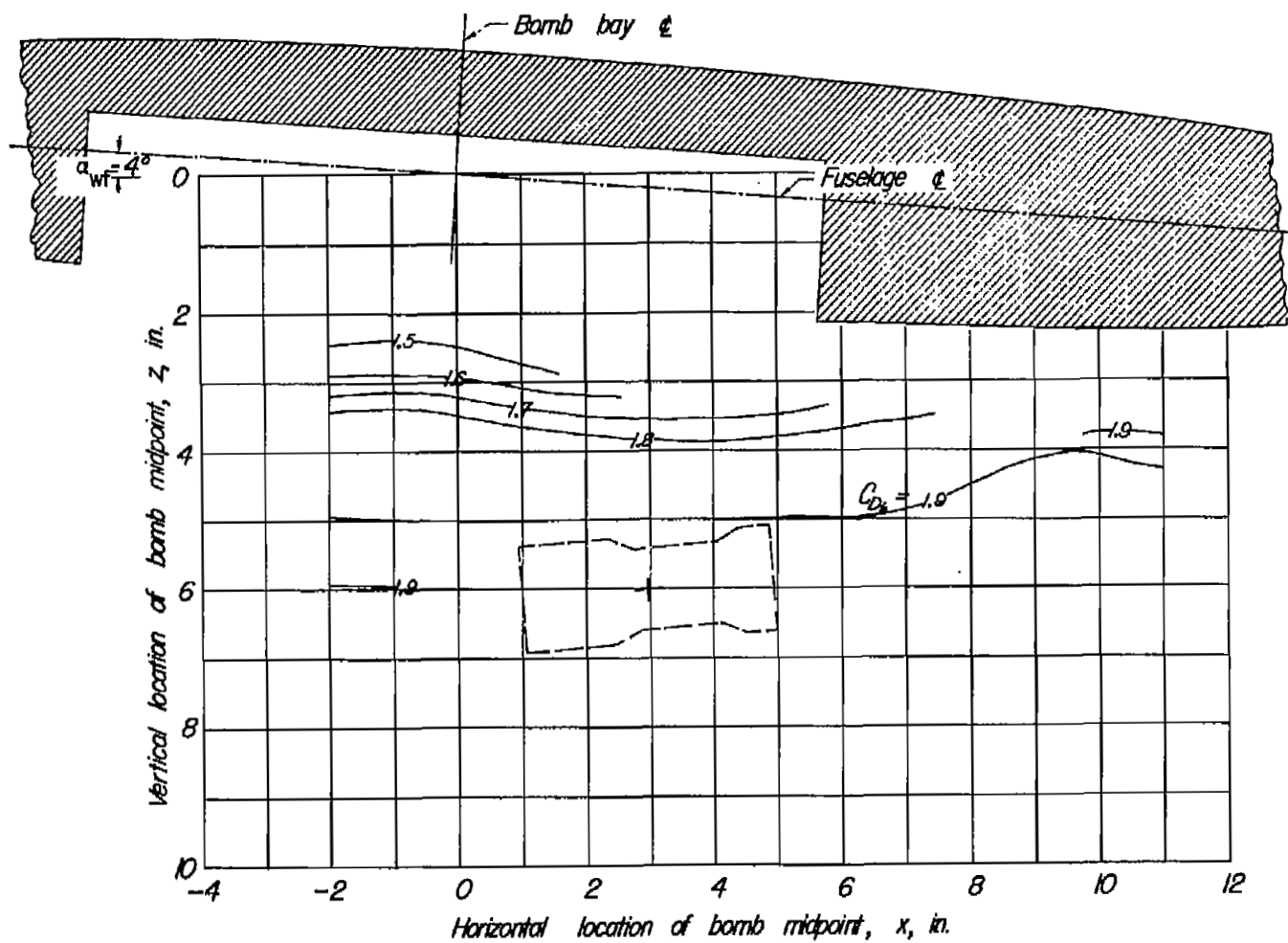
(c) $\alpha_b = 5^\circ$.

Figure 9.- Continued.



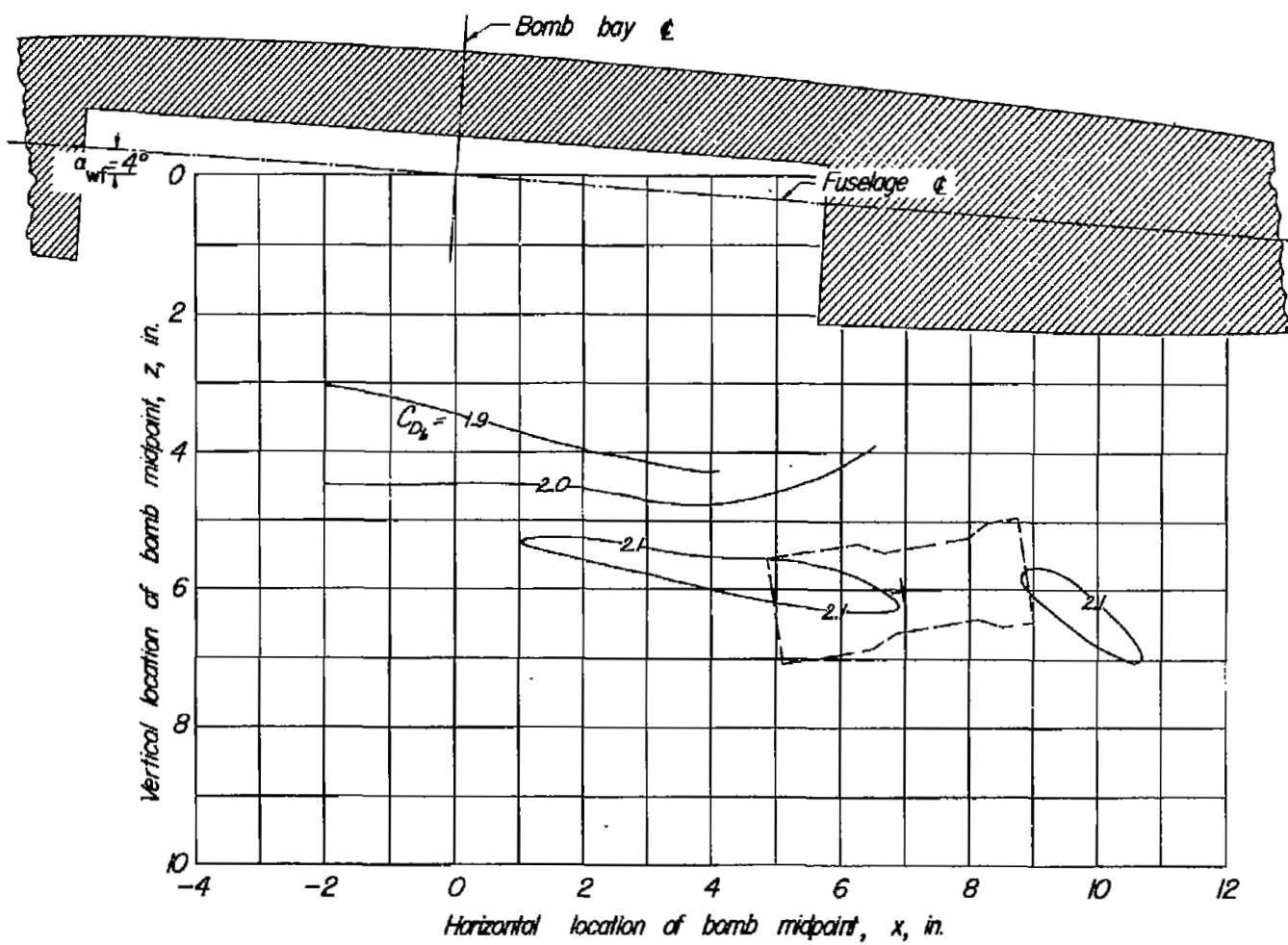
(d) $\alpha_b = 0^\circ$.

Figure 9.- Continued.



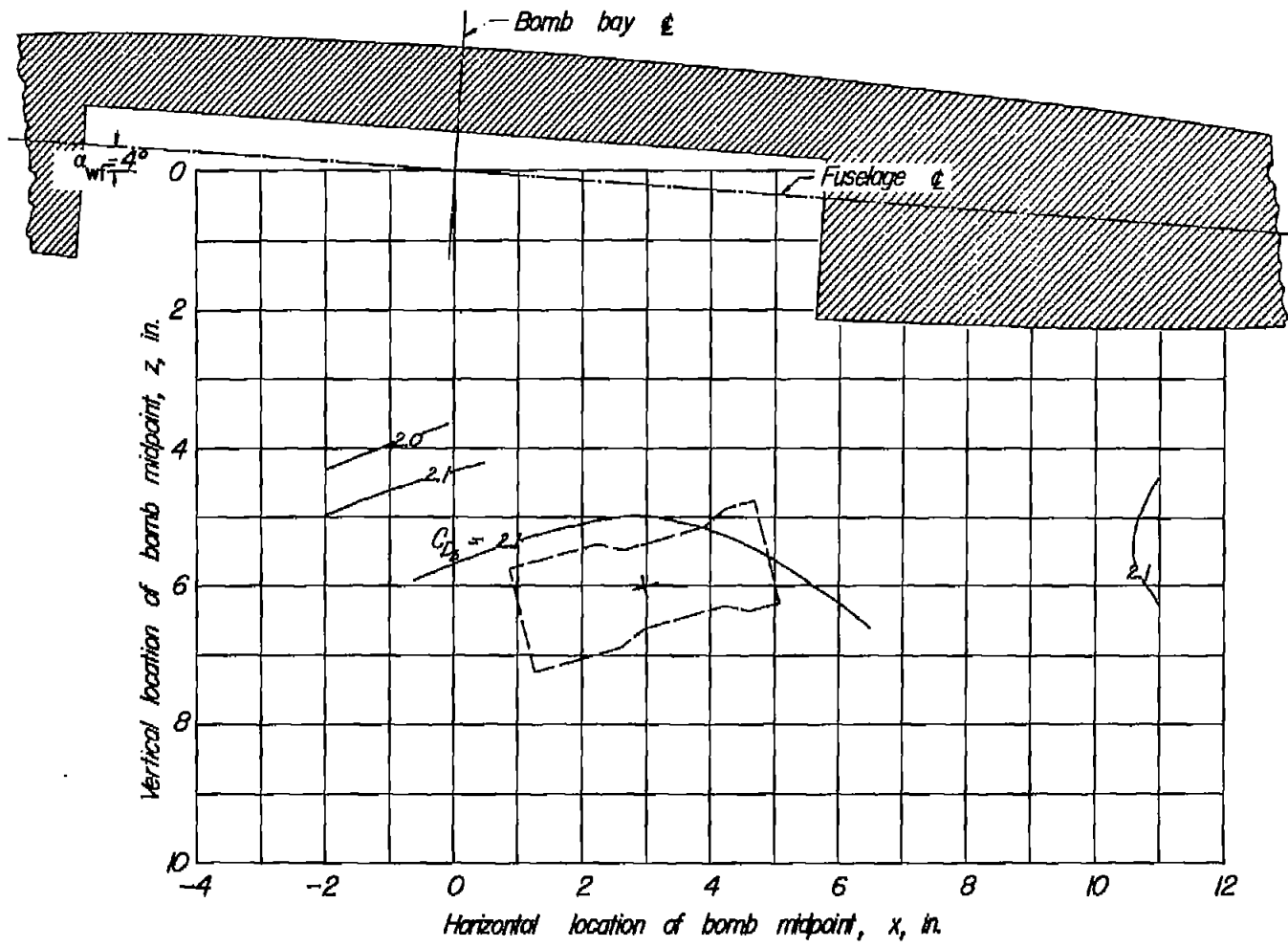
(e) $\alpha_b = -5^\circ$.

Figure 9.- Continued.



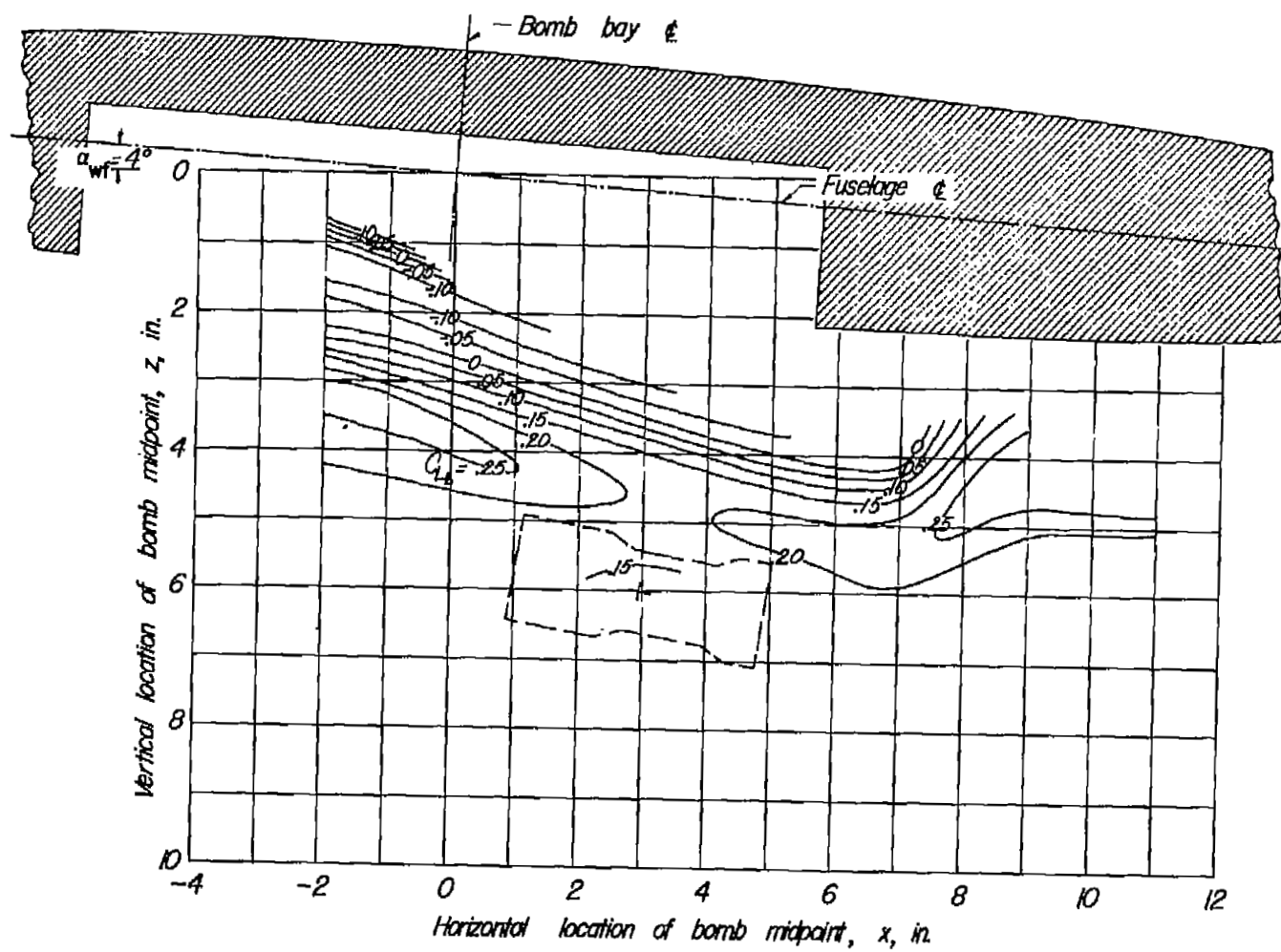
(f) $\alpha_b = -10^\circ$.

Figure 9.- Continued.



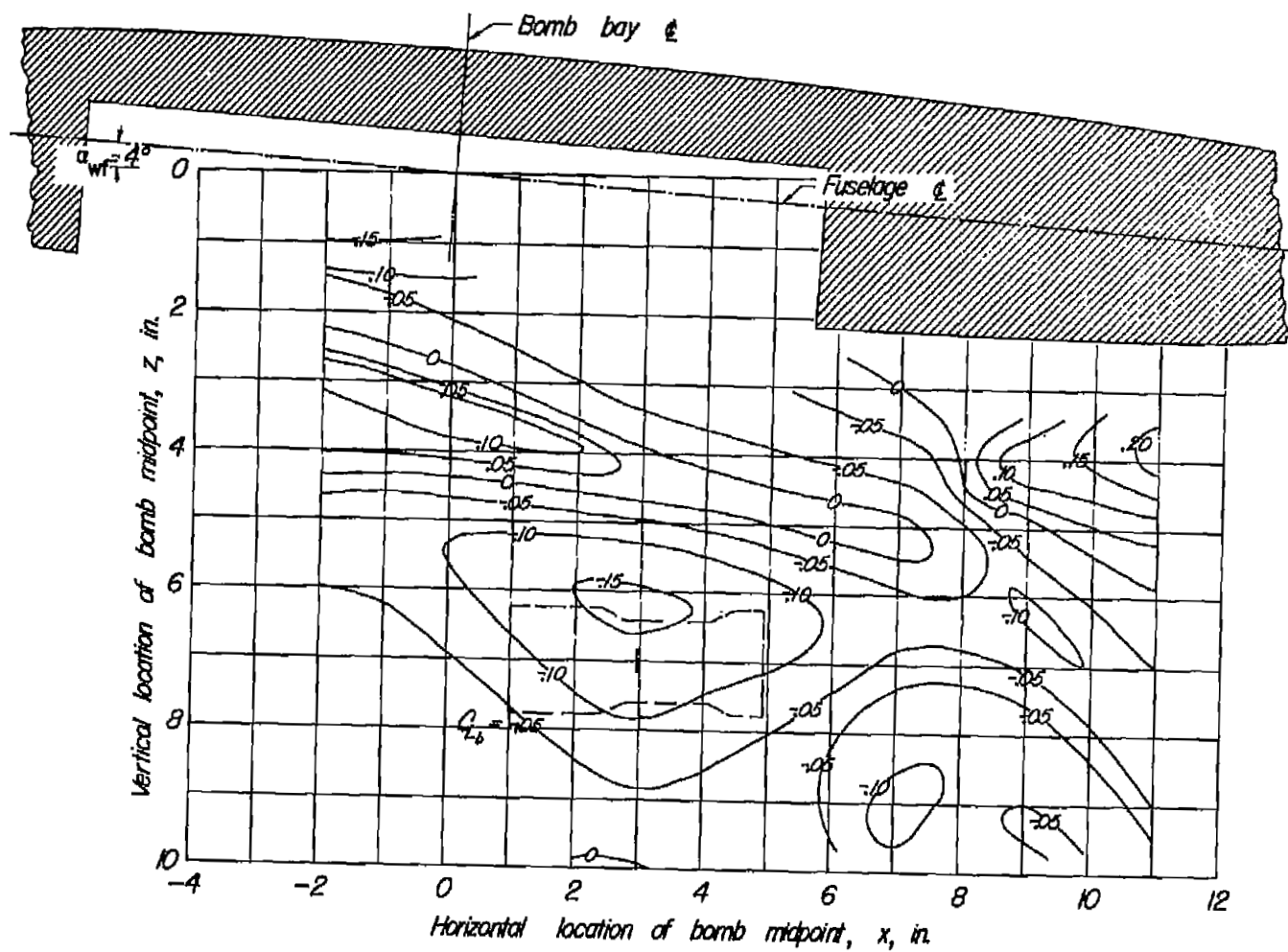
(g) $\alpha_b = -15^\circ$.

Figure 9.- Concluded.



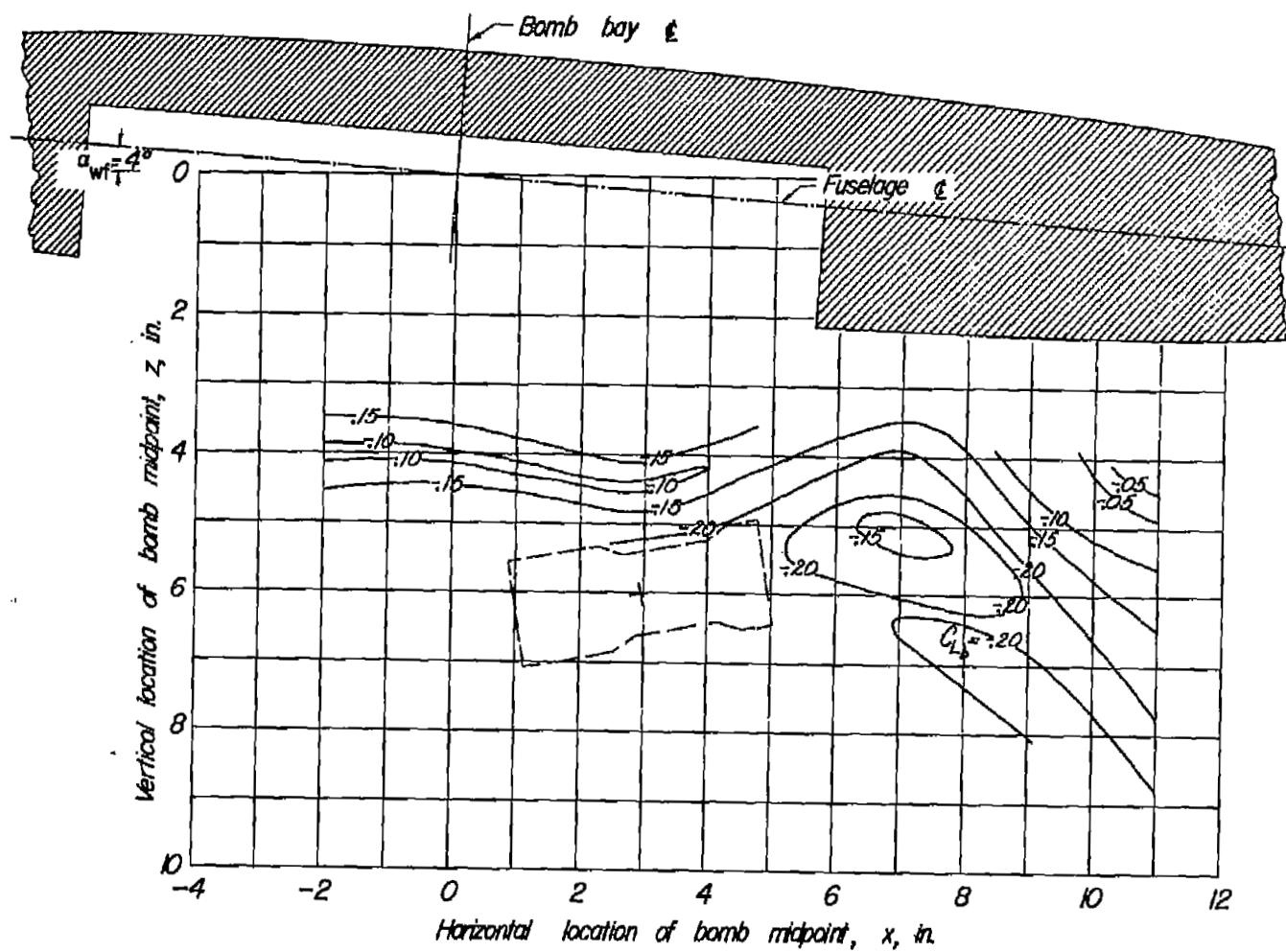
(b) $\alpha_b = 10^\circ$.

Figure 10.- Continued.



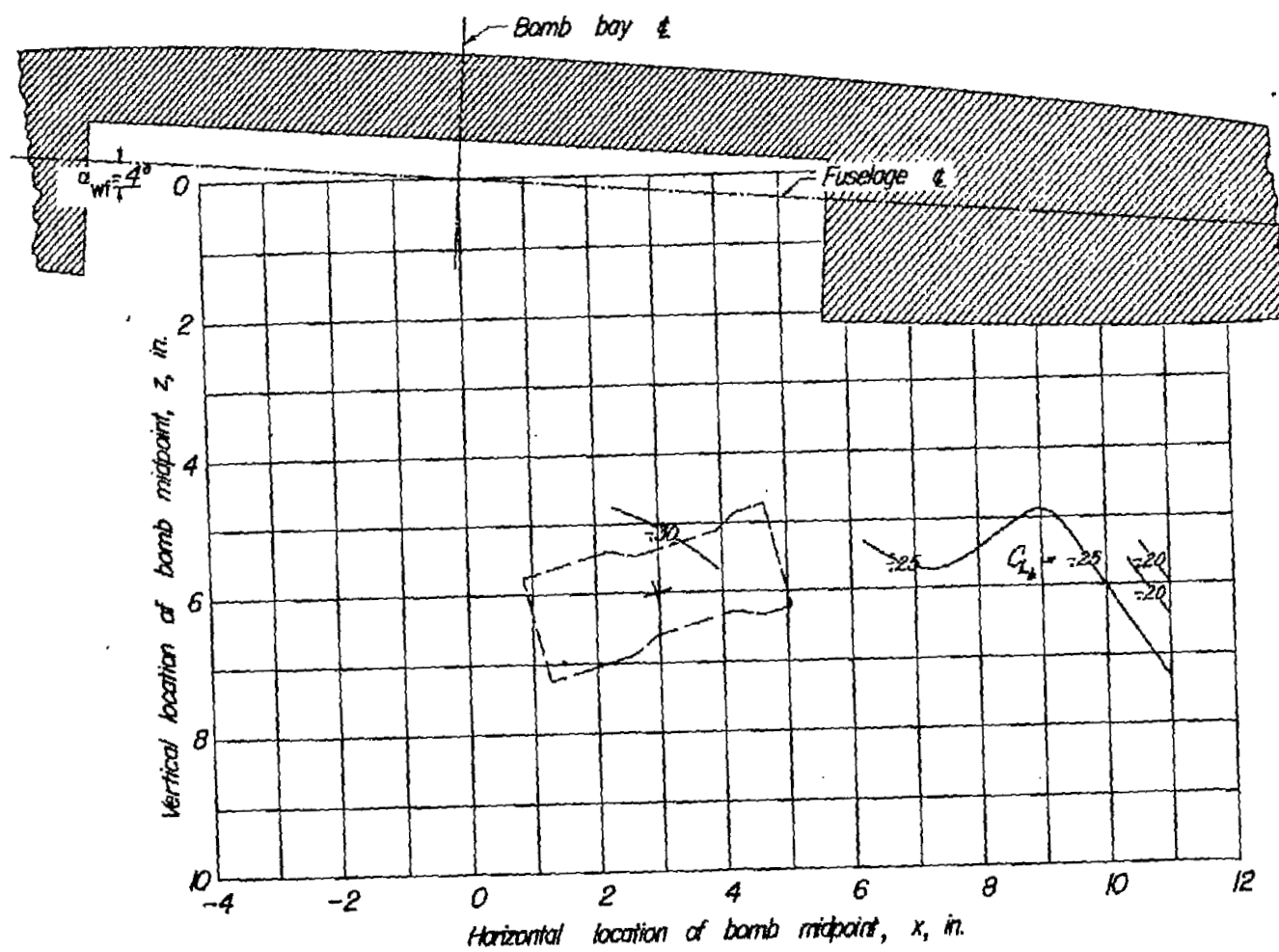
(d) $\alpha_b = 0^\circ$.

Figure 10.- Continued.



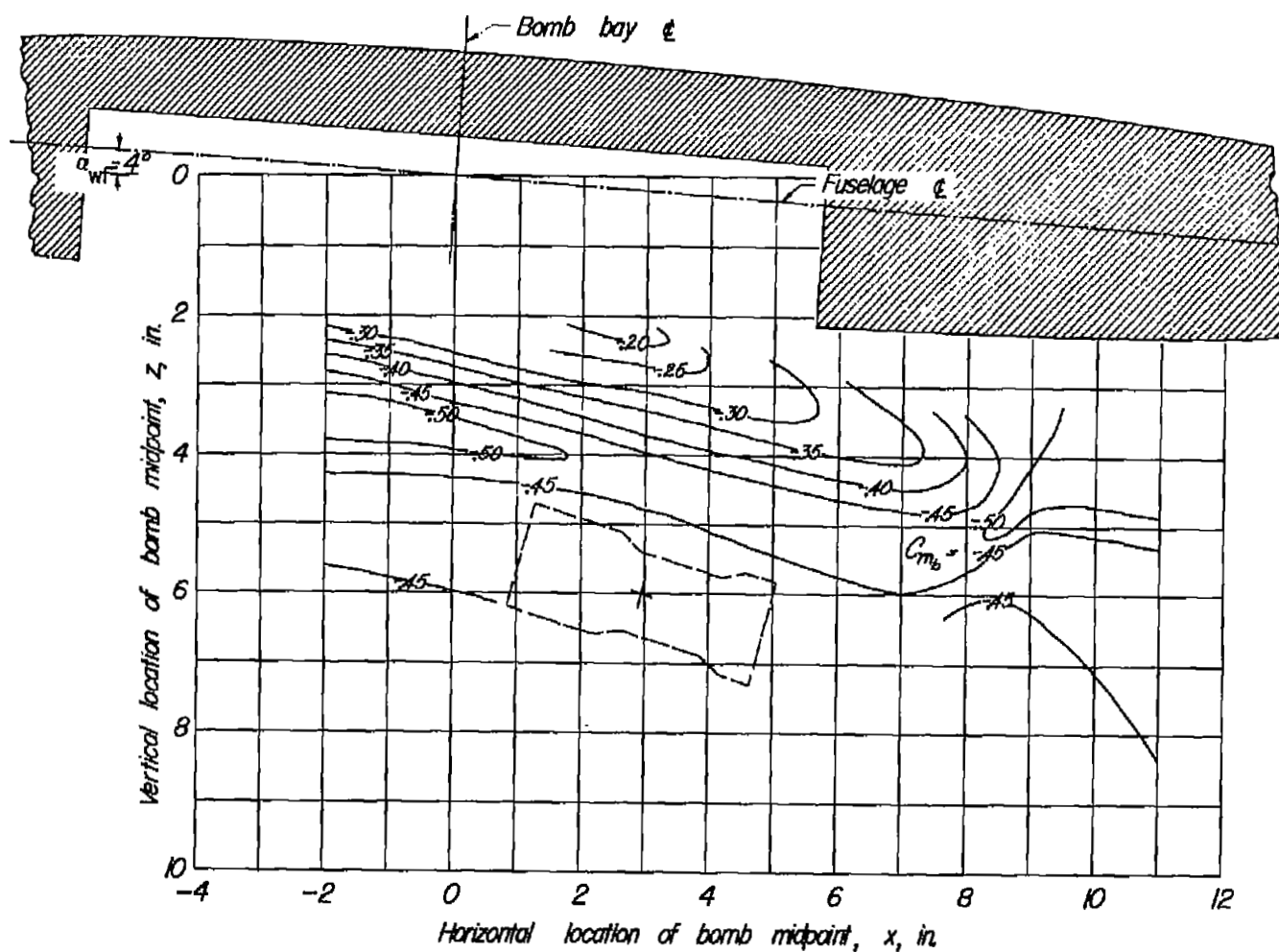
(f) $\alpha_0 = -10^\circ$.

Figure 10.- Continued.



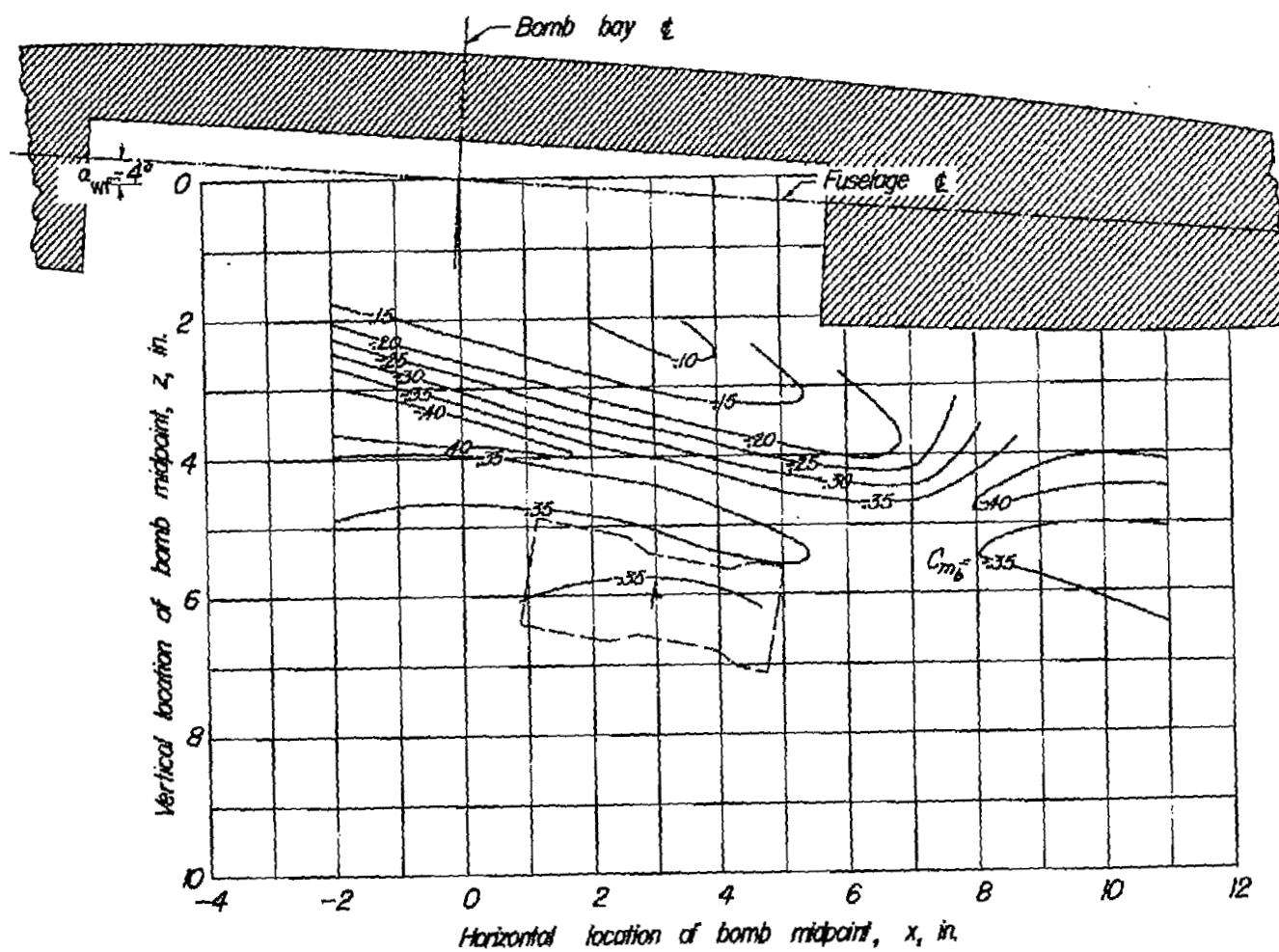
(g) $\alpha_b = -15^\circ$.

Figure 10.- Concluded.



(a) $\alpha_b = 15^\circ$.

Figure 11.- Contour plot of pitching-moment coefficients of spool bomb in presence of wing-fuselage combination.



(b) $\alpha_b = 10^\circ$.

Figure 11.- Continued.

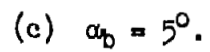
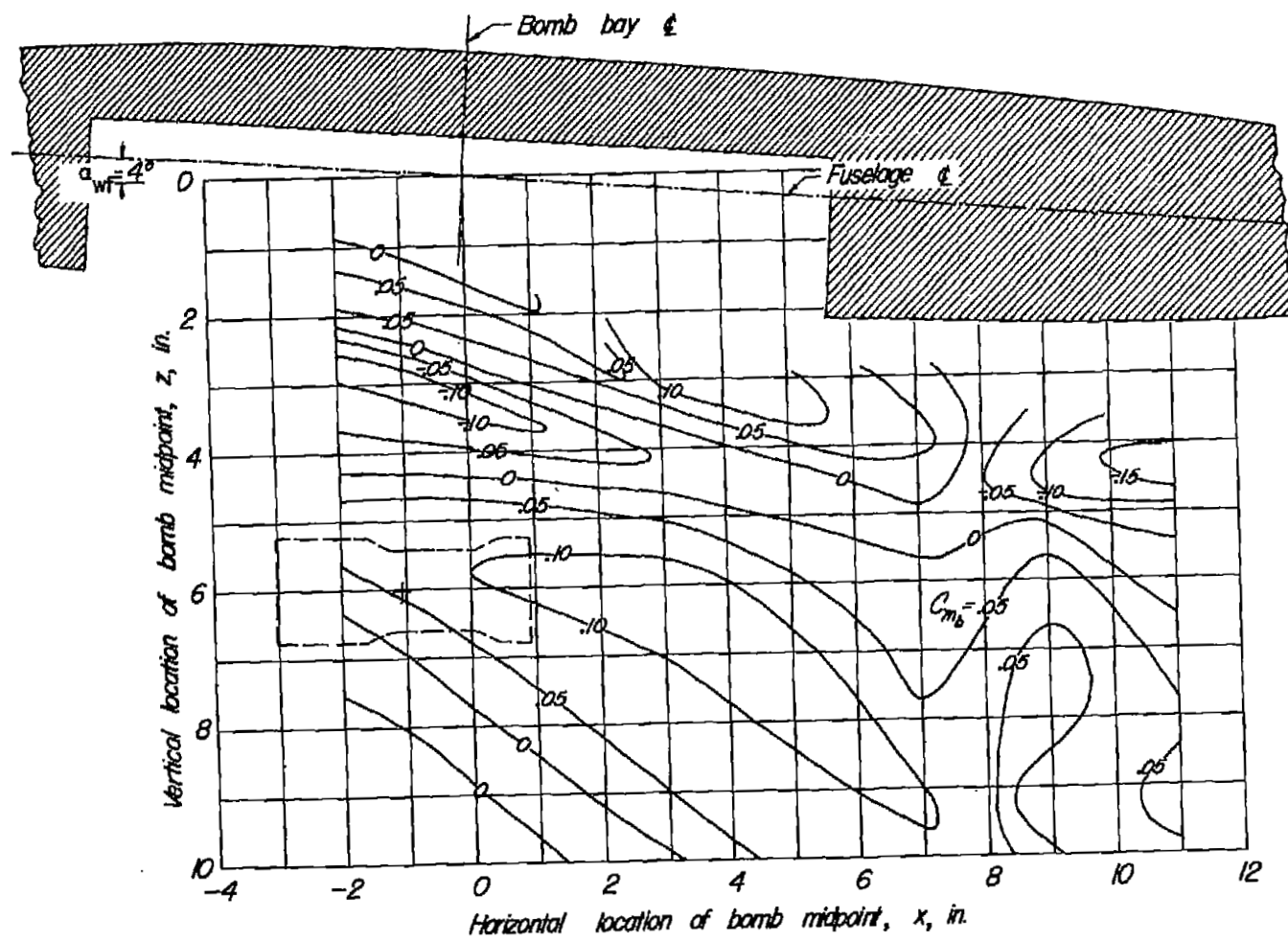
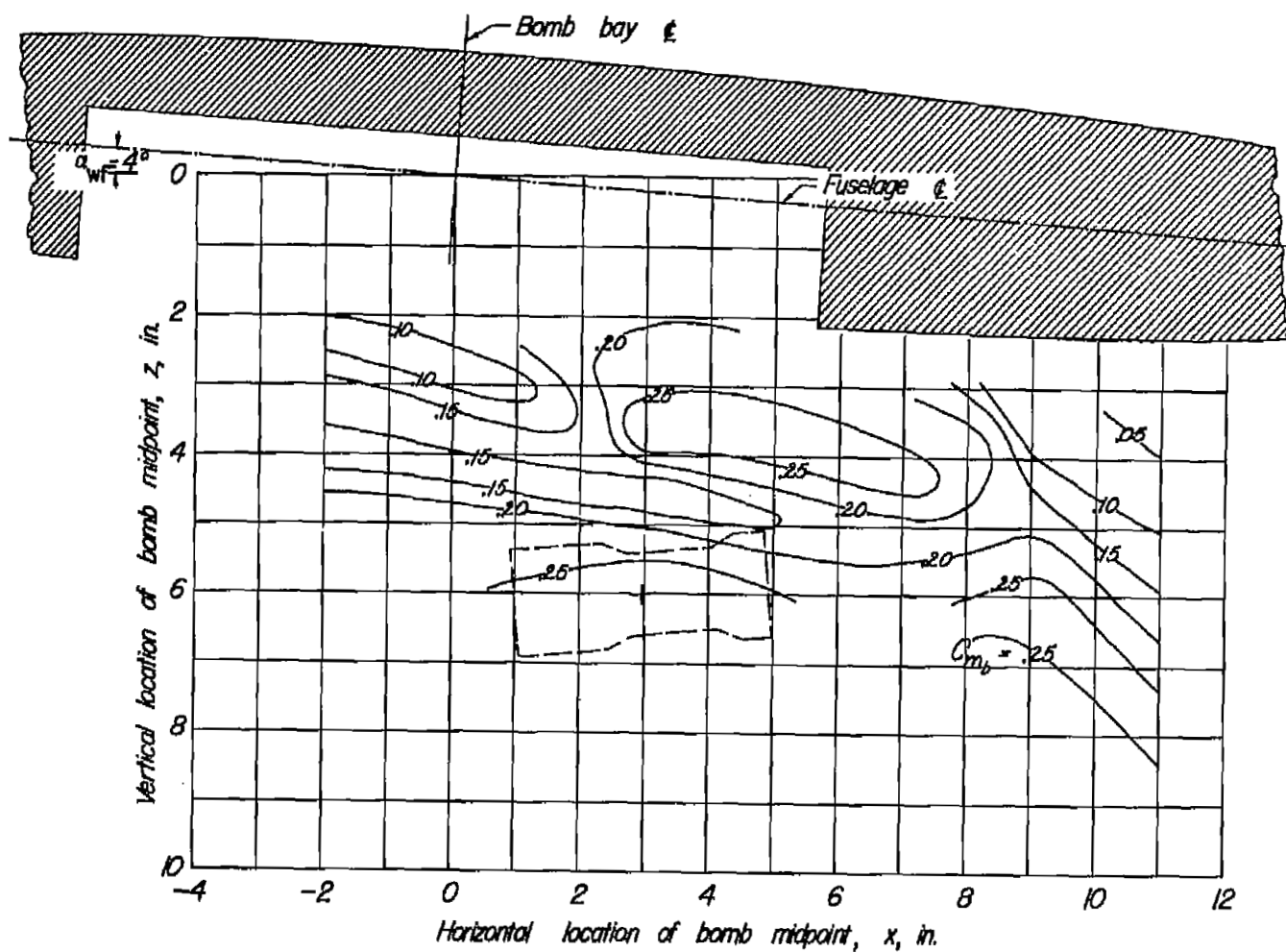


Figure 11.- Continued.



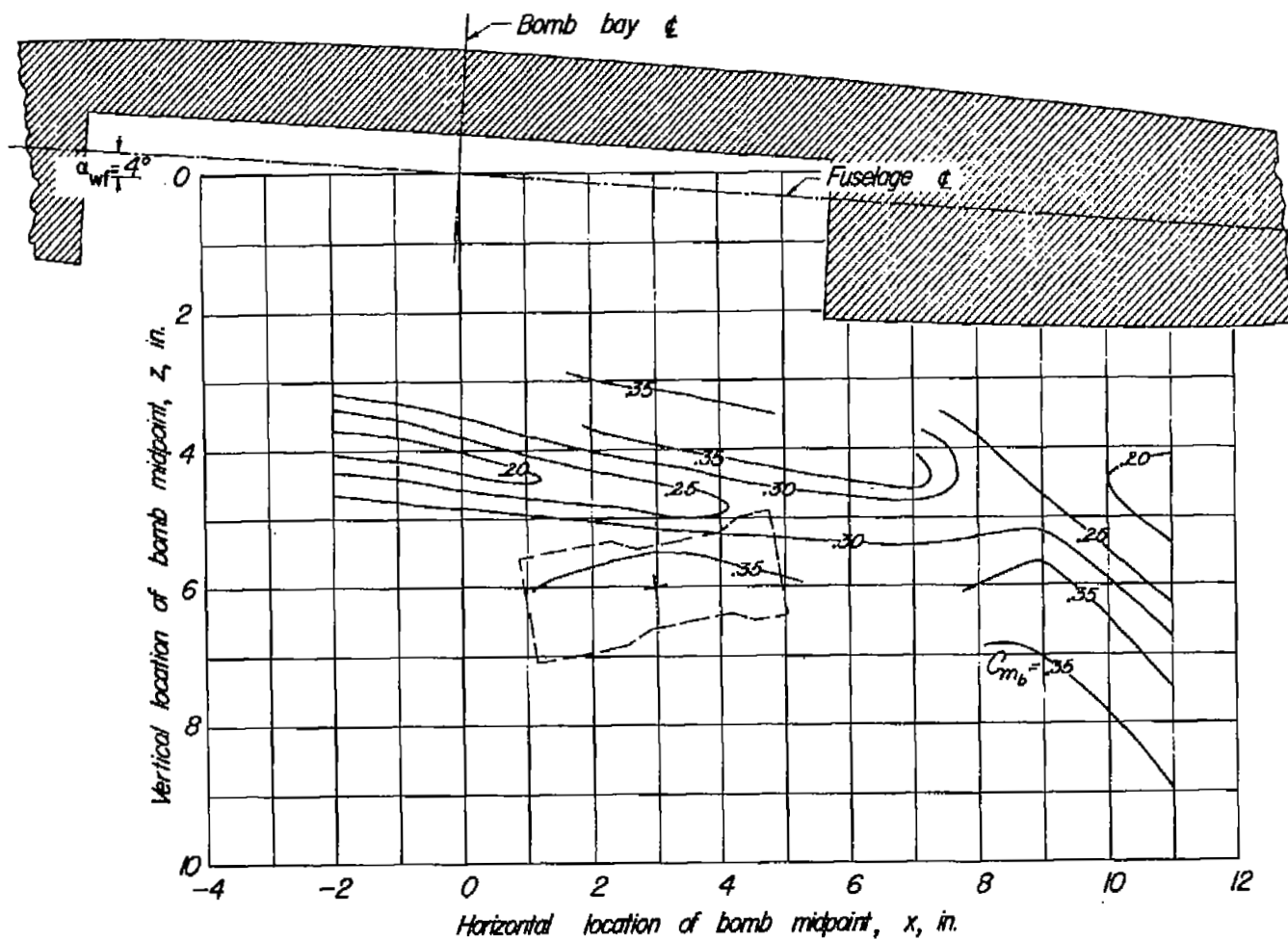
(d) $\alpha_b = 0^\circ$.

Figure 11.- Continued.



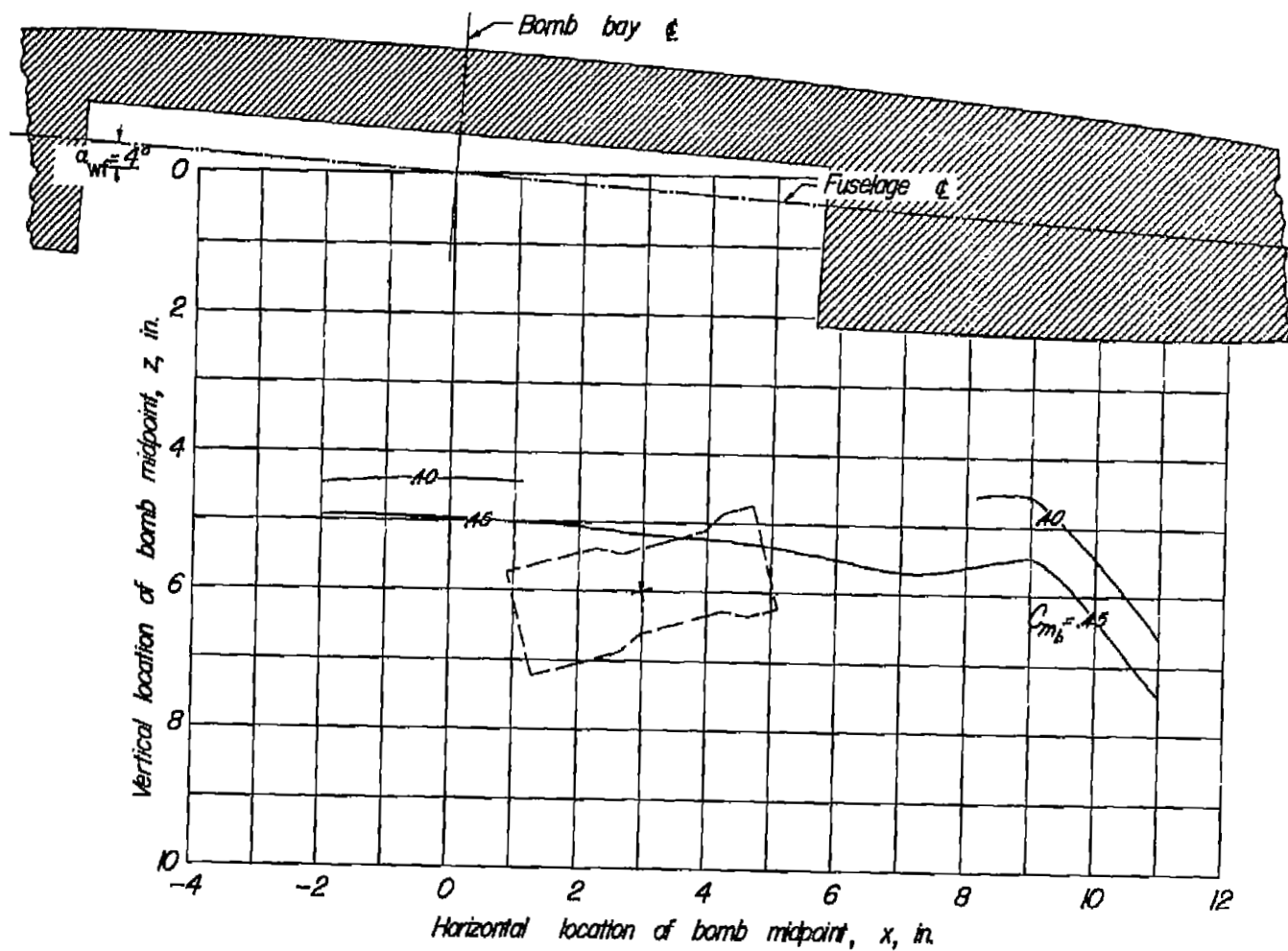
(e) $\alpha_b = -5^\circ$.

Figure 11.- Continued.



(f) $\alpha_0 = -10^\circ$.

Figure 11.- Continued.



(g) $\alpha_b = -15^\circ$.

Figure 11.- Concluded.

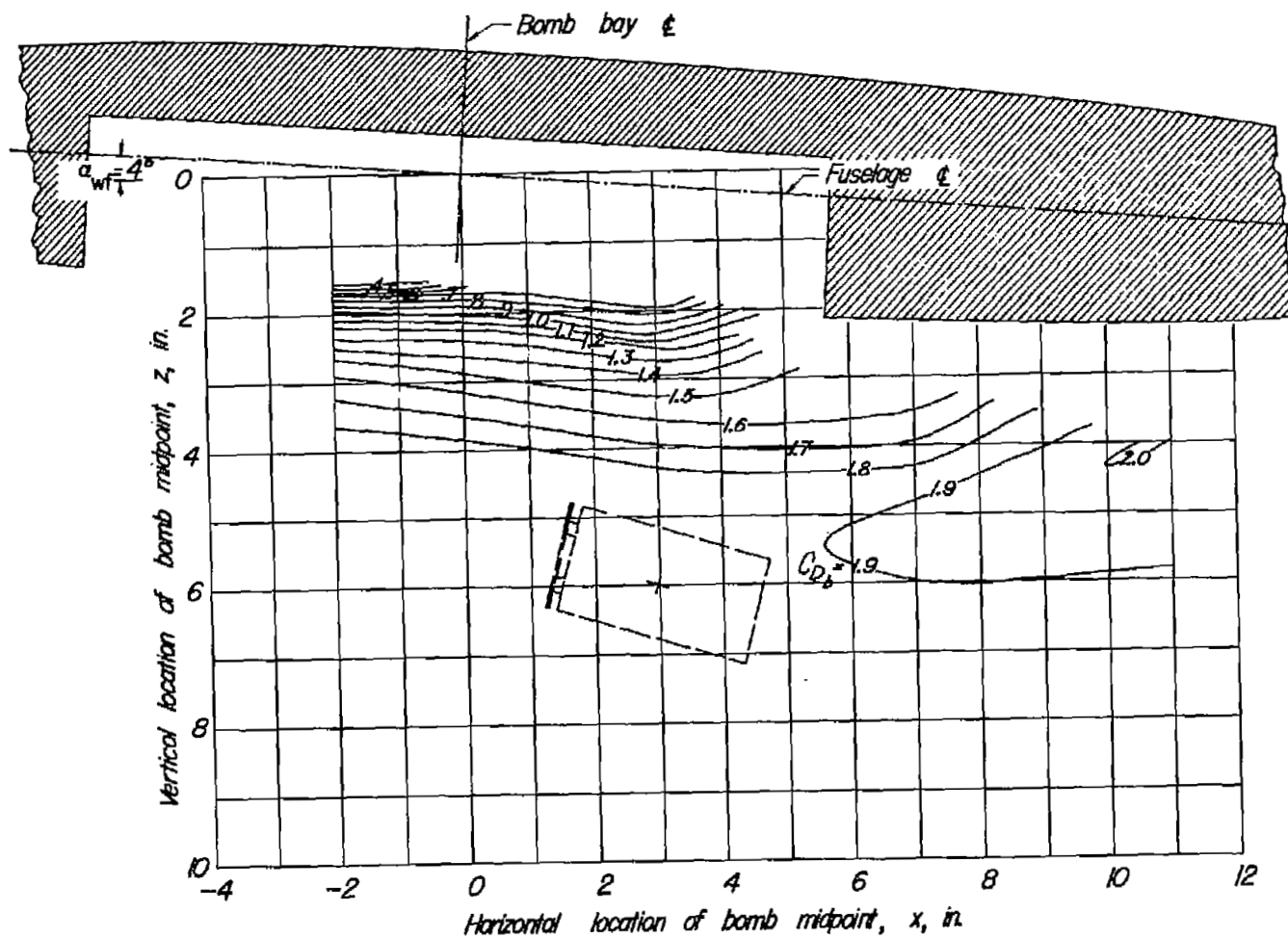
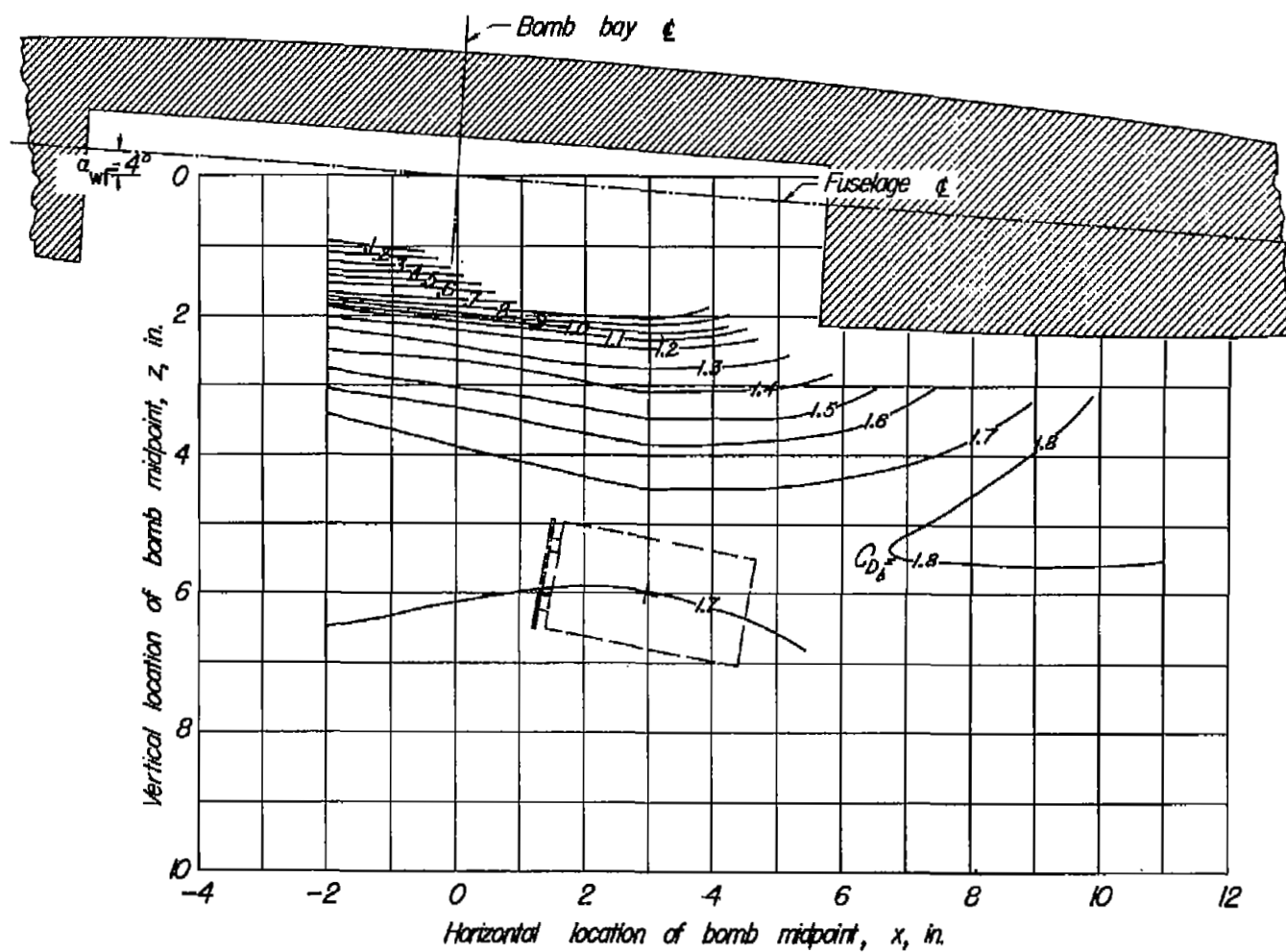
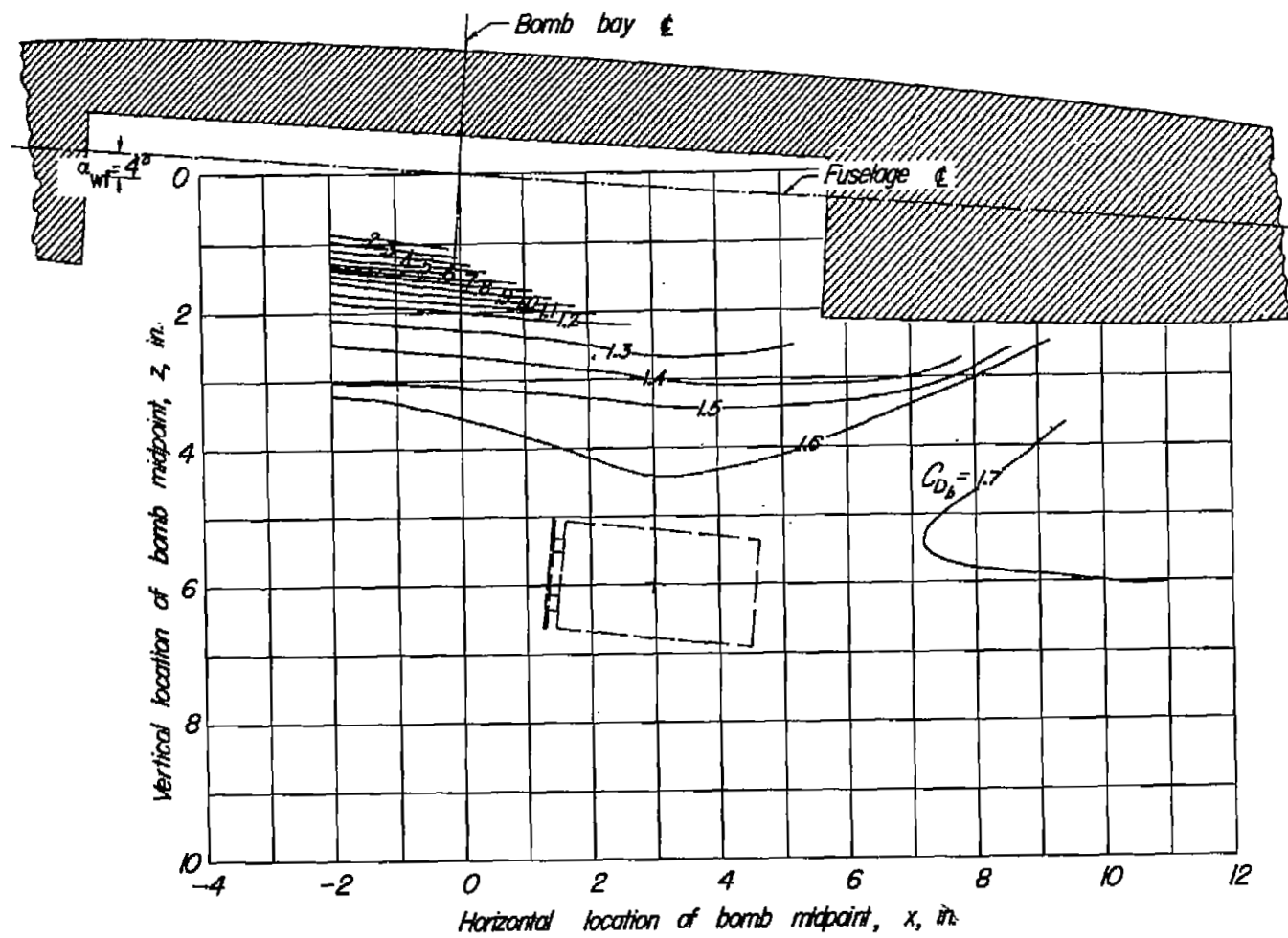


Figure 12.- Contour plot of drag coefficients of cylindrical bomb in presence of wing-fuselage combination.



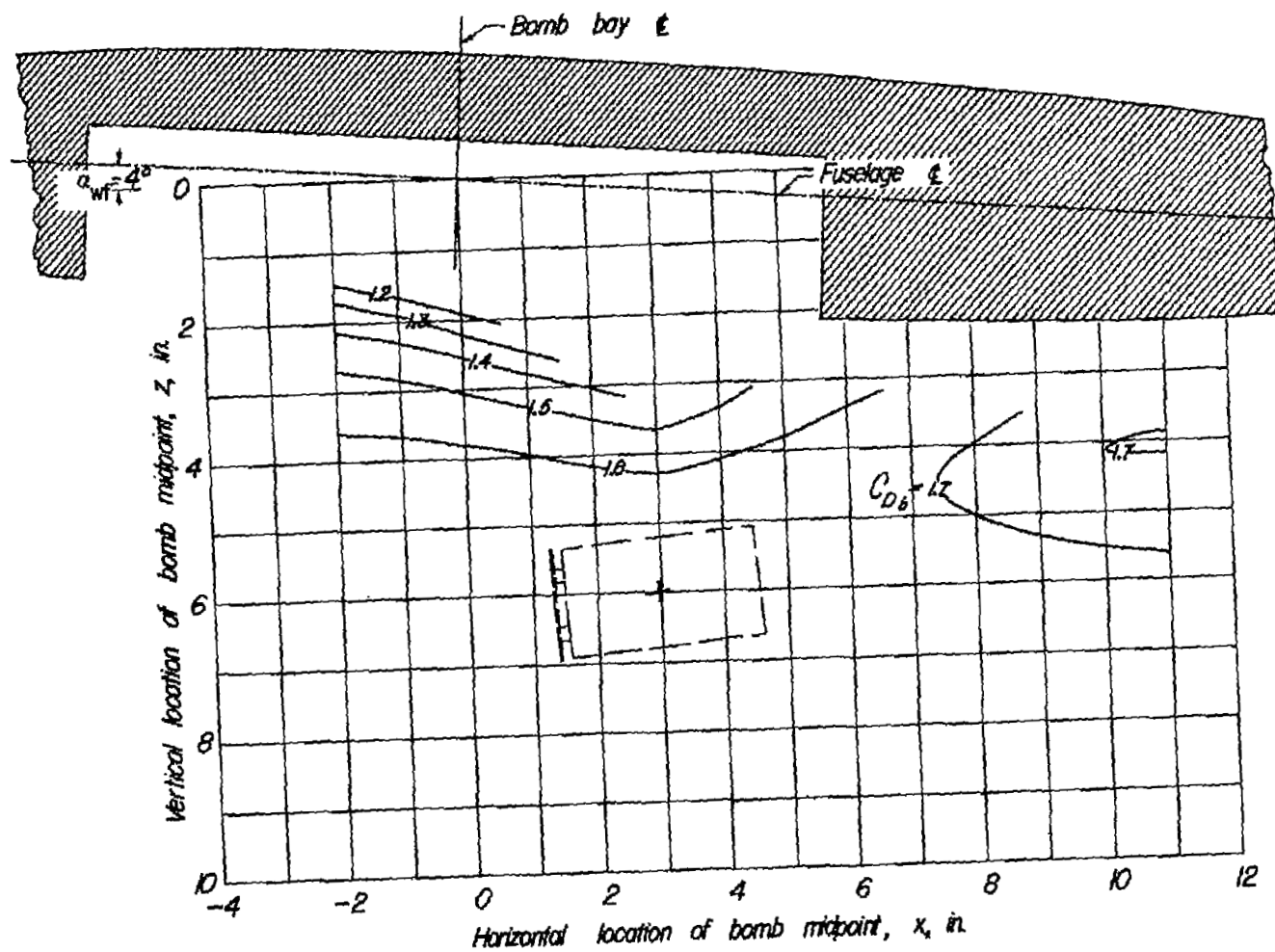
(b) $\alpha_0 = 10^\circ$.

Figure 12.- Continued.



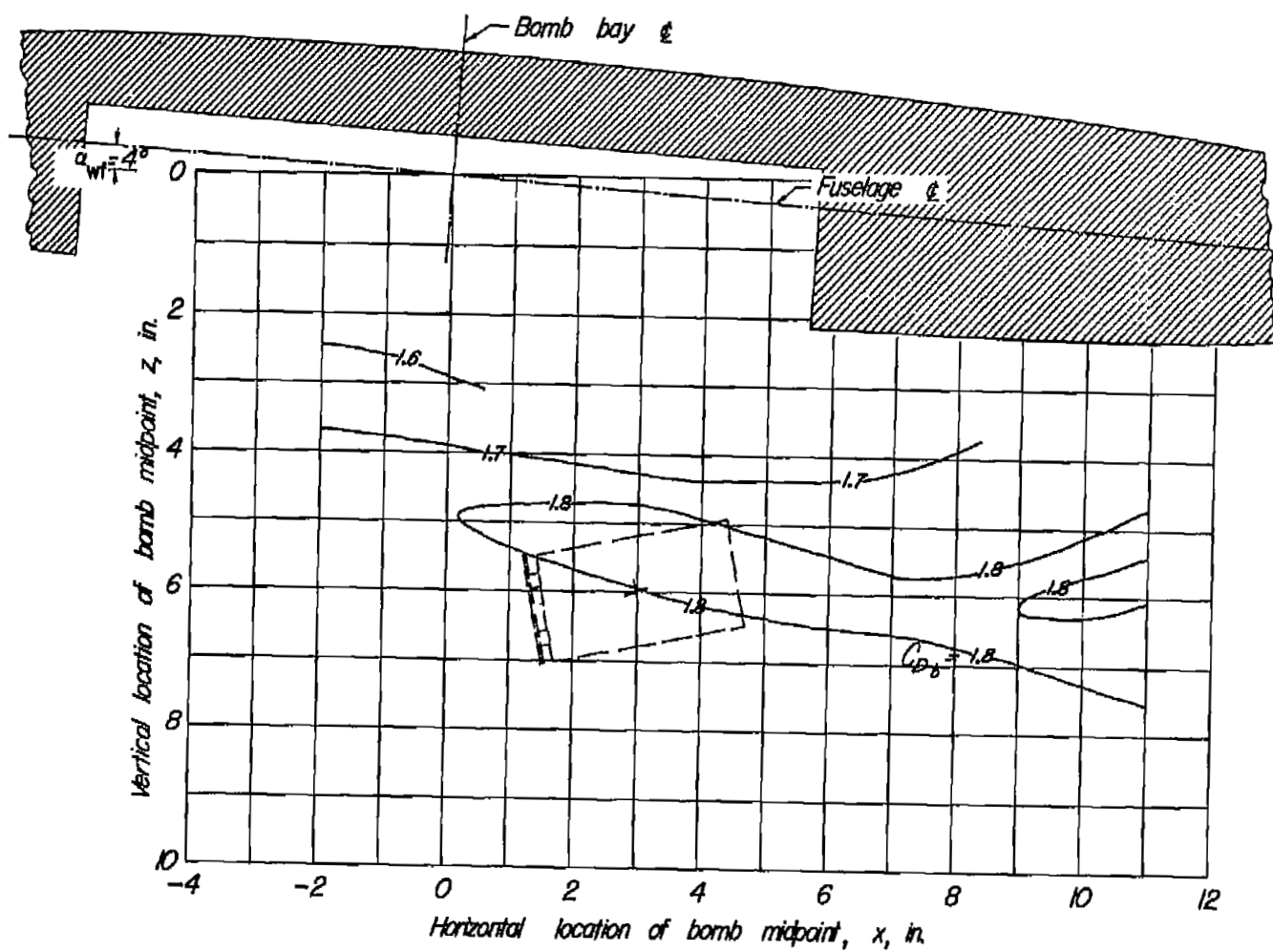
(c) $\alpha_b = 5^\circ$.

Figure 12.- Continued.



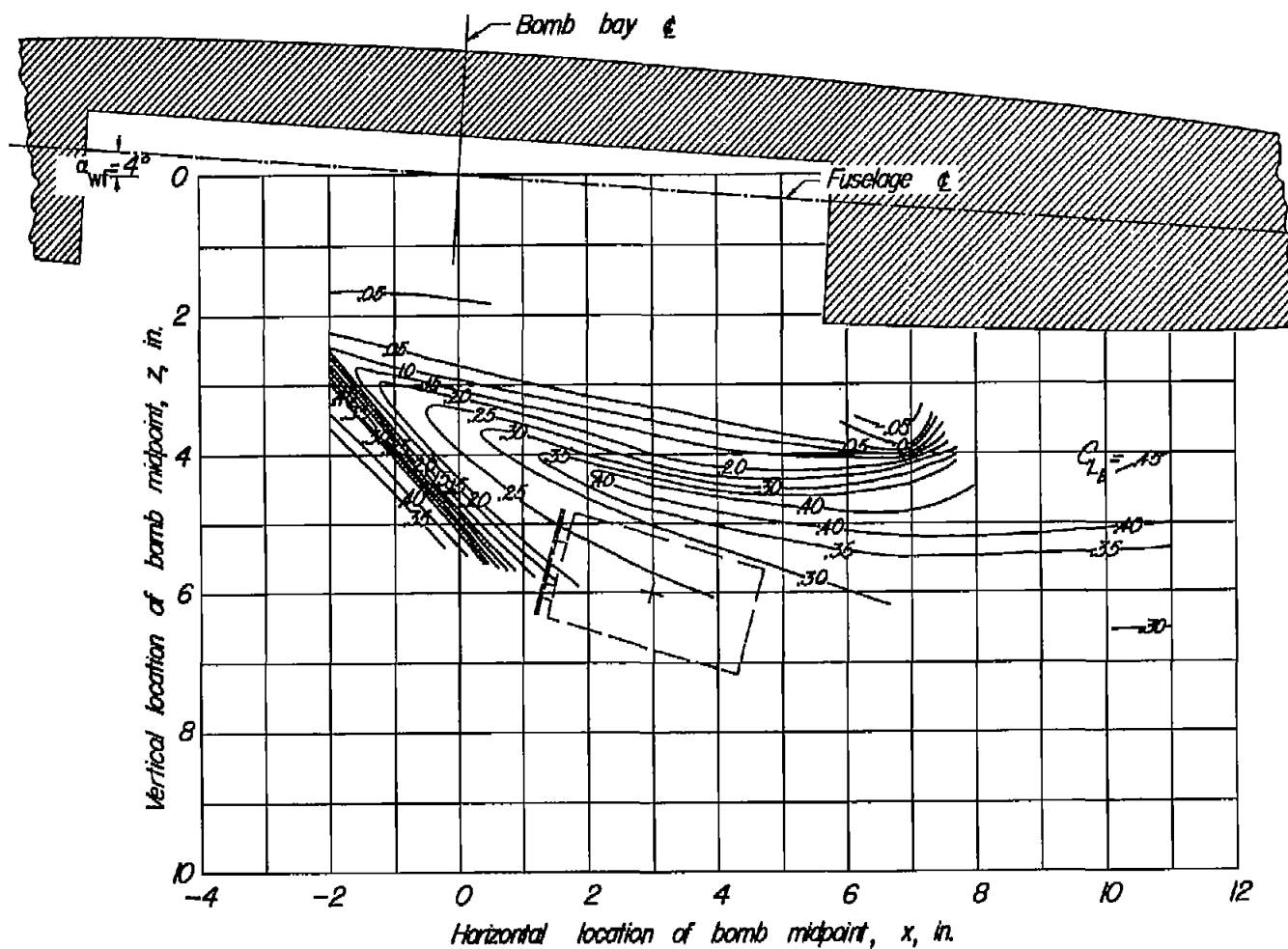
(e) $\alpha_b = -5^\circ$.

Figure 12.- Continued.



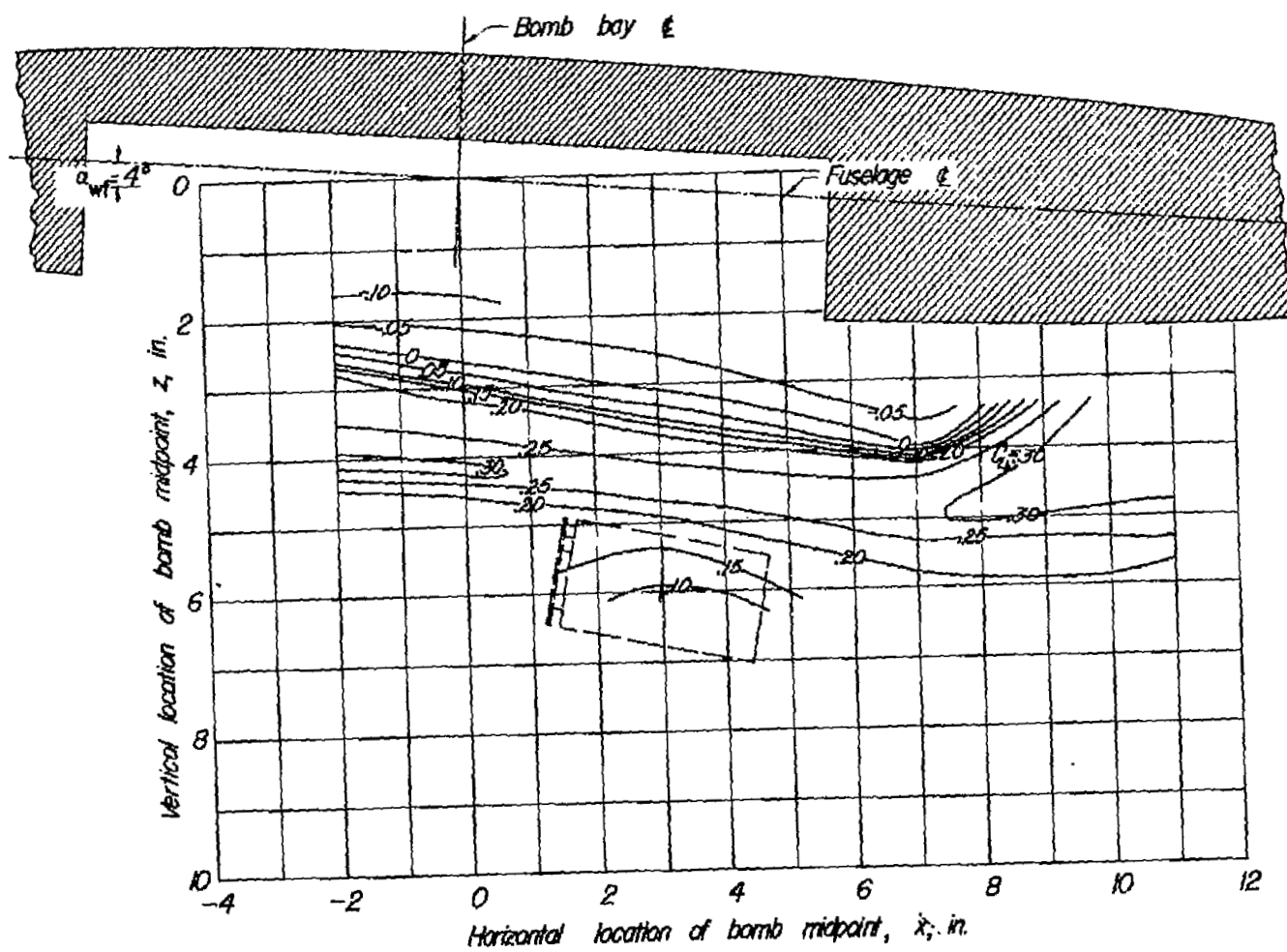
(f) $\alpha_b = -1.0^\circ$.

Figure 12.- Continued.



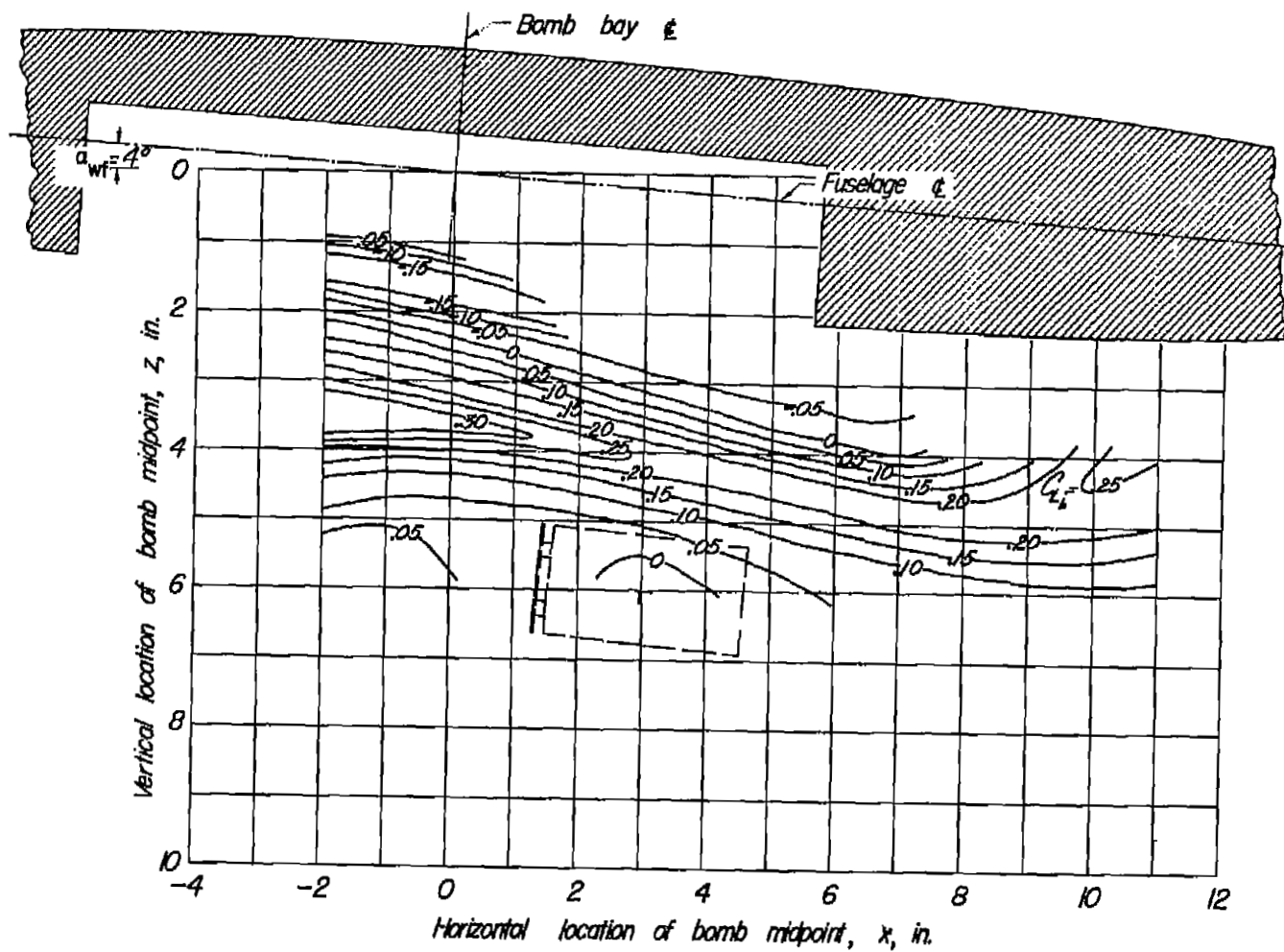
(a) $\alpha_b = 15^\circ$.

Figure 13.- Contour plot of lift coefficients of cylindrical bomb in presence of wing-fuselage combination.



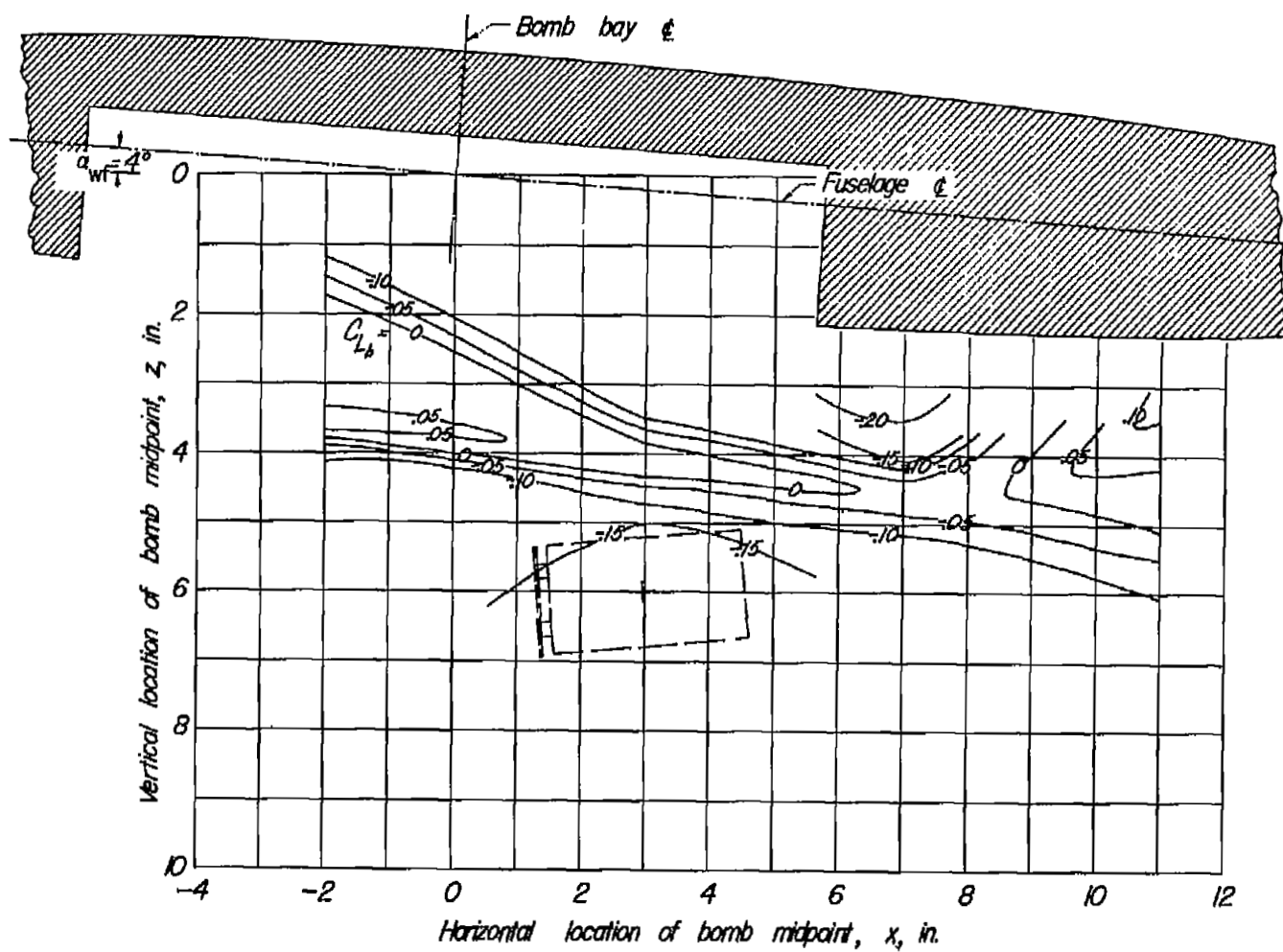
(b) $\alpha_b = 10^\circ$.

Figure 13.- Continued.



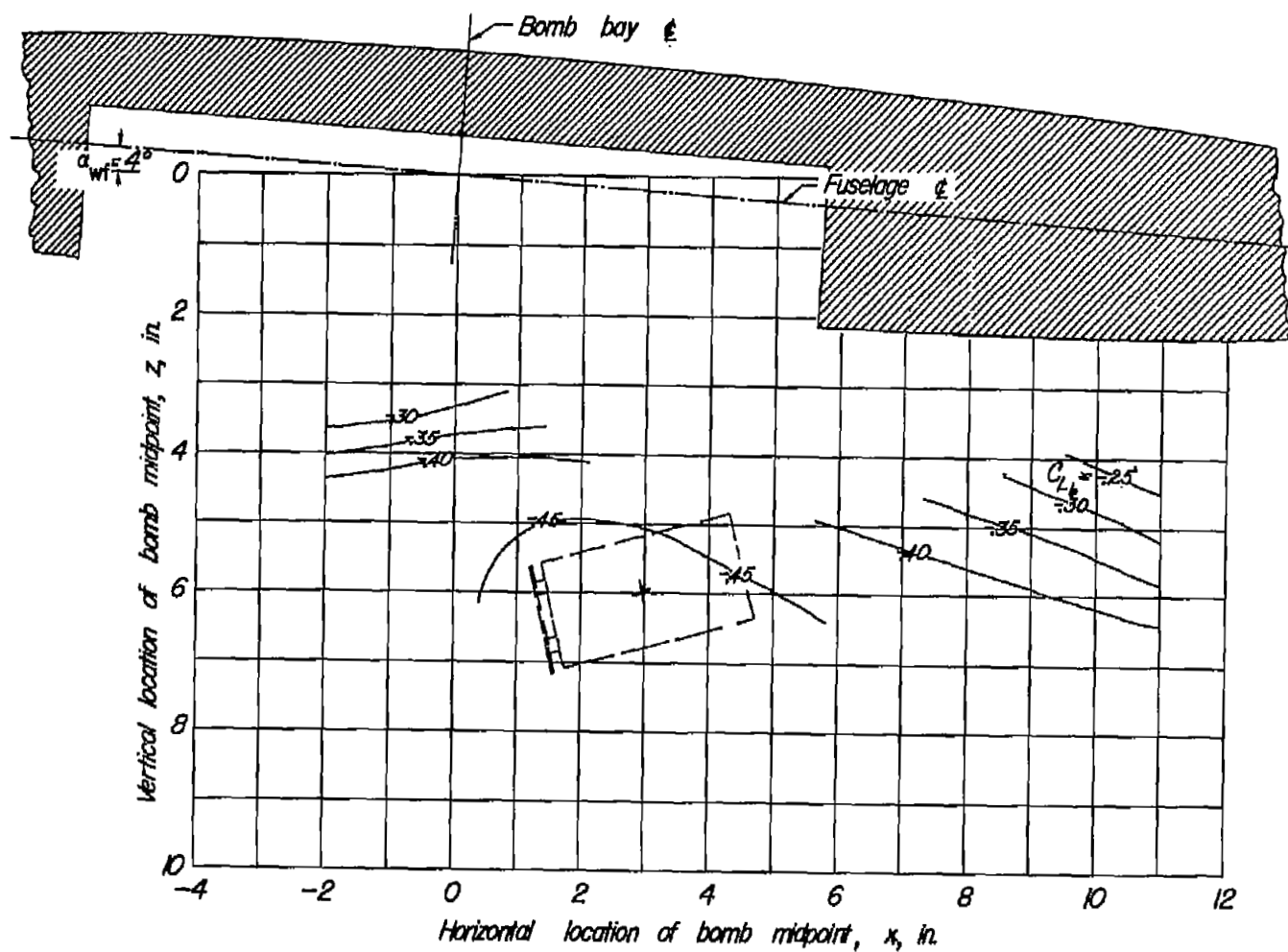
(c) $\alpha_b = 5^\circ$.

Figure 13.- Continued.



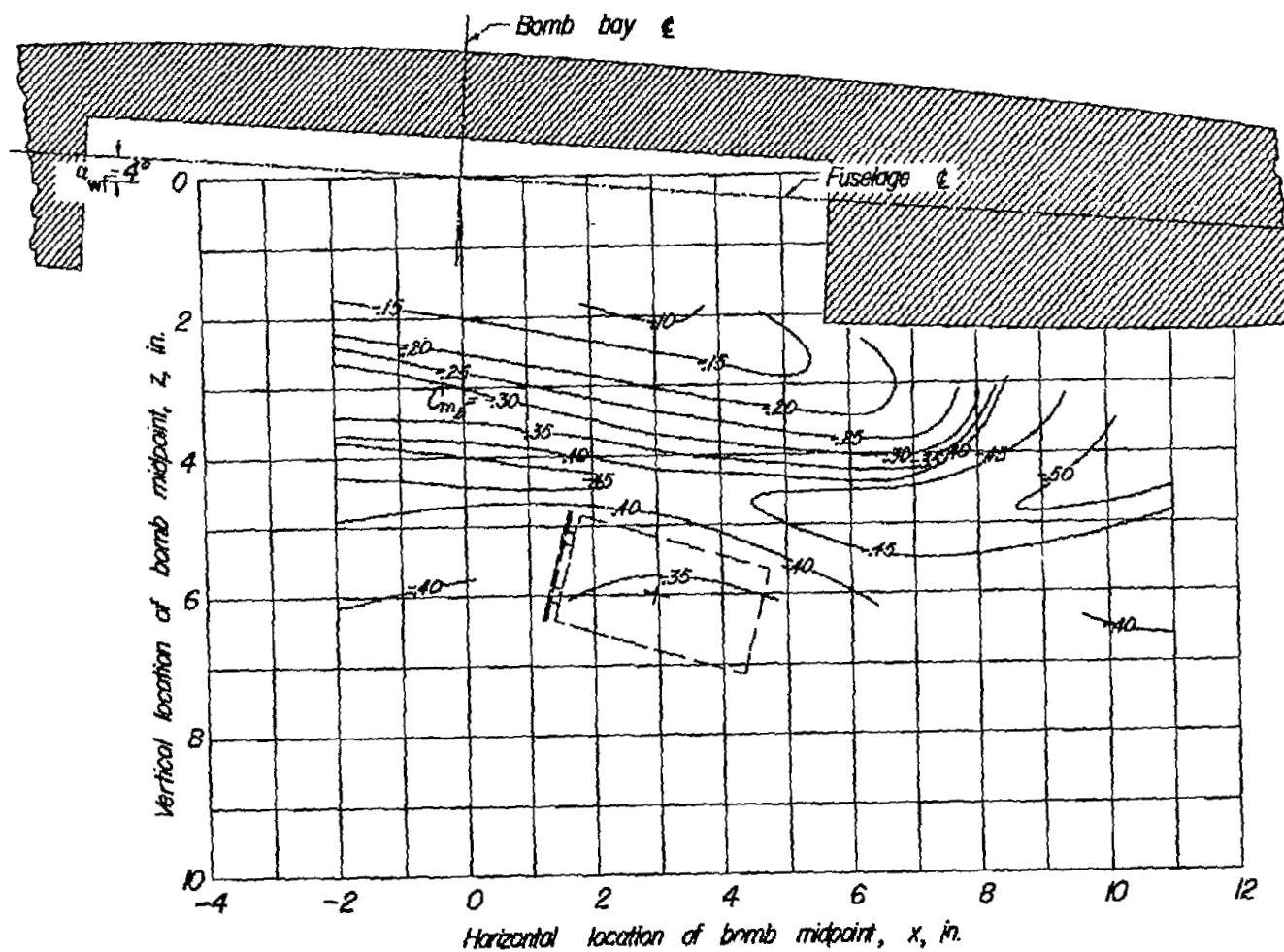
(e) $\alpha_D = -5^\circ$.

Figure 13.- Continued.



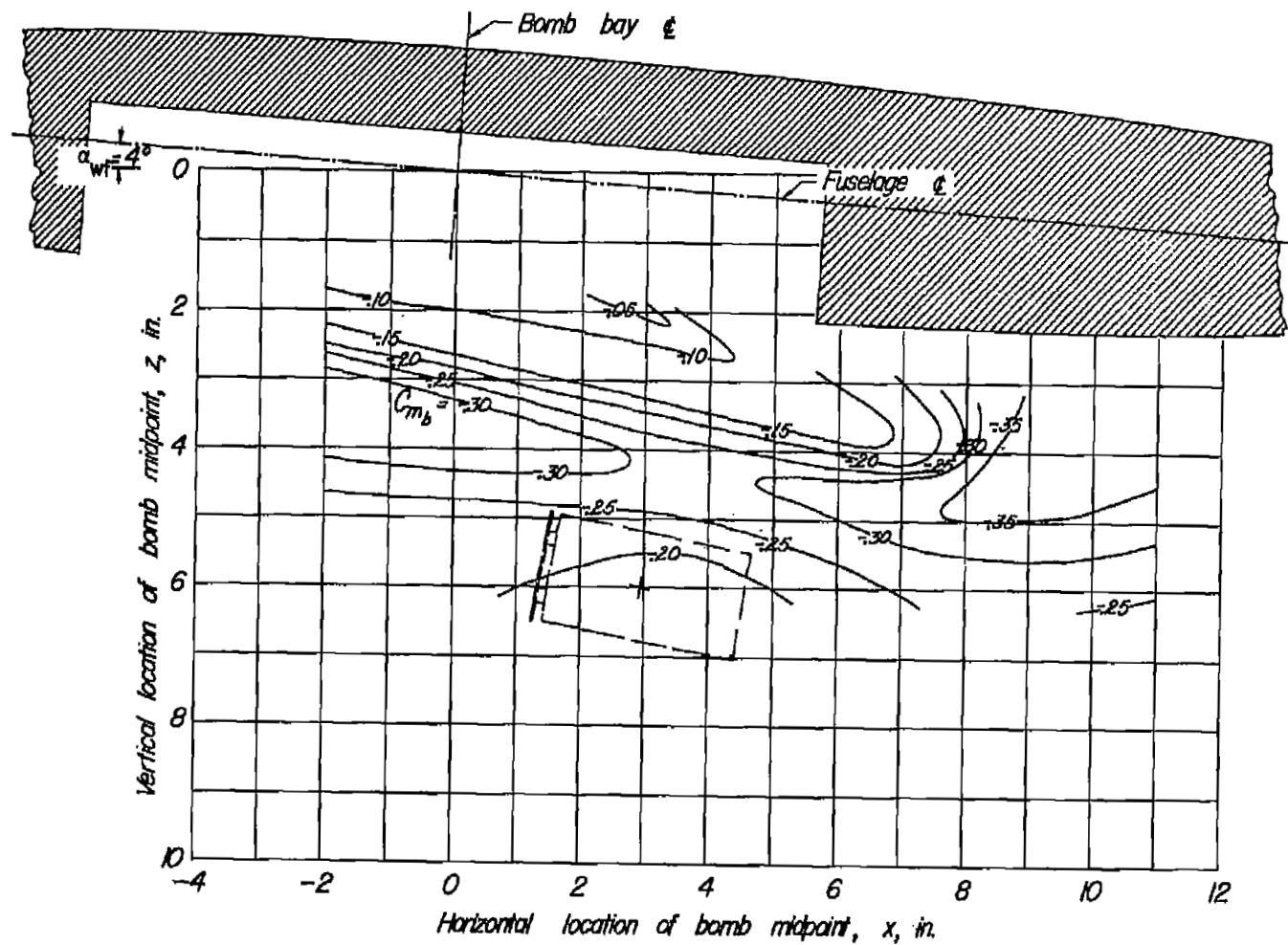
(g) $\alpha_b = -15^\circ$.

Figure 13.- Concluded.



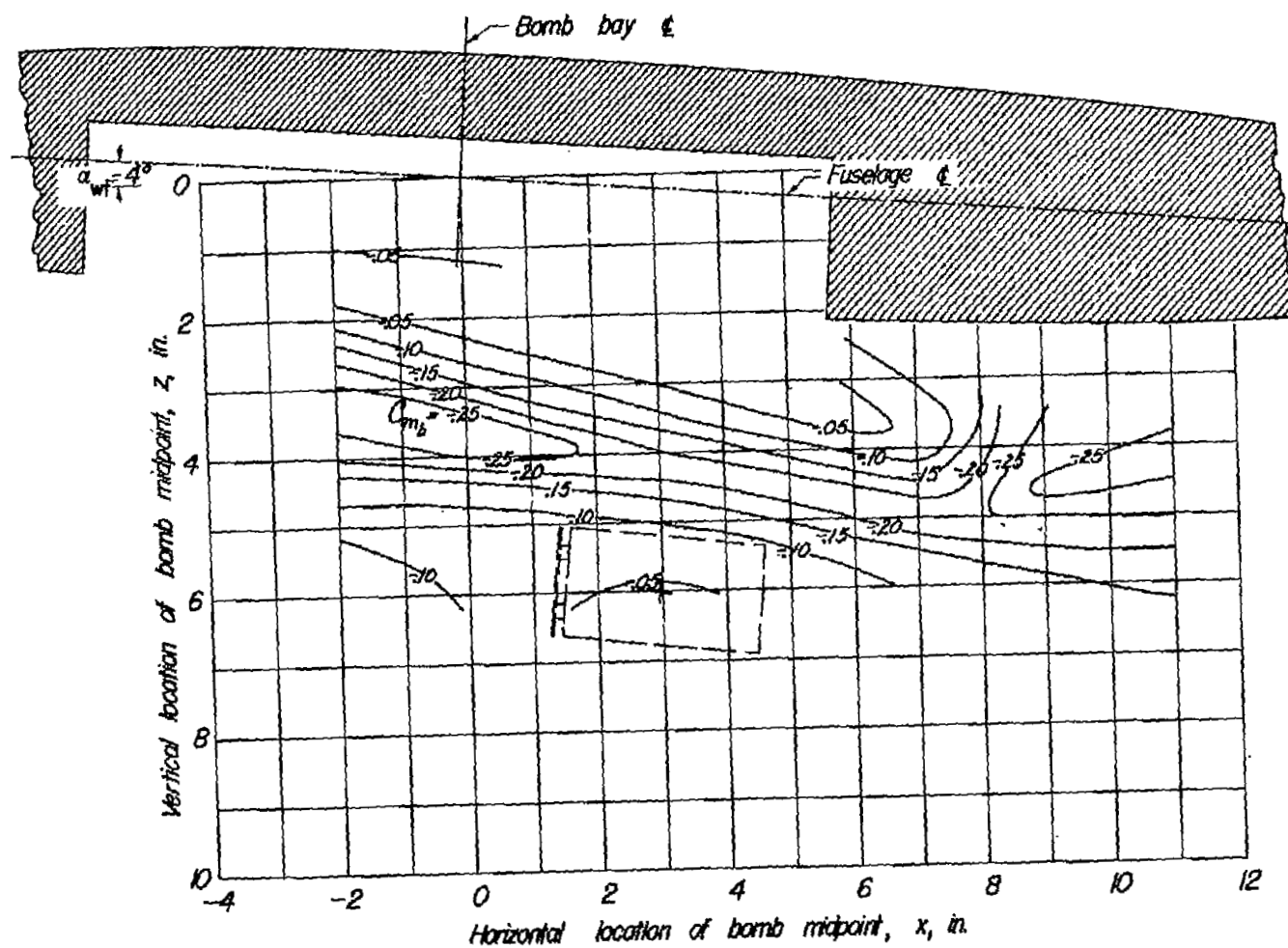
(s) $\alpha_D = 15^\circ$.

Figure 14.- Contour plot of pitching-moment coefficients of cylindrical bomb in presence of wing-fuselage combination.



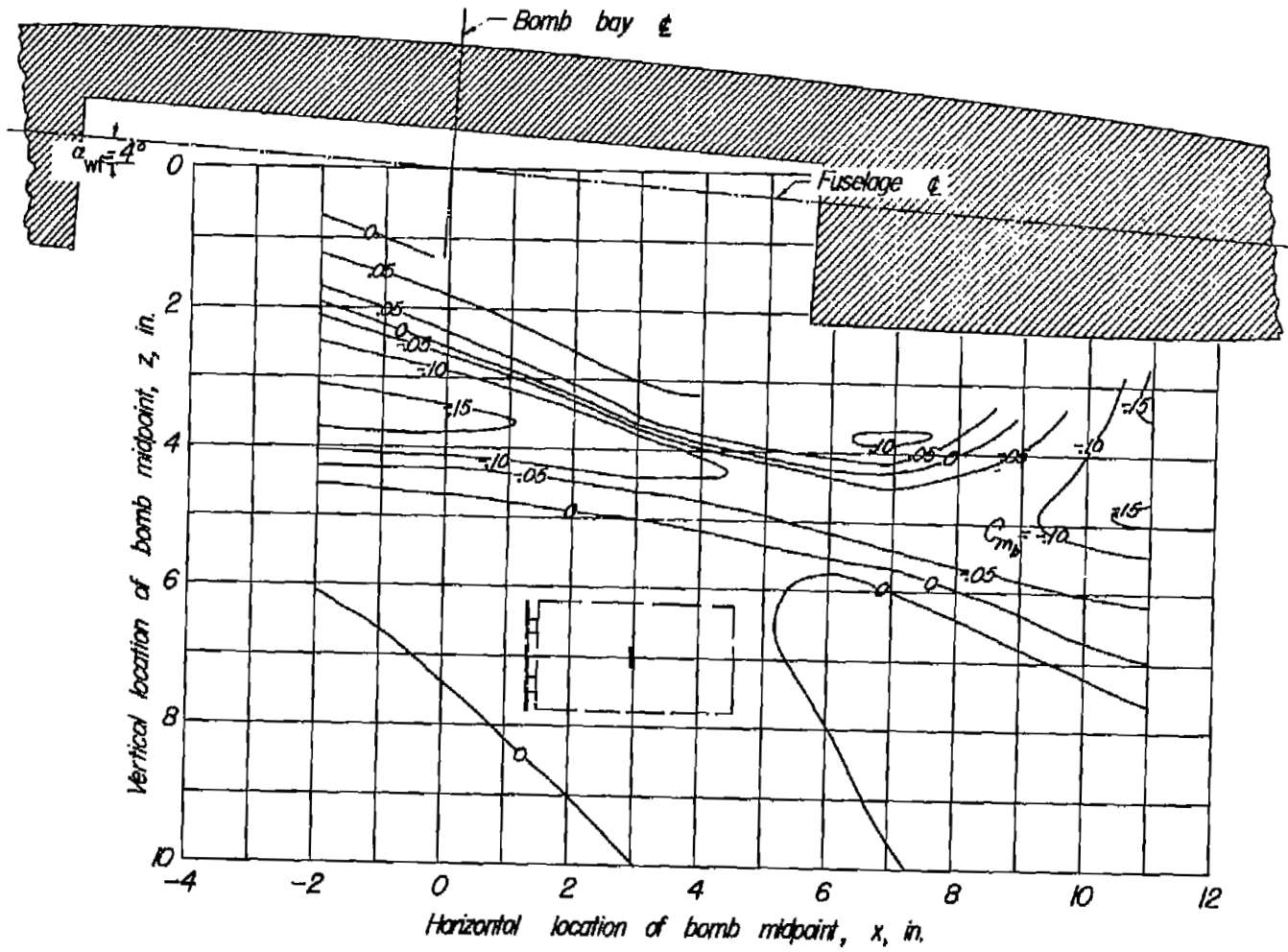
(b) $\alpha_b = 10^\circ$.

Figure 14.- Continued.



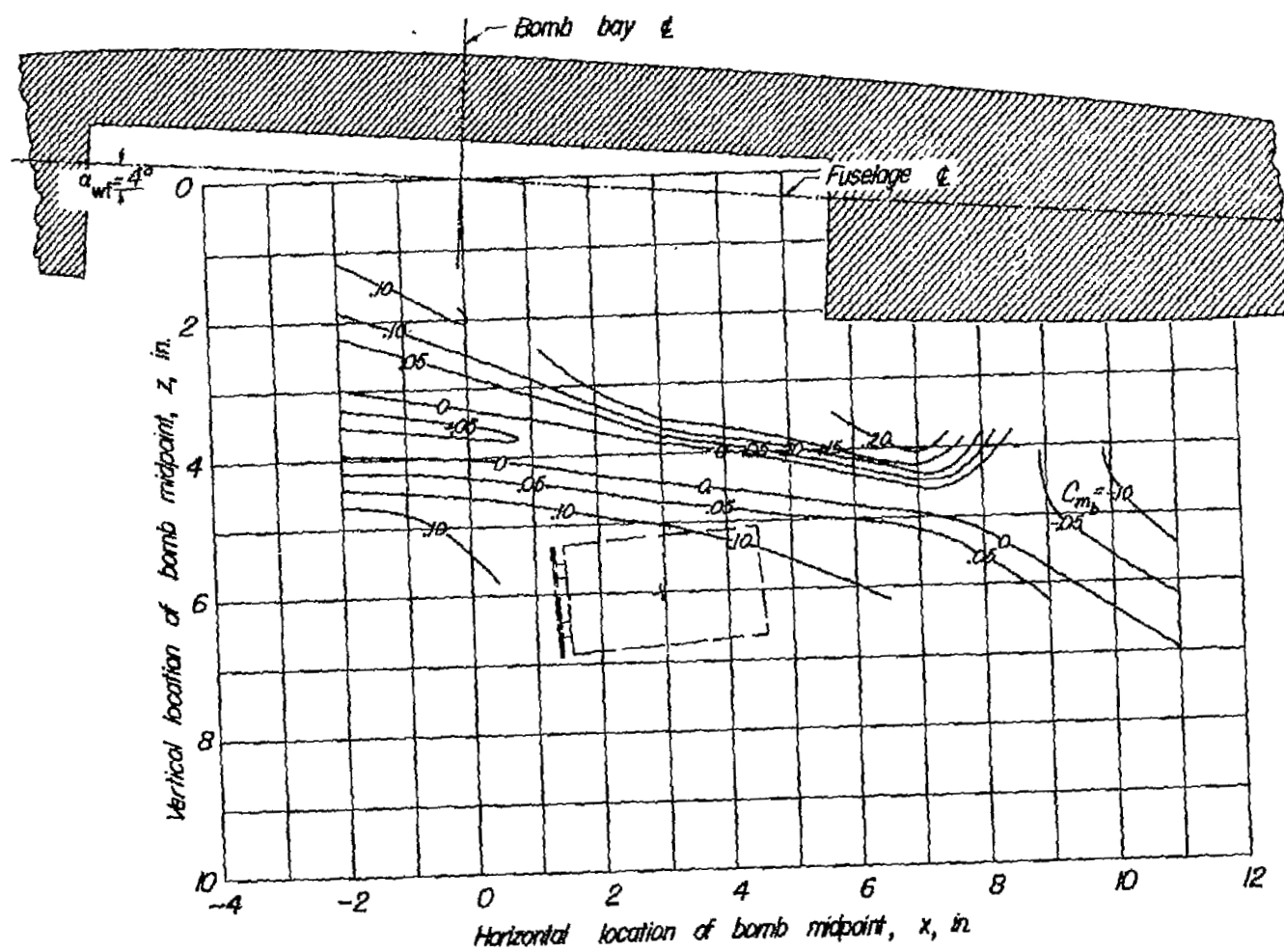
(c) $\alpha_D = 5^\circ$.

Figure 14.- Continued.



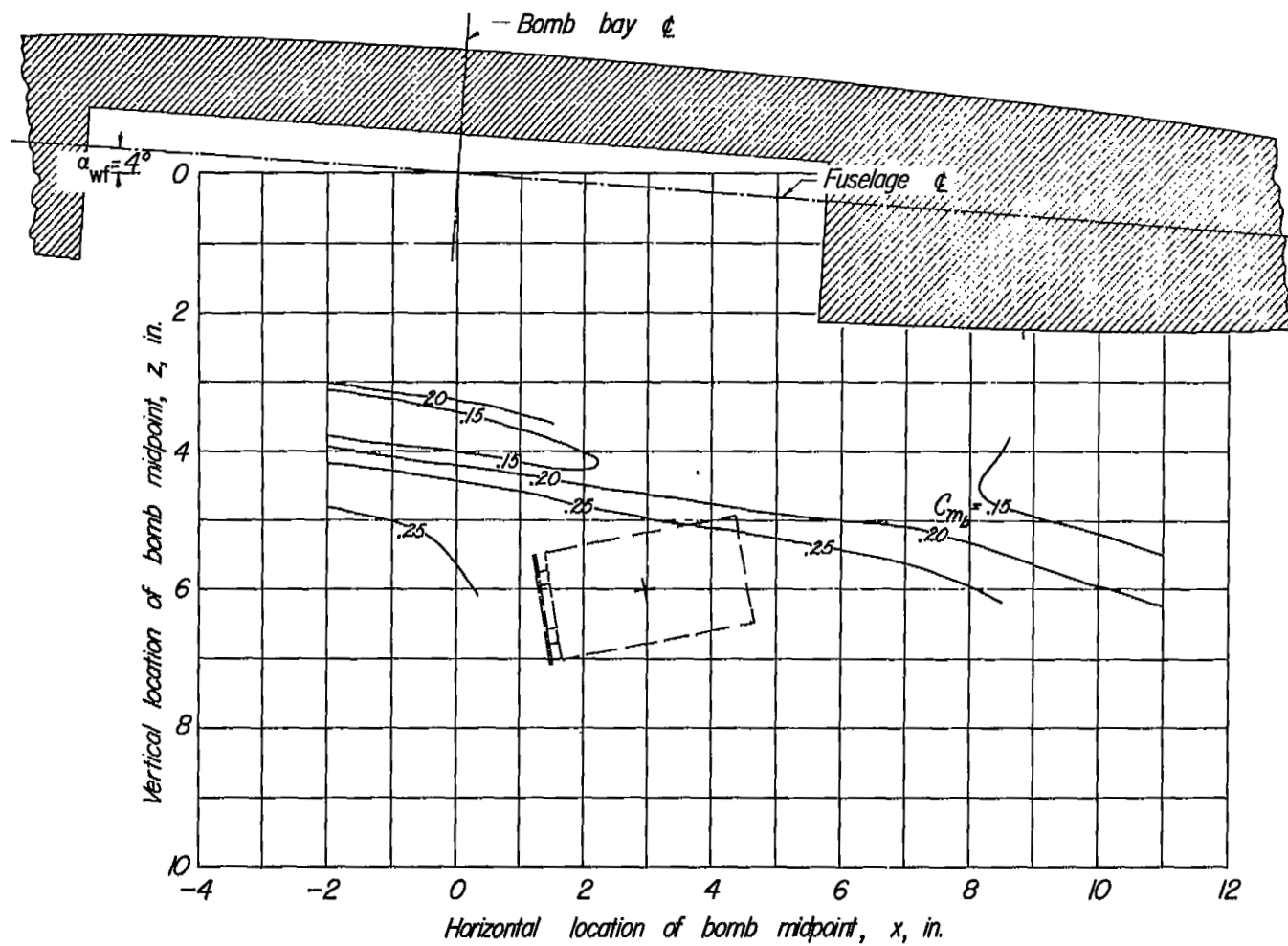
(d) $\alpha_0 = 0^\circ$.

Figure 14.- Continued.



(e) $\alpha_0 = -5^\circ$.

Figure 14.- Continued.



(f) $\alpha_b = -10^\circ$.

Figure 14.- Continued.

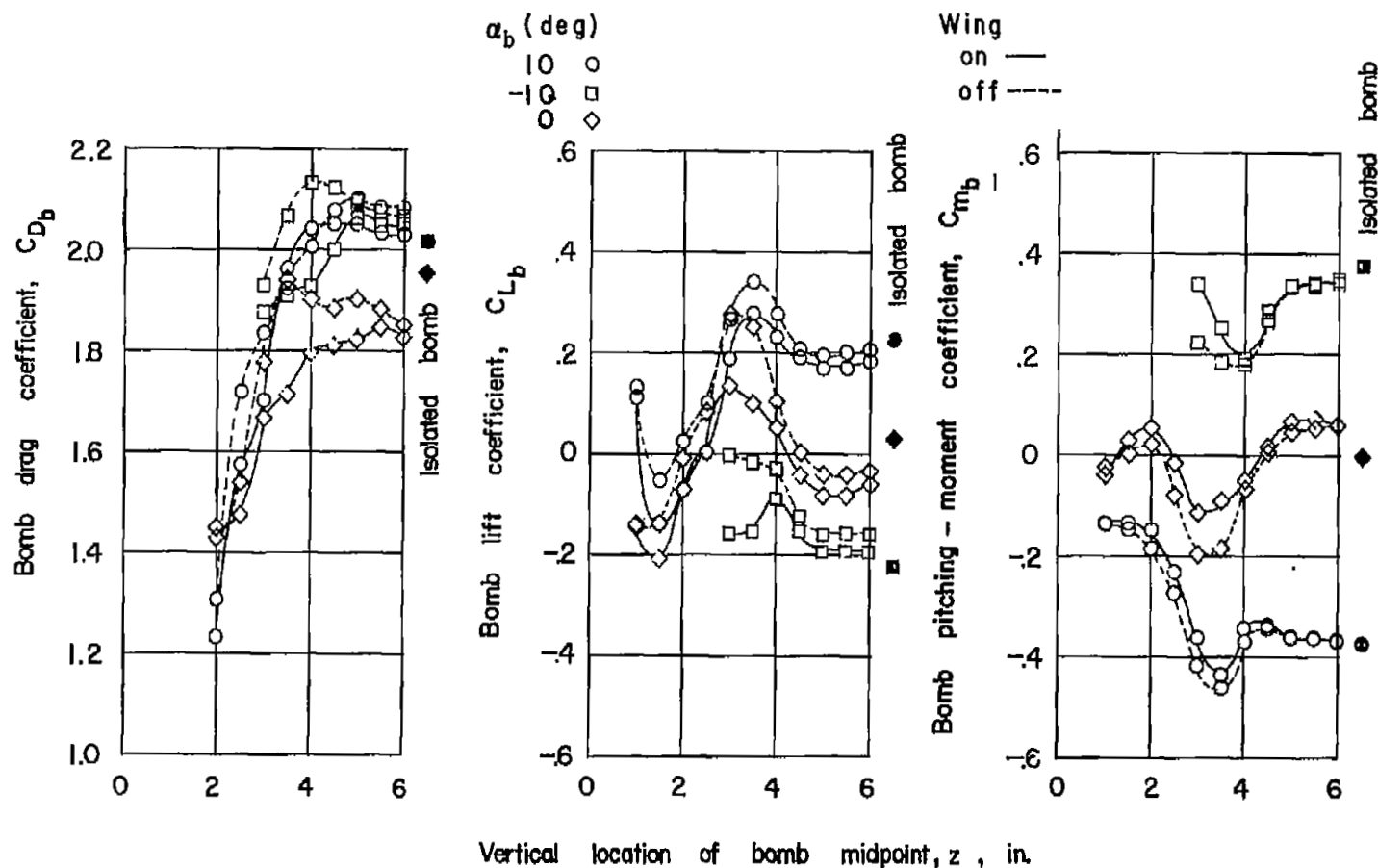


Figure 15.- Spool-bomb drag, lift, and pitching-moment coefficients in presence of wing-fuselage combination and fuselage alone. $x = -1.05$ inches; $\alpha_{wf} = 4^\circ$.

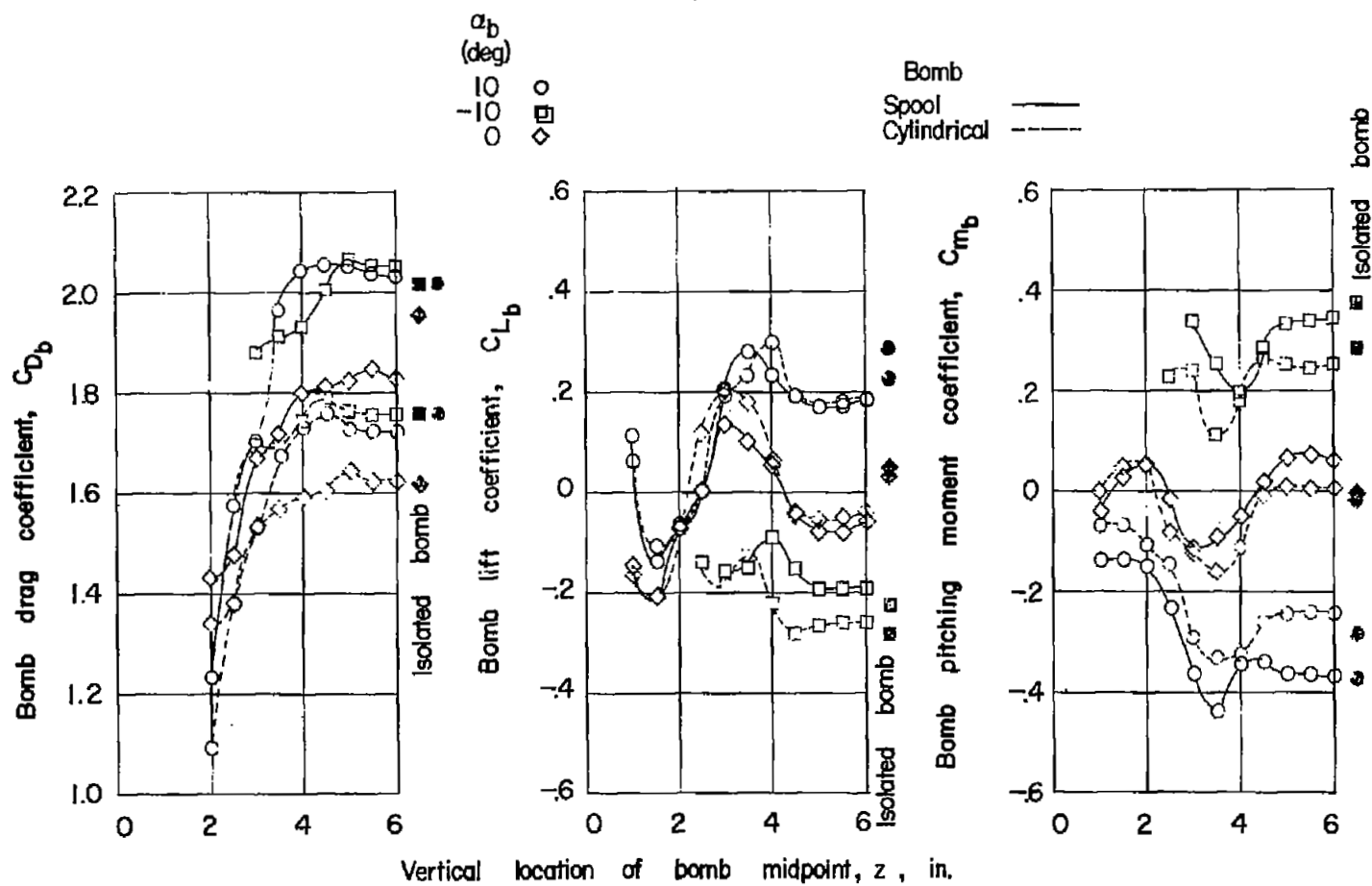
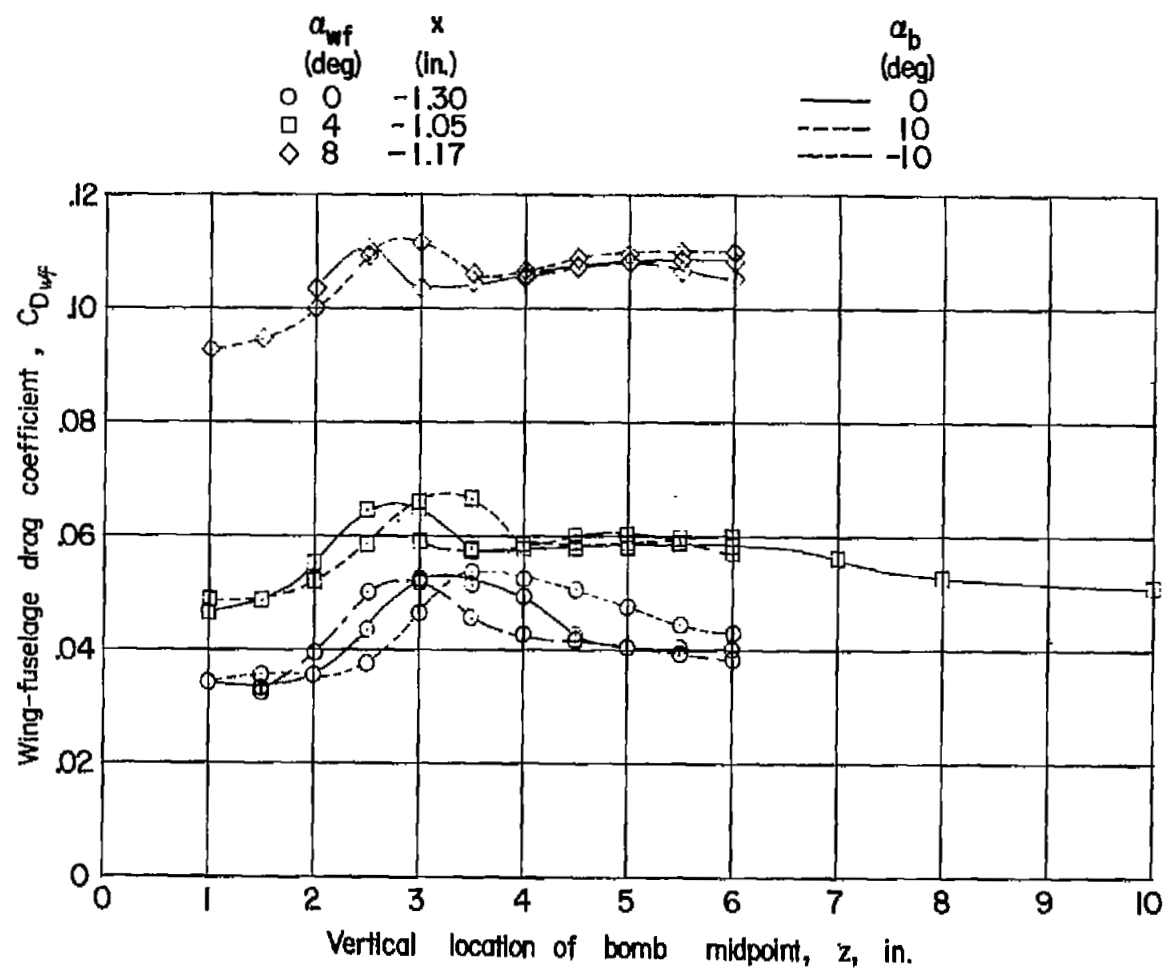
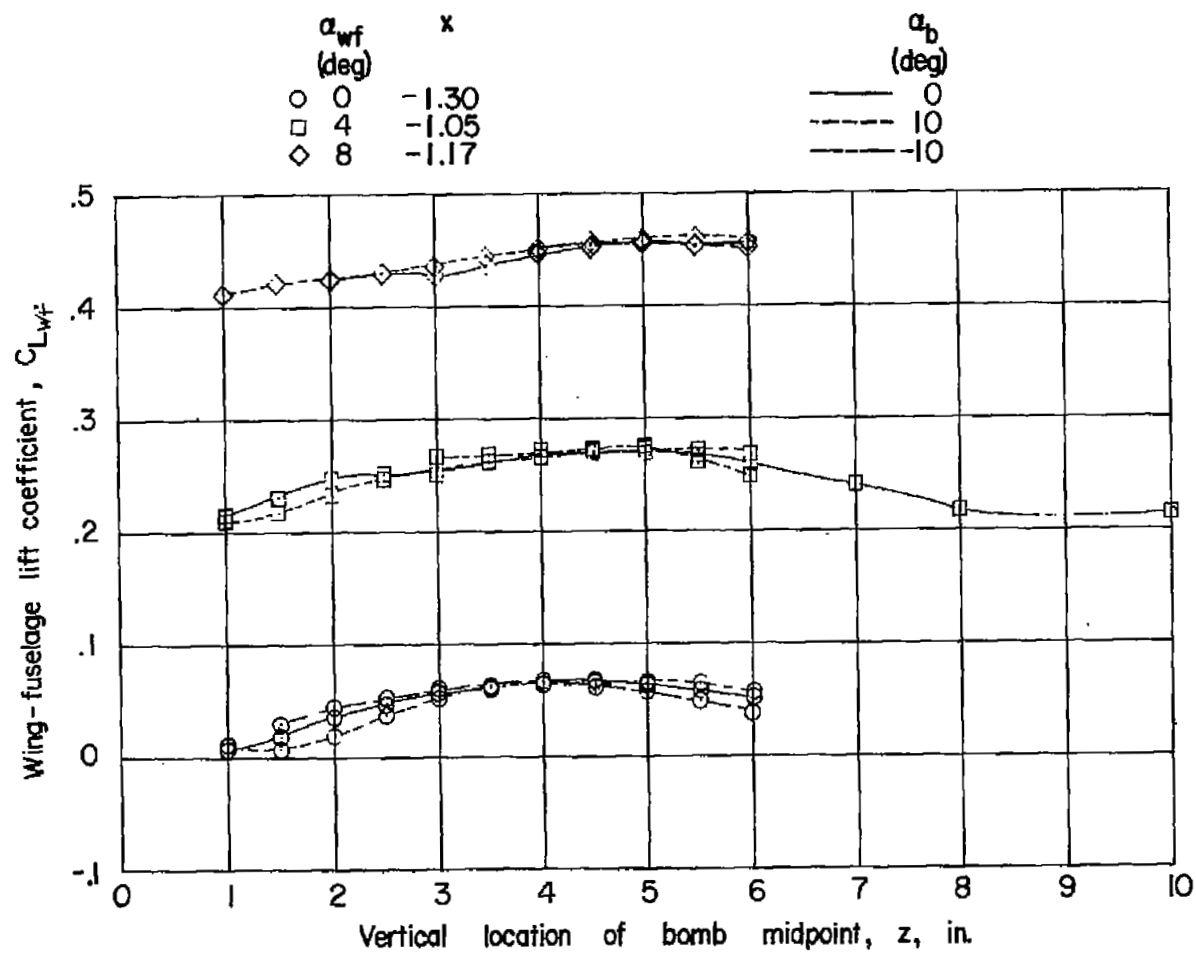


Figure 16.- Comparison of force and moment coefficients of spool and cylindrical bombs in presence of wing-fuselage combination. $x = -1.05$ inches; $\alpha_{wf} = 4^\circ$.



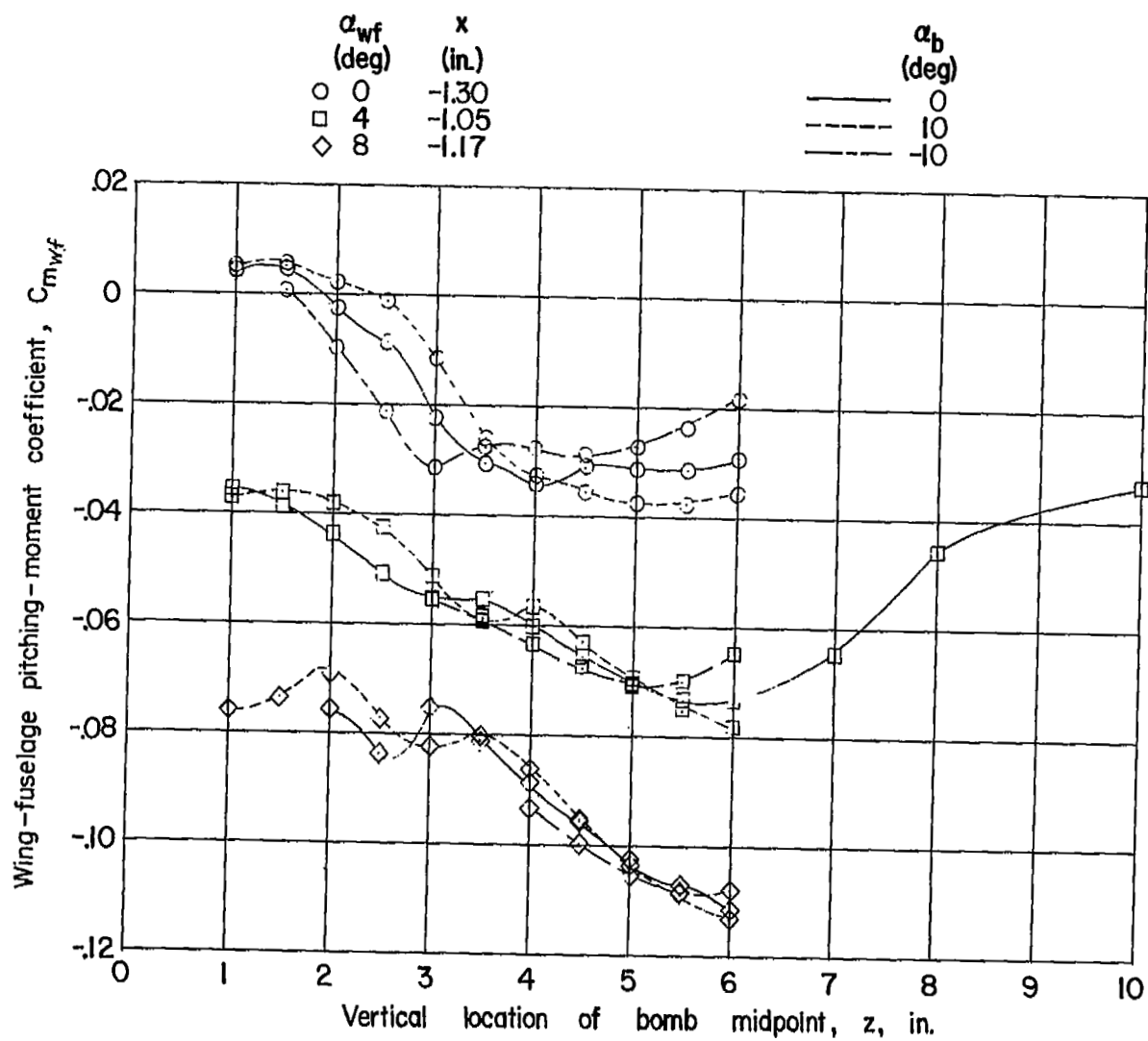
(a) Drag coefficient.

Figure 17.- Force and moment data for wing-fuselage combination in presence of spool bomb. Tail off; $x = -1.05$ to -1.30 inches.



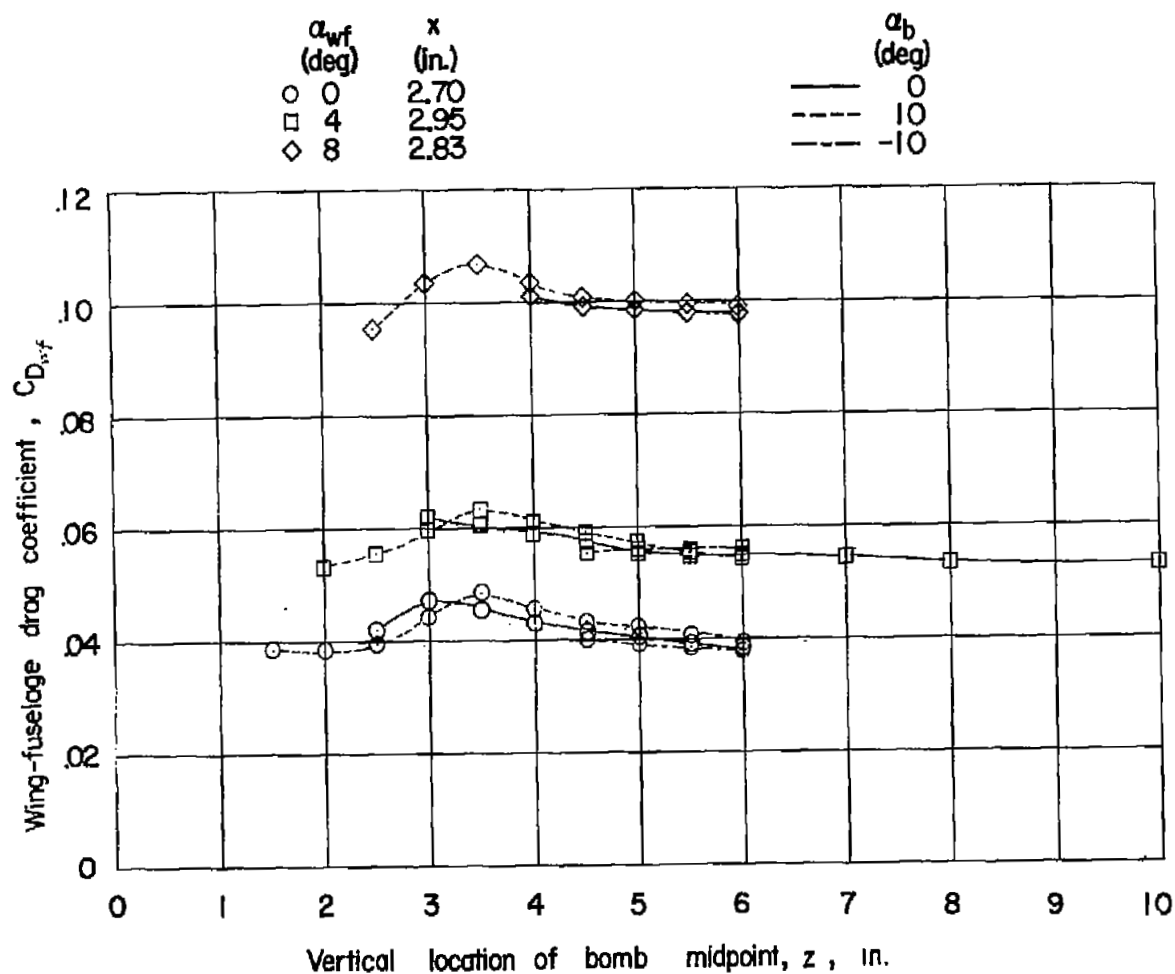
(b) Lift coefficient.

Figure 17.- Continued.



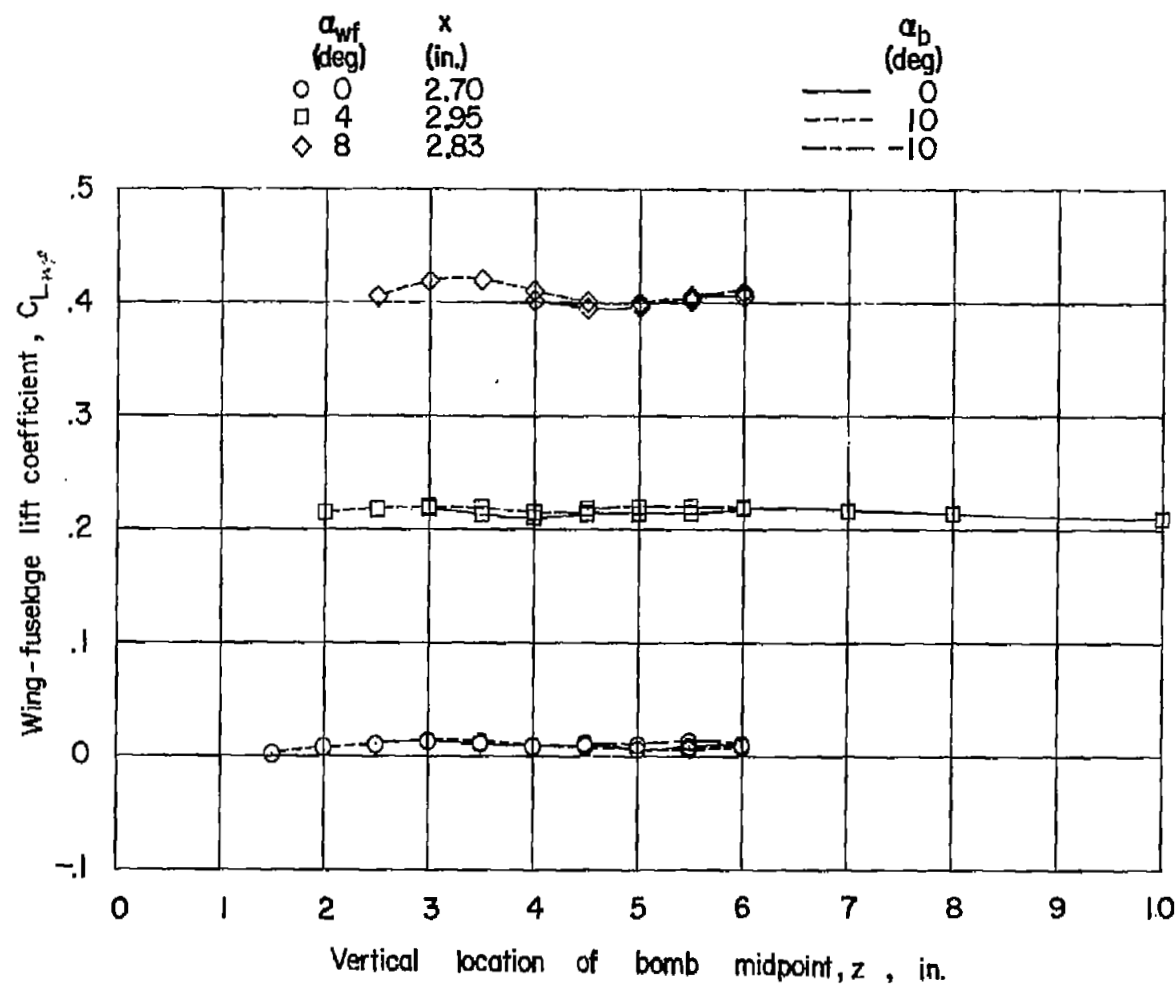
(c) Pitching-moment coefficient.

Figure 17.- Concluded.



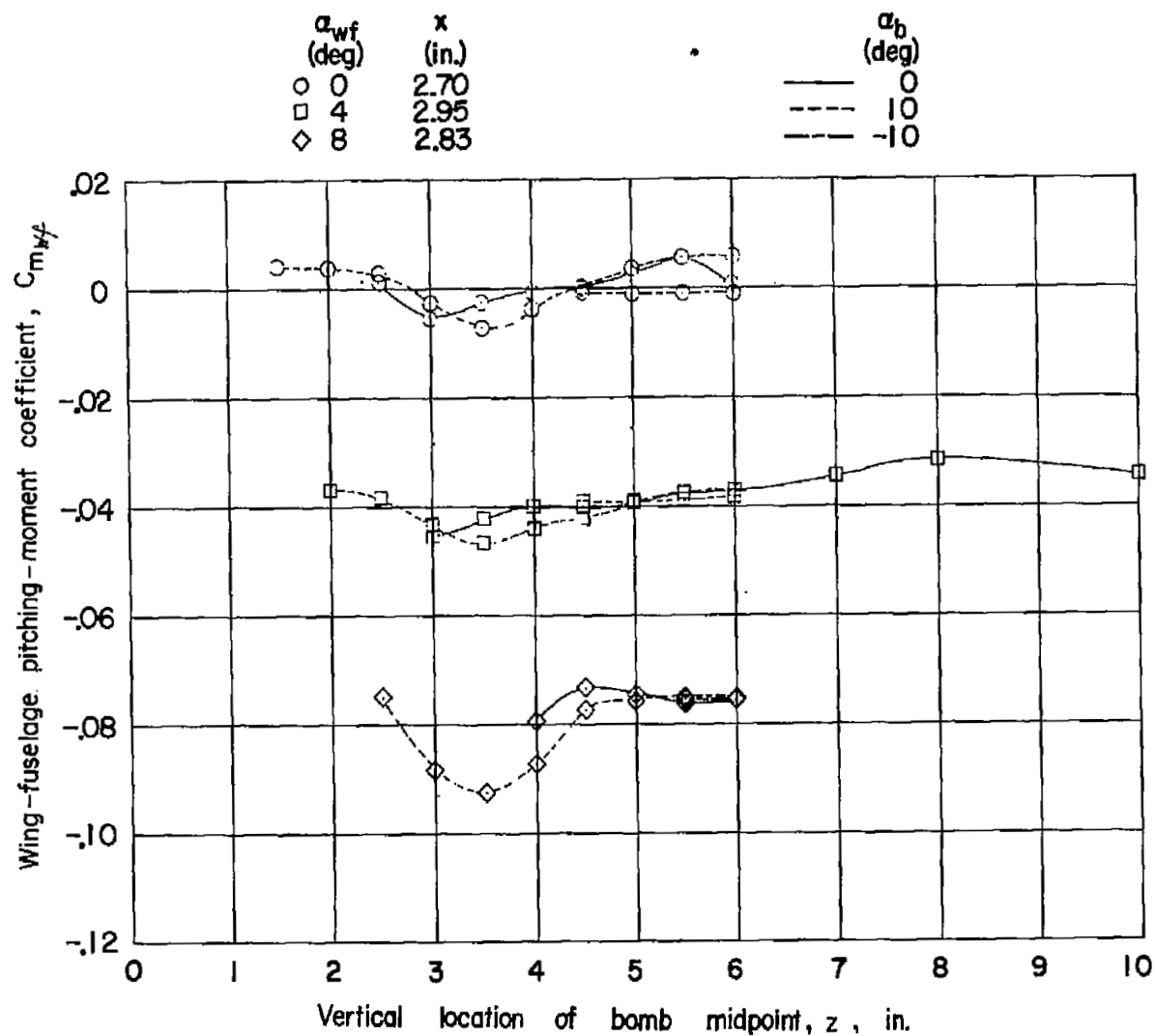
(a) Drag coefficient.

Figure 18.- Force and moment data for wing-fuselage combination in presence of spool bomb. Tail off; $x = 2.70$ to 2.95 inches.



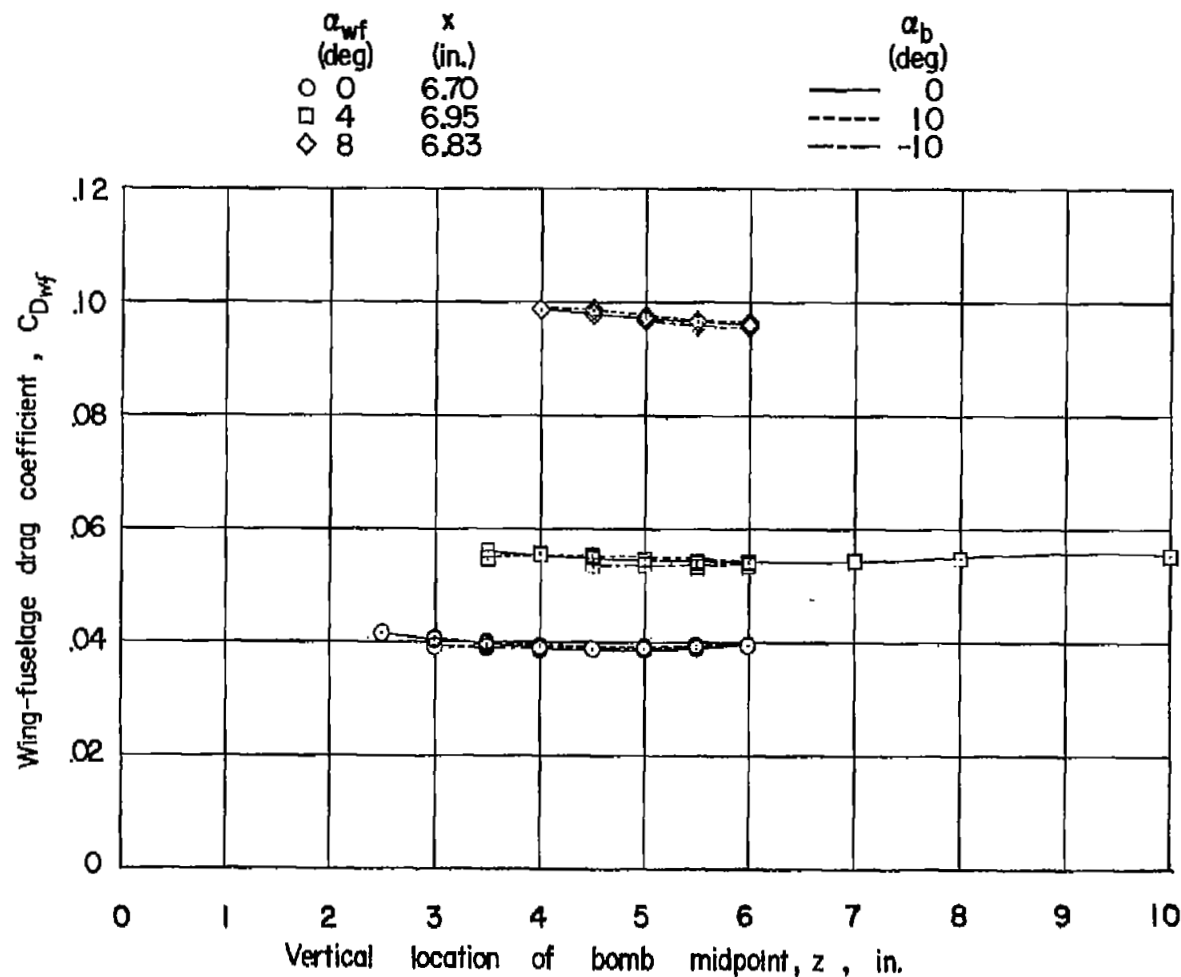
(b) Lift coefficient.

Figure 18.- Continued.



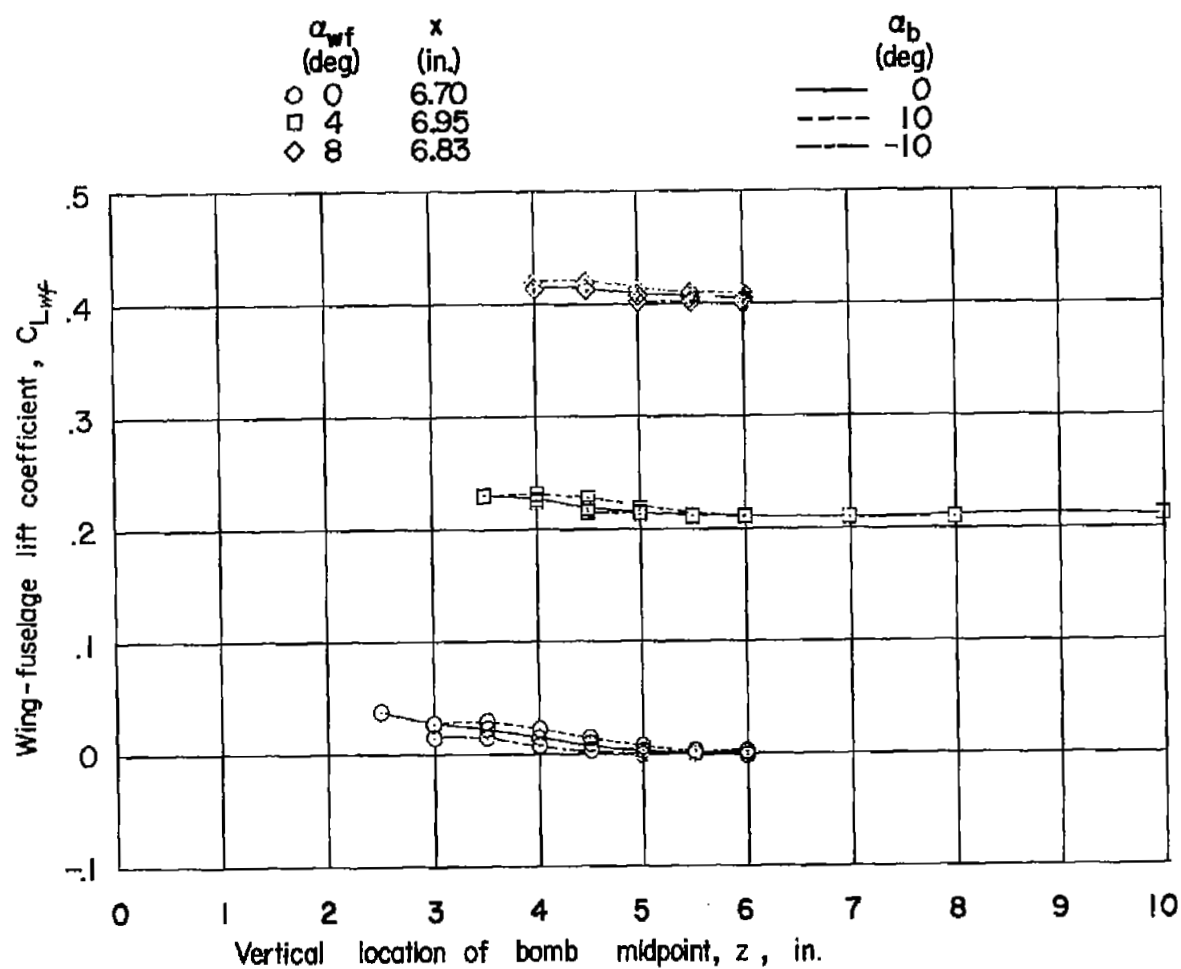
(c) Pitching-moment coefficient.

Figure 18.- Concluded.



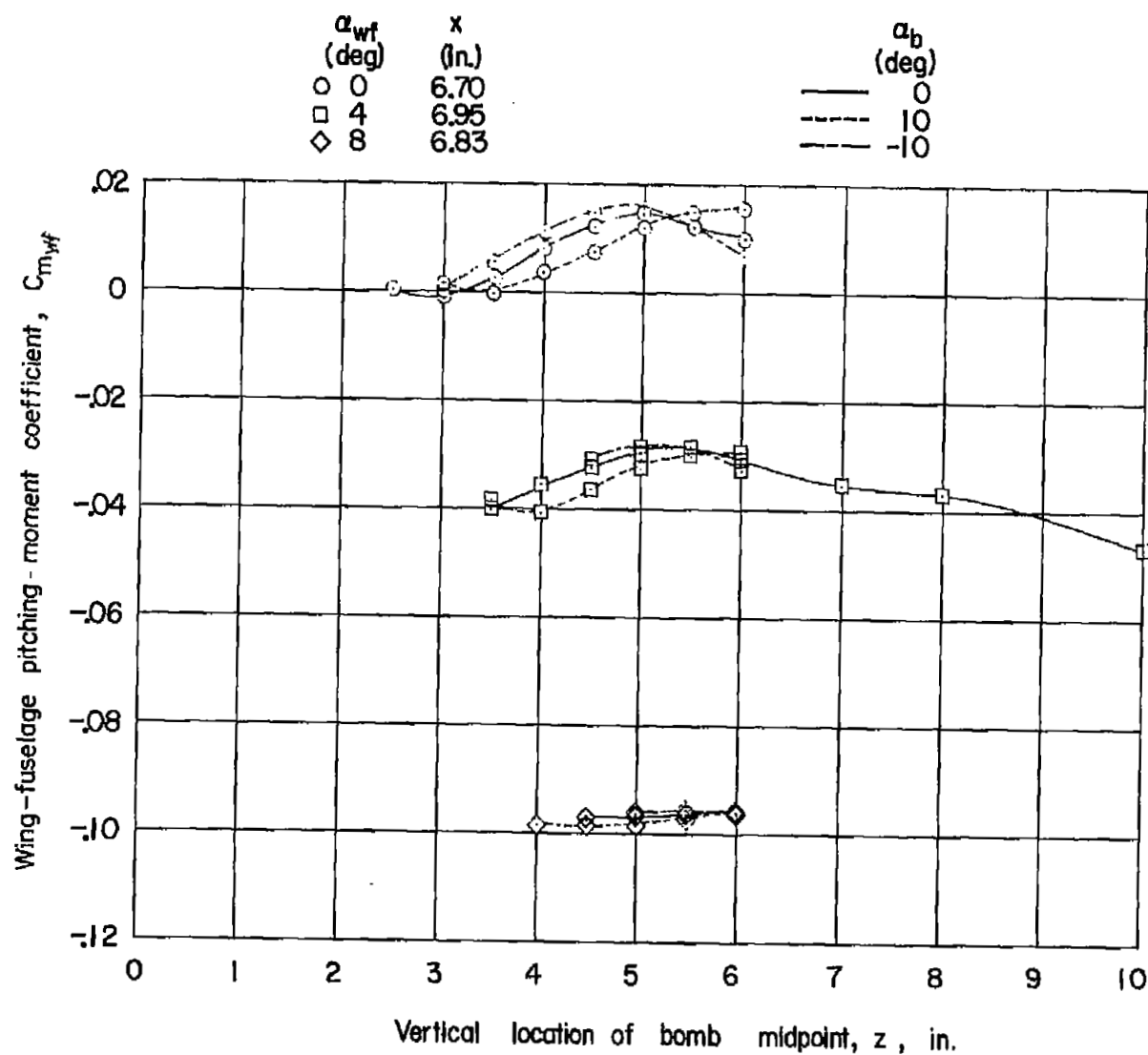
(a) Drag coefficient.

Figure 19.- Force and moment data for wing-fuselage combination in presence of spool bomb. Tail off; $x = 6.70$ to 6.95 inches.



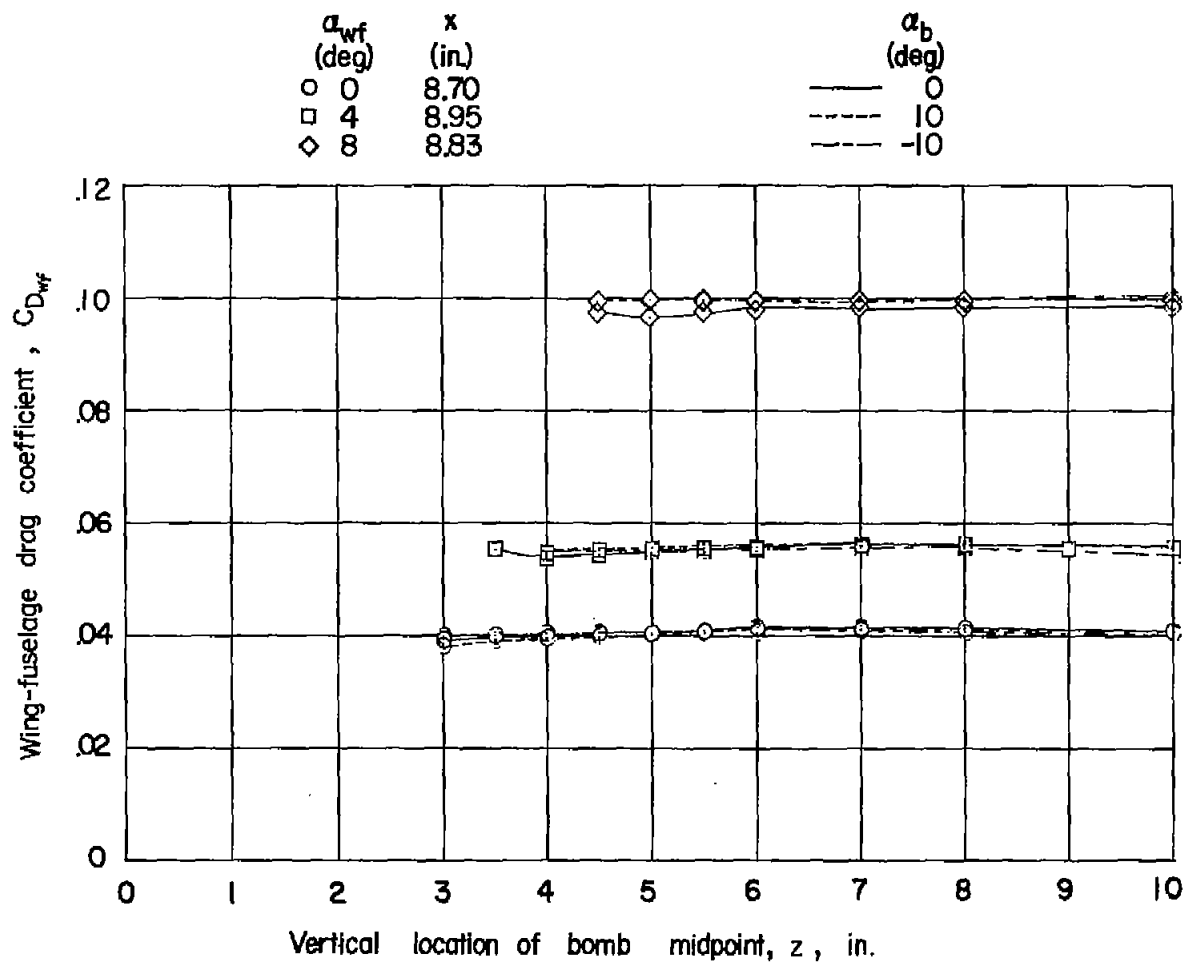
(b) Lift coefficient.

Figure 19.- Continued.



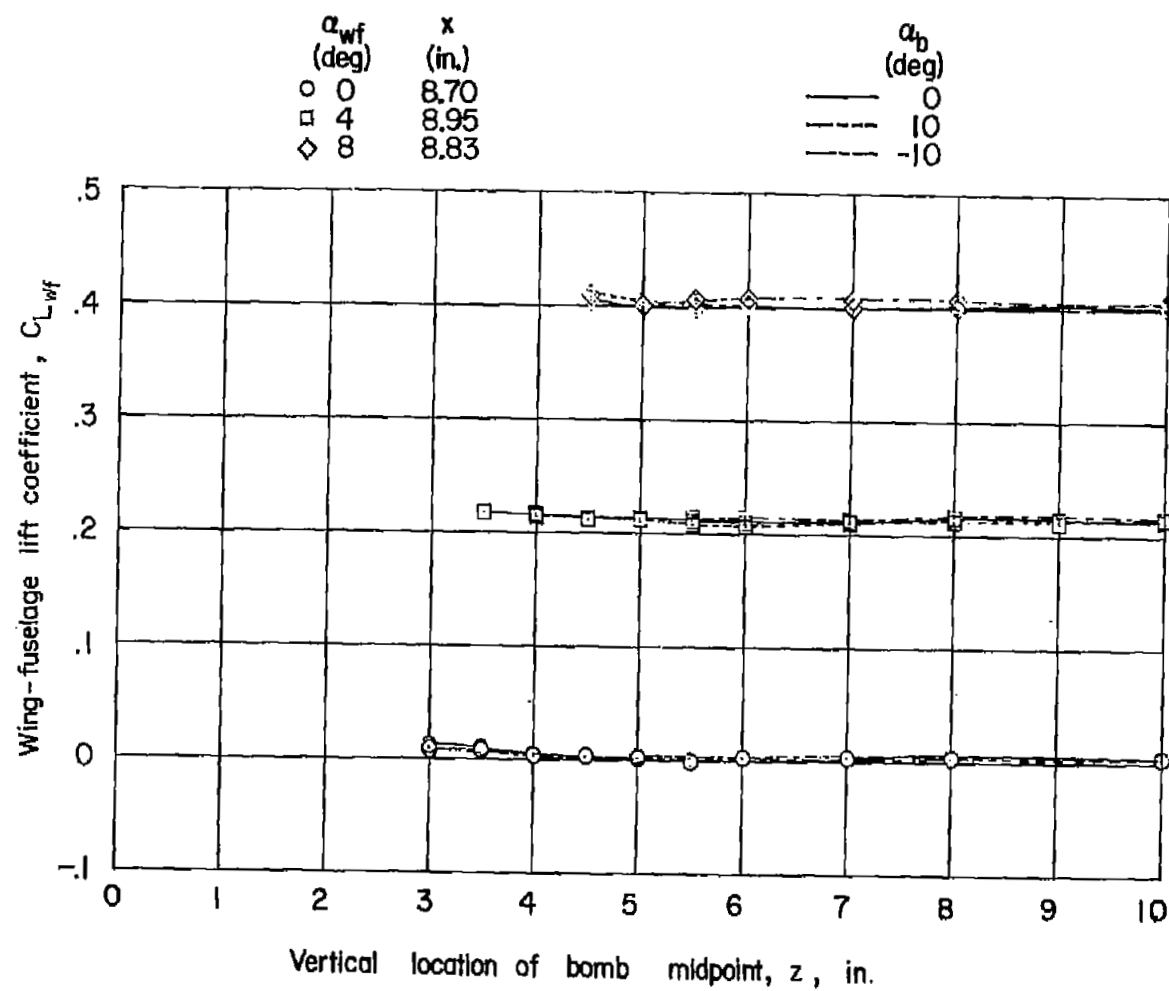
(c) Pitching-moment coefficient.

Figure 19.- Concluded.



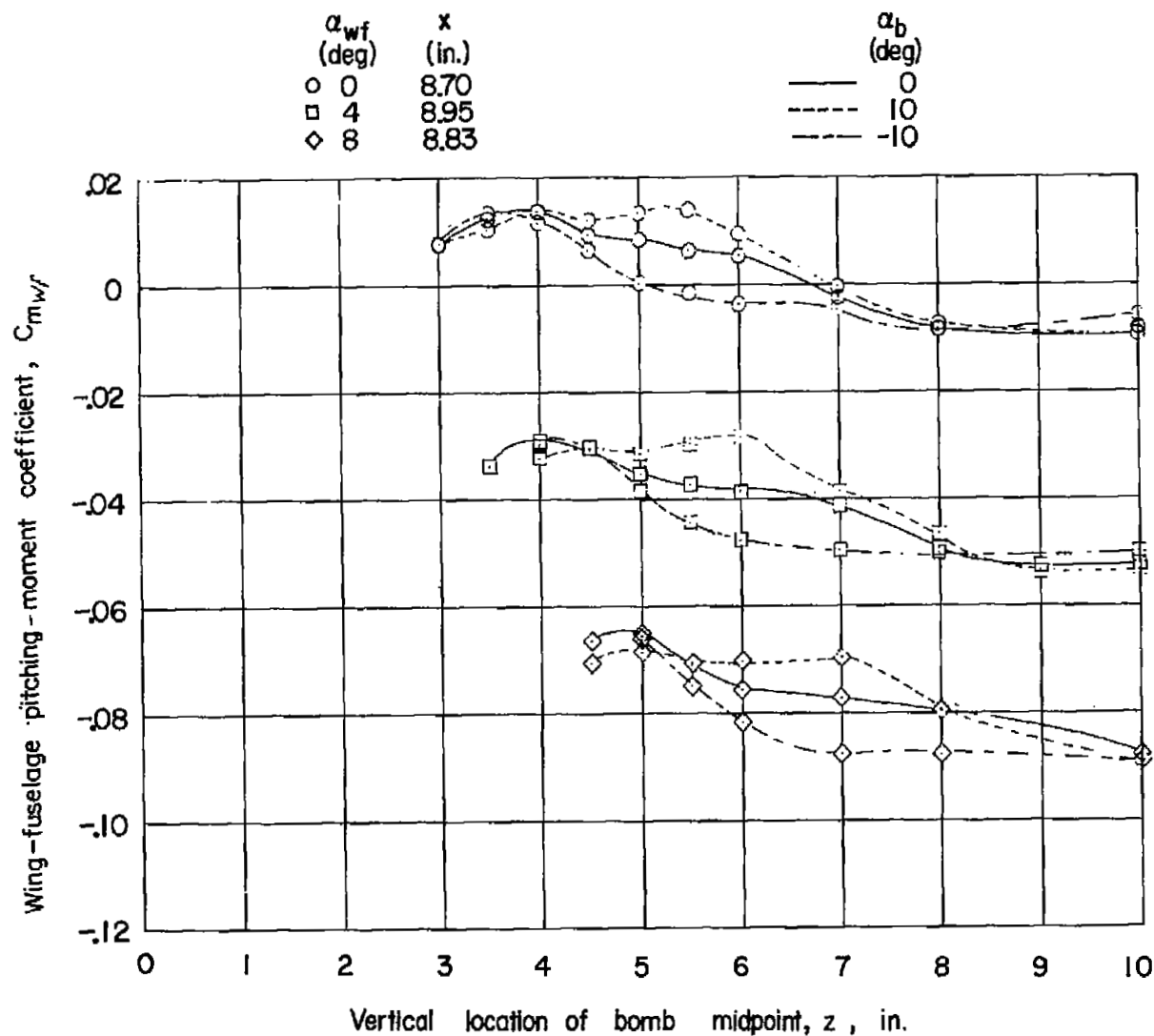
(a) Drag coefficient.

Figure 20.- Force and moment data for wing-fuselage combination in presence of spool bomb. Tail off; $x = 8.70$ to 8.95 inches.



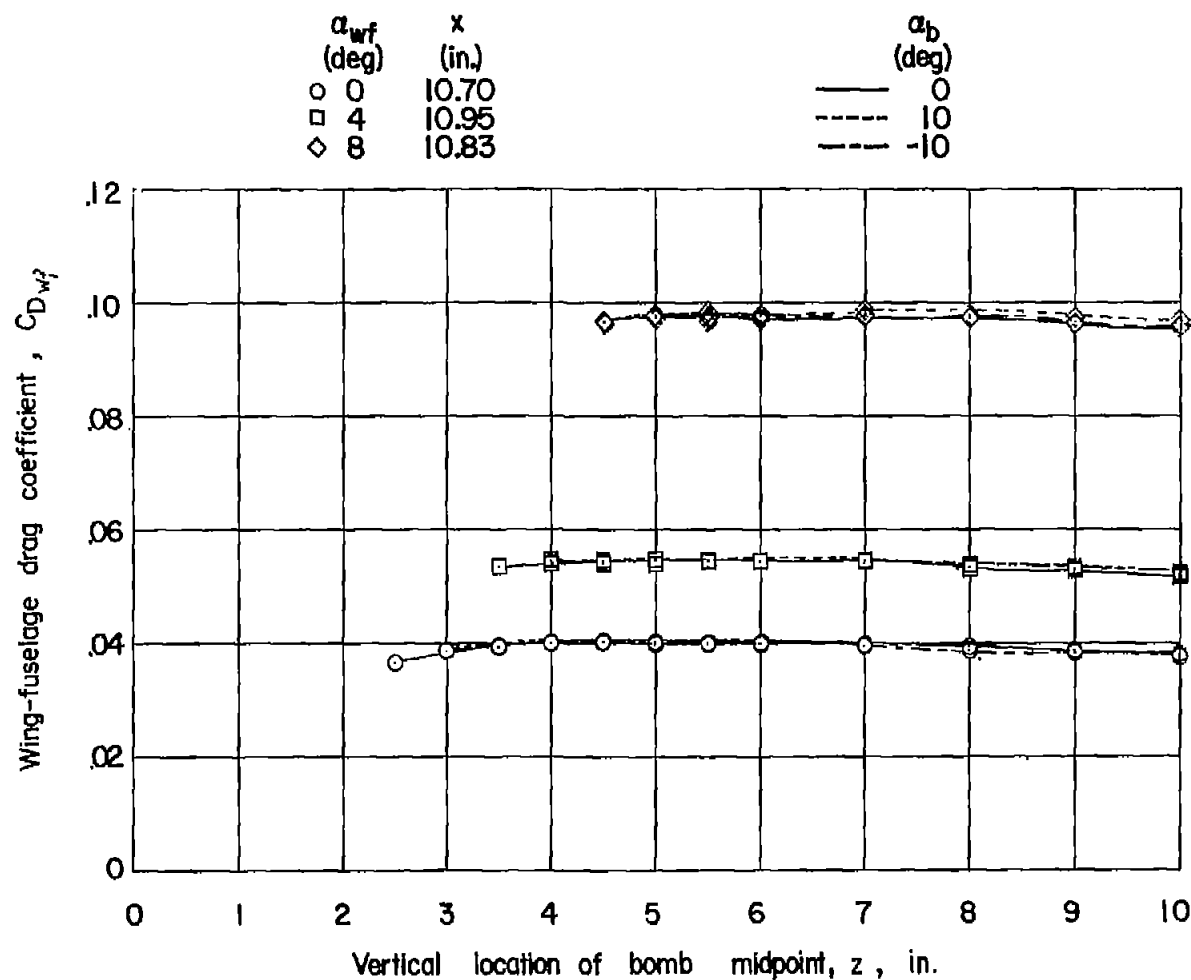
(b) Lift coefficient.

Figure 20.- Continued.



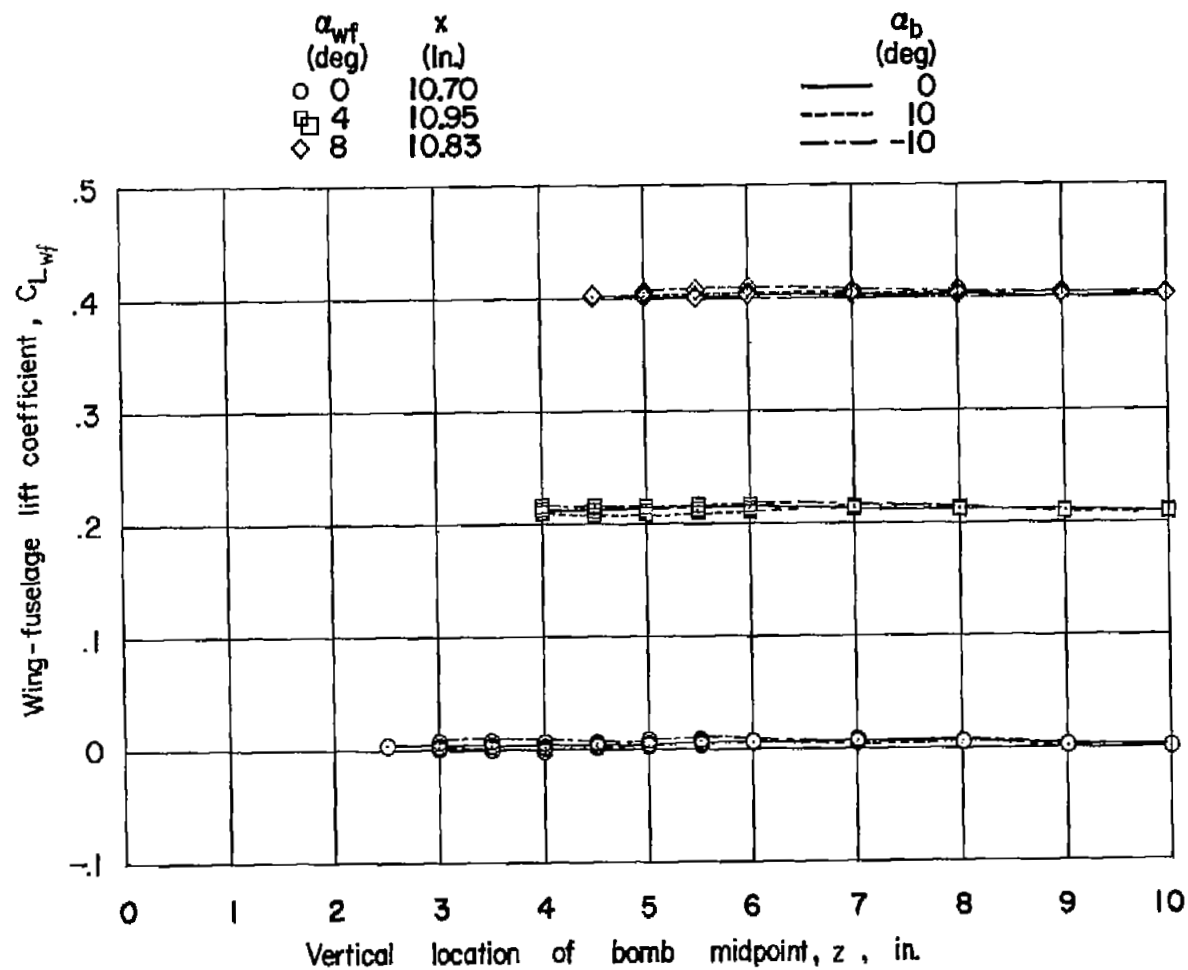
(c) Pitching-moment coefficient.

Figure 20.- Concluded.



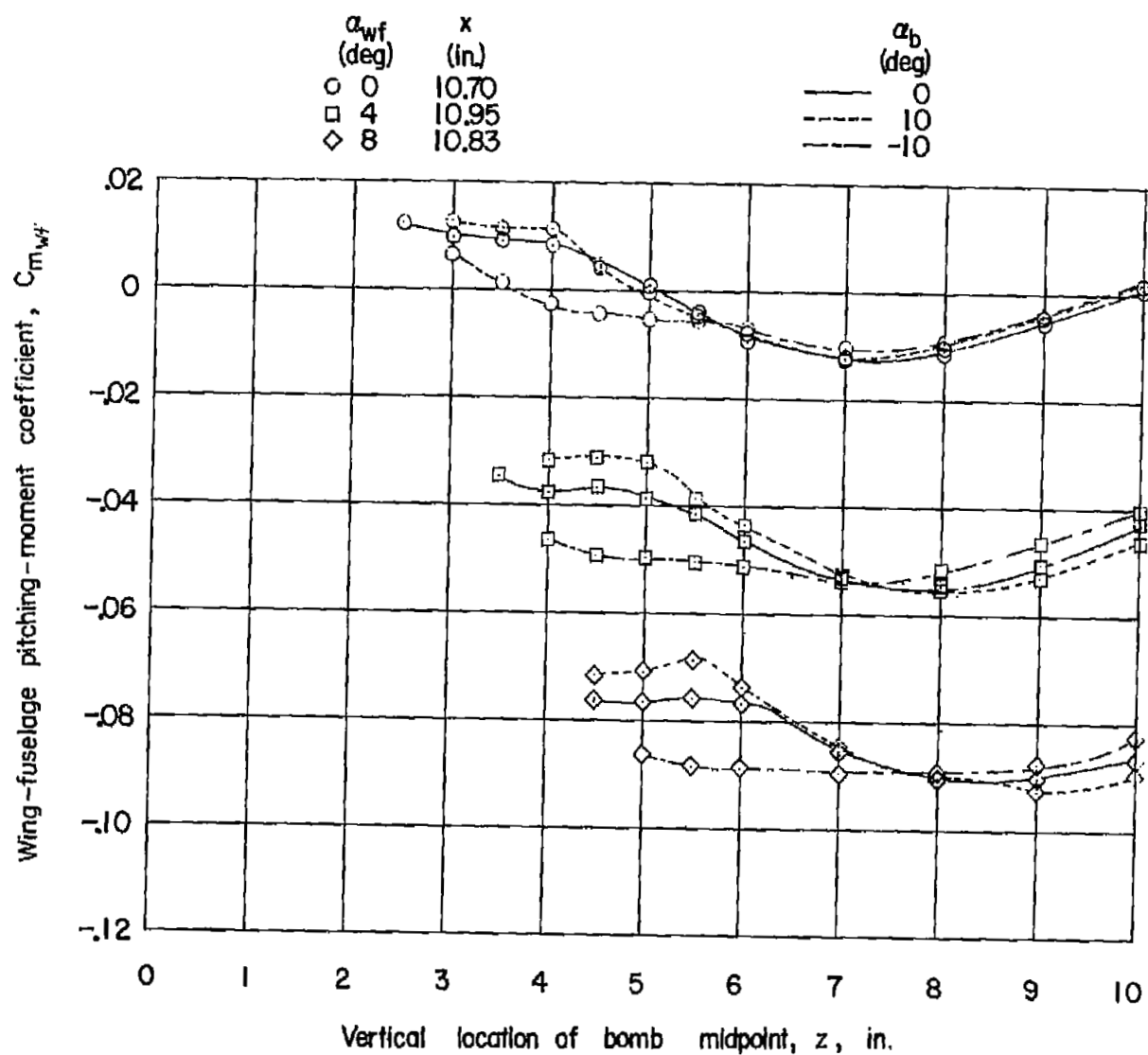
(a) Drag coefficient.

Figure 21.- Force and moment data for wing-fuselage combination in presence of spool bomb. Tail off; $x = 10.70$ to 10.95 inches.



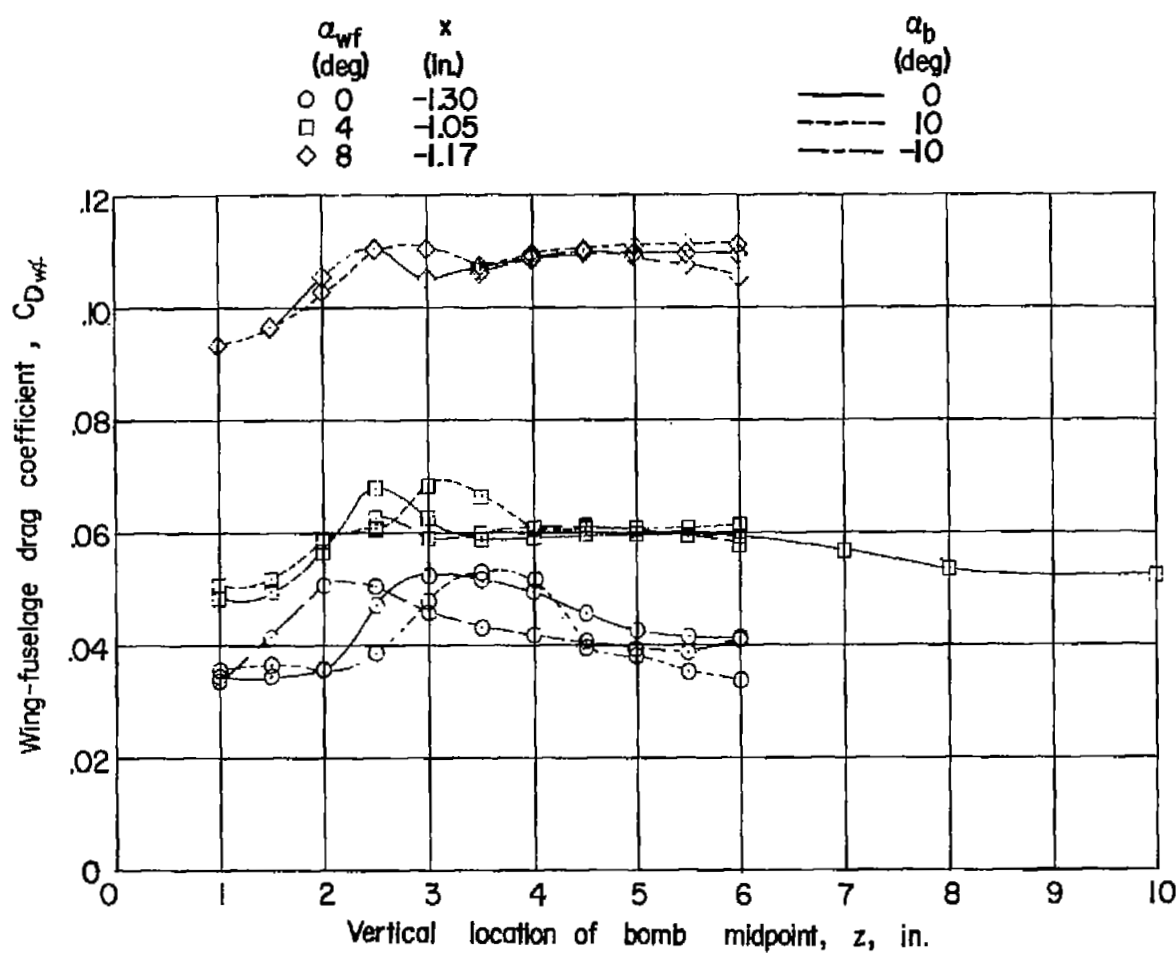
(b) Lift coefficient.

Figure 21.- Continued.



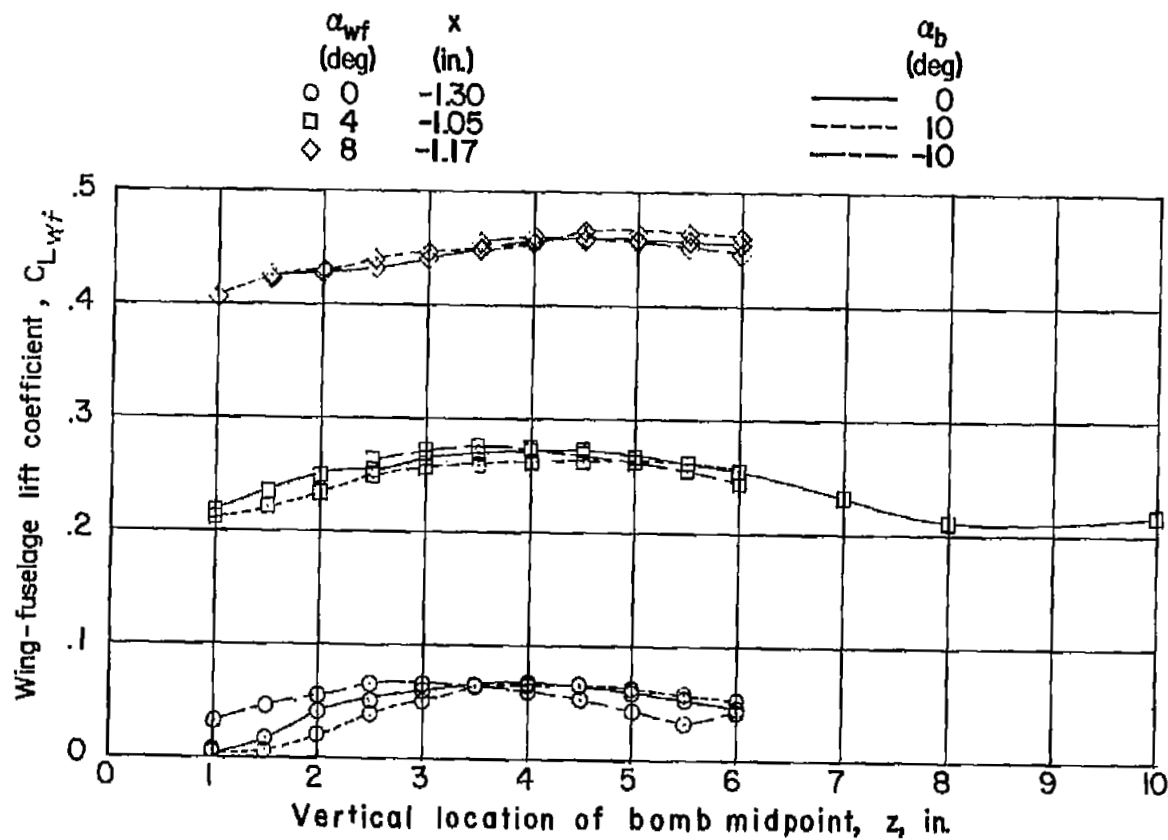
(c) Pitching-moment coefficient.

Figure 21.- Concluded.



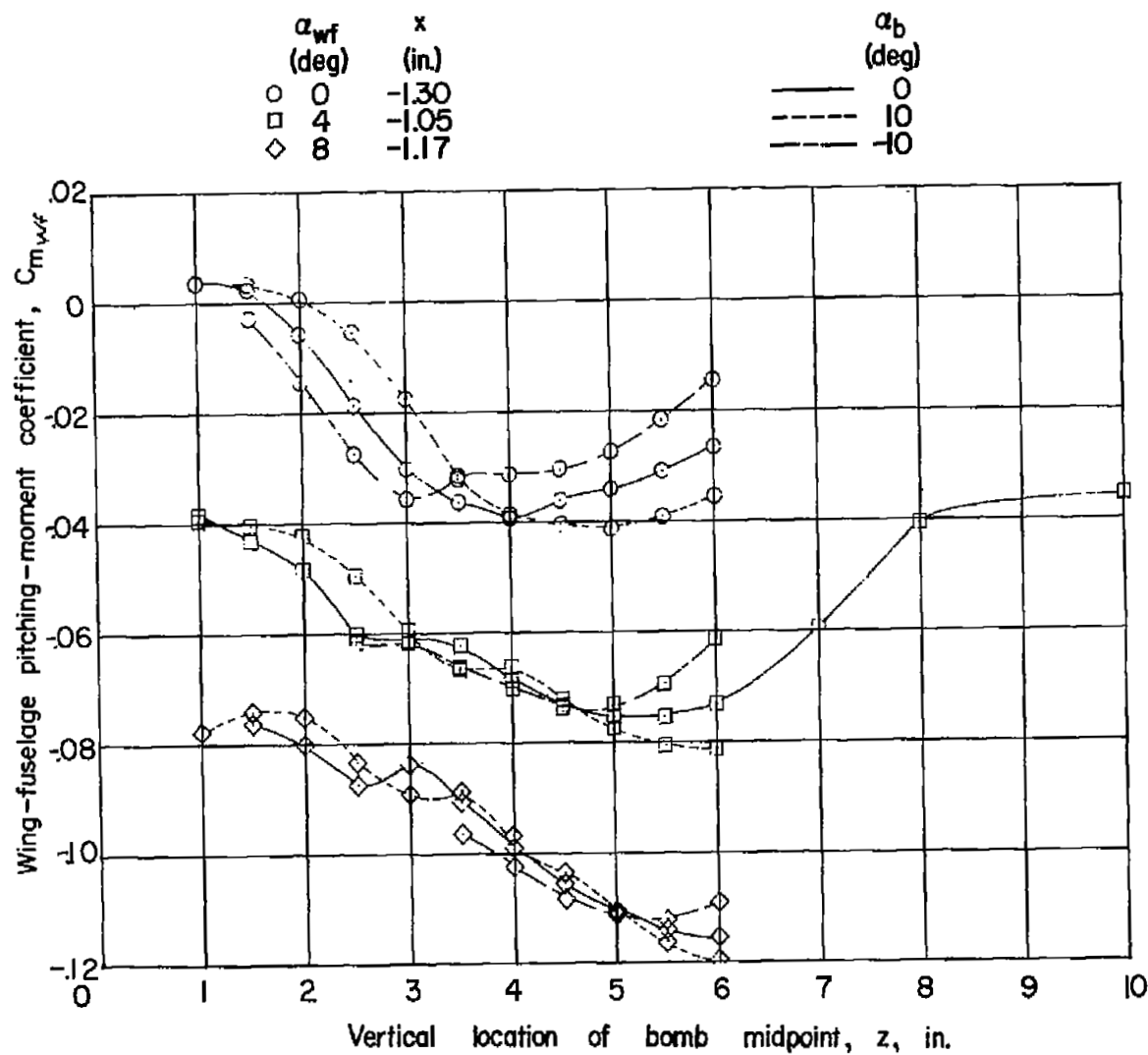
(a) Drag coefficient.

Figure 22.-- Force and moment data for wing-fuselage combination in the presence of cylindrical bomb. Tail off; $x = -1.05$ to -1.30 inches.



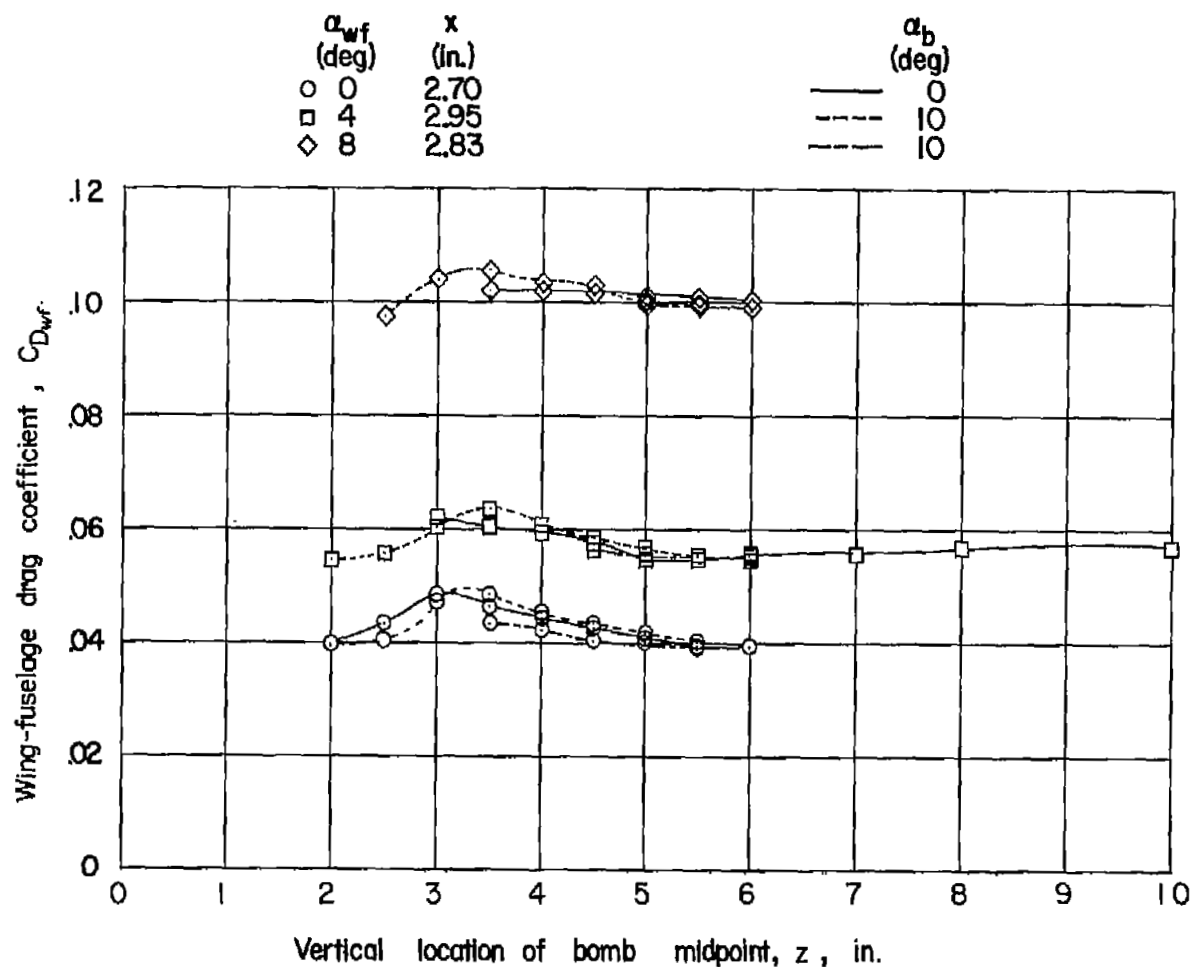
(b) Lift coefficient.

Figure 22.- Continued.



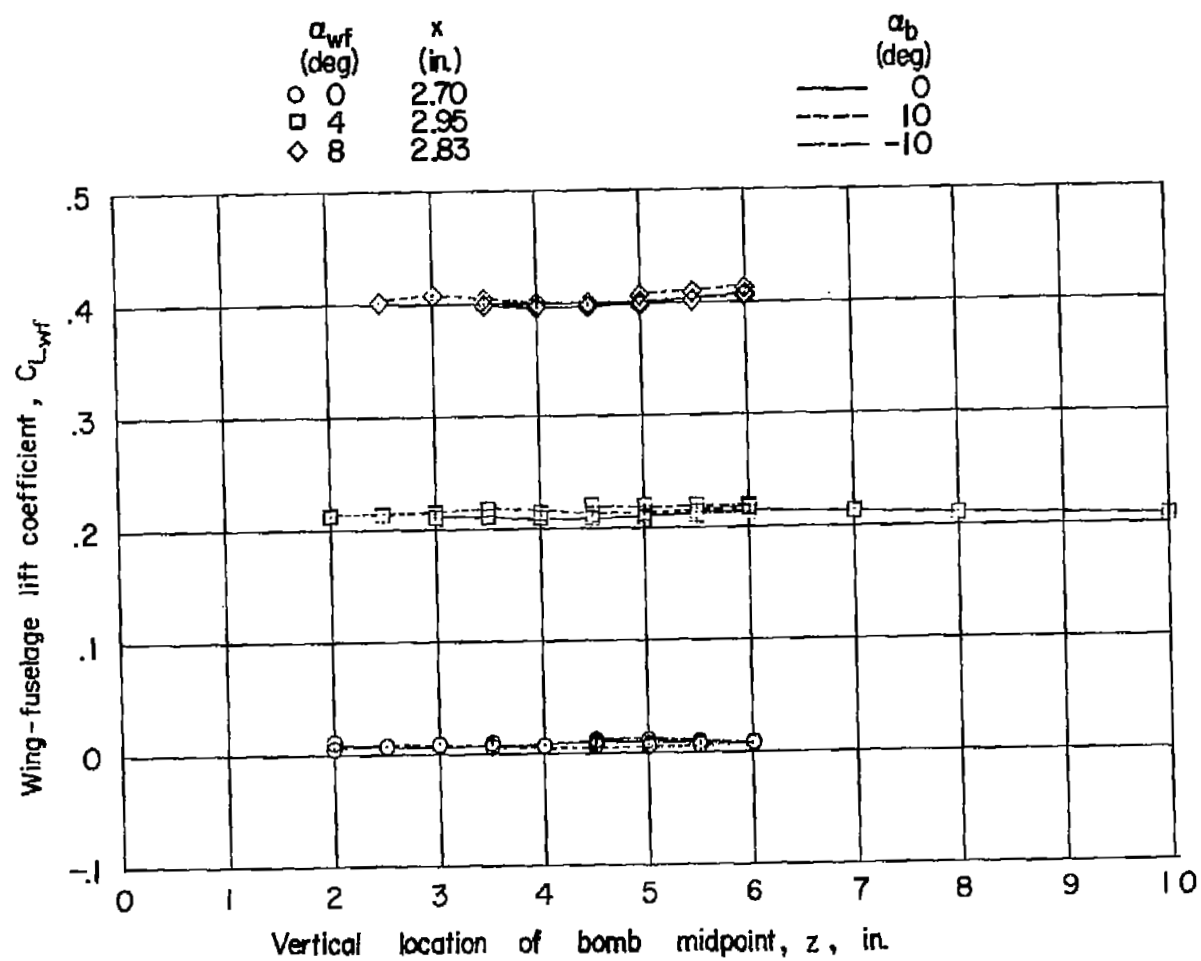
(c) Pitching-moment coefficient.

Figure 22.- Concluded.



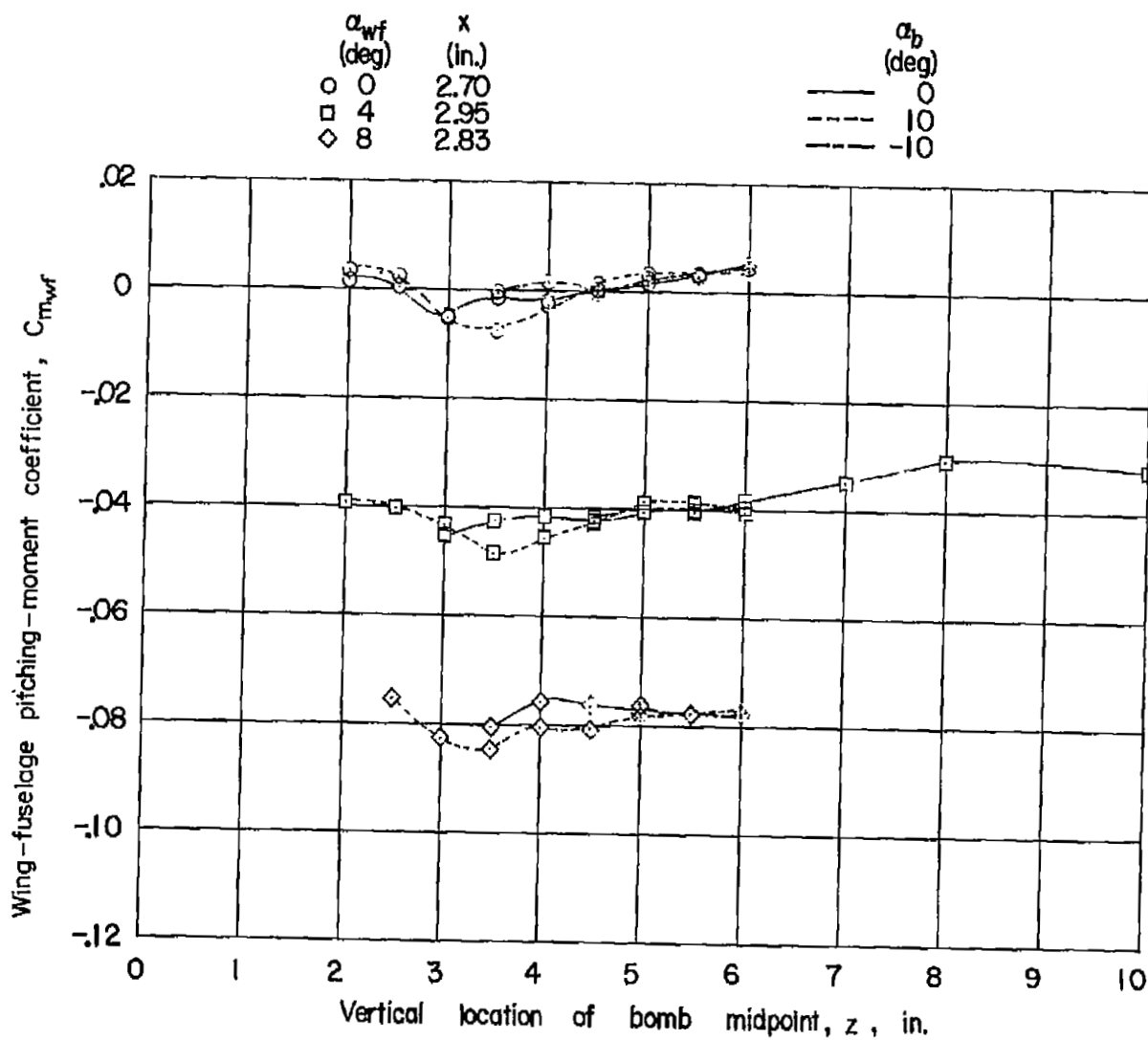
(a) Drag coefficient.

Figure 23.- Force and moment data for wing-fuselage combination in presence of cylindrical bomb.
Tail off; $x = 2.70$ to 2.95 inches.



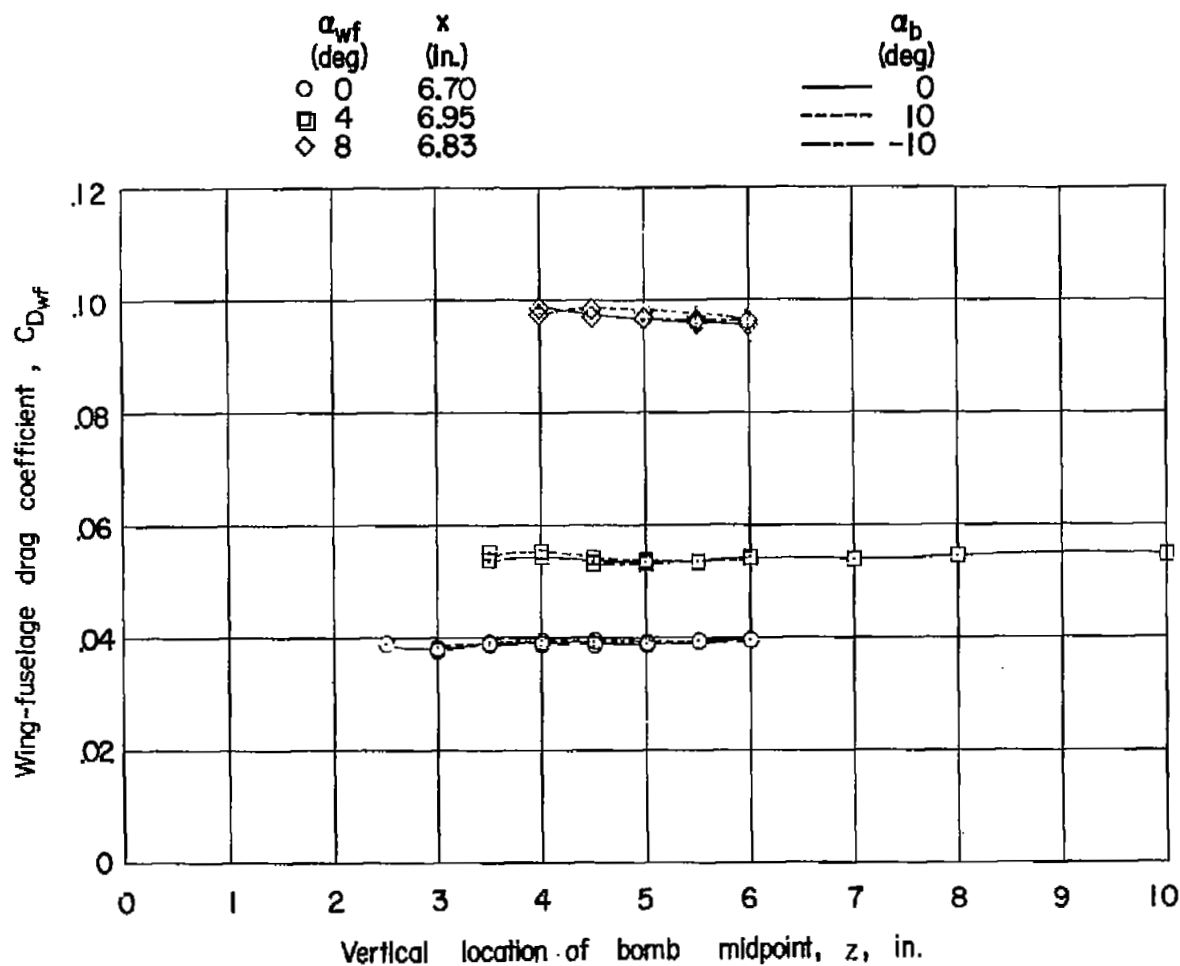
(b) Lift coefficient.

Figure 23.- Continued.



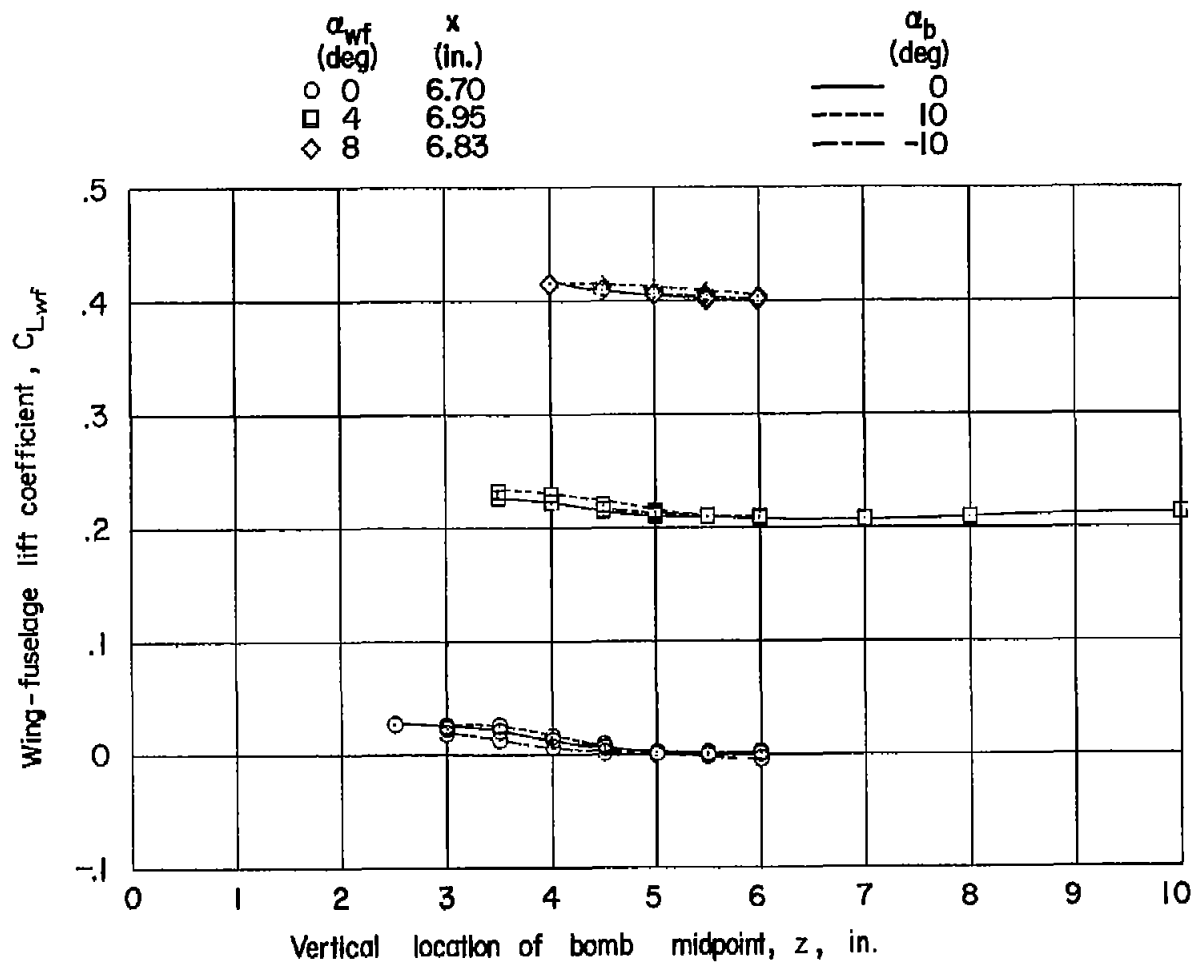
(c) Pitching-moment coefficient.

Figure 23.- Concluded.



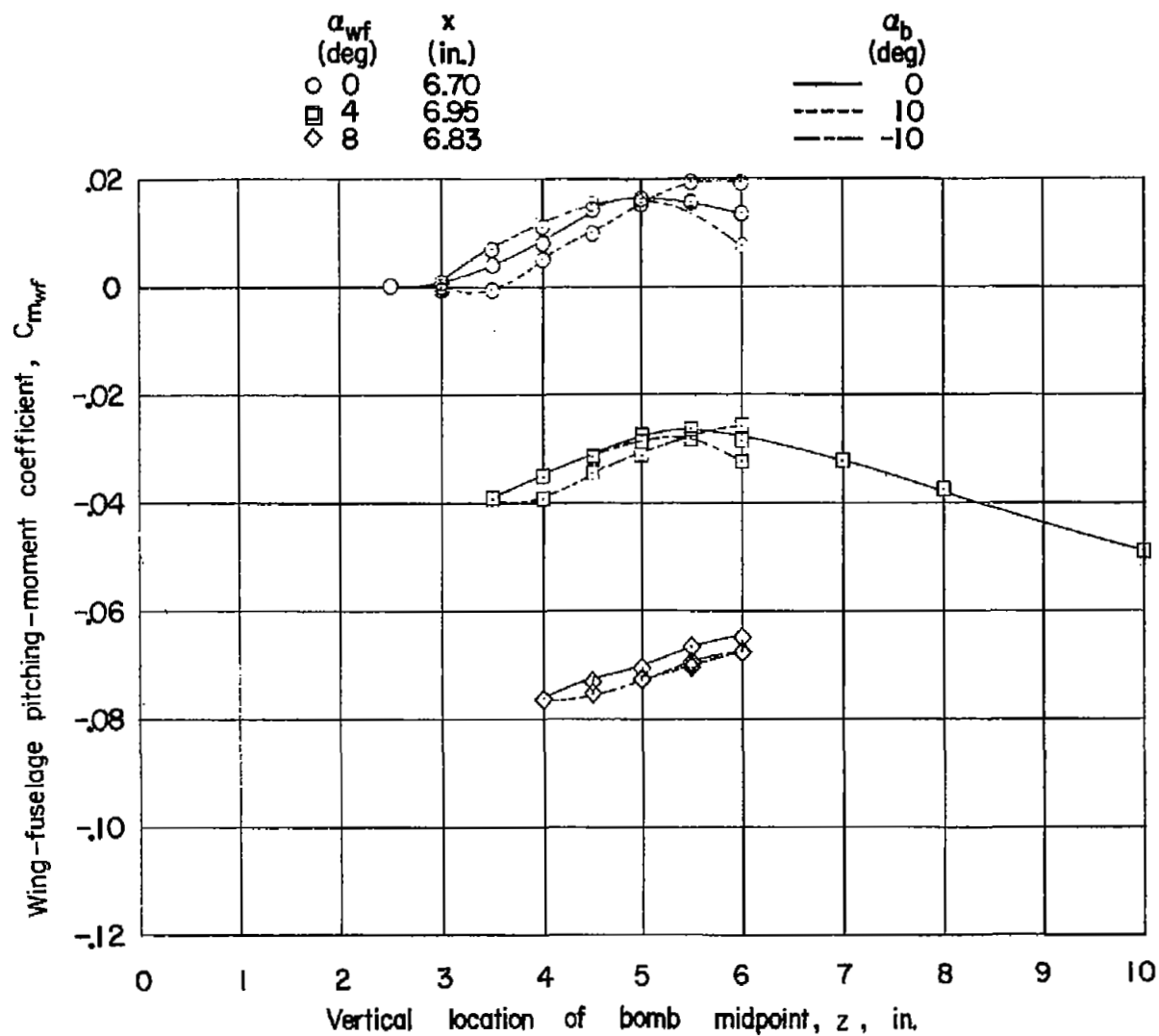
(a) Drag coefficient.

Figure 24.- Force and moment data for wing-fuselage combination in presence of cylindrical bomb.
Tail off; $x = 6.70$ to 6.95 inches.



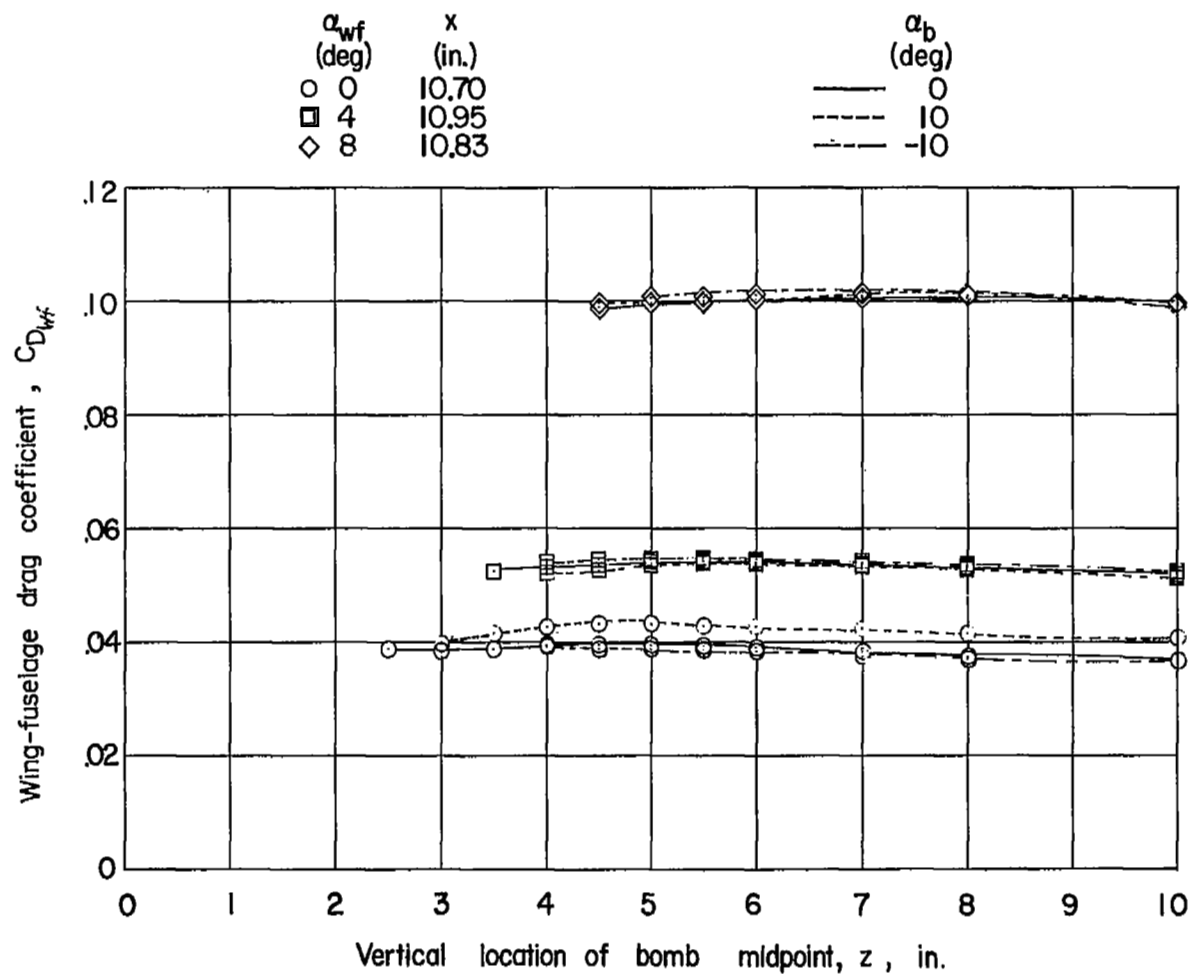
(b) Lift coefficient.

Figure 24.- Continued.



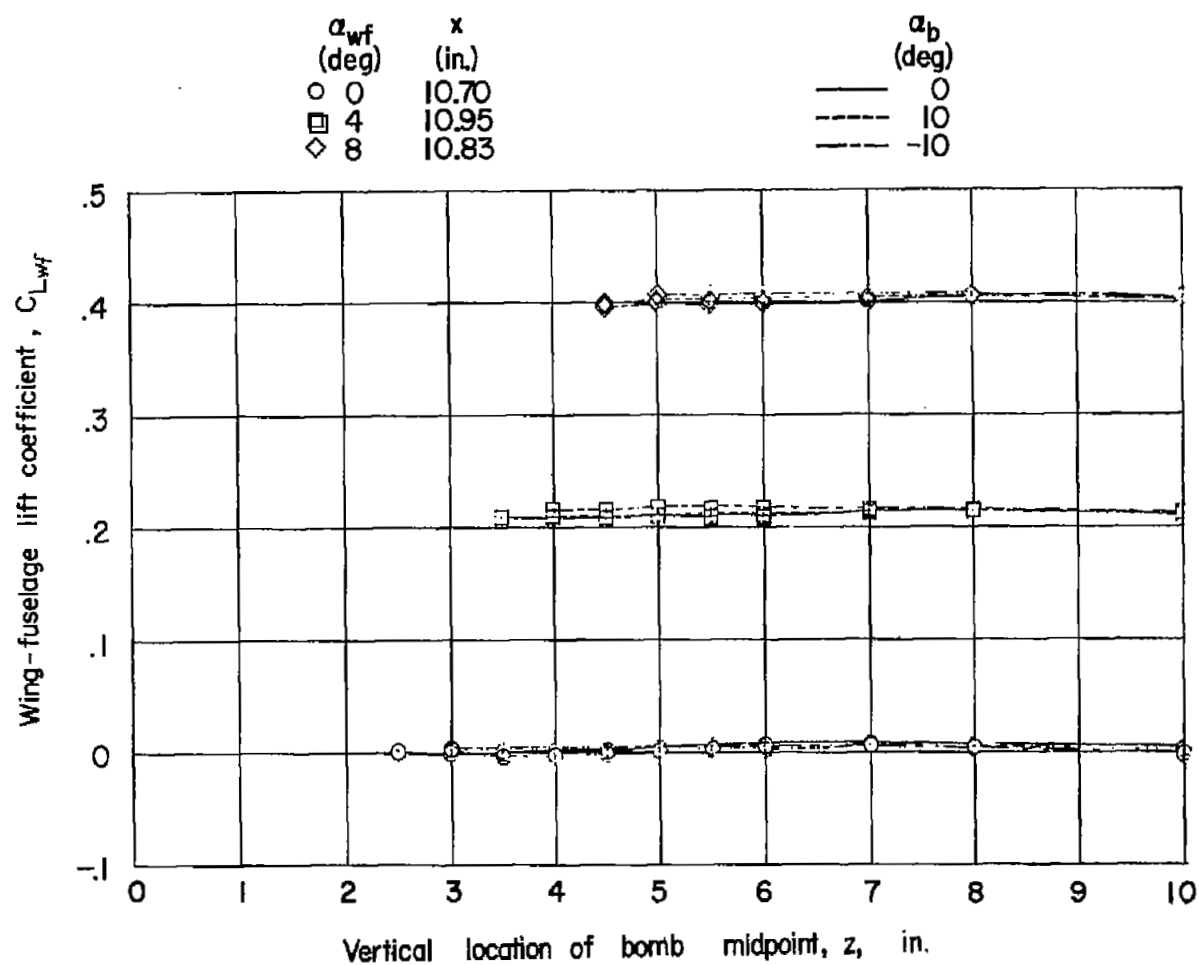
(c) Pitching-moment coefficient.

Figure 24.- Concluded.



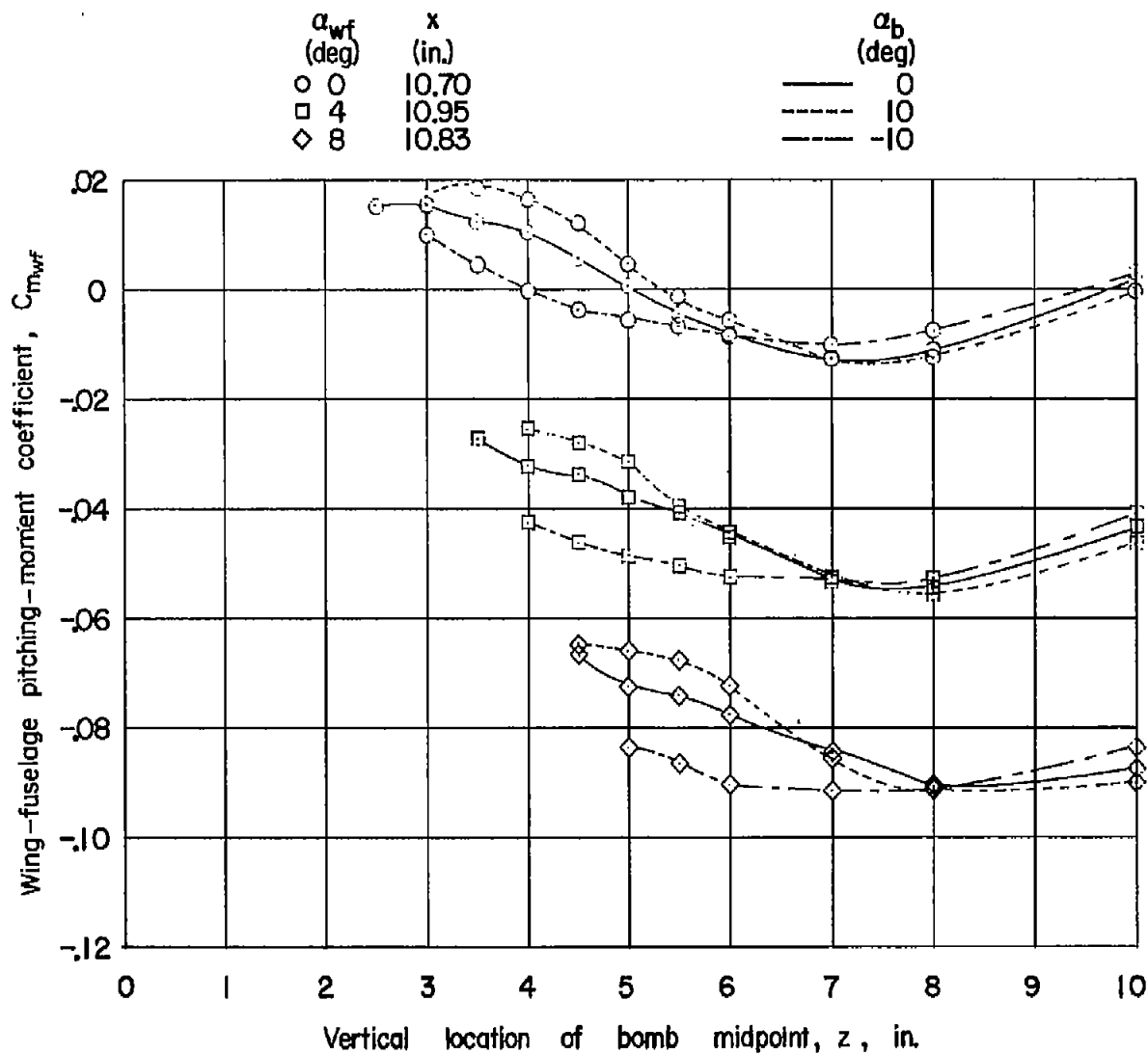
(a) Drag coefficient.

Figure 25.- Force and moment data for wing-fuselage combination in presence of cylindrical bomb.
Tail off; $x = 10.70$ to 10.95 inches.



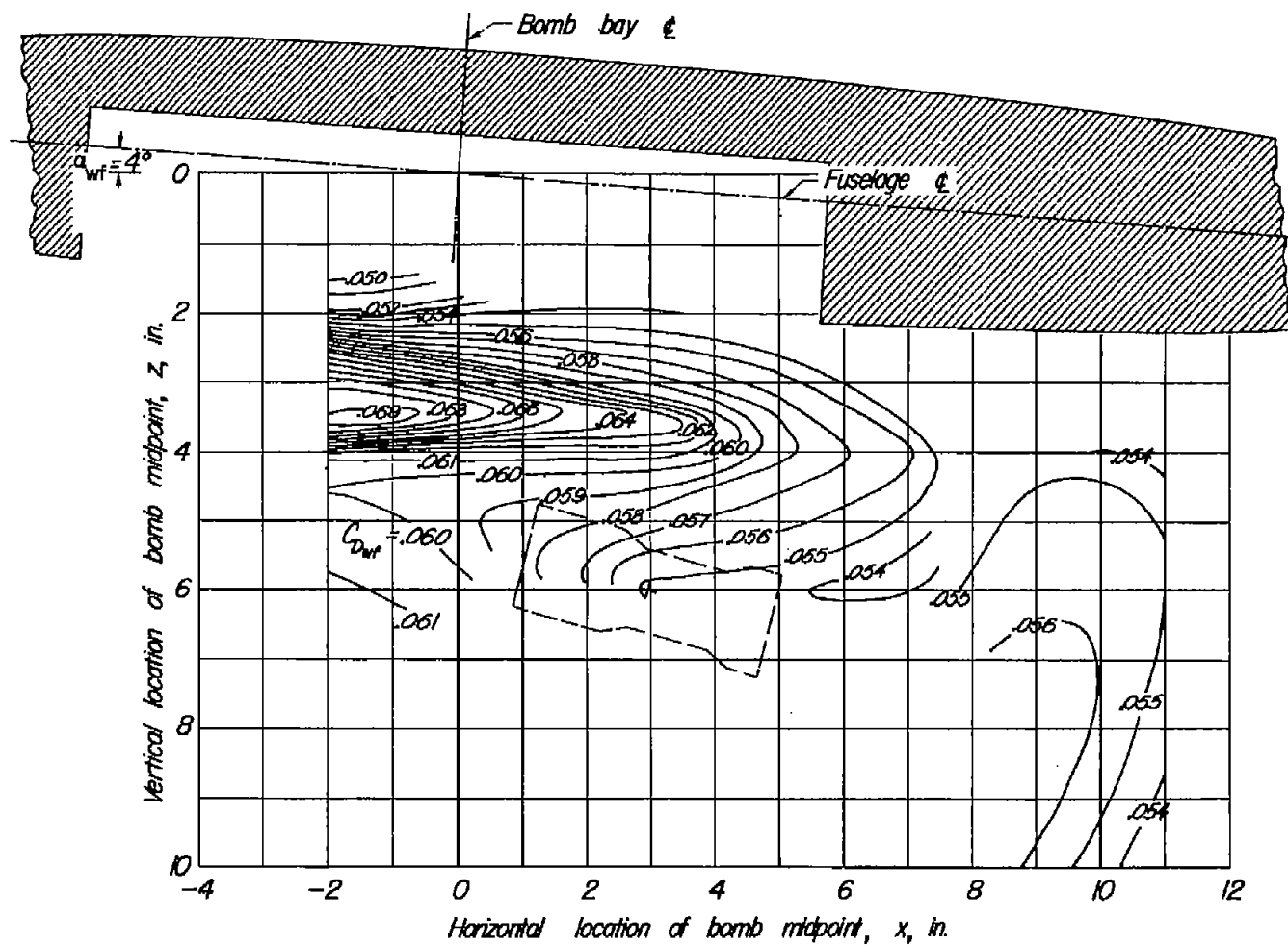
(b) Lift coefficient.

Figure 25.- Continued.



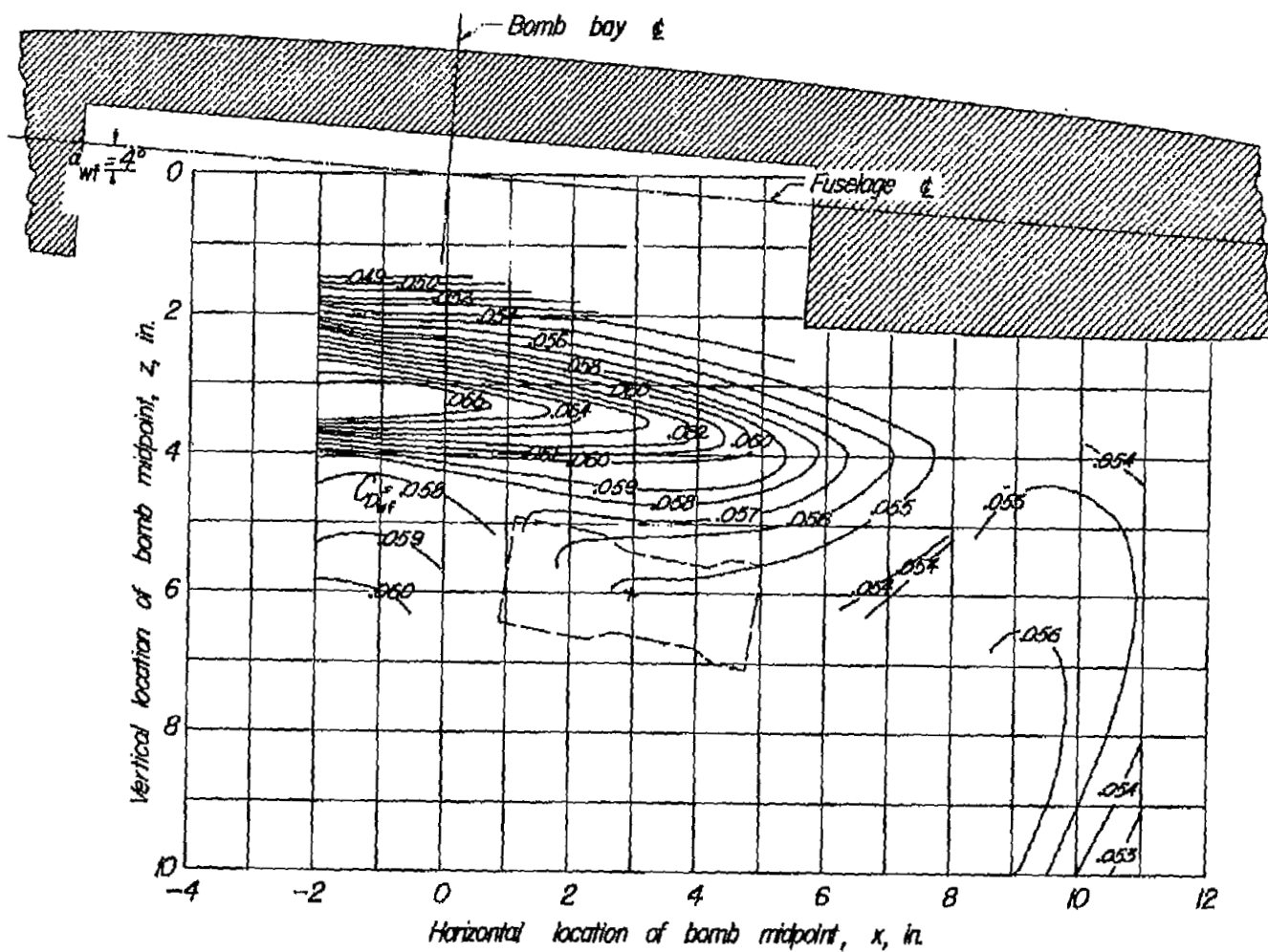
(c) Pitching-moment coefficient.

Figure 25.- Concluded.



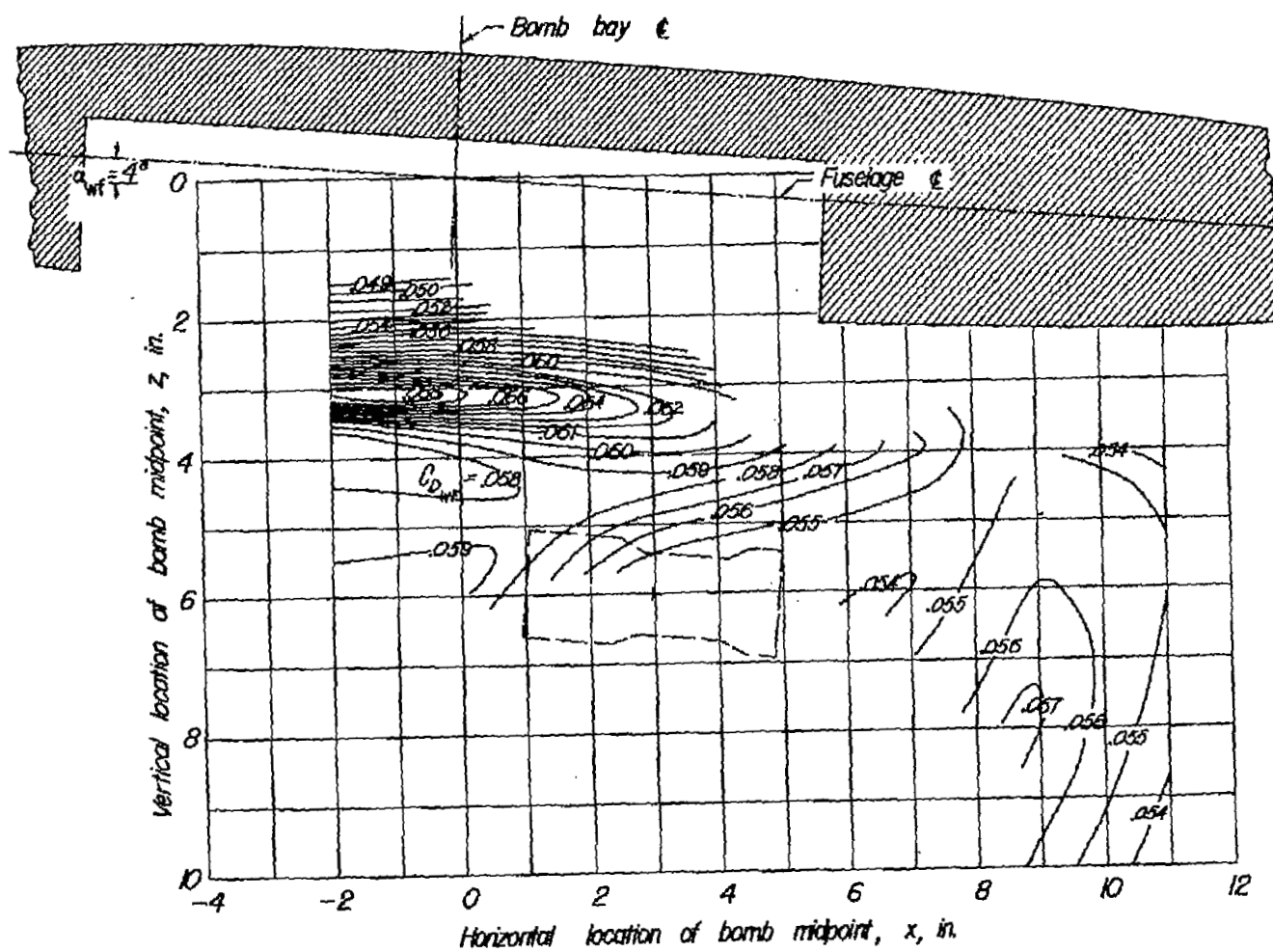
(a) $\alpha_b = 15^\circ$.

Figure 26.- Contour plot of drag coefficients of wing-fuselage combination in presence of spool bomb.



(b) $\alpha_D = 10^\circ$.

Figure 26.- Continued.



(c) $\alpha_b = 5^\circ$.

Figure 26.- Continued.

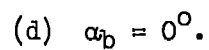
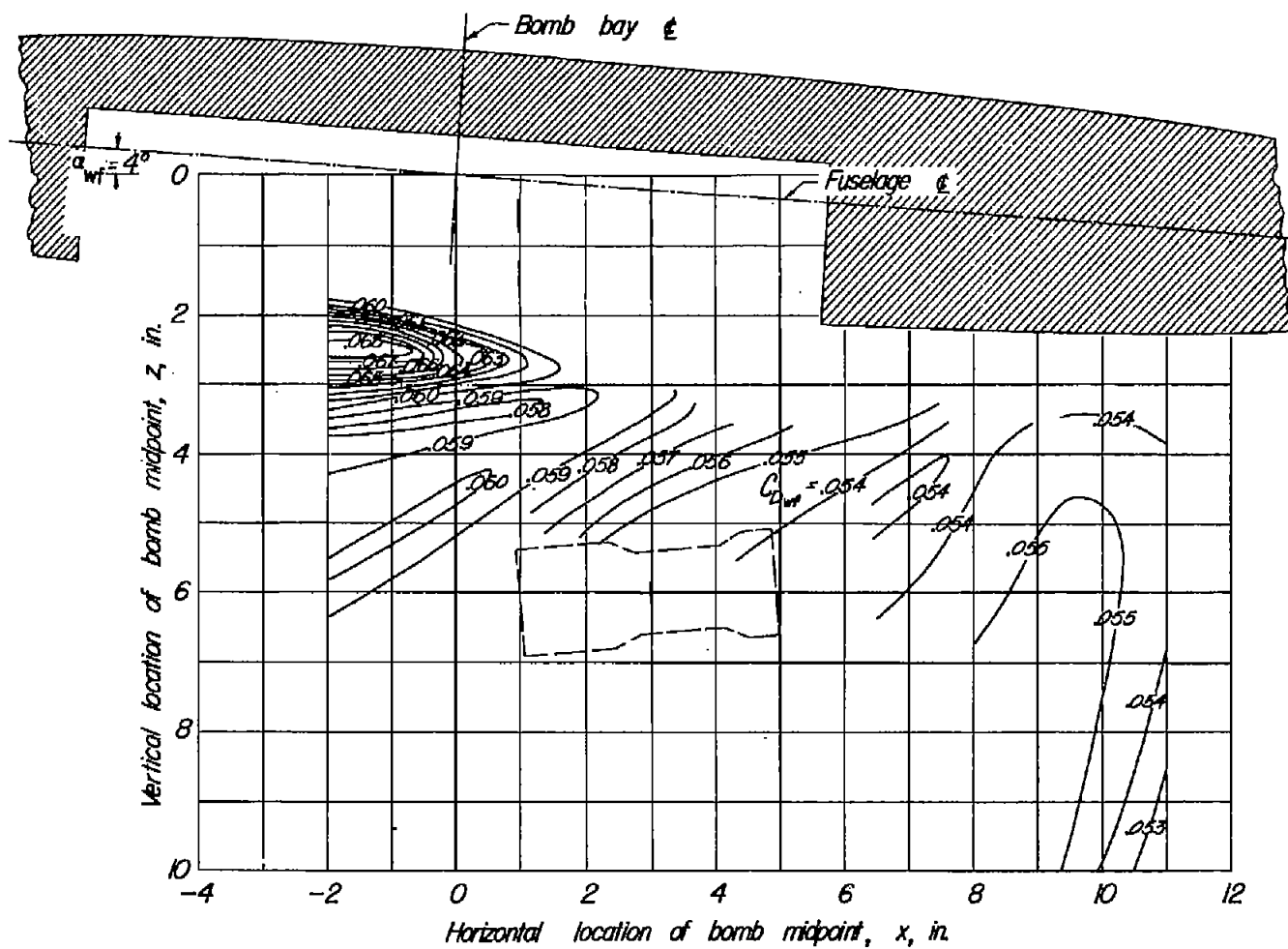
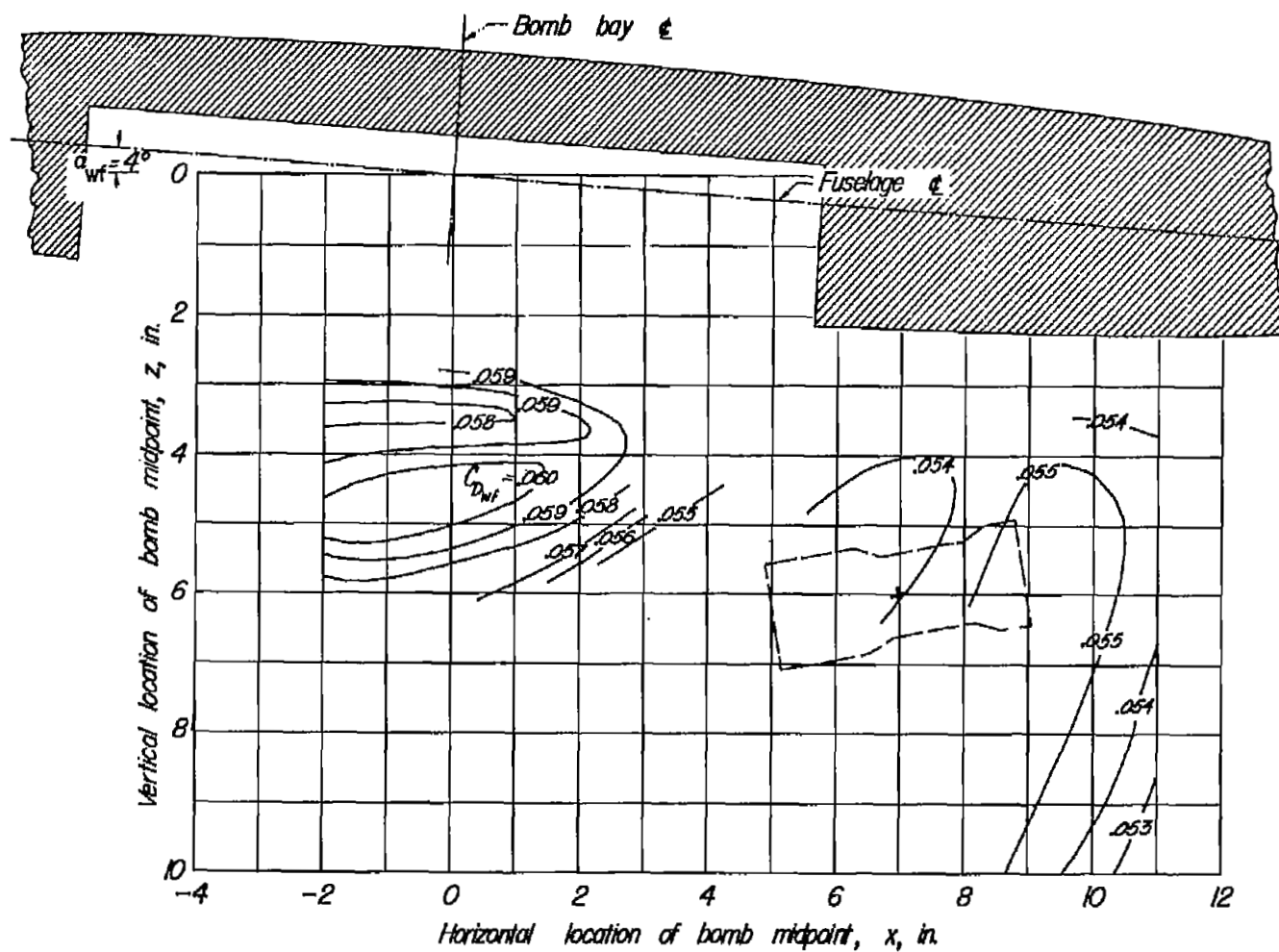


Figure 26.- Continued.



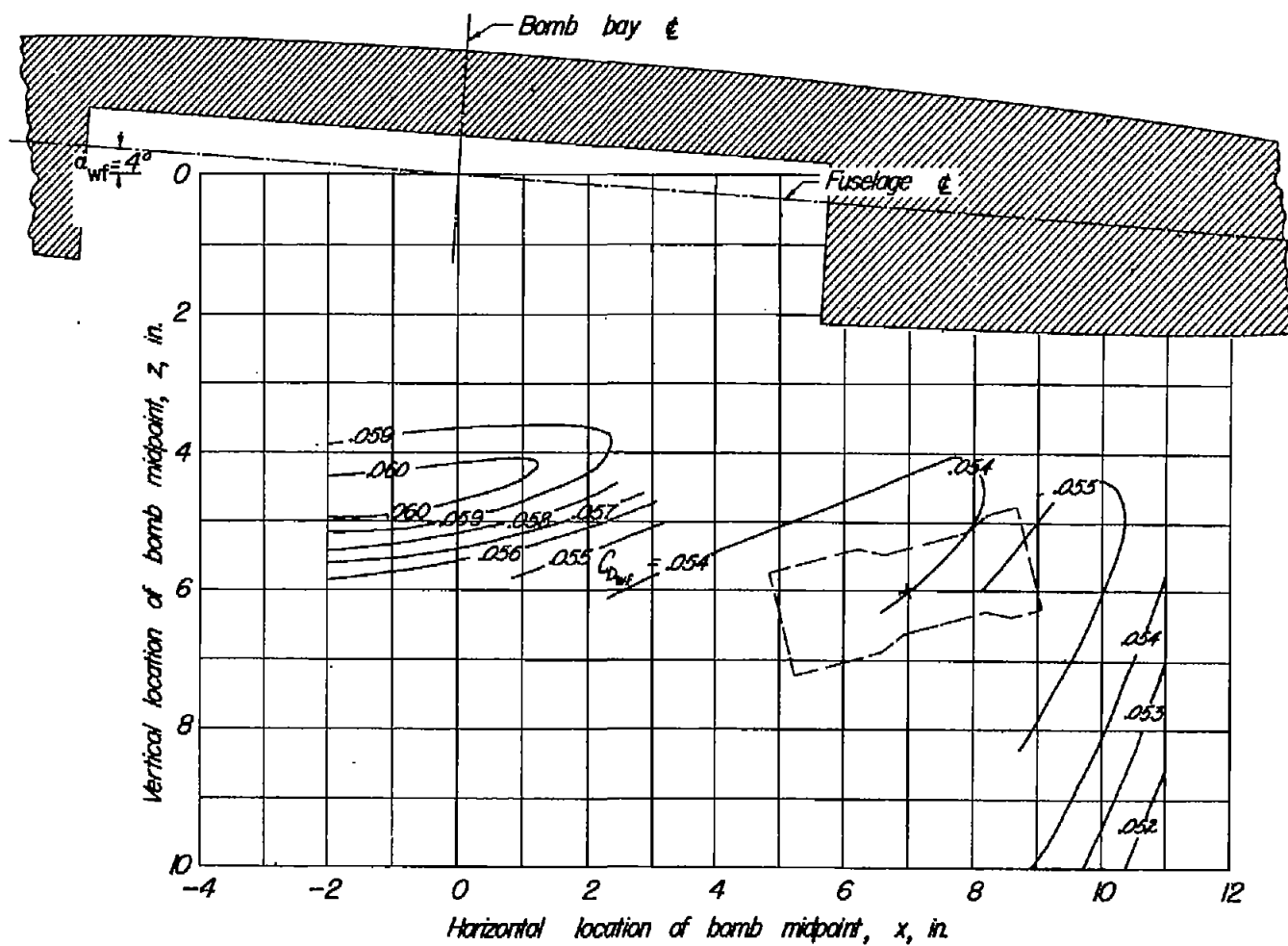
(e) $\alpha_0 = -5^\circ$.

Figure 26.- Continued.



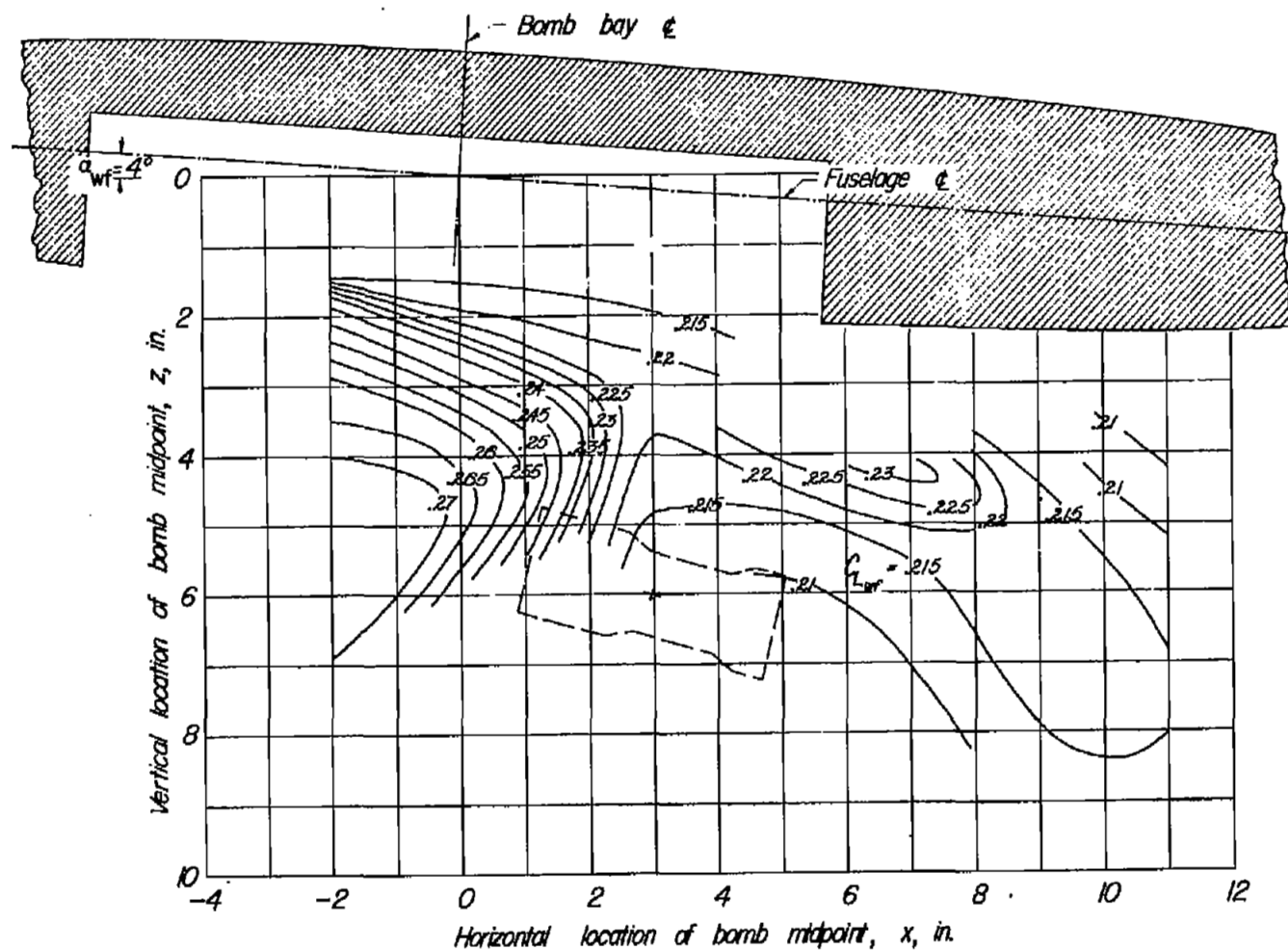
(f) $\alpha_b = -10^\circ$.

Figure 26.- Continued.



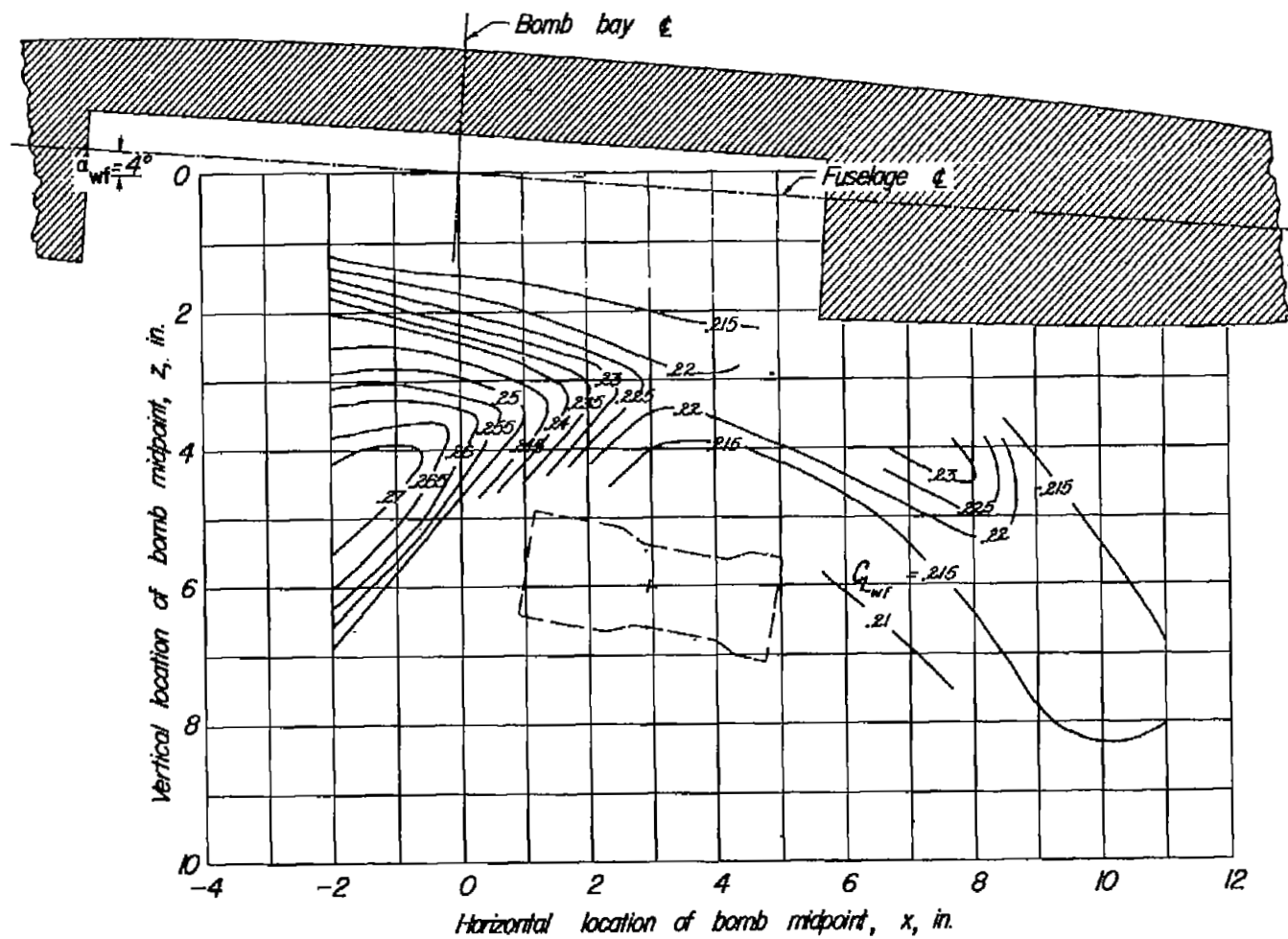
(g) $\alpha_p = -15^\circ$.

Figure 26.- Concluded.



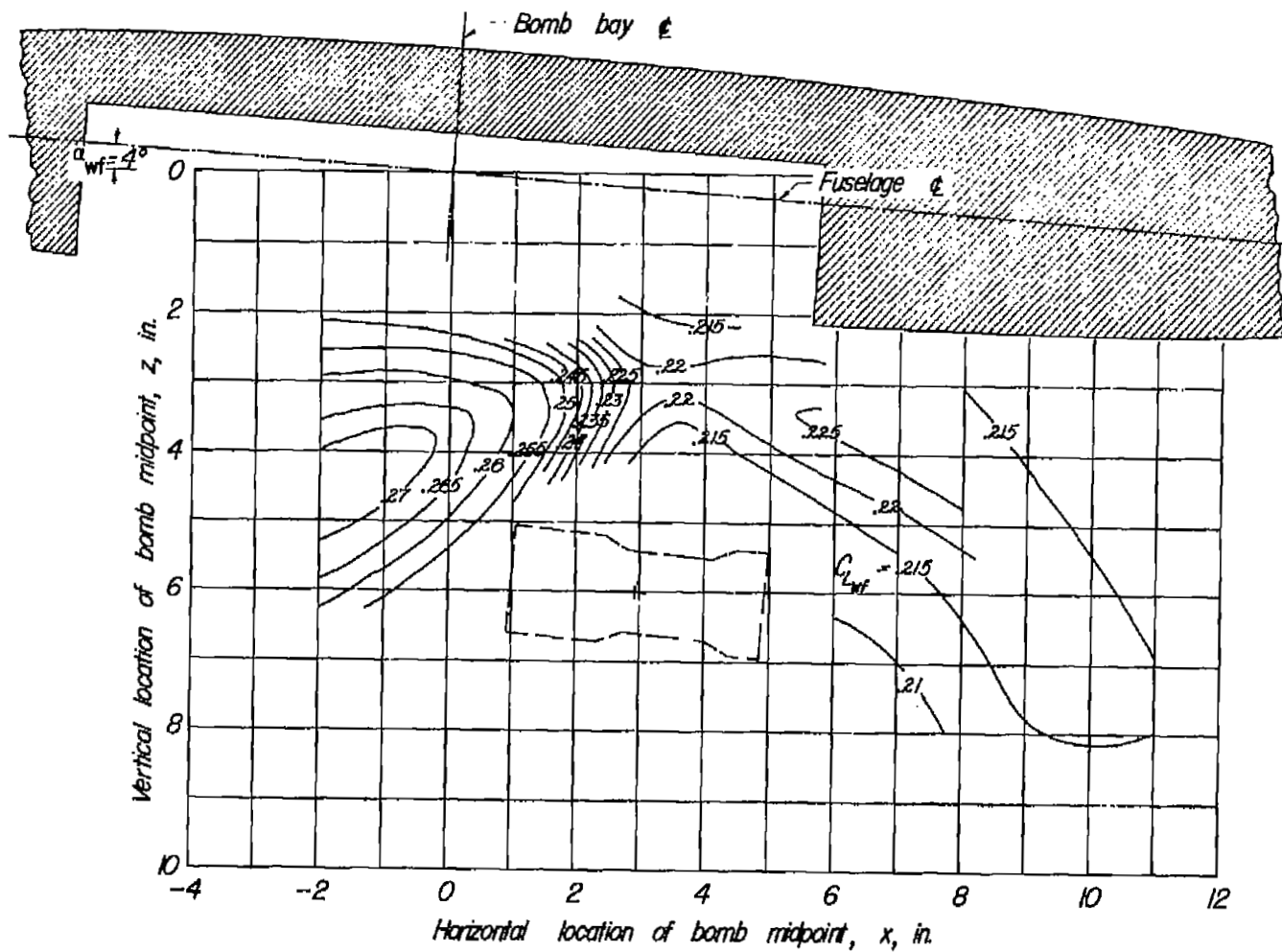
(a) $\alpha_b = 15^\circ$.

Figure 27.- Contour plot of lift coefficients of wing-fuselage combination in presence of spool bomb.



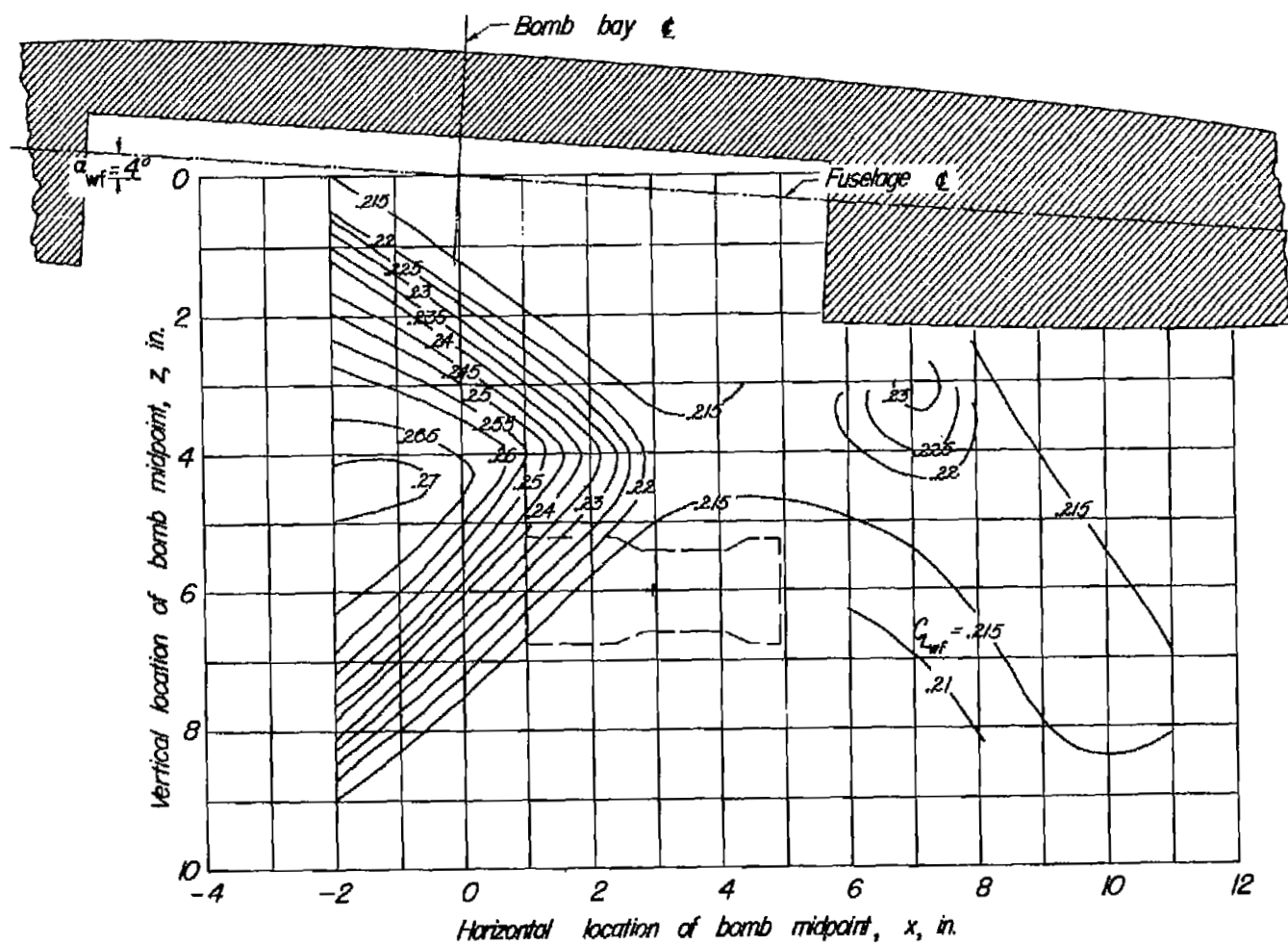
(b) $\alpha_b = 10^\circ$.

Figure 27.- Continued.



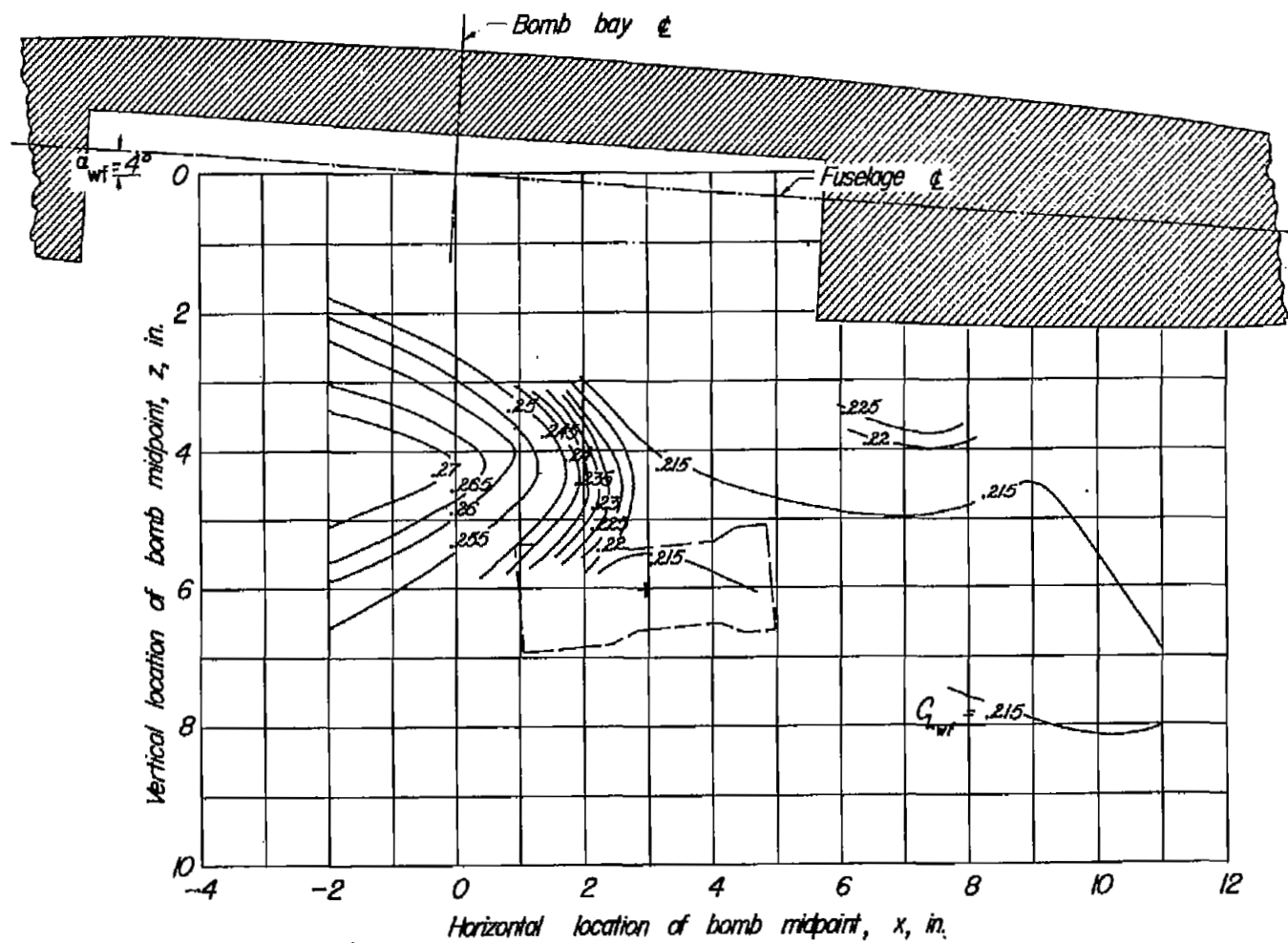
(c) $\alpha_b = 5^\circ$.

Figure 27.- Continued.



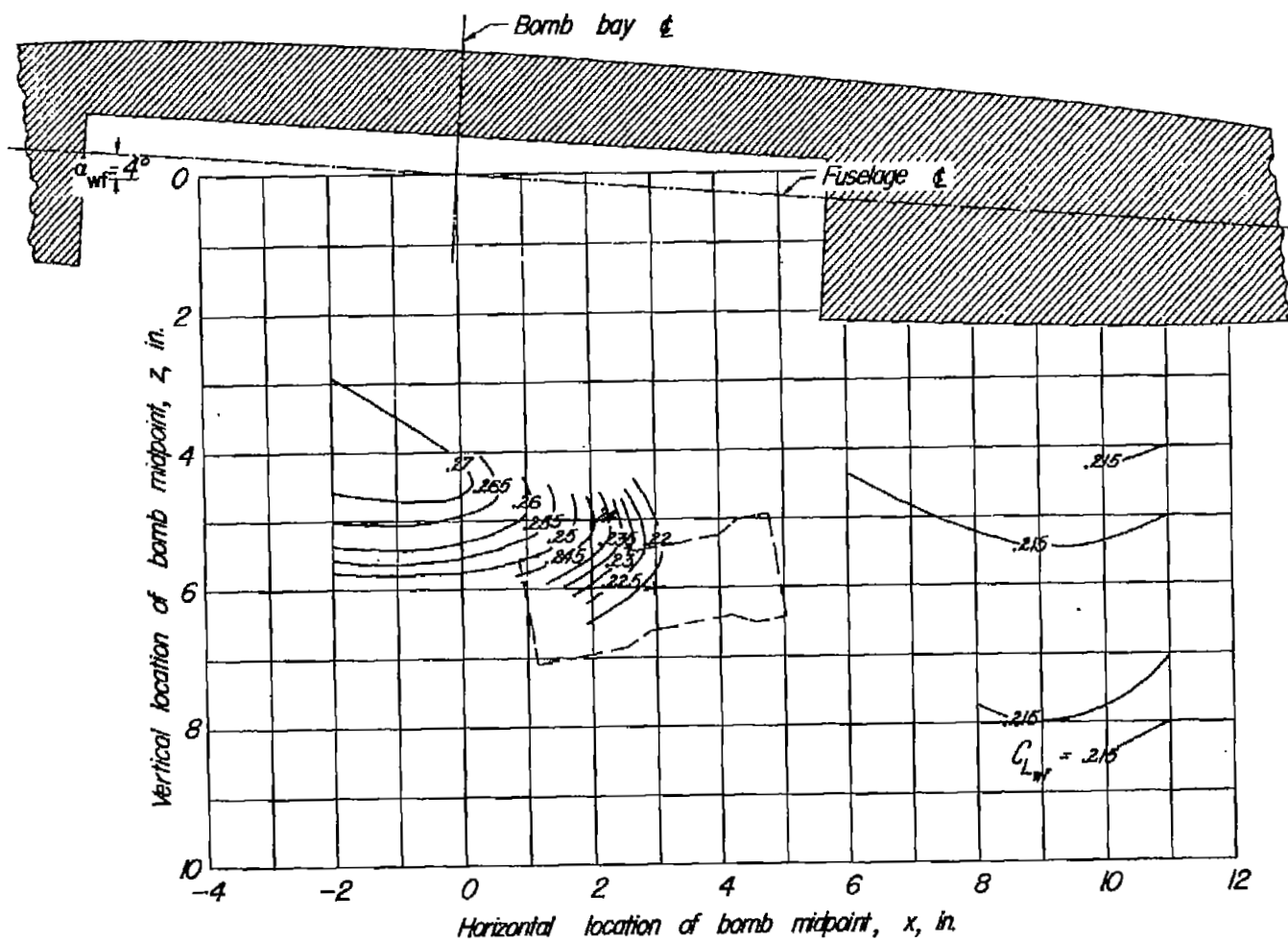
(d) $\alpha_b = 0^\circ$.

Figure 27.- Continued.



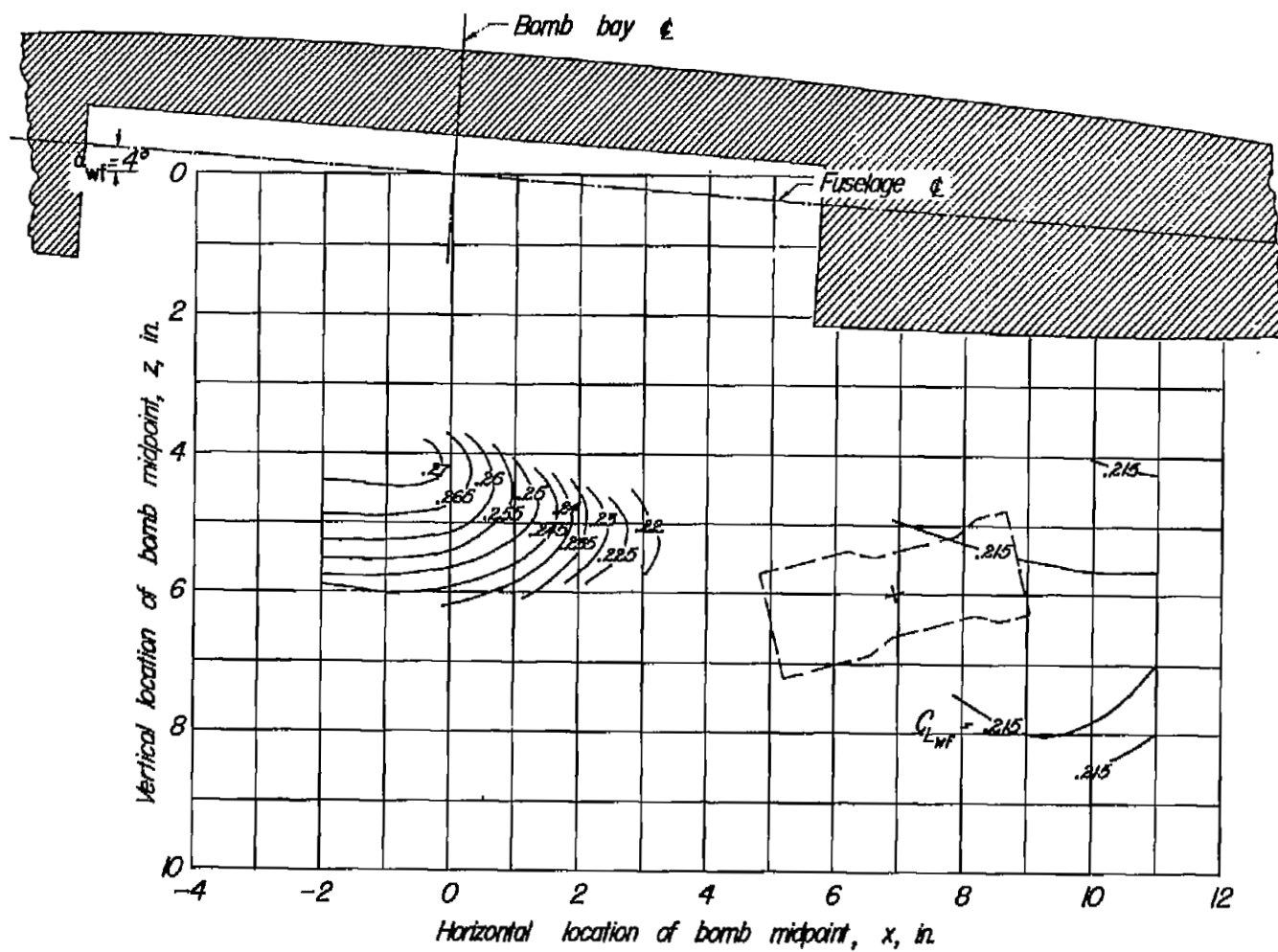
(e) $\alpha_0 = -5^\circ$.

Figure 27.- Continued.



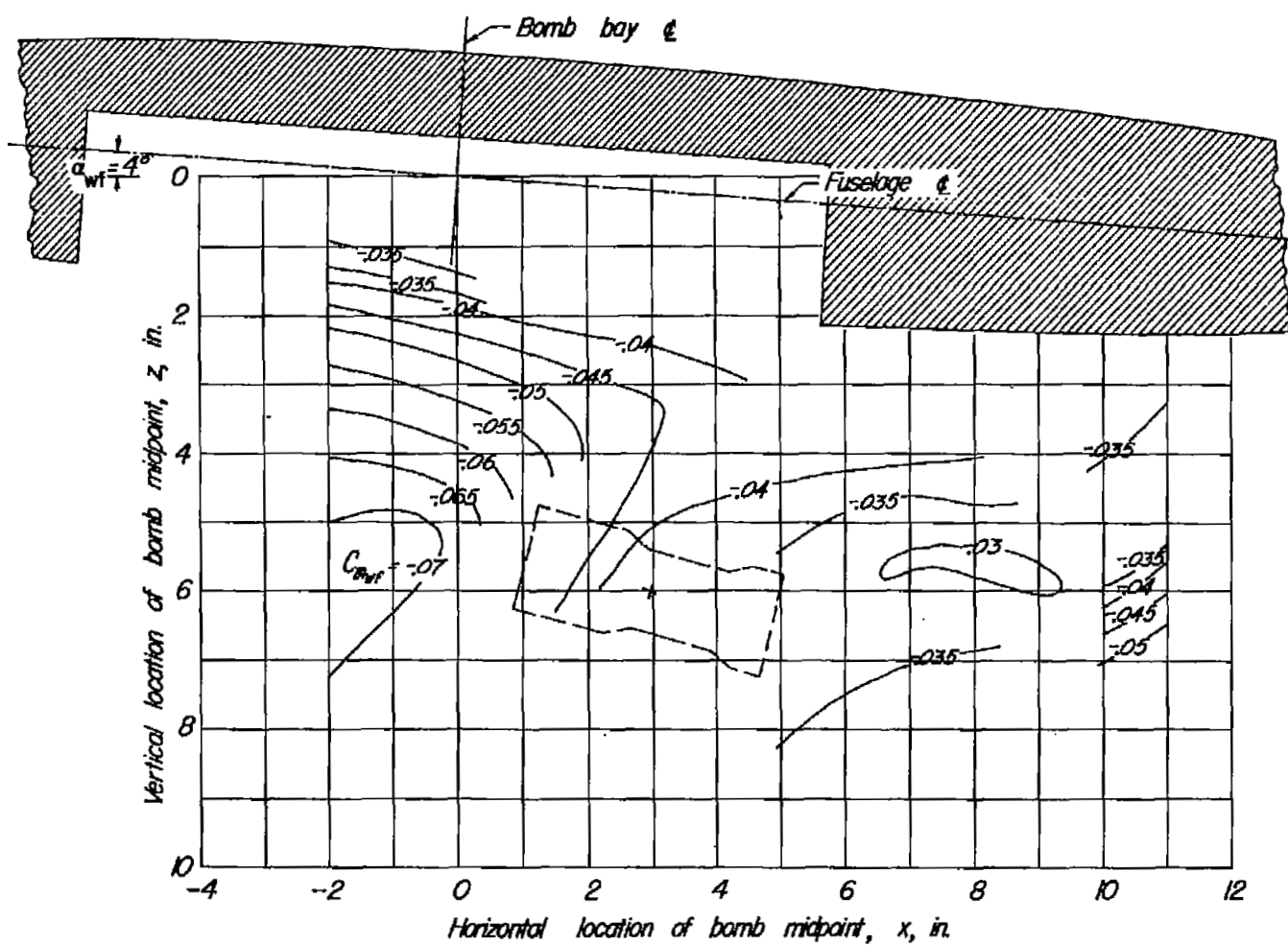
(f) $\alpha_b = -10^\circ$.

Figure 27.- Continued.



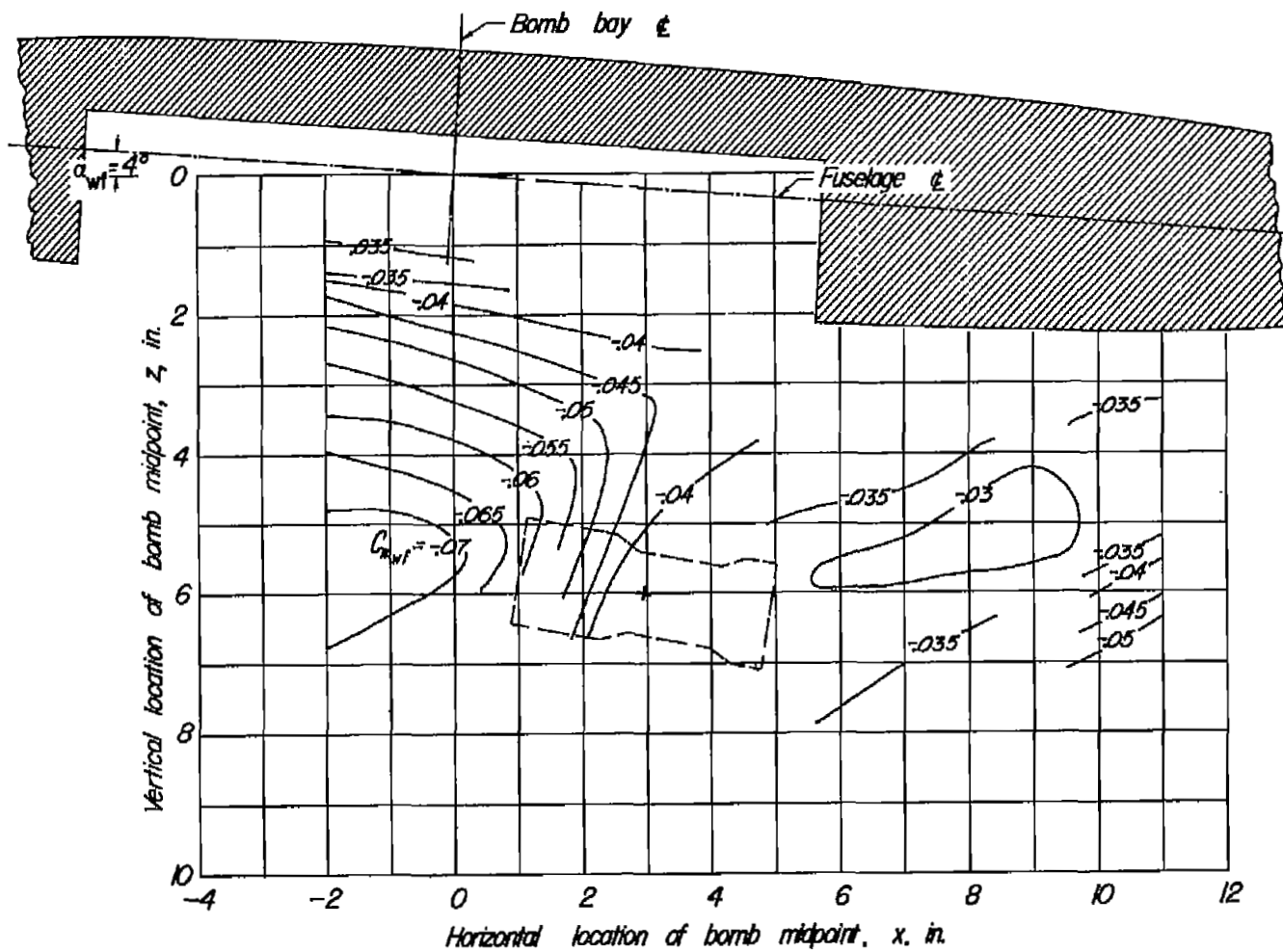
(g) $\alpha_b = -15^\circ$.

Figure 27.- Concluded.



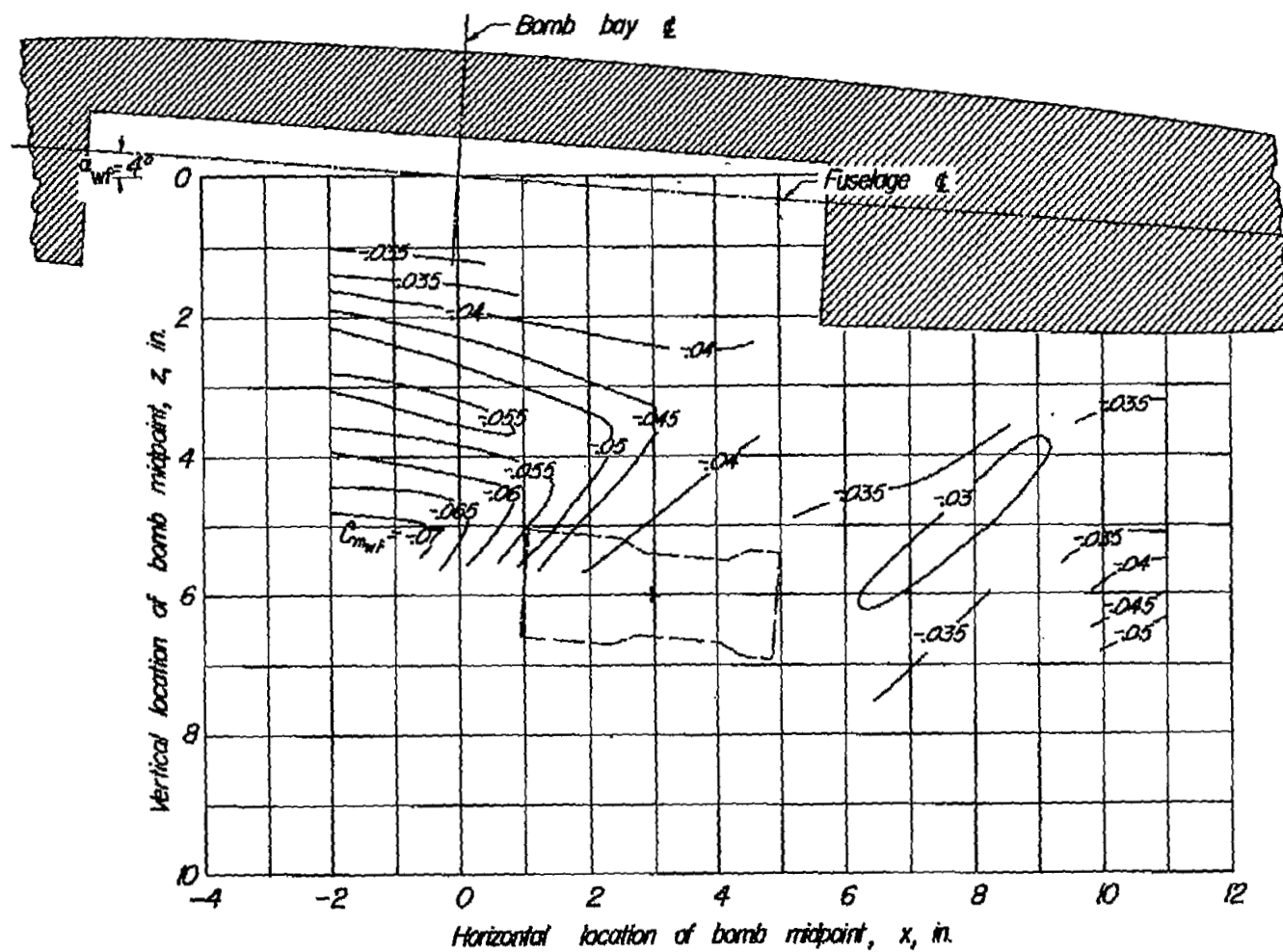
(a) $\alpha_0 = 15^\circ$.

Figure 28.- Contour plot of pitching-moment coefficients of wing-fuselage combination in presence of spool bomb.



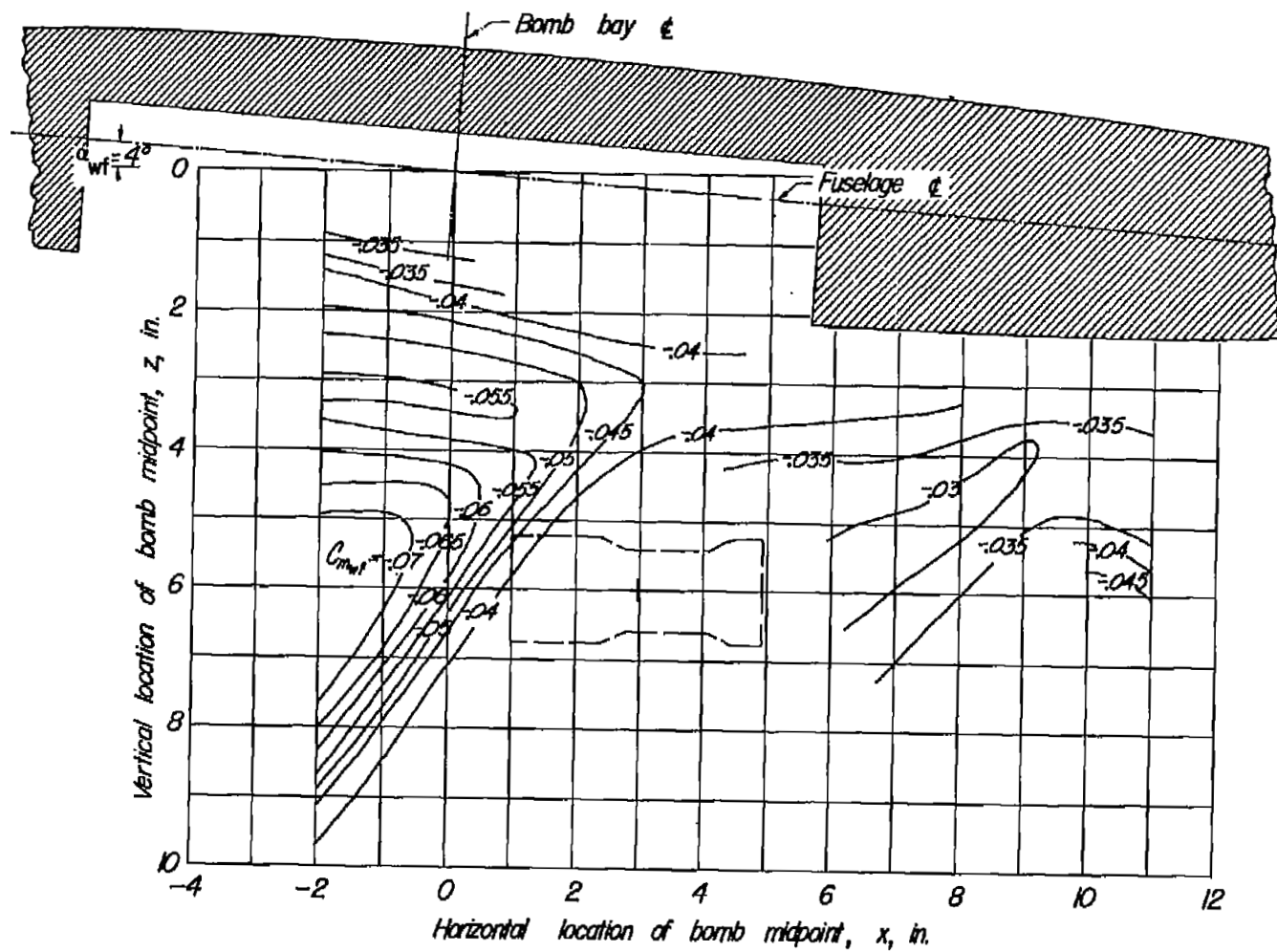
(b) $\alpha_0 = 10^\circ$.

Figure 28.- Continued.



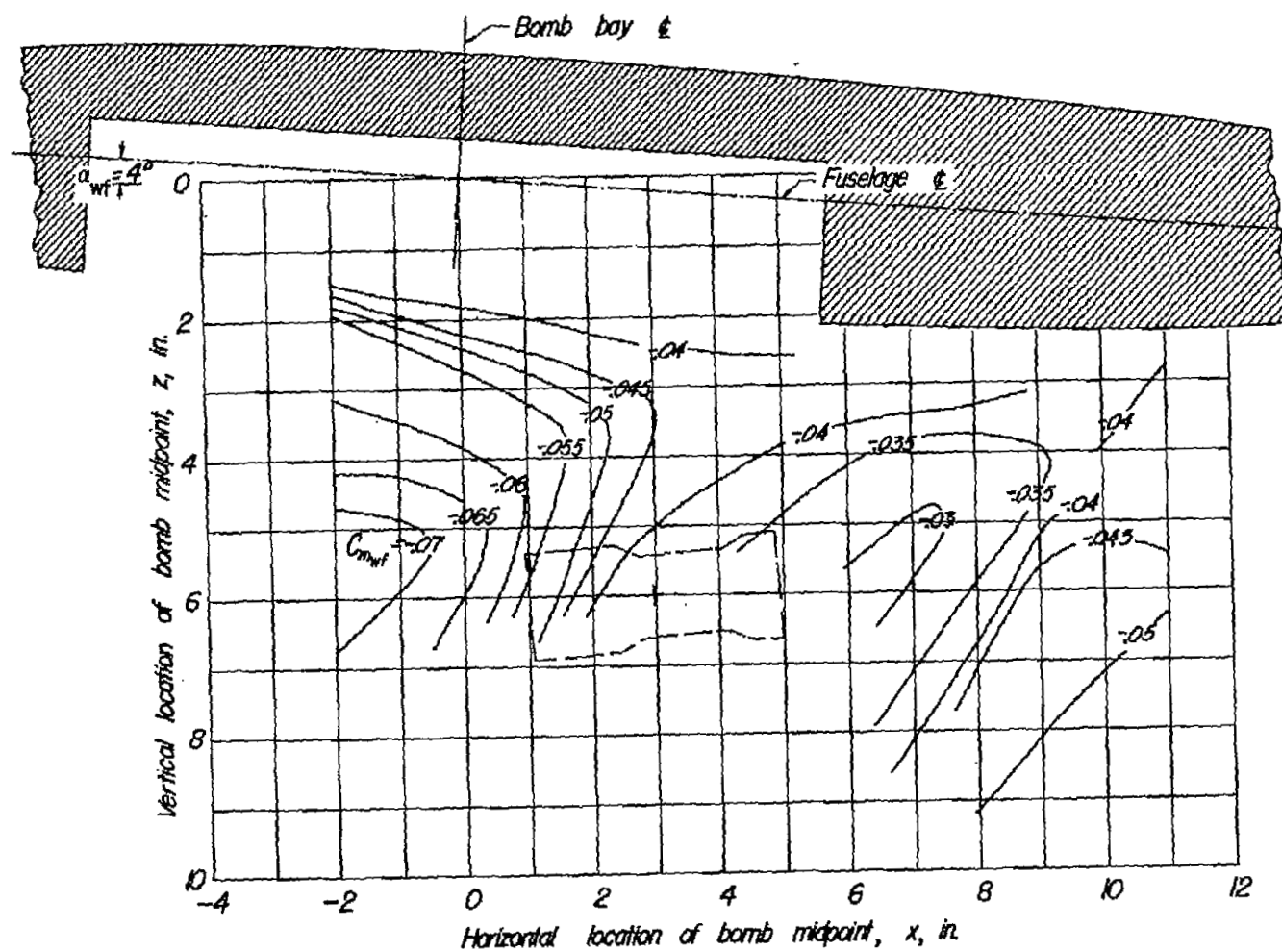
(c) $\alpha_b = 5^\circ$.

Figure 28.- Continued.



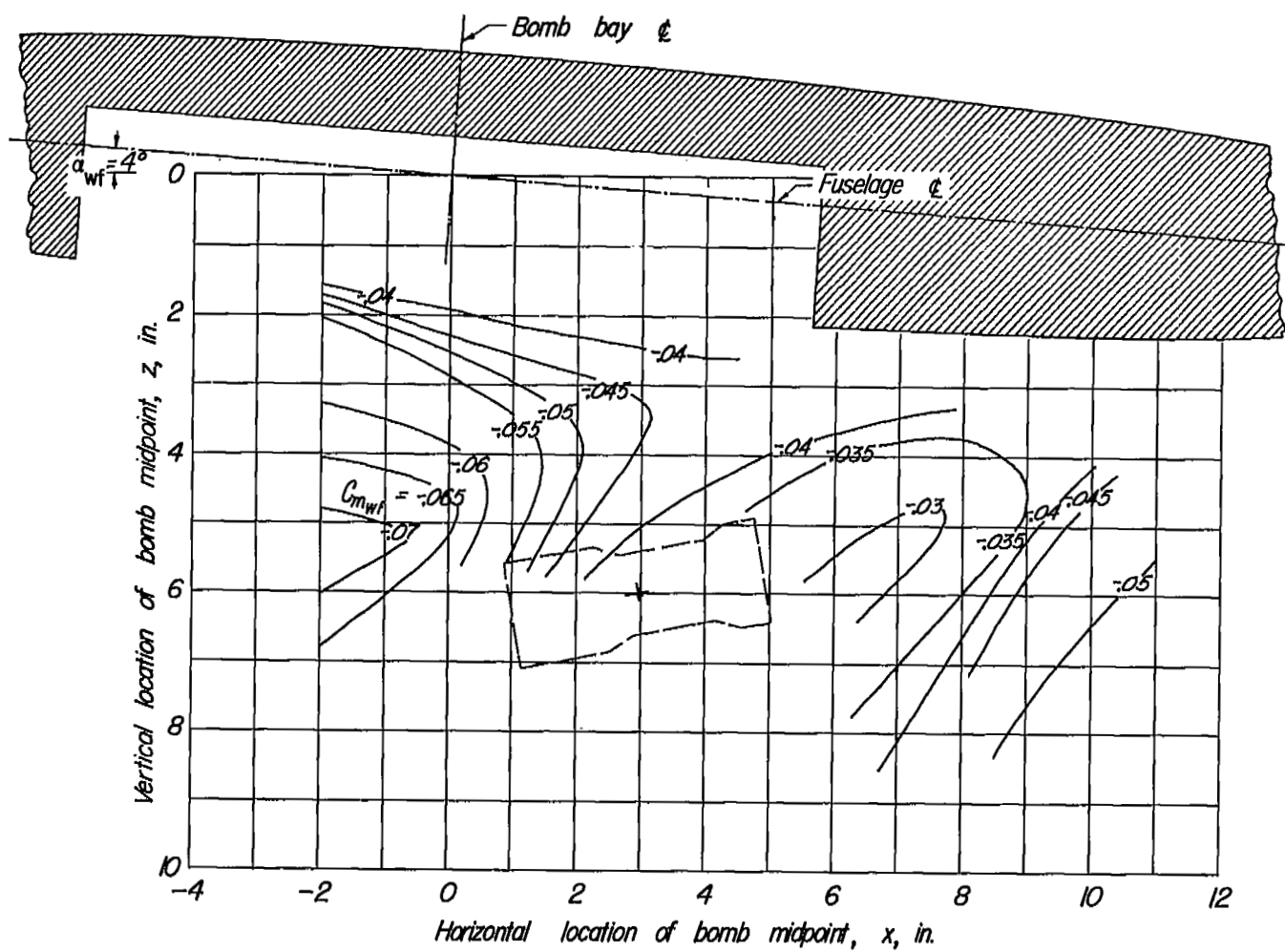
(d) $\alpha_b = 0^\circ$.

Figure 28.- Continued.



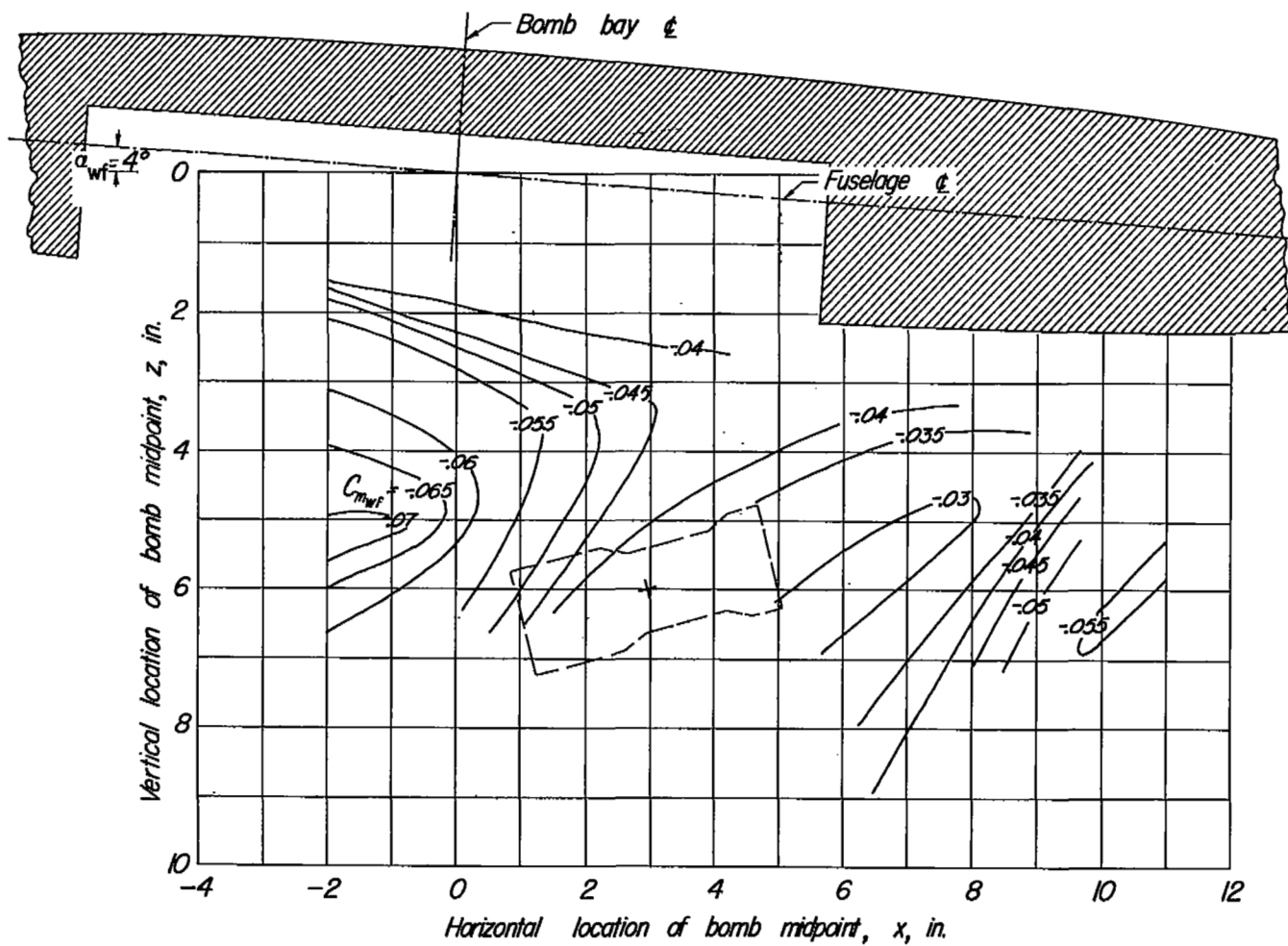
(e) $\alpha_b = -5^\circ$.

Figure 28.- Continued.



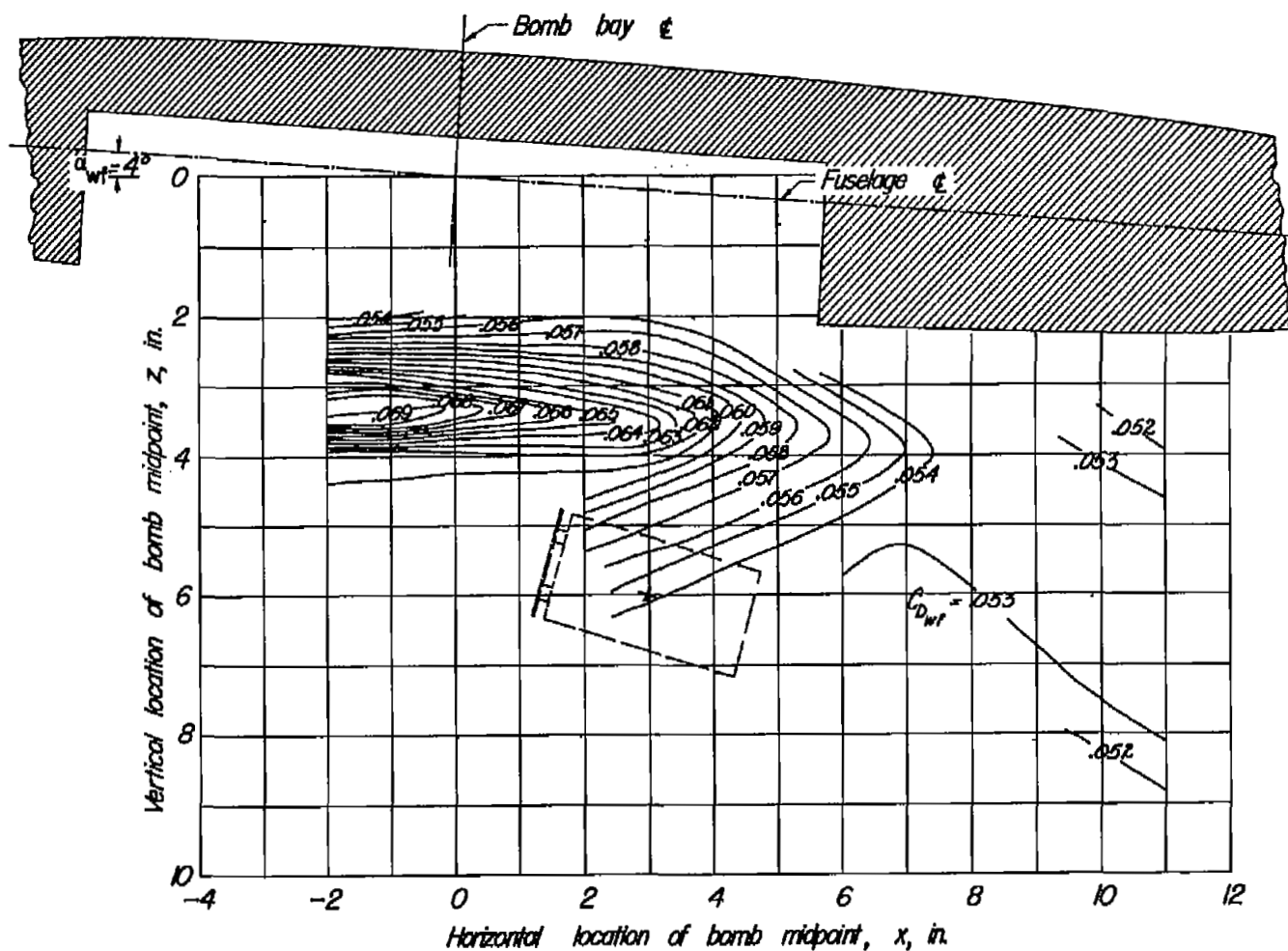
(f) $\alpha_p = -10^\circ$.

Figure 28.- Continued.



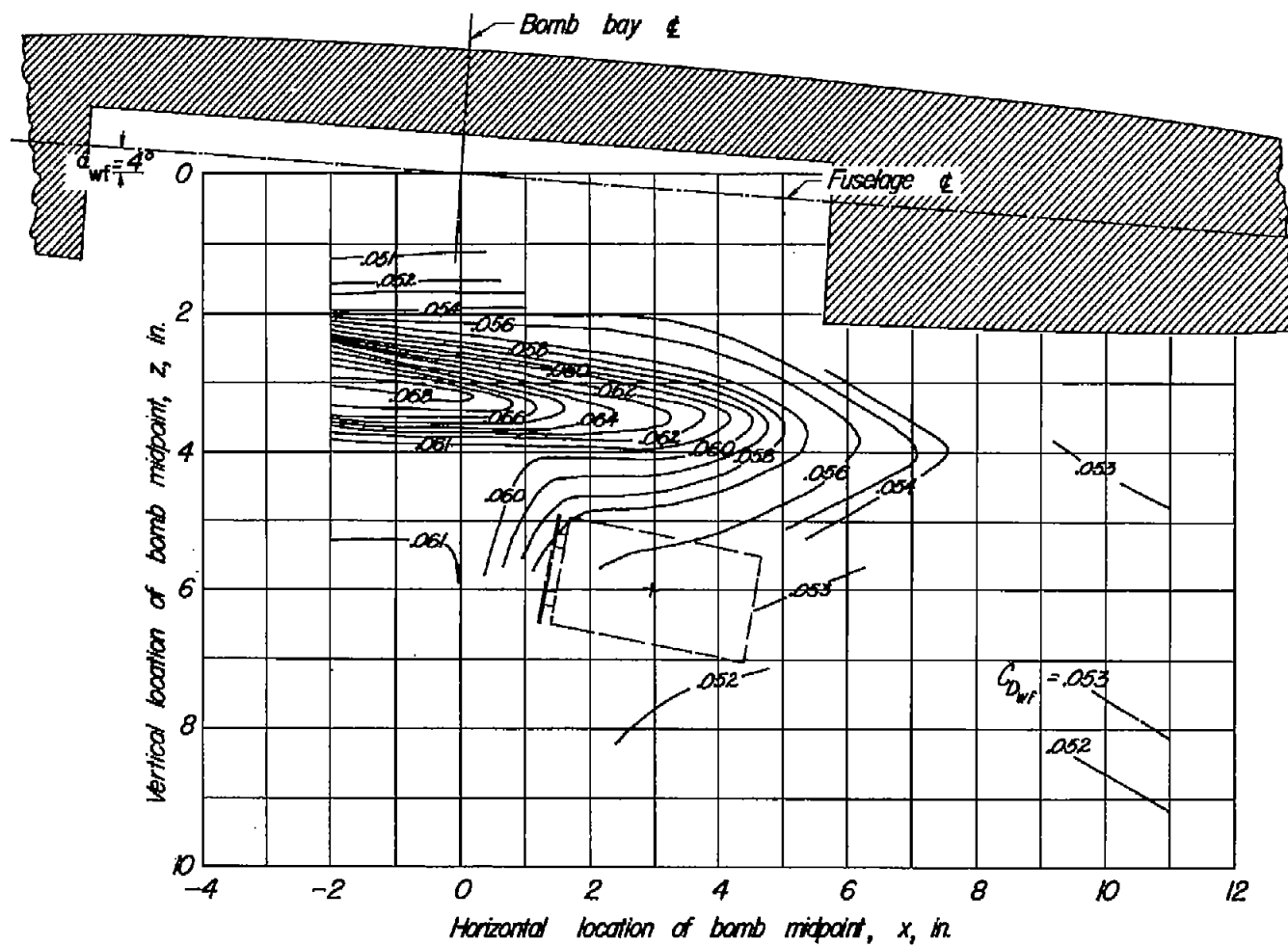
(g) $\alpha_0 = -15^\circ$.

Figure 28.- Concluded.



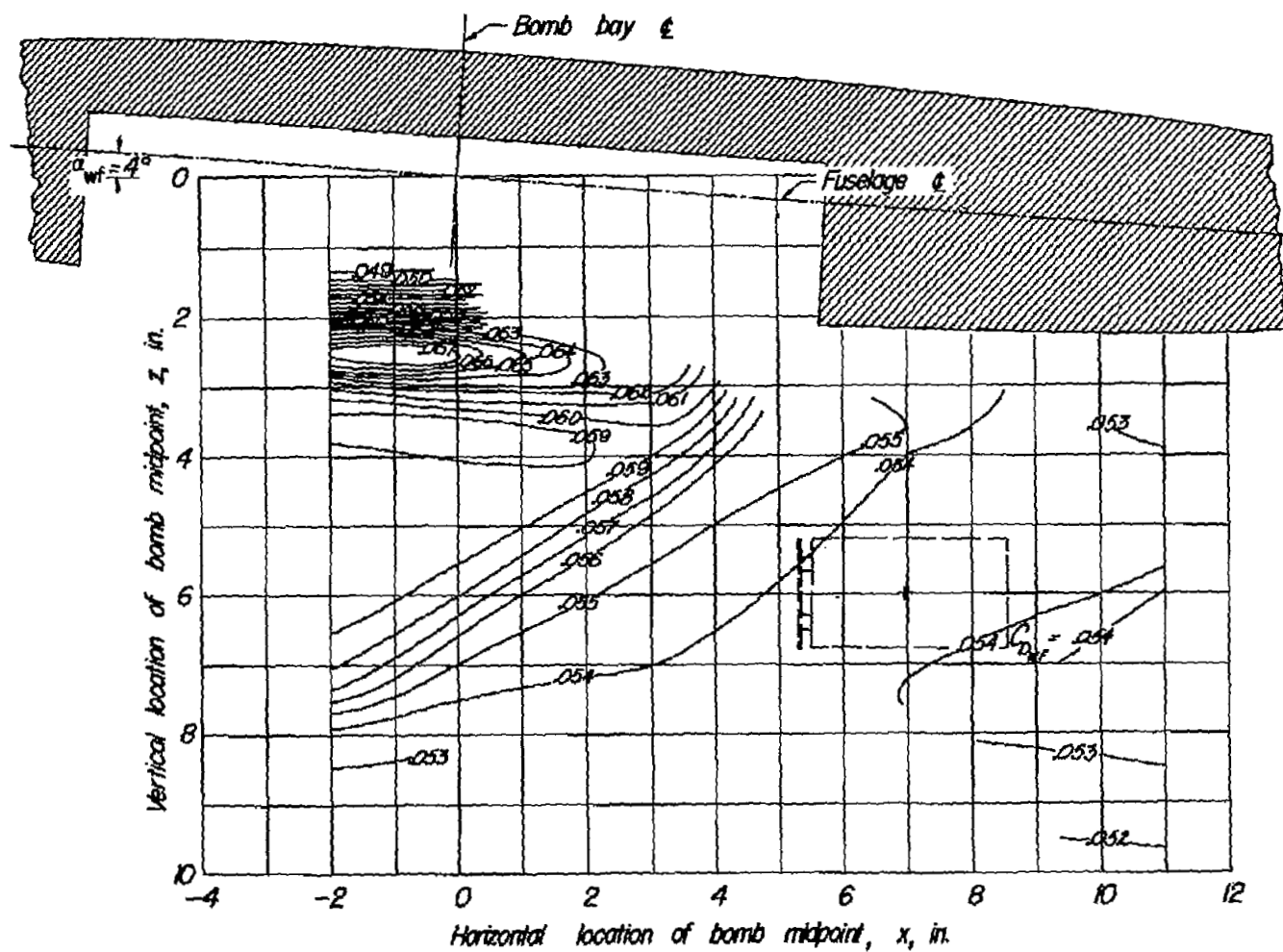
(a) $\alpha_b = 15^\circ$.

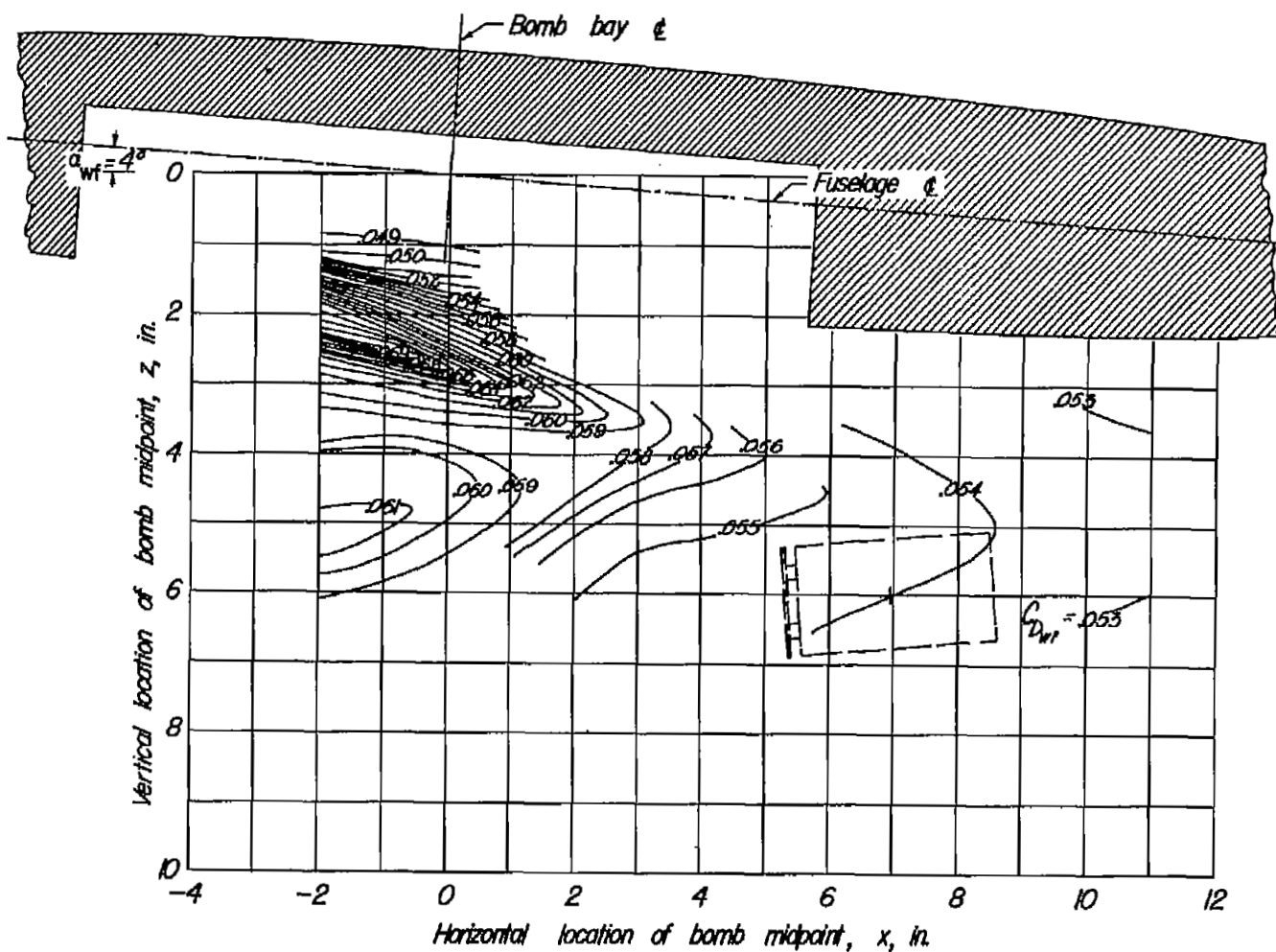
Figure 29.- Contour plot of drag coefficients of wing-fuselage combination in presence of cylindrical bomb.



(b) $\alpha_0 = 10^0$.

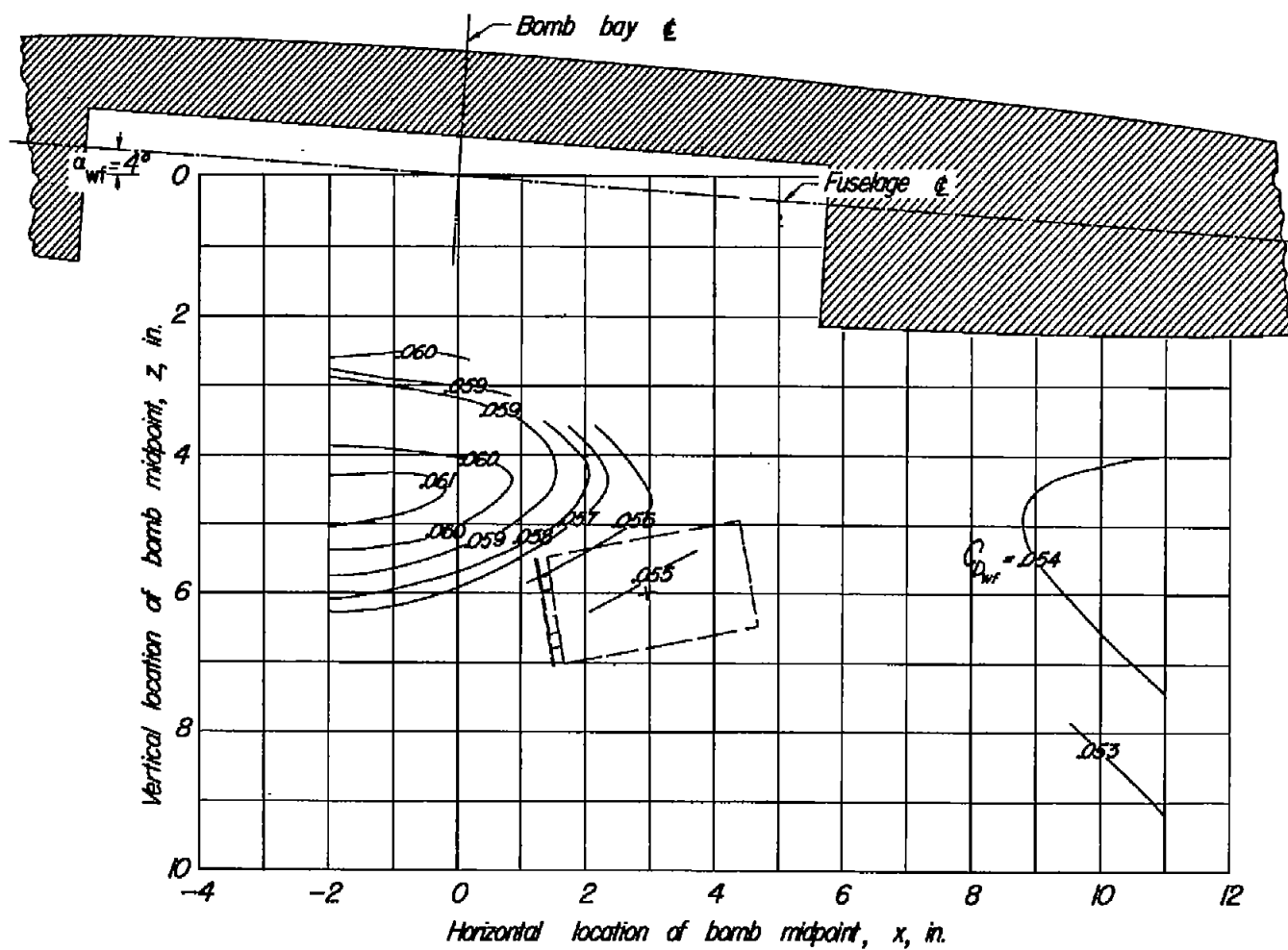
Figure 29.- Continued.





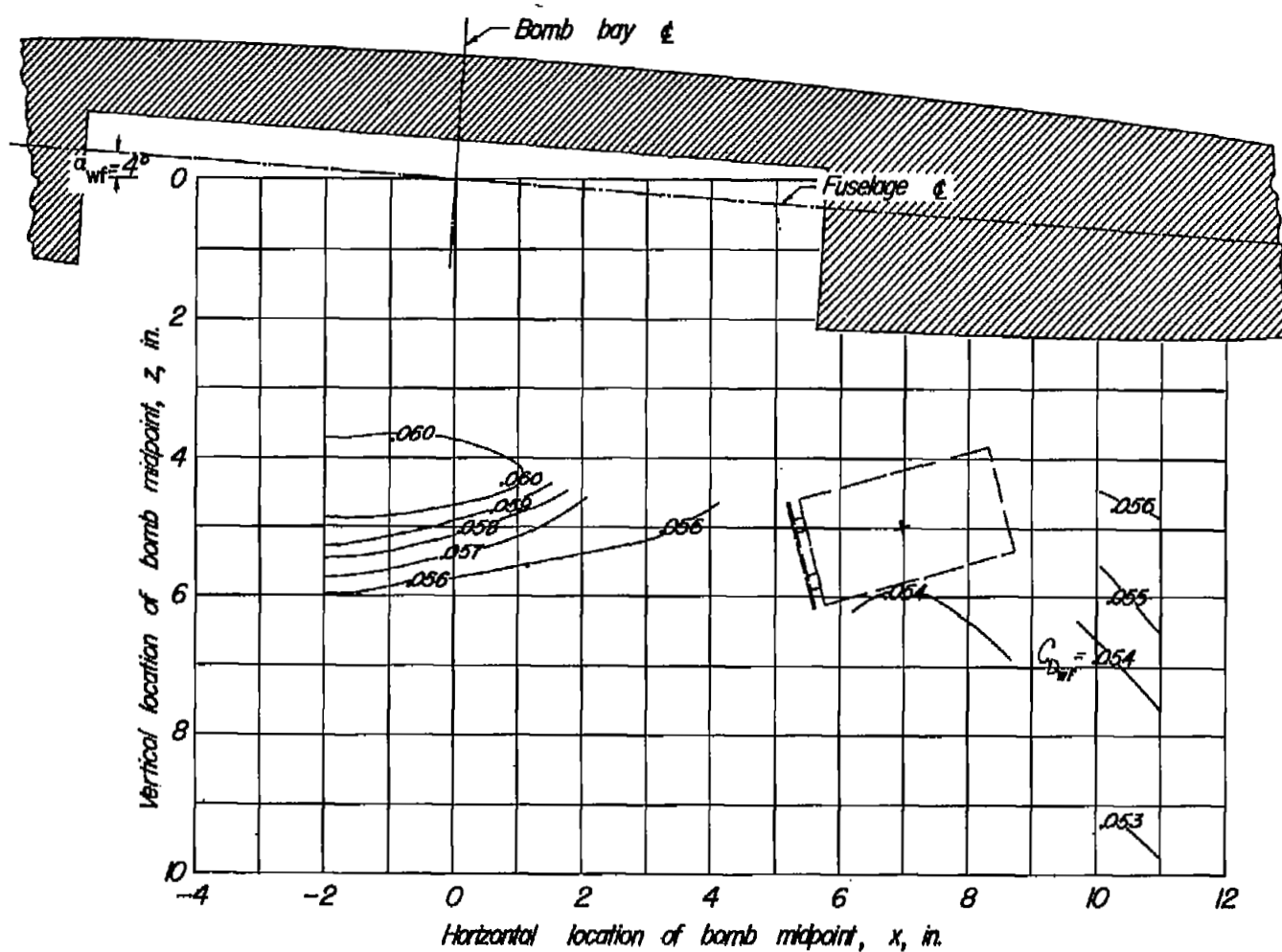
(e) $\alpha_b = -5^\circ$.

Figure 29.- Continued.



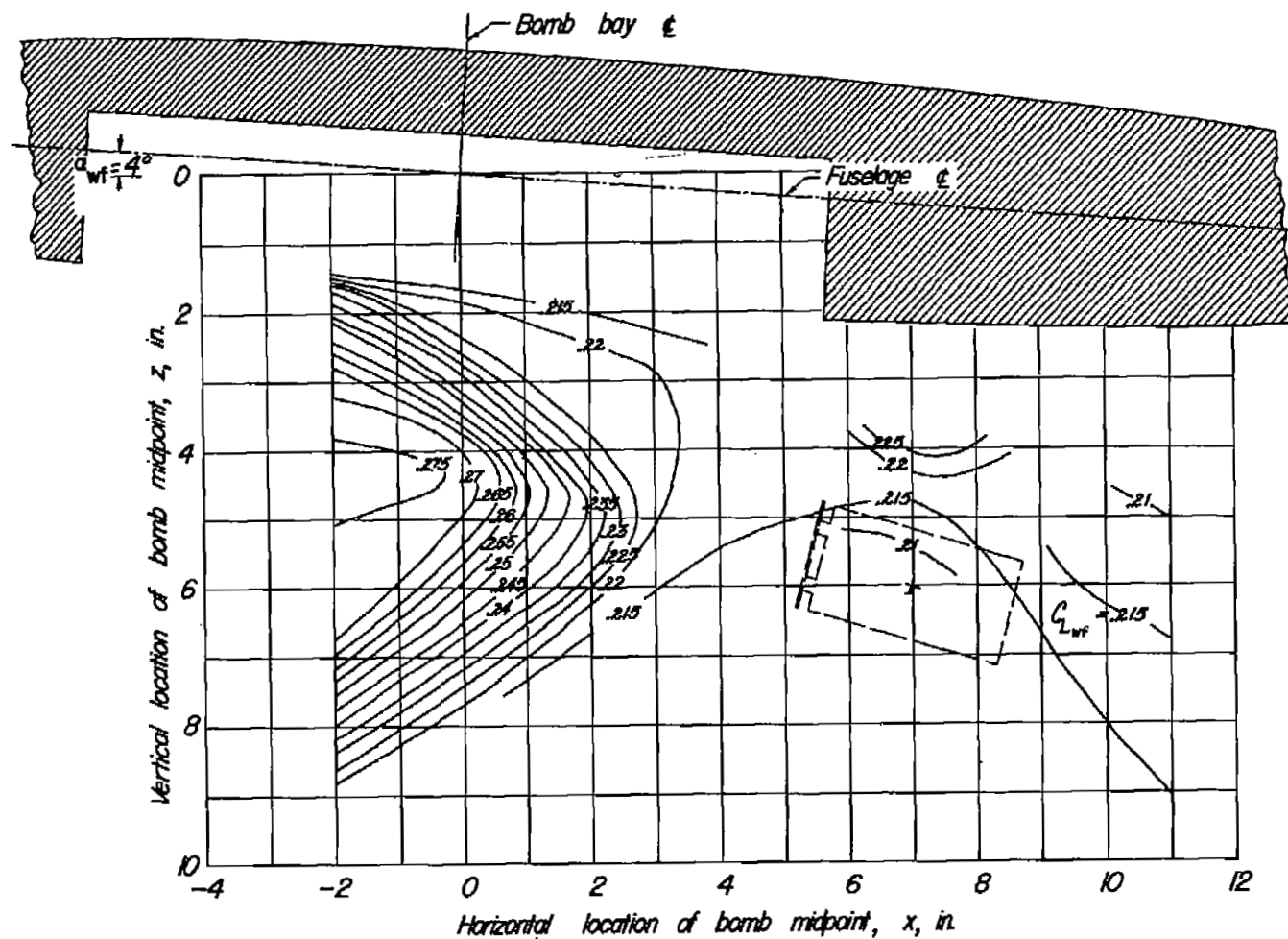
(f) $\alpha_0 = -10^\circ$.

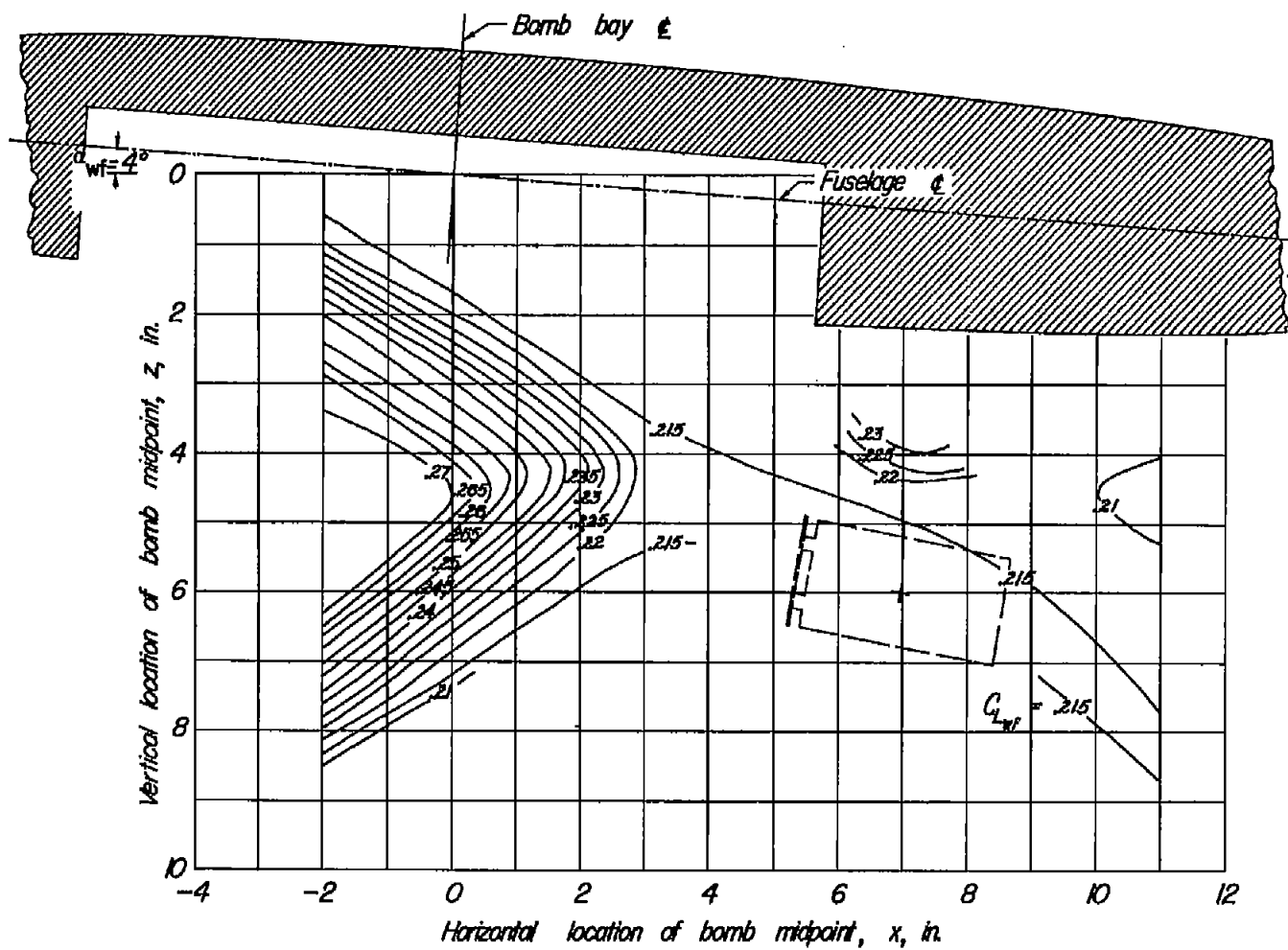
Figure 29.- Continued.



(g) $\alpha_b = -15^\circ$.

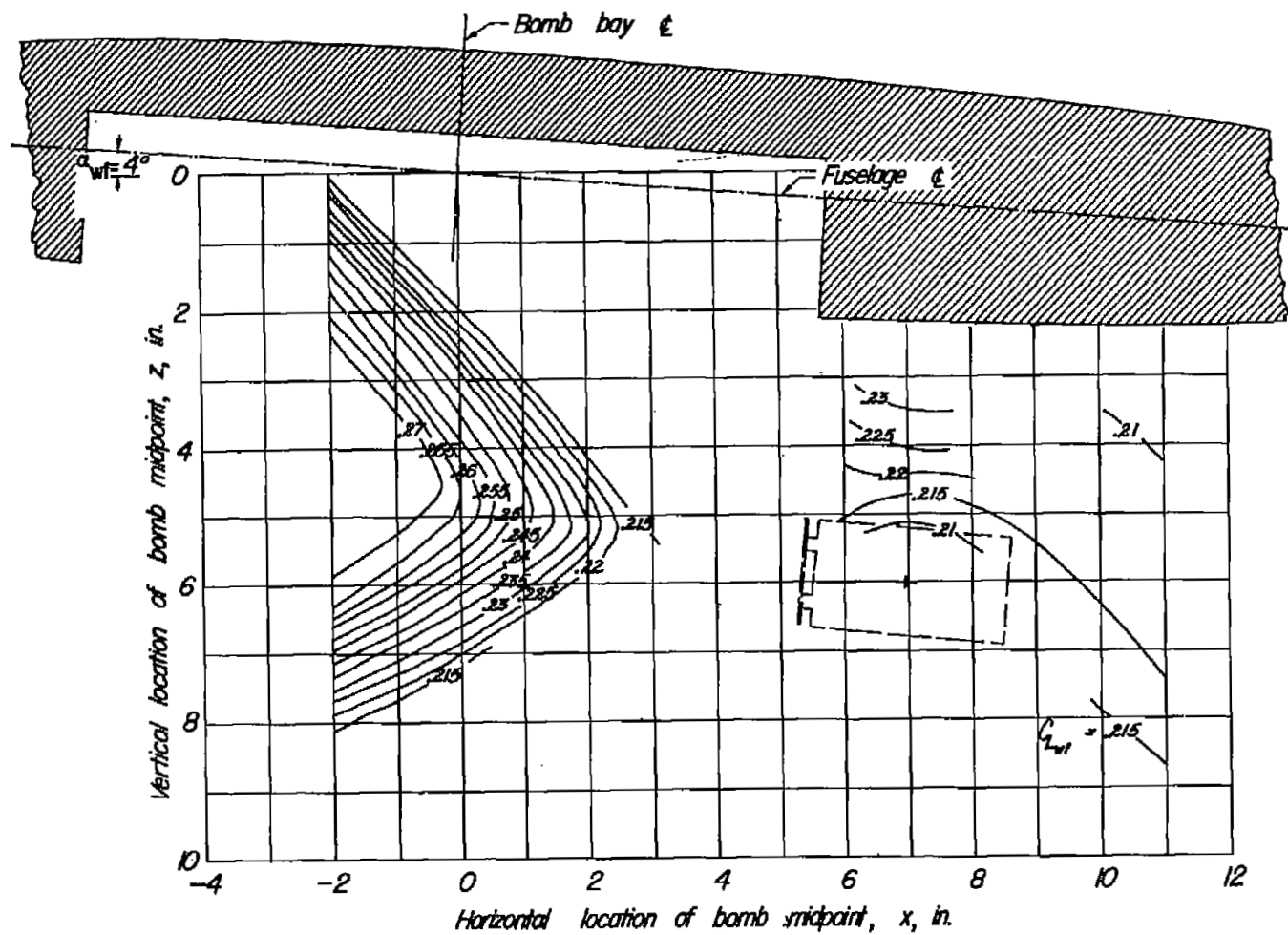
Figure 29.- Concluded.





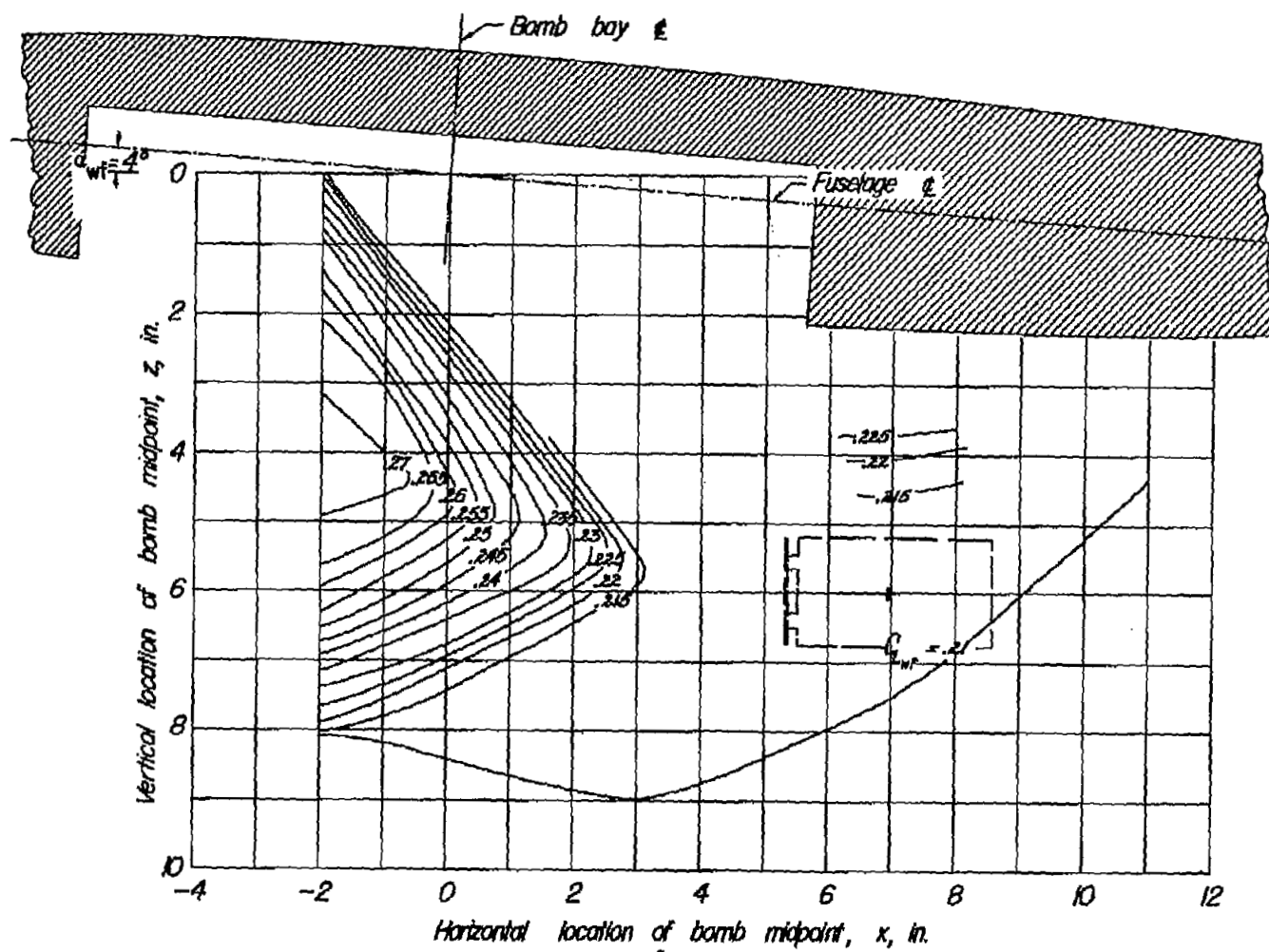
(b) $\alpha_b = 10^\circ$.

Figure 30.- Continued.



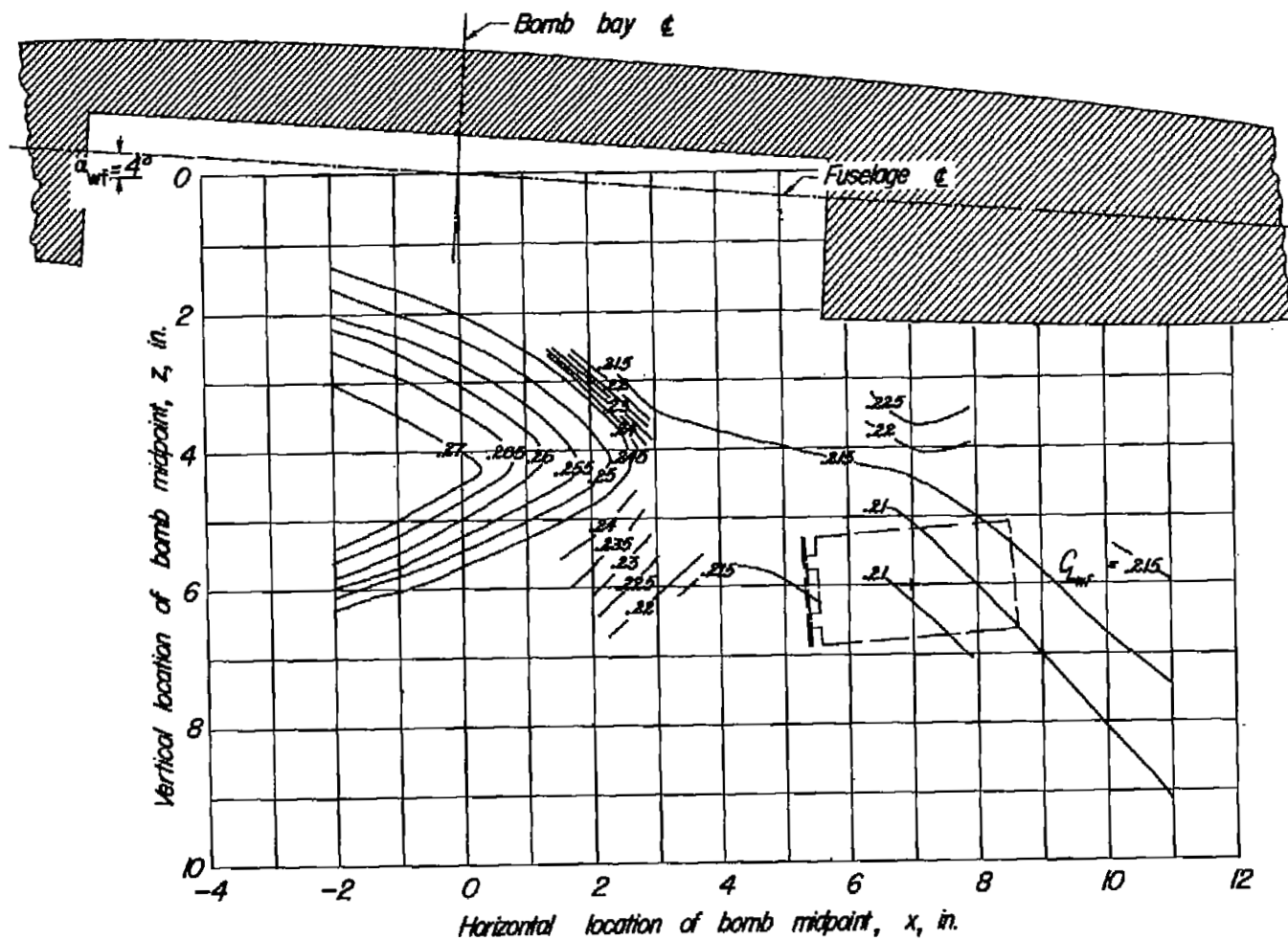
(c) $\alpha_0 = 5^\circ$.

Figure 30.- Continued.



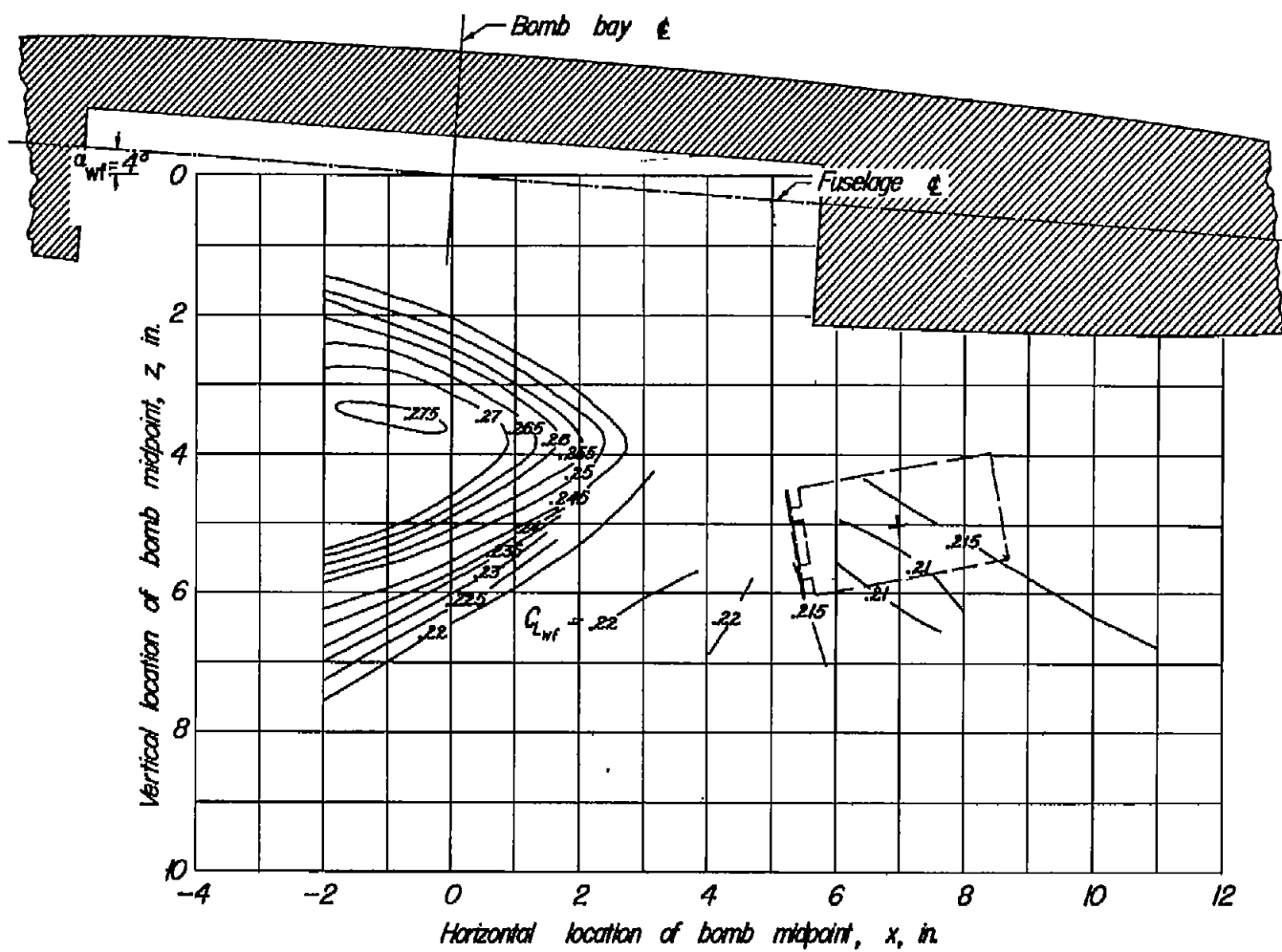
(d) $\alpha_0 = 0^\circ$.

Figure 30.- Continued.



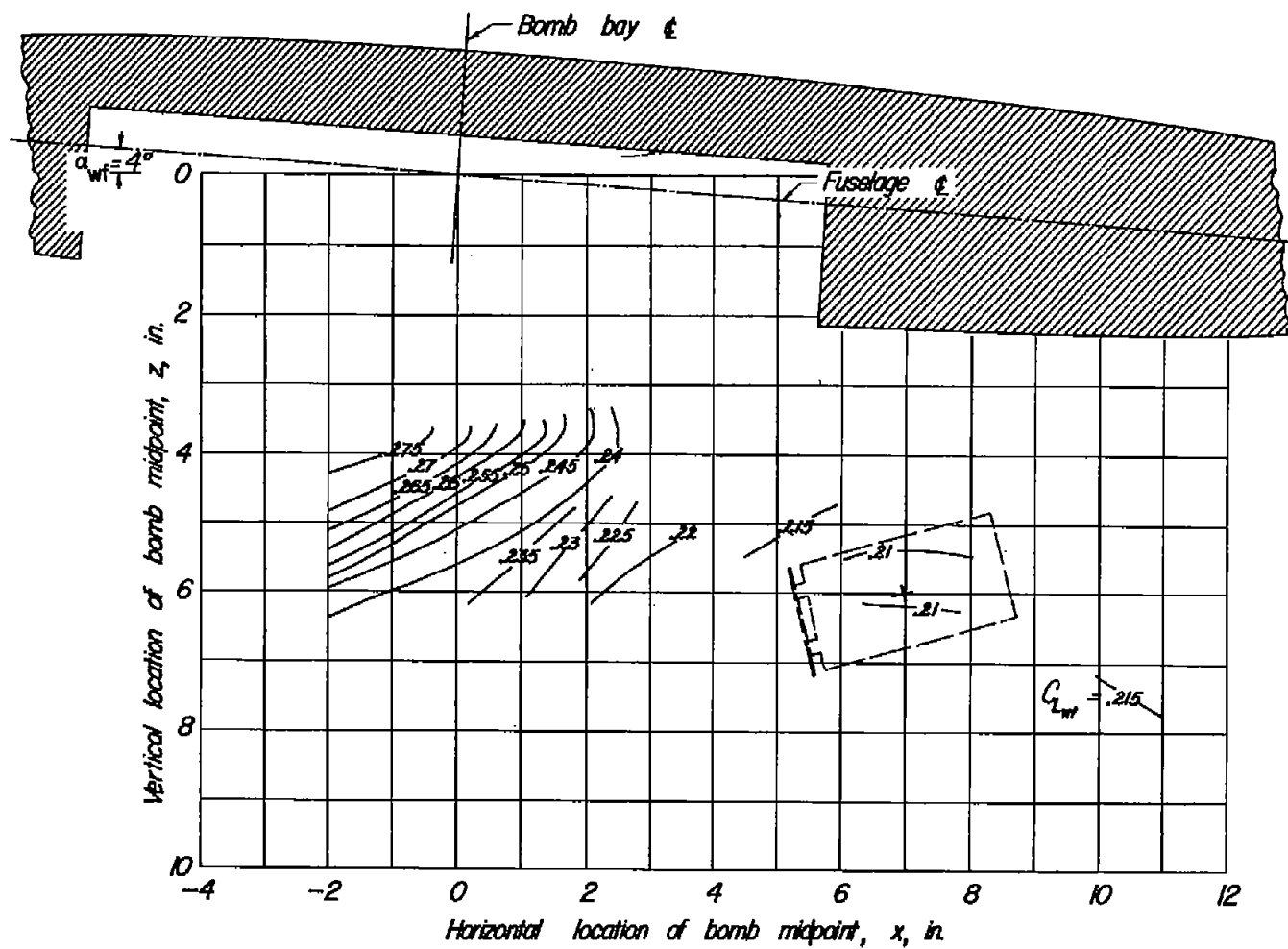
(e) $\alpha_b = -5^\circ$.

Figure 30.- Continued.



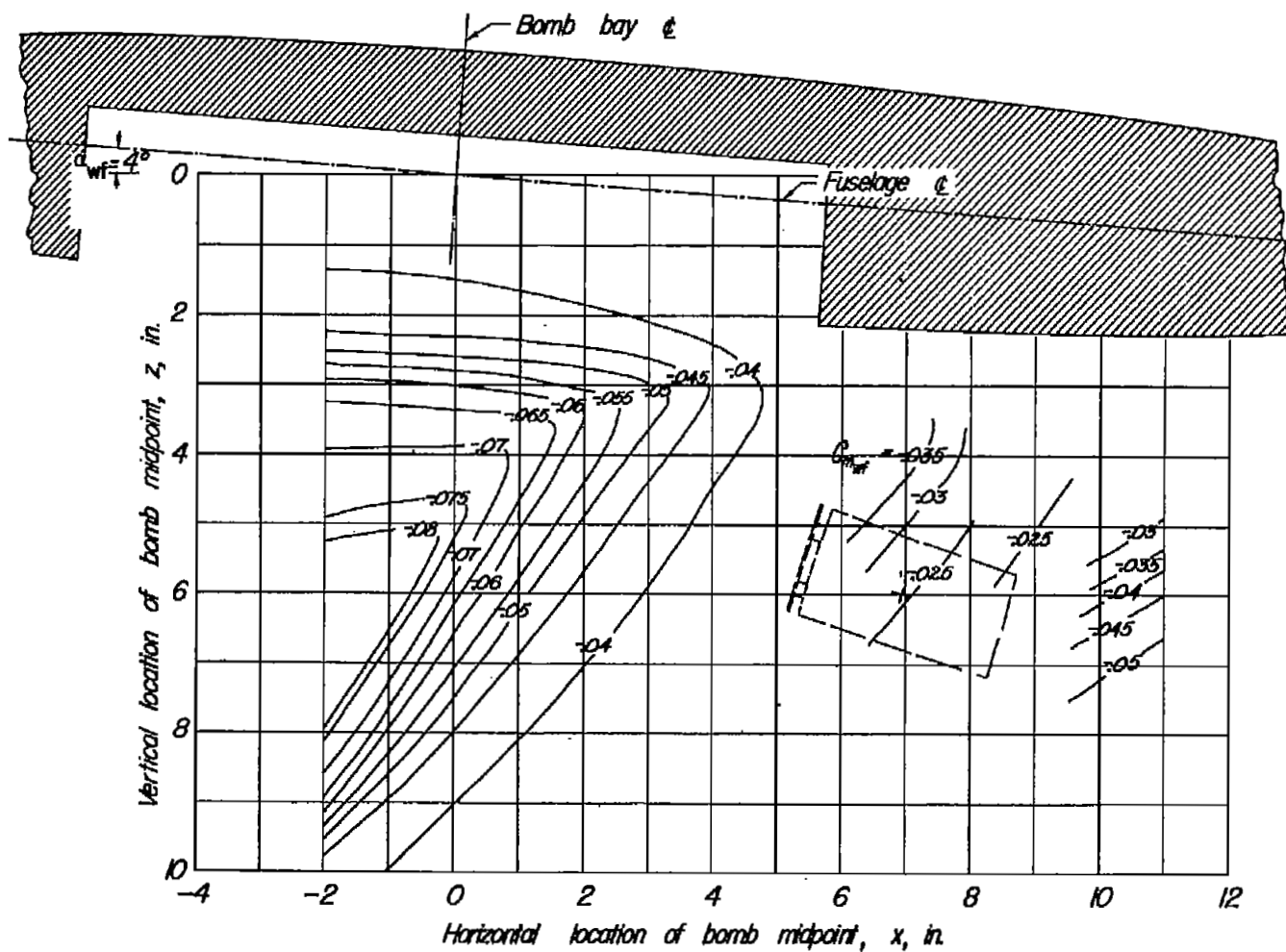
(f) $\alpha_b = -10^\circ$.

Figure 30.- Continued.



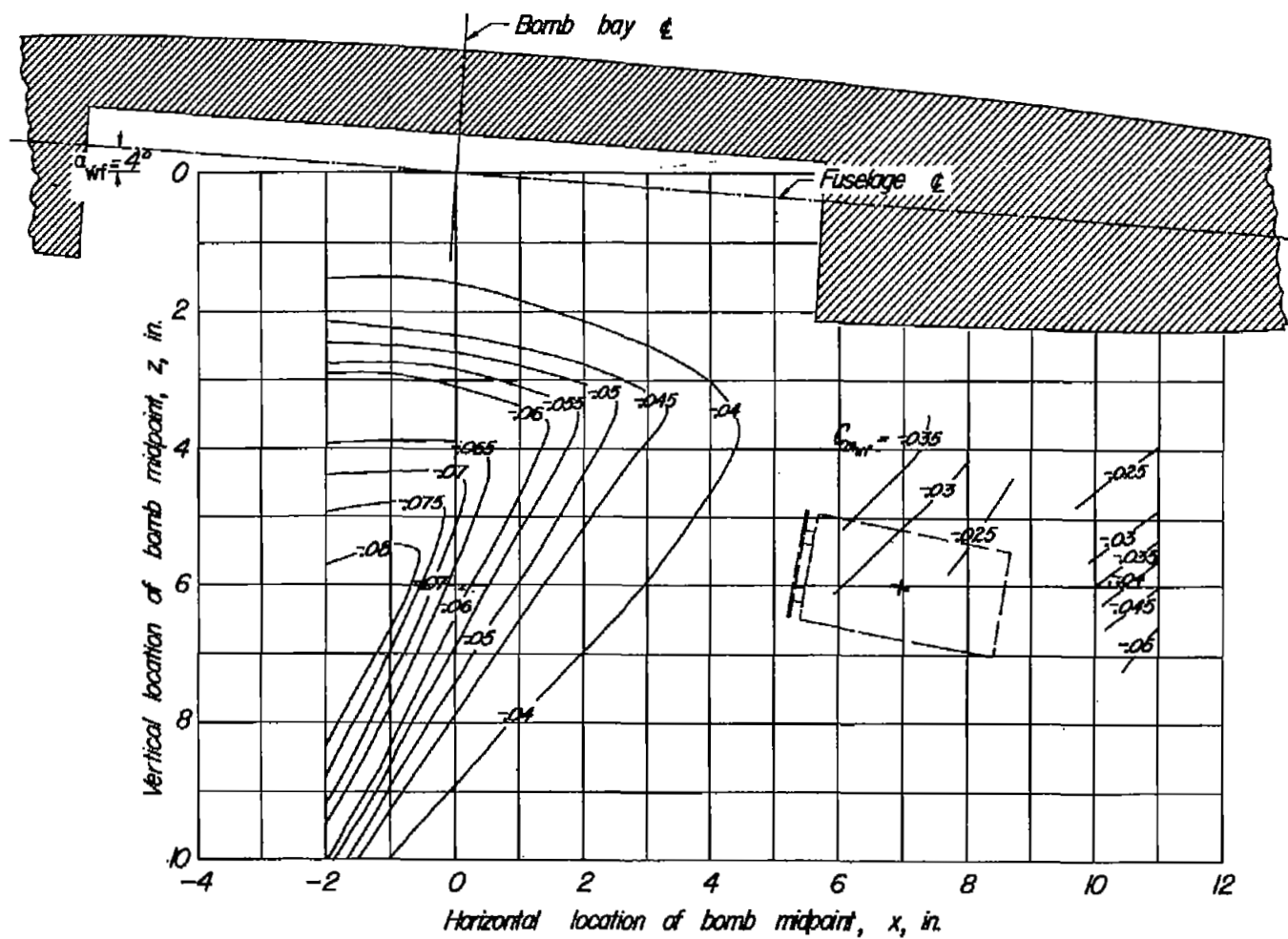
(g) $\alpha_b = -15^\circ$.

Figure 30.- Concluded.



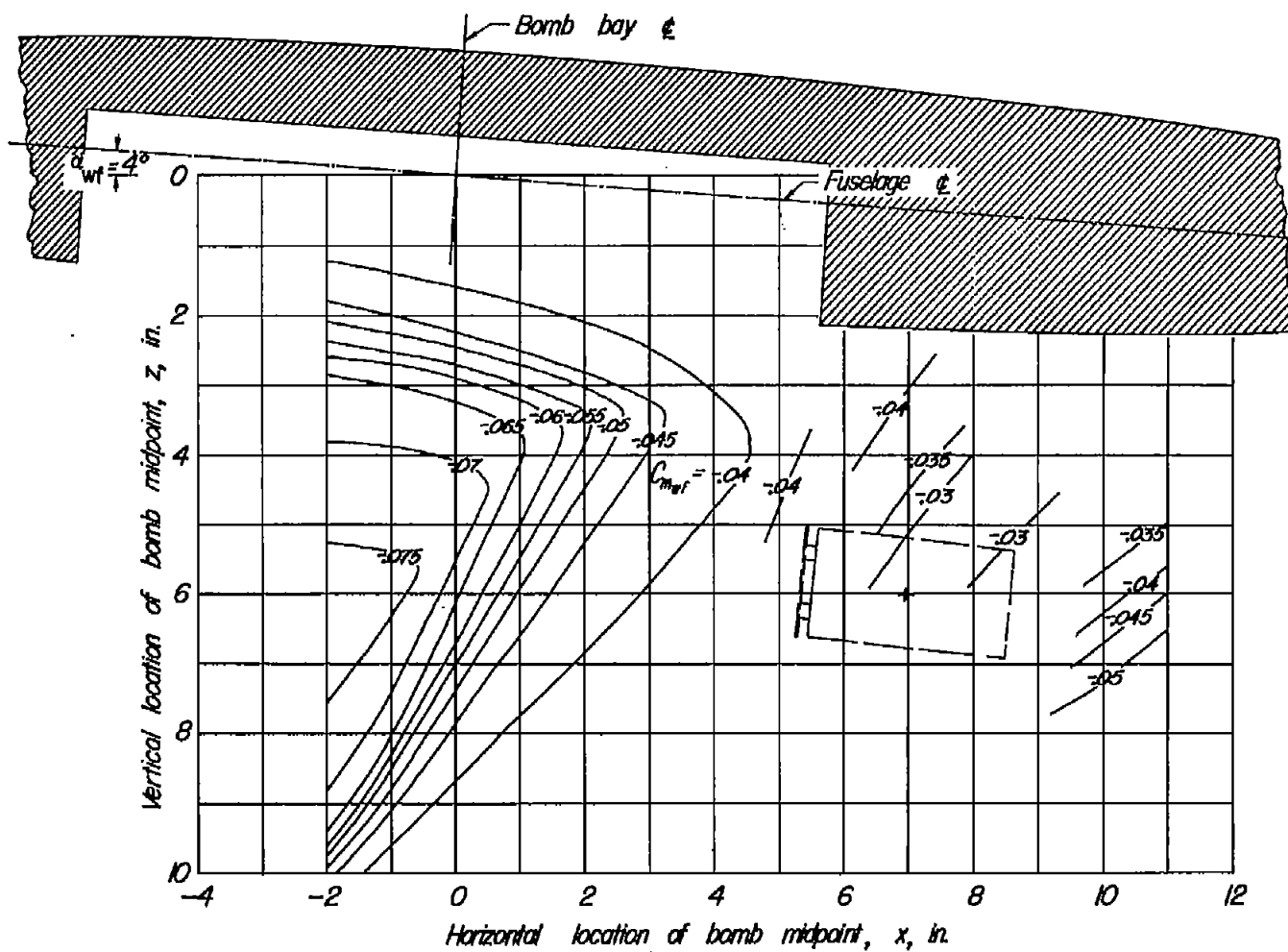
(a) $\alpha_b = 15^\circ$.

Figure 31.- Contour plot of pitching-moment coefficients of wing-fuselage combination in presence of cylindrical bomb.



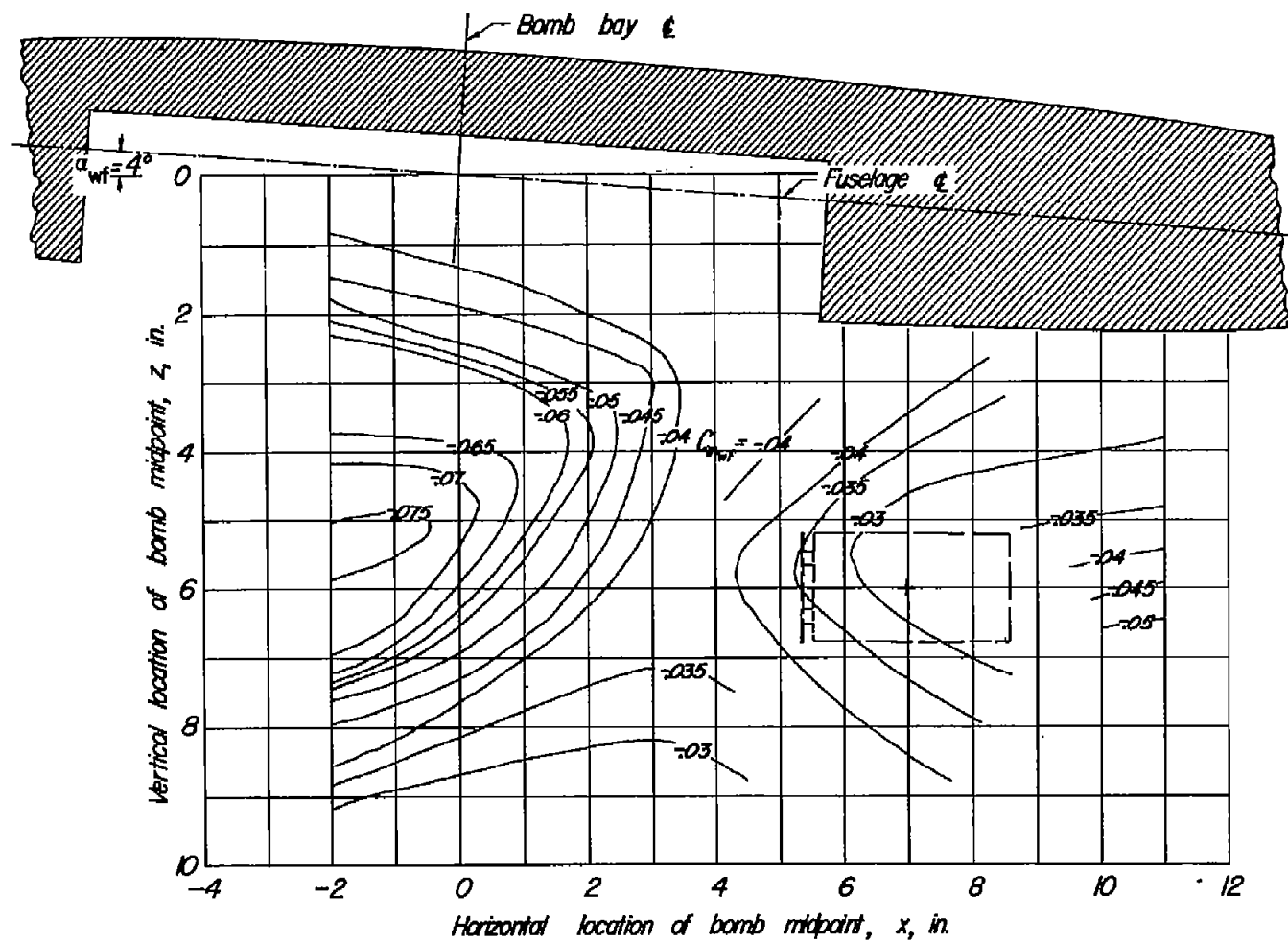
(b) $\alpha_b = 10^\circ$.

Figure 31.- Continued.



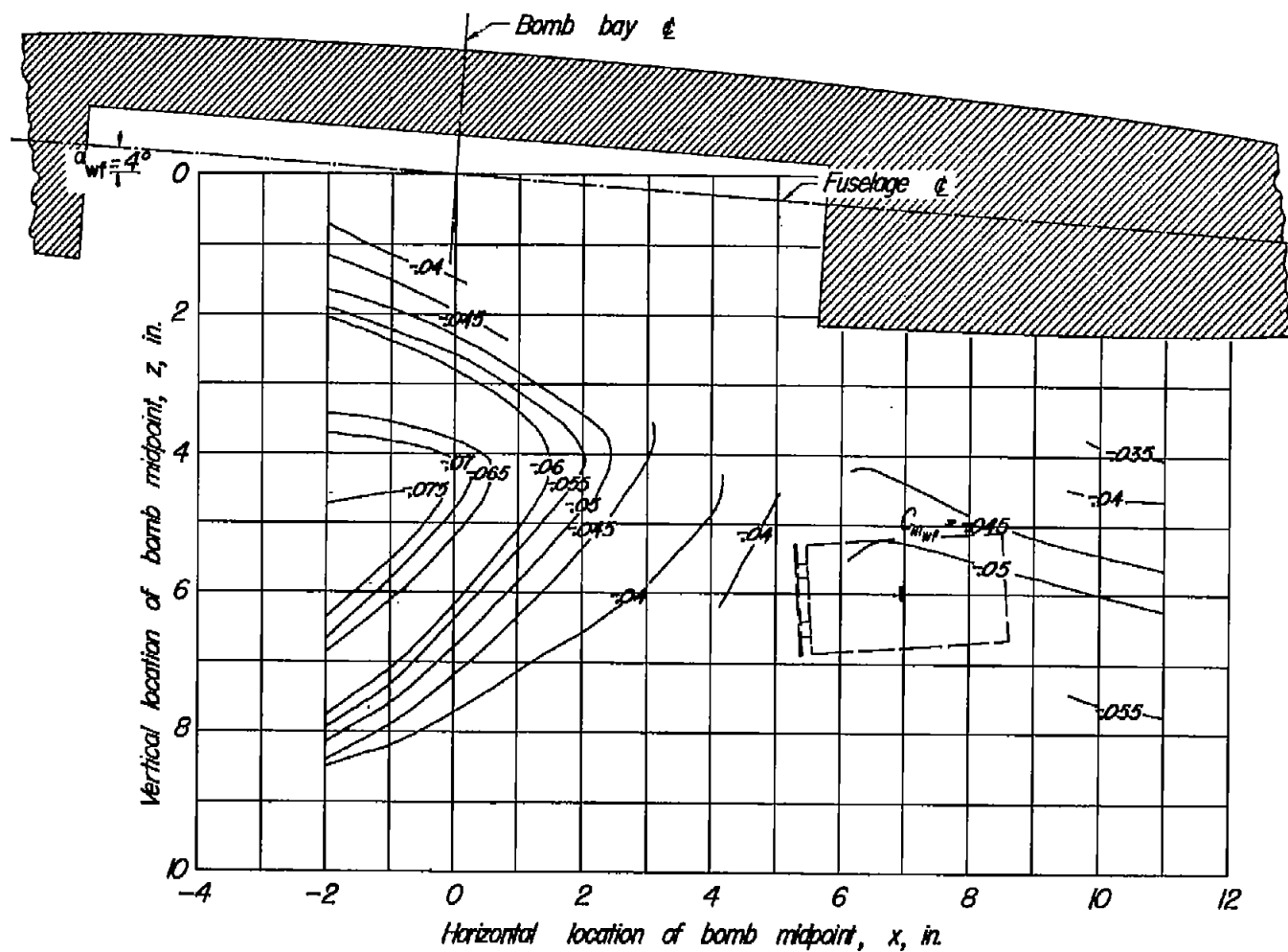
(c) $\alpha_b = 5^\circ$.

Figure 31.- Continued.



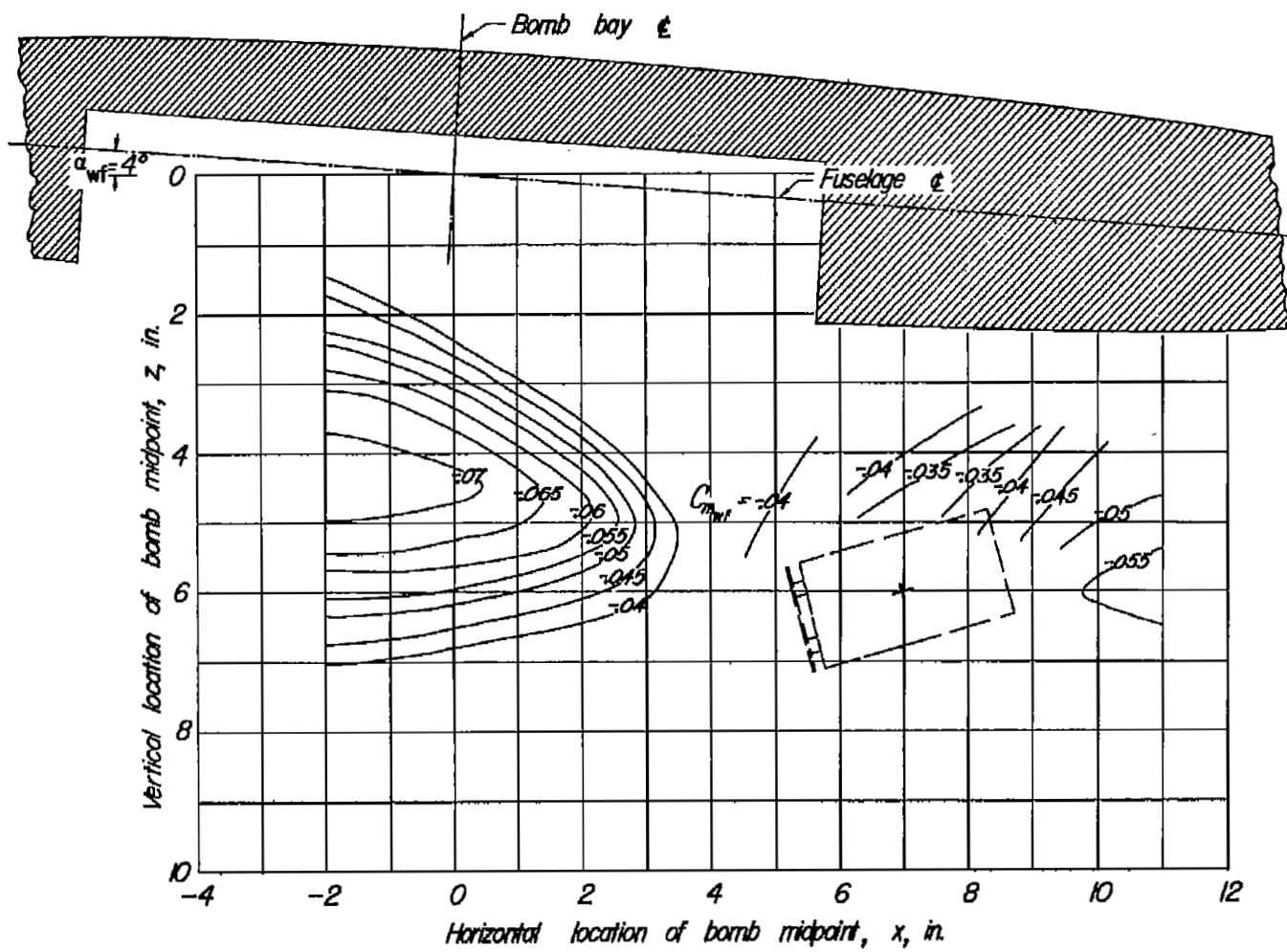
(d) $\alpha_b = 0^\circ$.

Figure 31.- Continued.



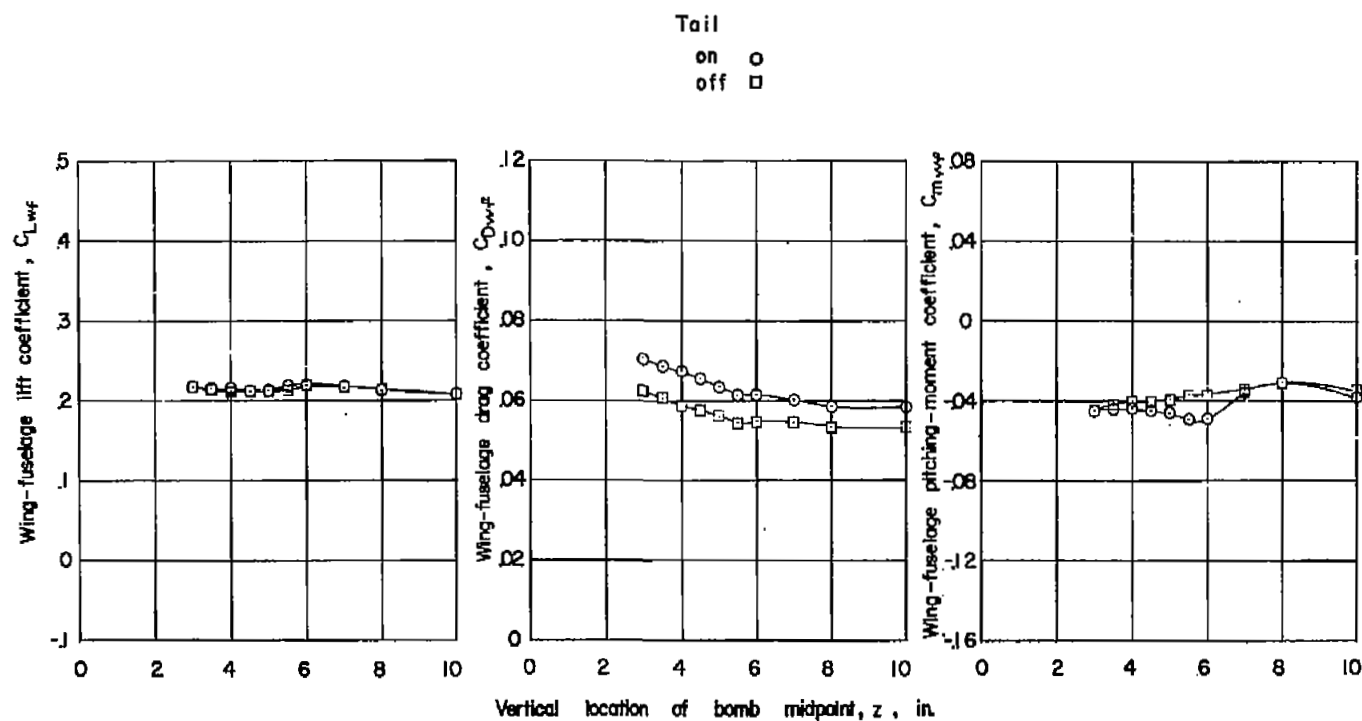
(e) $\alpha_b = -5^\circ$.

Figure 31.- Continued.



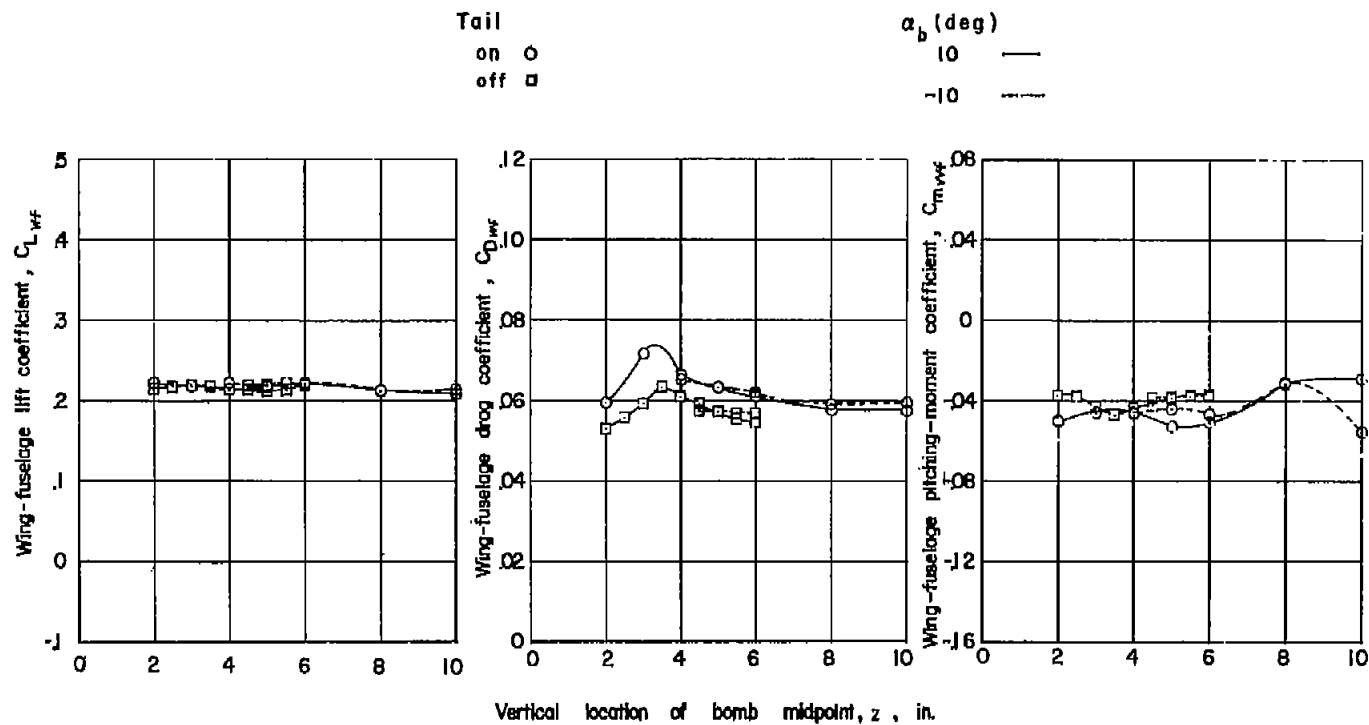
(g) $\alpha_b = -15^\circ$.

Figure 31.- Concluded.



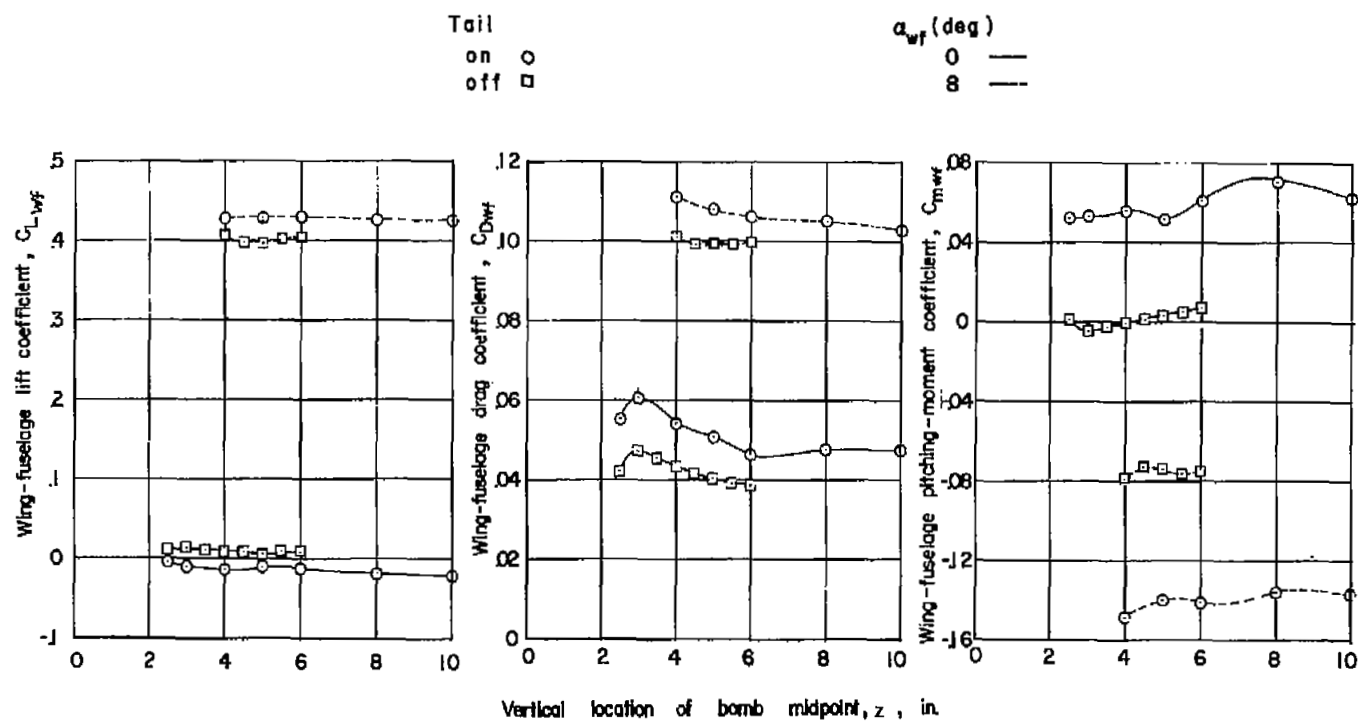
(a) $\alpha_{wf} = 4^\circ$; $\alpha_b = 0^\circ$; $x = 2.95$ inches.

Figure 32.- Lift, drag, and pitching-moment coefficients of wing-fuselage combination with and without a tail in presence of spool bomb in a forward position.



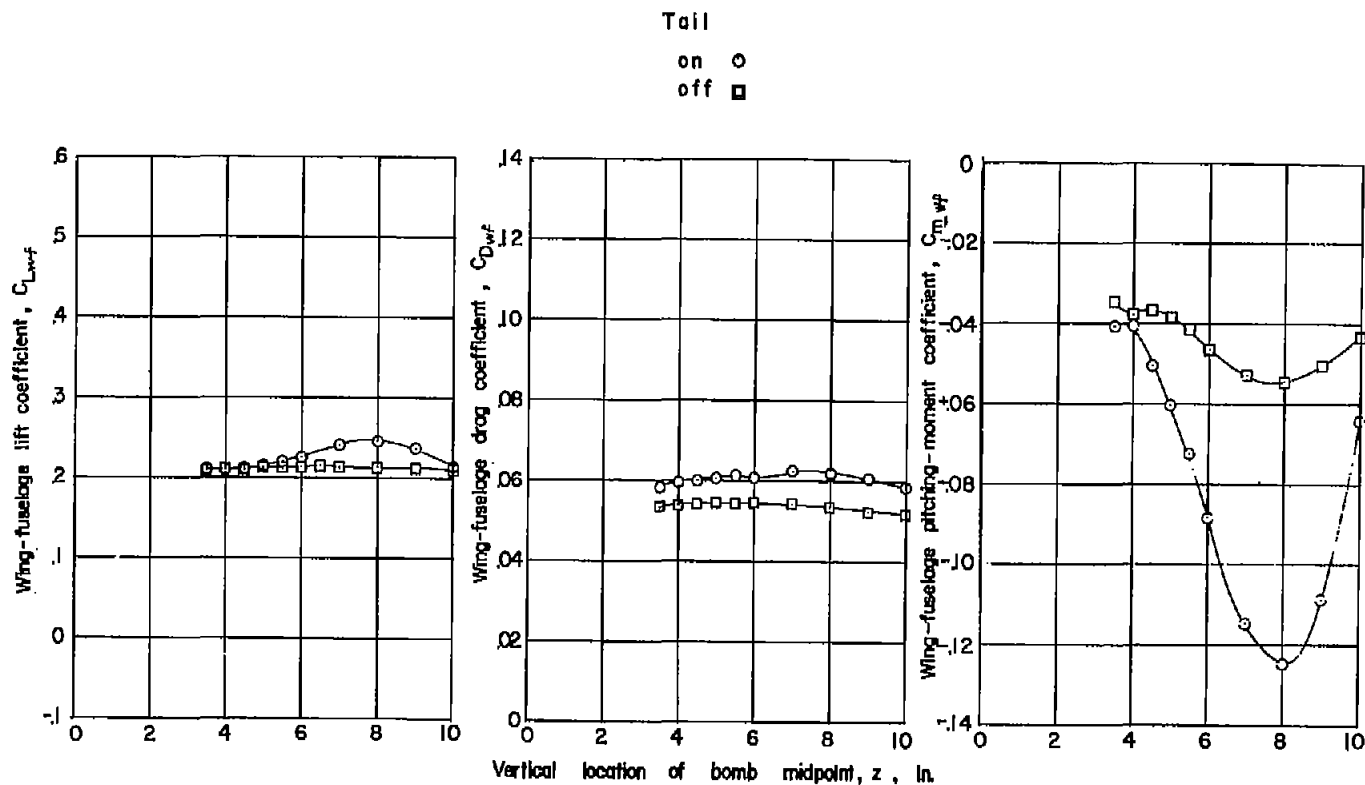
(b) $\alpha_{wf} = 4^\circ$; $x = 2.95$ inches.

Figure 32.- Continued.



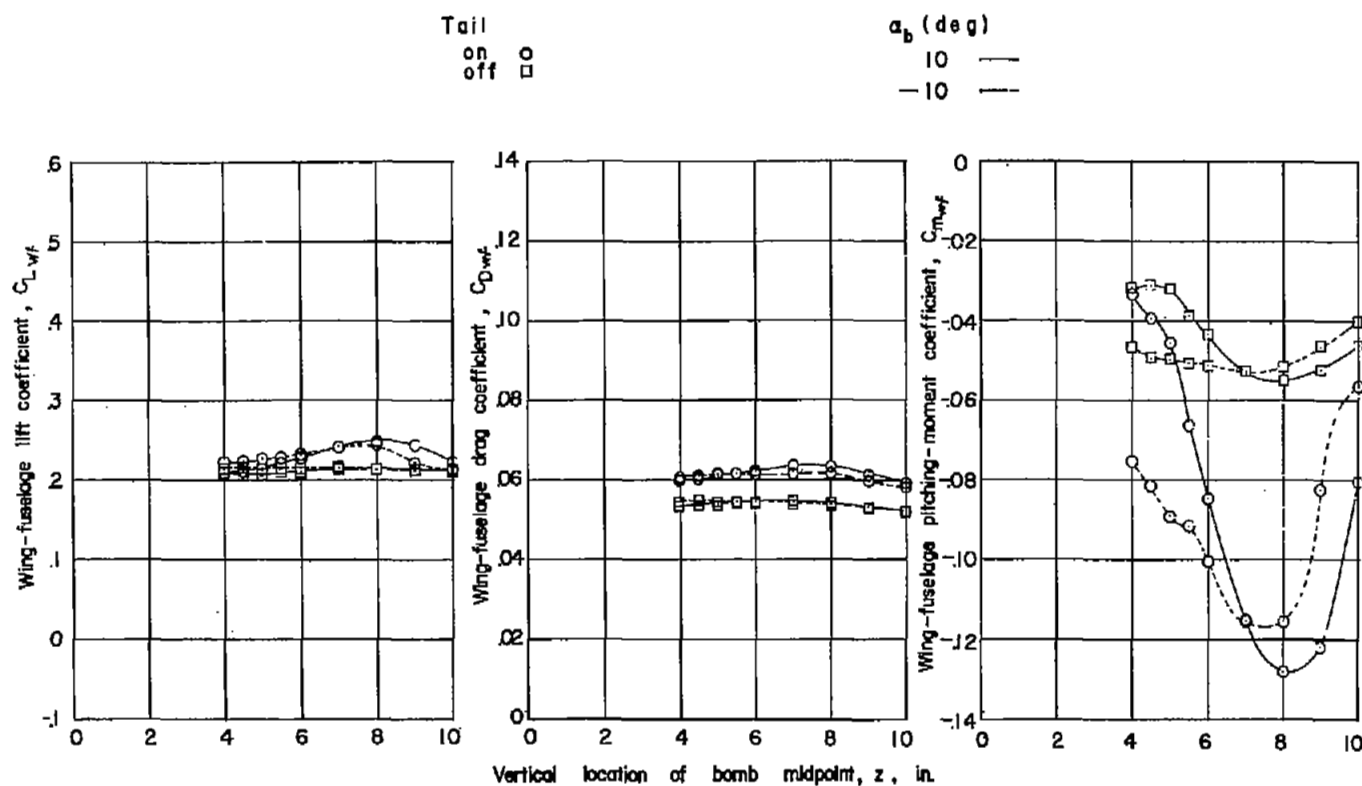
(c) $\alpha_{wf} = 0^\circ$; $x = 2.70$ inches; $\alpha_b = 0^\circ$.
 $\alpha_{wf} = 8^\circ$; $x = 2.83$ inches; $\alpha_b = 0^\circ$.

Figure 32.- Concluded.



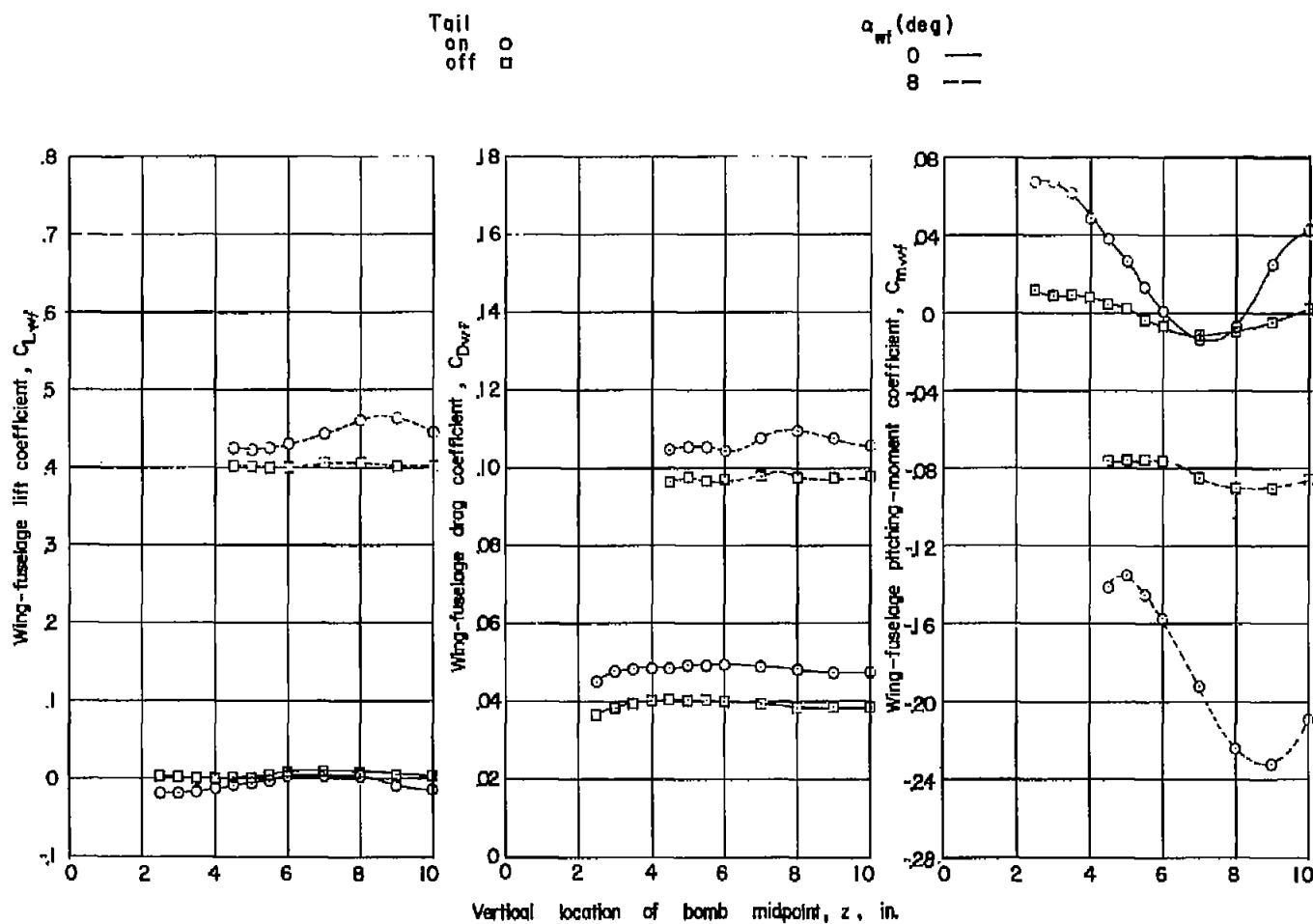
(a) $\alpha_{wf} = 4^\circ$; $\alpha_b = 0^\circ$; $x = 10.95$ inches.

Figure 33.- Lift, drag, and pitching-moment coefficients of the wing-fuselage combination with and without tail in presence of spool bomb in a rearward position.



(b) $\alpha_{wf} = 4^\circ$; $x = 10.95$ inches.

Figure 33.- Continued.



(c) $\alpha_{wf} = 0^\circ$; $x = 10.7$ inches; $\alpha_p = 0^\circ$.
 $\alpha_{wf} = 8^\circ$; $x = 10.83$ inches; $\alpha_p = 0^\circ$.

Figure 33.- Concluded.

UNCLASSIFIED

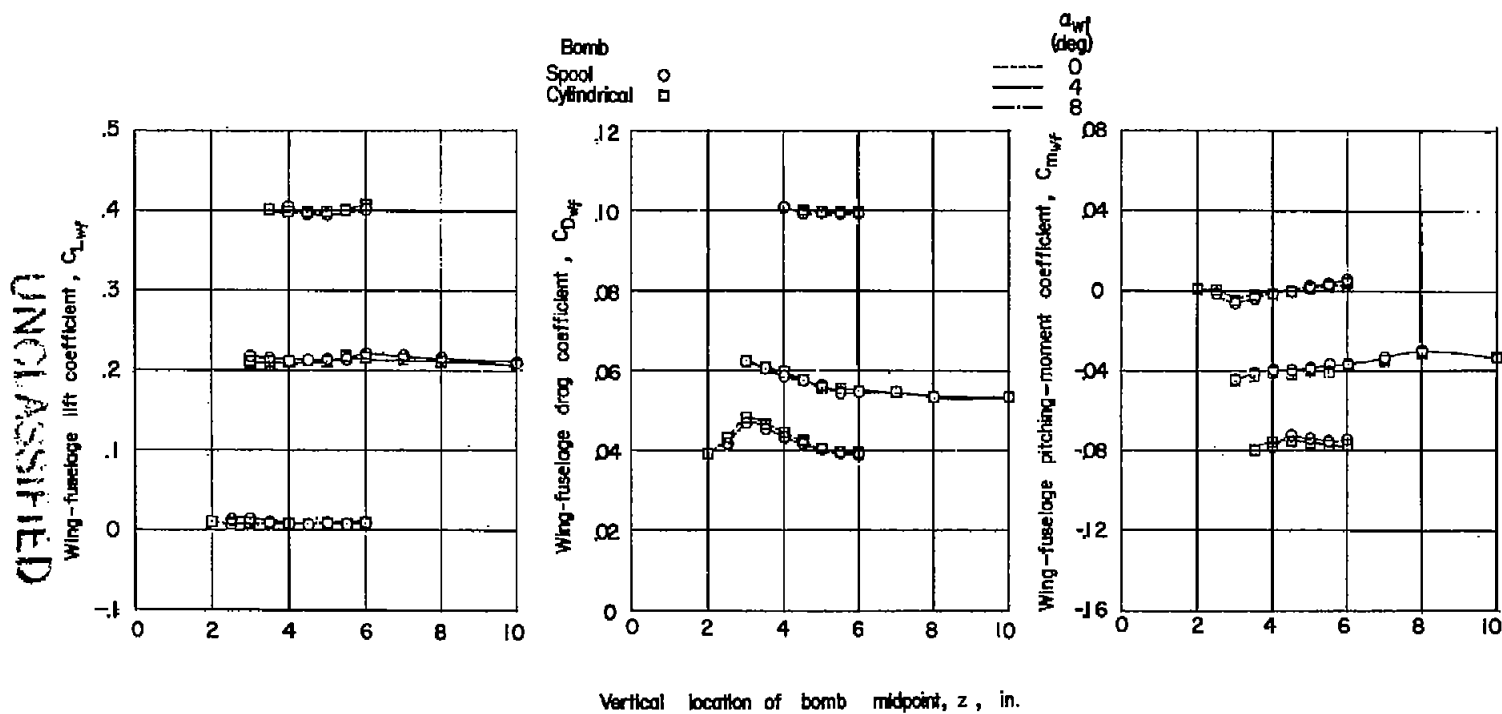


Figure 34.- Lift, drag, and pitching-moment coefficients of wing-fuselage combination in presence of spool and cylindrical bombs. $\alpha_b = 0^\circ$.